RPSEA

PREFORMED PARTICLE GEL FOR CONFORMANCE CONTROL

FINAL REPORT

CONTRACT NUMBER: 07123-2

March 1, 2012

Baojun Bai, PhD
Petroleum Engineering
Missouri University of Sciences and Technology
1400 N Bishop AV
Rolla, MO 65409
Email: baib@mst.edu
Tel: 573-341-4016

Final Report

Preformed Particle Gel for Conformance Control

Funded by RPSEA Small Producer Program

Members of the Consortium for the project

Missouri University of Science and Technology: PI, Baojun Bai, PhD

ChemEOR LLC: PI-Patrick Shuler, PhD

BJ Services (now with Baker-Hughes), PI-Qu Qi, PhD

Final report completed by

Baojun Bai

Hao Zhang

Patrick Shuler

Qi Qu

Yongfu Wu

Rajesh Challa

Mahmoud Elsharafi

Jia Zhou

Issued March 2012

LEGAL NOTICE

This report was prepared by Missouri University of Science and Technology as an account of work sponsored by the Research Partnership to Secure Energy for America, RPSEA. Neither RPSEA members of RPSEA, the National Energy Technology Laboratory, the U.S. Department of Energy, nor any person acting on behalf of any of the entities:

a. MAKES ANY WARRANTY OR REPRESENTATION, EXPRESS OR IMPLIED WITH RESPECT TO ACCURACY, COMPLETENESS, OR USEFULNESS OF THE INFORMATION CONTAINED IN THIS DOCUMENT, OR THAT THE USE OF ANY INFORMATION, APPARATUS, METHOD, OR PROCESS DISCLOSED IN THIS DOCUMENT MAY NOT INFRINGE PRIVATELY OWNED RIGHTS, OR

b. ASSUMES ANY LIABILITY WITH RESPECT TO THE USE OF, OR FOR ANY AND ALL DAMAGES RESULTING FROM THE USE OF, ANY INFORMATION, APPARATUS, METHOD, OR PROCESS DISCLOSED IN THIS DOCUMENT.

THIS IS A FINAL REPORT. THE DATA, CALCULATIONS, INFORMATION, CONCLUSIONS, AND/OR RECOMMENDATIONS REPORTED HEREIN ARE THE PROPERTY OF THE U.S. DEPARTMENT OF ENERGY.

REFERENCE TO TRADE NAMES OR SPECIFIC COMMERCIAL PRODUCTS, COMMODITIES, OR SERVICES IN THIS REPORT DOES NOT REPRESENT OR CONSTIITUTE AND ENDORSEMENT, RECOMMENDATION, OR FAVORING BY RPSEA OR ITS CONTRACTORS OF THE SPECIFIC COMMERCIAL PRODUCT, COMMODITY, OR SERVICE.

THIS PAGE INTENTIONALLY LEFT BLANK

Principle Investigator: Baojun Bai

Signature: 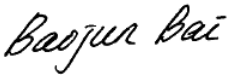

Date: 3/1/2012

ABSTRACT

This report summarizes work performed for the research project of "preformed particle gel for conformance control". The goal is to develop methods to optimize preformed particle gel (PPG) treatments to increase oil recovery and reduce water production by improving waterflood sweep efficiency.

Field applications of PPG conformance control treatments in various reservoir conditions were summarized. Reservoirs where PPG has been successfully applied include those with high temperatures, high salinity in the formation water, thick heterogeneous zones with crossflow, severe sand production, polymer flooding, and CO_2 flooding. Guidelines for PPG treatment design were provided.

Lab experiments were run to quantify PPG propagation through fractures and fracture-like channels, and the results can guide the selection of best particle gels for specific reservoirs. The results indicate that PPG injectivity increases with fracture width and flow rate; it decreases with brine concentration on which the PPG swollen ratio is dependent. Increasing particle sizes and injection rates cannot significantly increase injection pressure. Fracture models showed that PPG propagated like a piston along a fracture during injection and a gel pack formed in the fracture after PPG placement. Gel packs are permeable and their permeability can be controlled by particle strength and size, and by formation pressure; thus, they can be used to optimize PPG design.

A new technology called forced surfactant imbibition was initiated by combining PPG with surfactant. Results showed that most surfactants are not absorbed into particle gels, and certain surfactants can significantly reduce gel strength. However, gel strength can be recovered after the surfactants have been removed.

A series of customized, well-characterized laboratory scale PPG products were successfully synthesized. These products cover a wide range of particle size and chemical characteristics for laboratory performance testing. The results will aid in the field design of PPG treatments for a large range of well conditions. The swelling behavior of these products was evaluated as a function of salt type, concentration, and temperature. Results indicate that the swelling ratio is generally significantly higher in a sodium chloride brine than in a calcium chloride brine.

The possible damage caused by PPG to unswept areas was investigated in the lab. Preliminary results show that certain millimeter-sized gel particles neither penetrate into conventional rock with a permeability of less than 100 md nor form gel cake on the surface of the rock; thus, they do not damage unswept zones if the particle type and size are properly selected.

TABLE OF CONTENTS

LIST OF ILLUSTRATIONS

LIST OF TABLES

Executive Summary

This project began on October 1, 2008, and ended on March 30, 2011. Its goal was to develop methods to optimize preformed particle gel (PPG) treatments to increase oil recovery and reduce water production by improving waterflood sweep efficiency. The project involved four research tasks: First, we reviewed field application data to determine where particle gels can be effective and how best to use them. Second, we quantified the propagation of different particle gels through open fractures and fracture-like channels. The results will guide the proper selection of particle gels for fractures and channels with different widths. Third, we conducted laboratory flow tests to evaluate a novel process that could improve gel particle treatment efficiency. Finally, we developed a series of commercialized PPGs in which particles of various sizes are well distributed. The results are summarized below.

The project began with the summary and analysis of field applications of PPG conformance control treatments in various reservoir conditions. This analysis determined where PPGs can best be applied. Reservoirs where PPG has been successfully applied include those with high temperatures, high salinity in the formation water, thick heterogeneous zones with crossflow, severe sand production, polymer flooding, and CO_2 flooding. An example of field application was provided to demonstrate the proper design and implementation of a successful PPG treatment. A specification form for PPG treatment design was posted in the website http://web.mst.edu/~baib/PPG.htm for those who are interested in applying the PPG treatment technology.

Lab experiments were run to quantify PPG propagation through open fractures and fracture-like channels, and the results can guide the selection of best particle gels for specific reservoirs. Four experimental models were designed for the purpose, including screen models, tube models, transparent fracture models, and semi-transparent fracture models. The results indicate that PPG injectivity increases with fracture width, open hole size, and flow rate; it decreases with brine concentration on which the PPG swollen ratio is dependent. Increasing particle sizes and injection rates cannot significantly increase injection pressure. This observation agrees closely with the real-time injection pressures and injection rate changes observed during practical particle gel treatments. These gel particle injection behaviors are completely different from those of conventional particles in that the gels are elastic and deformable during extrusion. Transparent fracture models showed that PPG propagated like a piston along a fracture during injection and a gel pack formed in the fracture after PPG placement. Gel packs are permeable and their

permeability can be controlled by particle strength and size, and by formation pressure. The gel pack can be used to optimize PPG design.

This work also developed a fast, cost-effective method to screen PPG for fractures. The results of screening model experiments correlated well with those of fracturing model experiments; therefore, the screen model experiments, which are much simpler than fracture model experiments, can be used to screen PPGs for a reservoir with a specific fracture width.

A new technology called forced surfactant imbibition was initiated by combining PPG with surfactant. The method was developed based on a study of the compatibility of particle gels and surfactants. Results showed that most surfactants are not absorbed into particle gels, and certain surfactants can significantly reduce gel strength. However, gel strength can be recovered after the surfactants have been removed. The new technology will greatly benefit the oil industry by improving oil recovery while reducing water production.

A series of customized, well-characterized laboratory scale PPG products were successfully synthesized. These products cover a wide range of particle size and chemical characteristics for laboratory performance testing. The results will aid in the field design of PPG treatments for a large range of well conditions. The swelling behavior of these products was evaluated as a function of salt type, concentration, and temperature. Results indicate that the swelling ratio is generally significantly higher in a sodium chloride than that in a calcium chloride brine. The PPG-8B product exhibits gradual swelling, taking as many as five days to swell to its maximum extent at room temperature. The PPG-9B product is better suited for lower temperature conditions, but it takes less time to swell to its full extent.

The possible damage caused by PPG to unswept areas was investigated in the lab. Preliminary results show that certain millimeter-sized gel particles neither penetrate into conventional rock with a permeability of less than 100 md nor form gel cake on the surface of the rock; thus, they do not damage unswept zones if the particle type and size are properly selected. This lack of damage may explain why PPG treatments in field applications have rarely had negative effects on oil production.

1. Introduction

1.1. Background

One out of every six barrels of crude oil produced in the United States comes from stripper wells. These wells produce oil and gas at low rates of less than 10 barrels per day of oil or 60,000 cubic feet per day of natural gas, and they represent typical operations for many of the small producers in U.S. About 80 percent of oil wells in U.S. are now classified as marginal wells. Tapping into additional oil and gas supplies within the nation's stripper wells for smaller producers will be an important contribution to U.S. energy security. Water production is a major problem for most small producers. High level of water production results in increased level of corrosion and scale, increased load on fluid-handling facilities, increased environmental concerns, and eventually could lead to well shut-in (with associated workover costs). Consequently, producing zones are often abandoned in an attempt to avoid water contact, even when the intervals still retain large volumes of recoverable hydrocarbons. Controlling water production has been a major objective for the oil industry. Gel treatment is one of the most cost-effective methods to control water production.

1.2. Technologies/Tools Being Used

Gel treatments are applied widely to improve conformance and reduce water or gas channeling in reservoirs. The main objective of a gel treatment is to reduce water or gas flow through highly permeable channels or fractures without damaging productive zones. Two kinds of gels are applied to control conformance: in-situ crosslinking gels and Preformed Particle Gels (PPGs).

An in-situ gelling system is usually composed of polymer, crosslinker and some other additives. Polymer is usually HPAM, while crosslinkers can be the compounds of Cr^{3+}, Cr^{6+}, or Al^{3+}, or resin. Additives are used to adjust gelation time, control gel strength and thermo-stability. The mixture of polymer and crosslinker called gelant is injected at a high water cut production well into a target formation and reacts in the formation (mainly via temperature effect) to form gel and thus fully or partially seal the formation where gel is placed. Therefore the gelation process occurs in reservoir conditions. Typical in-situ gels included bulk gel (BG) and colloid dispersion gel (CDG).

In-situ crosslinked polymer gels are traditionally mostly applied for conformance control treatments because they have the advantages of controllable gelation time, adjustable strength, and good injectivity. However, there are distinct drawbacks inherent in in-situ gelation systems, such as uncontrolled gelation times and variations in gelation due to shear degradation, and gelant compositional changes induced by contact with reservoir minerals and fluids. In addition, in-situ gelation systems behave as a polymer solution before gelation. According to polymer flooding mechanisms, polymer solution will more enter the zones unswept by water during water flooding. Once gelant forms gel in unswept zones, it will seriously damage the potential oil production zones.

Preformed gel is formed at surface facilities before injection, and then gel is injected into reservoirs. For this technology the gel treatment occurs in injection well. So no gelation occurs in reservoirs. The current available preformed particle gels include mm-size preformed particle gel (Coste, 2000; Bai, 2008), microgels (Chauveteau, 2000; Zaitoun, 2007), and swelling micron-sized polymers (Bright Water®) (Pritchett 2003; Frampton, 2004). Field applications of some gels resulted in very positive results (Pritchett, 2003; Bai, 2008; Liu, 2006; Zaitoun, 2007; Cheung, 2007; Abbasy, 2008; Pyziak, 2007; Larkin and Creel, 2008). Their major differences are their sizes and swelling times.

Preformed particle gels have become a newer trend because they can overcome some distinct drawbacks inherent in in-situ gelation system such as lack of gelation time control, uncertainness of gelling due to shear degradation, chromatographic fractionation or change of gelant compositions, and dilution by formation water. The preformed particle gels (PPG) that is the focus in this study have the following unique advantages over traditional in-situ gel, including: (1) PPG are strength- and size-controlled, environmentally-friendly, and they are stable in the presence of almost all reservoirs minerals and formation water salinity; (2) PPG can preferentially enter into fractures or fracture-feature channels while minimizing gel penetration into low permeable hydrocarbon zones/matrix. Gel particles with the appropriate size and properties should transport through fractures or fracture-feature channels, but they should not penetrate into conventional rock or sand; (3) PPG has only one component during injection. Thus, it is a simpler process, and does not require many of the injection facilities and instruments that

often are needed to dissolve and mix polymer and crosslinker for conventional in-situ gels, and (4) PPG can be prepared with produced water without influencing gel stability. In contrast, traditional in-situ gels are often very sensitive to salinity, multivalent cations, and H2S in the produced water. This not only can save fresh water but it also can protect our environment.

However, the PPG injectivity is still questionable to many reservoir engineers because its size is usually much larger than the pore sizes of conventional cores from reservoirs. PPG treatments have been successfully used for more than 2,000 wells in China (Bai, 2007; Liu, 2006), Halliburton (Abbasy, 2008), Occidental oil company (Pyziak et al., 2007) and Kinder-Morgan (Larkin and Creel, 2008), but its mechanisms to control conformance and its applied conditions are still not clear. And due to its large size, it cannot be used in the reservoirs without super-high permeability channels or fractures.

1.3. Justification for the New Research or Technology

Unless special efforts are made during gel placement (e.g., zone isolation), theoretical studies and field applications demonstrate that gel treatments are most likely to be successful when treating fractures or fracture-like features that cause channeling in reservoirs. Seright has studied the propagation of preformed bulk gels through open fractures since 1992. They have also performed extensive core flooding experiments and successfully developed a series of theories and methods to characterize the propagation of preformed bulk gels through porous media. However, although the preliminary studies of particle gel propagation through porous media were performed by the product inventors, all core flooding tests used porous media without channels. The smallest gel particles, such as microgels, colloidal dispersion gels, and micron-sized swelling polymers, were marketed only for treatment of matrix problems. However, we are interested in whether these particles gels might have applicability to fractures and fracture-like channels. The ultimate purpose of the project is to provide the fundamental information to select particle gels for mitigating water production and extending field life.

1.4. Problems Addressed in this Research Project

Our work features the following innovations:

The transport of particle gels through fractures and channels were tested using screens and core flooding experiments. These experiments provided a design basis for fractured or channeled reservoir gel treatments.

The analysis of connecting laboratory and field data resulted in models to optimize particle treatments in fractured reservoirs.

Novel methods were tested to improve PPG treatments.

1.5. Research Tasks in the this Research Project

The project involved four research tasks:

- First, it reviewed field application data to determine where particle gels can be effective and how best to use them.
- Second, particle gel propagation for different PPG products was quantified during extrusion through open fractures and fracture-like channels. The results will guide the proper selection of particle gels for fractures and channels with different widths.
- Third, laboratory flow tests were conducted to evaluate novel processes that could improve gel particle treatment efficiency.
- Finally, it developed PPGs in which particles of various sizes are well distributed.

1.6. Structure of the Report

Following is the structure of this report:

Chapter 1 is a review of the current status of gel treatments and the significance of preformed particle gel treatments to small producers. Different gel treatments are compared and current technology being used was introduced. The problems and research tasks in this project are also defined.

Chapter 2 is the summary of field applications of PPG conformance control treatments in various reservoir conditions. It addressed the first task in this project. This analysis determines where PPGs can best be applied. Reservoirs where PPG has been successfully applied include those with high temperatures, high salinity in the formation water, thick heterogeneous zones with crossflow, severe sand production, polymer flooding, and CO_2 flooding. An example of field application is provided to demonstrate how to properly design and implement a successful PPG treatment.

Chapters 3-7 report lab experiments using four experimental models (screen models, tube models, transparent fracture models, and semi-transparent fracture models) for quantifying PPG propagation through open fractures and fracture-like channels. They address the second task in this project. The results can guide the selection of best particle gels for specific reservoirs.

Chapter 3 shows the experimental results from screen models that are used to test the strength of the swollen particle gel and the effect of injection rate on the injectivity of particle gels. The results indicate injectivity mainly depends on the swelling capacity and the open hole size of a screen. Increasing particle sizes and injection rates can not significantly increase the injection pressure.

Chapter 4 reports experiments using tubes of various internal diameters to study the PPG propagation and extrusion behavior through tubes. It considered several factors that influence PPG behavior during extrusion, including particle gel swelling ratio (brine concentration), and internal diameter of tube through which particle gel is injected. Effect of gel flow resistance factor on the tube internal diameter and the brine concentration of the PPG were also discussed.

Chapter 5 reports the experimental results from transparent fracture models which were constructed to visually track swollen preformed particle gel (PPG) propagation through open fractures and water flow through PPG placed in fractures. Investigation of factors that influence PPG injectivity and plugging efficiency revealed that PPG injectivity increases with fracture widths and flow rates but decreases with brine concentrations. PPG can reduce the permeability for the fractures with different widths to the same level. Full-factorial experimental design analysis was performed to rank the influence of injection rate, fracture width, and PPG swelling ratio on pressure response, resistance factors, and injectivity.

Chapter 6 used semi-transparent fracture models to understand the propagation of preformed particle gel along the fractures and the leakoff properties in the matrix rock. The effects of injection rate, gel concentration, gel particle size, and particle gel swelling ratio (depending on brine concentration) on particle gel intrusion were also examined in this chapter. Experiential results showed no progressive plugging was in any part of the

fracture models, and the required volume and time for injecting gels into a given fracture were much smaller compared to those in bulk gel treatments.

Chapter 7 developed a fast, cost-effective method to screen PPG for fractures by using screen tests. The results of screening model experiments correlated well with those of fracturing model experiments; therefore, the screen model experiments, which are much simpler than fracture model experiments, can be used to screen PPGs for a reservoir with a specific fracture width. Considering the shear-thinning properties of PPG, a theoretical mathematical model using a general power law equation to predict the pressure gradient of swollen PPG during its extrusion through a fracture was developed. Then the model was modified by correlating screen test results with fracture experiment results. These correlations correlated effective viscosity with flow rate, fracture width, apparent consistency constant and apparent flow index together. The newly developed correlations were validated and the results show that a single group of screen test measurements can be applied to determine the effective viscosity of PPG in a fracture with limited errors.

Chapter 8 reports our research results about the compatibility of particle gels and surfactants. This delivers the third task in this project. The objective of this research is to test if the combined technology of PPG treatments and surfactant injection can significantly improve the gel particle treatment efficiency and thus improve overall oil recovery. Results show (1) surfactants have negligible effect on PPG swelling ratio; (2) Equilibrium surfactant concentration in excess brine increases after swelling of gel particles; (3) Gel strength in terms of dynamic modulus G' (storage modulus) and G" (loss modulus) can be reduced to a much lower value. But the gel strength can be recovered after the surfactants have been removed. Moreover, a new technology of forced surfactant imbibition can be developed by combination of particle gel and surfactant. The new technology will greatly benefit to oil industry by the way to improve oil recovery while reduce water production.

Chapter 9 presents a series of customized, well-characterized laboratory scale PPG products which have been successfully synthesized. This is the fourth task in this project. These products cover a wide range of particle size and chemical characteristics for laboratory performance testing. The results will aid in the field design of PPG

treatments for a large range of well conditions. The swelling behavior of these products was evaluated as a function of salt type, concentration, and temperature. Results indicate that the PPG swelling ratio is generally significantly higher in a sodium chloride than that in a calcium chloride brine.

Chapter 10 shows the preliminary results about possible damage caused by PPG to unswept areas. Results show that millimeter-sized gel particles neither penetrate into conventional rock with a permeability of less than 100 md nor form gel cake on the surface of the rock; thus, they do not damage unswept zones if the particle type and size are properly selected. This lack of damage may explain why PPG treatments in field applications have rarely had negative effects on oil production.

Chapter 11 indicates the impact to small producers by applying PPG treatments and the technology transfer efforts in this project.

Chapter 12 concludes all the results in this project and provides several recommendations for future research in PPG treatment area.

2. Field Application and Data Analysis of Preformed Particle Gel for Conformance Control

2.1. Summary

The purpose of this chapter is to provide an overview and analysis of known work that has been done in the field of PPG, presenting a broad view of the various applications for which it might prove useful. This chapter reviews field applications of preformed particle gel (PPG) treatments for conformance control in various reservoir conditions, including reservoirs with high temperatures, high salinities, thick heterogeneous zones, severe sand production, polymer flooding and CO_2 flooding. Detailed information is described about an application of PPG treatment for in-depth fluid diversion in four injection wells in a sandstone reservoir with thick net zones. In addition, theoretical models are used to discuss why a large amount of large particles can be injected into the reservoir.

2.2. Overview of PPG Treatment Technology and Field Applications

2.2.1. What is PPG?

PPG (mm-sized preformed particle gel) is an improved super adsorbent polymer (SAP). SAPs are a unique group of materials that can absorb over a hundred times their weight in liquids and do not easily release the absorbed fluids under pressure. Superabsorbent polymers are primarily used as an absorbent for water and aqueous solutions for diapers, adult incontinence products, feminine hygiene products and the agriculture industry. However, the traditional SAPs in the markets do not meet the requirements for conformance control due to their fast swelling time, low strength and instability at high temperature. A series of new SAPs called preformed particle gels (PPGs) have developed for the conformance control purposes (Li et al, 1999; Bai et al, 2004, 2007). PPG properties are summarized as follows:

- PPG sizes are adjustable: μm-cm.
- Swelling ratio in formation water: 30~200 times original size.
- Salt resistance: all kinds of formation salts and concentrations are acceptable.
- Thermal stability: more than 1 year below 110 ºC (230 ºF).
- Strength: adjustable, high strength product available.

- Swelling rate: slightly controlled.

2.2.2. Why Select Preformed Particle Gel Treatments?

Our lab tests have shown that gelants will form dispersed gels rather than bulk gels in the porous media without open fractures at flowing conditions, shown in Figure 2-1. Therefore, gel treatments in porous media are particle gel treatments.

Particle gels have great potential due to their unique advantages over traditional the traditional in-situ gels discussed in the first chapter.

Preformed Particle Gels (PPGs) also have unique properties compared to other preformed gels. PPGs are mm-sized gel particles, so they cannot be injected into conventional porous media without fractures or void. They can effectively plug fractures or high permeability streaks/channels in mature oilfields which cannot be successfully implemented by nanosized particle gel-Bright Water® (Pritchett, et al. 2003; Frampton, et al., 2004) or microsized preformed particle gels-microgels (Chauveteau, et al., 2001, 2003; Rousseau, et al, 2005; Zaitou, et al, 2007). In addition, the PPG has the following advantages:

1. PPG can preferentially enter into fractures or fracture-feature channels while minimizing gel penetration into low permeable hydrocarbon zones/matrix. PPG has adjustable sizes, from a few hundred micrometers to a few centimeters. Gel particles with the appropriate size and properties could transport through fractures or fracture-feature channels, but they should not penetrate into conventional rocks or sandstones. The minimized gel penetration in low permeability zones results in significant reduction in required gel volumes because fracture or fracture-like channels usually comprise less than 10% of the reservoir volume (Tang, 2005). This is in contrast to in-situ gels, which behave as polymer solutions when they are injected as gelants. According to polymer flooding mechanisms, more gelants will sweep into un-swept low permeability oil zones than water. Once the gelants crosslink in these oil zones, not only they will waste polymer but they will also block these zones, which will cause serious damage in these potential productive oil zones.
2. PPG suspension can be prepared with produced water without influencing gel stability. This can not only save fresh water but it can also protect our

environment. In contrast, traditional gels and nano-sized particle gel Bright Water® are very sensitive to salinity, multivalent cations, and H_2S in the produced water.

3. The adjustable size and strength of PPG particles make them suitable to use a "trial and error" method for better conformance control results. Real-time monitoring data can be used to adjust the previous design for better gel treatment results. The success of gel treatments depends on accurate reservoir problem identification, appropriate well candidate selection, gel selection, parameter design, and gel placement. However, most reservoirs remain somewhat of a "black box", and are not completely understood. The "trial and error" provides an effective method to improve treatment of the reservoir during the course of the treatment based on empirical data obtained during monitoring.

Field experiences have demonstrated mm-sized particle gels are feasible for mature water flooded reservoirs. Fractures or high permeability streaks/channels are well documented to exist in mature water-flooded reservoirs (Seright, 1999; Bai, et al, 2007). Field tests and successful injections of particle-type conformance control agents in China have demonstrated that reservoir pore structures and physical parameters have been significantly changed by long-term waterflooding. The existence of induced fractures or high permeability streaks/channels is evidenced by the following field experiences:

- Interwell tracer tests. Many reservoirs have no initial fracture(s), but tracer tests showed in many cases that it took less than 15 days, or even a few days or hours for the tracers to move from an injector to its adjacent producers with a distance of around 100-300 meters (328-984 ft). Tracer test data interpretation using simulation software shows that the permeabilities of these channels or streaks are usually around a few hundred to tens of thousands of Darcies. Although their volumes are only 1 to 10% of the reservoir volume, these high permeability zones may take in up to 80-90% of the injected water (Tang, 2005).
- Gel treatments. Large-volume gel treatments (more than 5,000 m^3 or 31,449 barrels) using in-situ gelation systems were performed on hundreds of wells in China's oilfields in the 1990s. Their gelation times were usually only a few hours to less than one day. All gelants were successfully injected even though the

injections continued from anywhere between 15 days up to a few months. In addition, many treatments did not increase water injection pressure enough as expected after treatments. This indicates much of the gel was getting "lost" in the very high-permeability zones.

- Particle injections. Many kinds of particles such as montmorillonite clay and fly ash were applied to control conformance in China in 1990s. Many wells were successfully injected with a few thousands of cubic feet of the particle-type conformance control agents without any injection problems, which also indicated the formations had extremely large voids or fractures.

Based on above field practices, millimeter-sized PPG treatments were proposed to control conformance (Li, 1999; Coste, 2000; Bai, 2004, 2007). Field applications have demonstrated the mm-sized gel particles have no significant injectivity problems in most mature reservoirs.

2.3. Application Cases of Preformed Particle Gel for Conformance Control in Different Reservoir Conditions

The following sections describe a number of different applications where PPGs were successfully used in reservoir treatment. Many of the early applications were performed in China, so reservoir units have been reported in metric units. A conversion table is provided at the end of the text (SI Metric Conversion Factors).

2.3.1. Application Case in a Reservoir with High Salinity and High Temperature

This case was the first PPG treatment in Zhongyuan oilfield, SINOPEC. It includes two adjacent injection wells, W51-75 and P-72, in Pucheng reservoir of the oilfield. Three production wells are connected with the two injectors. It is a sandstone reservoir with an average permeability of 121 md without fractures. The formation temperature is 107 ºC (224.6 ºF) and the total salinity of the formation water is 15×10^4 mg/l (ppm). The reservoir has been developed by water flooding since 1979. The two wells were not hydraulically fractured. The two wells were treated using PPG in 1999 due to the following reasons:

- Each of the two wells has high water injectivity. The injectivity index of W51-75 is 20 m^3/(MPa•day) (0.867 bbl/(psi•day)) with threshold pressures (which is defined as the minimum injection pressure that water can be injected) of 9.2 MPa

(1,334 psi), and the injectivity index of P-72 is 18 m^3/(MPa•d) (0.78 bbl/(psi•day)) with threshold pressure of 8.5 MPa (1,233 psi);

- Connected production wells had a high average water cut of more than 85%;
- Water injection profile results showed that the wells had an extreme vertical heterogeneity;
- Tracer test results showed that the wells had an extreme severe areal heterogeneity and channel between injectors and producers (tracer breakthrough in two days).

The injected PPG volume of each well was optimized by systematically considering injectivity, water injection profile and tracer test results. 4,300 m^3 (36,062 barrels) PPG suspension prepared with 13,000 kg (28,660 lbs) dry PPG was injected into W51-75 and 2,500 m^3 (20,966 barrels) PPG suspensions prepared with 7,500 kg (16,535 lbs) dry PPG was injected into P-72. PPG concentration is 3,000 mg/L (ppm). Produced water was used to prepare the PPG suspensions. PPG size ranges from 0.8 to 2.0 mm (0.0315 to 0.0787 inch) with a median diameter of 1.5 mm (0.0591 inch).

The injection rate was determined by the injectivity index of each well. The highest injection pressure was limited to 80% of the fracturing pressure of the formation. An alternate injection method of water (treated produced water) and PPG suspension was applied: PPG suspension injection was done during the daytime and water injection was done at night.

After the PPG treatment, injection wells and their corresponding production had the following responses:

(1) Injection pressure was increased: the water injection pressure of P-72 increased from 19.5 MPa (2,828 psi) to 24 MPa (3,481 psi) and W51-75 from 16 MPa (2,320 psi) to 19 MPa (2,756 psi). The higher injection pressure continued for more than two years, indicating the PPG is stable for more than one year at the formation conditions.

(2) Vertical injection profile was modified. The improvement of the vertical profile was confirmed by a profile test survey before and after the PPG treatment shown in Figure 2-2. In this figure, each layer represents a separate layer and there is an impermeable barrier between layers (assuming no vertical fracture). As shown in

this figure, only two layers took water before treatment, but another two layers began to accept water after the treatment. Of course, it should be noted that the injection well profile results sometimes are not instructive when channels or fractures exist near the wellbore due to the limited depth of investigation. In this case, if the channel or fracture just exists in one layer, the comparison results are meaningful because some new layers were affected after the treatment. However, the results are meaningless if the fracture or channel penetrates most layers of the well. Because the detection of fracture penetration is difficult, it cannot be proven whether the channels or fractures penetrate most layers or just one layer.

(3) Water cut of corresponding producers was decreased and daily oil production rate was increased. Figure 2-3 presents a typical production curve of well W51-172, which connects with both W51 and P72. The water cut was decreased from about 80% to about 70% and daily oil production was increased from 40 tons/day (293.2 bbl/day) to 439.8 tons/day.

The two well PPG treatments resulted in a total 3,239 tons (23,742 barrels) of oil increase or 525 barrels of incremental oil per 1,000 lb PPG.

2.3.2. Application Case in a Sandstone Reservoir with Thick Layers

This example documents the first PPG treatment in Daqing oilfield, PetroChina. The selected injection well is Xing-7-24 in Xingbei oilfield. The reservoir formation is characterized by thick oil layers with severe vertical heterogeneity. Formation temperature is about 45 °C (113 °F) and salinity is about 4,500 mg/L (ppm). The perforated depth is from 890 to 1051.4 m (2,920 to 3,450 ft). Net pay of the well is 24.5 m (80 ft). The initial permeability is from several md to more than 1,200 md. The well was changed from a producer to a water injection well in November 1992, and the cumulative water injection volume had been 763,758 m^3 (4,803,893 barrels) until August 2000. Four adjacent producers were confirmed to be connected with the injection well with a total of more than 700 m^3/day (4,403 bbl/day) of liquid and average water cut of more than 90%. Profile tests showed that about 85% injected water directly passed through high permeability parts of the oil zones, which occupied less than 1/5 of the total thickness. Inter-well potential measurements demonstrated that the well group had severe areal heterogeneity, shown as Figure 2-4. PPG treatment was performed in August 2000.

The produced water was used to prepare PPG suspension. As is known, for a normal in-situ polymer gelling system, it usually takes some time to prepare polymer and crosslinker before it is injected. But PPG is completely different, and it can be easily dispersed into water. Figure 2-5 shows the flow scheme of PPG mixing and injection system. The procedure is simple, and it can also reduce some operation and labor costs.

Table 2-2 shows the injection scheme of PPG suspension. A total of 3,100 m^3 (19,498 barrels) PPG suspension was injected into the well in multiple stages. For the first stage, 100 m^3 (629 barrels) of 5 mm (0.2 inch) PPG suspension was injected into the well at a higher flow rate of 25 m^3/h (157 bbl/h) and a higher concentration of 1%. The objective of the first stage was to inject the PPG at higher pressure so that the PPG suspension could start in all open layers. Because the PPG cannot penetrate into zones with permeability below 1,000 md, it will form face plugging at these zones that can prevent subsequent PPG from entering and damaging these zones. For the second and third stages, an alternative injection method of PPG suspension and water was used: 10 hours of PPG suspension injection followed by 14 hours of water injection. The difference between the 2nd and 3rd stage is their particle sizes. In fact, we initially designed them to be the same size, but the injection pressure increase did not achieve our expectation, and so we increased particle size from 1.5 mm (0.059 inch) to 3 mm (0.118 inch). For the fourth stage, 5 mm (0.2 inch) PPG was continually injected so that the final injection pressure can achieve expected results. Figure 2-6 shows the monitoring injection pressure result during PPG injection while not including water injection periods. As we saw, the injection pressure oscillates, which is caused by the alternating injection of PPG suspension and water. When PPG suspension was injected, the injection pressure gradually increased, but when changed to water injection, the pressure decreased, which indicated injection water could displace part of the PPG away from wellbore.

The injection wells and their corresponding producers showed the following results after the treatment.

- Injection pressure increased from an initial 5.0 MPa (725 psi) to 11.6 MPa (1,682 psi).
- Potential test results showed that the areal heterogeneity was effectively controlled.

- About 2,400 tons (17,592 barrels) of incremental oil was obtained with 8% water cut decrease.
- The useful life of PPG is more than 6 months.

The above results show that the PPG treatment is positive. In this case, 15.5 tons (34,171 lbs) of 1.5~5 mm (0.059~0.197 inch) particles were injected into the wells, but no injectivity problem was encountered. According to the theoretical particle size of PPG propagation through porous media, this reservoir should have a channel with a permeability of hundreds of Darcies. Of course, there are two other possibilities for this case. The first possibility is that the particles may have been broken into small pieces when they were injected or transported through porous media. But for this possibility, no matter how small, the particles still are a gel and it is very difficult to transport gels through normal porous media without the presence of a fracture or channel. Another possibility is that there exists a "cave" which is often caused by sand-production near the wellbore. For Daqing oilfield, sand-production is not severe, so there is only a low probability that caves exist near the wellbore. From the injection history, it can be inferred that the reservoir has some fractures or channels. Otherwise, it is improbable that such a large volume of PPG could be injected. Of course, it cannot be proven that fractures or channels exist nor how far they might extend from the injection well.

2.3.3. Application in a Reservoir with Severe Sand Production

Two injection wells were selected for PPG treatments in Shengli oilfield, SINOPEC in 1999. Both selected wells (Bin 24-4 and Bin 24-17) are in the block 255 of Shangdian reservoir, which is a sandstone faulted-block reservoir with severe sand production. The oil production layers in the block are named as S3 and S4. The average thickness of layer S3 is 4.6 meter (15 ft) with a high permeability of 2-6 Darcy and an average porosity of 31%. The crude oil viscosity in the layer ranges from 57 to 148 cp. The average thickness of S4 layer is 1.6 meter (5.25 ft) with a low permeability of 0.04 to 0.5 Darcy and an average porosity of about 25%. The oil viscosity in the S4 layer is high to 7,731 cp (with an average value of 721 cp).

The selection of PPG treatment was selected based on the following considerations:

- The reservoir is mainly composed of unconsolidated sand. Sand production has resulted in voids or channels with super-high permeability in the water-flooded areas.
- PPG particles are soft and deformable and could move more deeply into the very high permeability channels to redirect the fluid flow away from there.
- The high salinity of the reservoir is not favorable for other gel treatments.
- The PPG injection process is simple compared to in-situ gel treatments.
- The treatment cost is low due to the little requirement of workover.

The reasons for choosing wells Bin 24-4 and 24-17 were:

- High contrast in the vertical fluid distribution (see the injection before treatment in Figures 2-7 and 2-8).
- Most of the offset producers had a water cut of above 90%.
- Both wells were previously unsuccessfully treated with other water control techniques.

The information for the two injection wells is shown on Table 2-3. Table 2-4 provides information for the offset producers of well Bin 24-4 and Table 2-5 for the offset producers of well Bin 24-17.

The equipment designed for PPG injection is shown on Figure 2-9. The particles and water were mixed prior to injection in a standard tank and then were injected into the formation through the tubing string. Table 2-6 shows the designed injection parameters for the two well treatments.

Figure 2-10 shows the monitored real time pressure response during PPG injection. The pressure curve in both tests can be divided in two parts: In the first part the injection pressure increases steadily indicating the buildup of resistance to flow, the second part is almost a plateau which can be attributed to the in-depth propagation of the gel particles.

The profile surveys for the two injection wells indicated significant change of the vertical fluid distribution for the well Bin 24-4 (Figure 2-7). After treatment, one of the two initial water “thief” intervals was almost shut off, and water was redistributed toward the six remaining open intervals. For well Bin 24-17 (Figure 2-8) the distribution of the

fluid was much more homogeneous than that before treatment. The sweep in the low permeability (S4) layer was improved in both treatments.

For wells Bin 24-4 and Bin 24-17, respectively, three and two offset wells responded favorably to the job. The average water-cut decreased and a total of 2,278 tons (16,698 barrels) of incremental oil was produced within 8 months following the treatment. Table 2-7 gives the data for the responding producing wells.

2.3.4. Application in Polymer Flooding Areas

Four injection wells in polymer flooding areas were treated using PPG to control conformance in LMD reservoir, Daqing oilfield, PetroChina. Totally 18,400 m^3 (115,732 barrels) of PPG suspension (99 tons (218,255 lbs) of dry particles) were injected into the four injection wells. The selected four injectors have 46 connected producers with average water cut of 95.4% before treatment. The treatment results were very successful as indicated by the following:

The injection pressure for each well significantly increased after treatment. The average water injection pressure after treatment increased 0.6 MPa (87 psi) compared to pretreatment injection pressure at the same injection rates, shown as Table 2-8.

Injection profiles were greatly improved. Polymer injection in well 6-P173 started in Feb 1999 and a total of 3.157×10^5 m^3 (2.6476×10^6 barrels) of 1,000 ppm polymer solution was injected before PPG treatment. The polymer injection pressure was 13.2 MPa (1,914.5 psi) at the injection rate of 200 m^3/d (1,677 bbl/d). The relative polymer absorbent rate of Layer PI2 changed from 96.49% to 52.67% due to the treatment and the reduced absorbent rate contributed to other layers.

Treatment slowed pressure drop rates during pressure drawdown tests. Figure 2-11 compares the drawdown test results of well 4-P163 before and after treatment. The pressure drop decreased very quickly before treatment, which suggesting the presence of fractures or fracture-like channels. The pressure drop rate changes slowly after treatment, indicating that the channels have been effectively plugged.

The oil production rates of connected wells were increased and the water production rates were decreased after PPG treatment. Figure 2-12 compares the oil production rates and water cut of eleven connected production wells before and after PPG treatments. The average oil produced increased 3.8 tons (27.9 barrels) and water cut

reduced 2.8% and produced polymer concentration reduced 33 mg/L (ppm) due to the PPG treatments.

2.3.5. Remediate Unwanted Communication in a CO_2 Flooding Reservoir.

Larkin et al (2008) described a case study of conformance problems aggravated by apparent direct communication channels between injector and offset producer(s) in certain patterns of SACROC unit CO_2 EOR project and their practice of controlling the conformance by the injection of swelling gel particles---crystal polymer (CP).

SACROC Unit within the Kelly-Synder field is located outside the city of Snyder in Scurry County, TX. It was discovered in November 1948. Water flooding started in 1954 and CO_2 flooding in 1972. To date, the field has 1956 well bores and 815 active wells in its 50,000 acres with average depth of 6,700 ft and average net pay thickness of 260 ft (up to 800 ft). Average porosity is 7.6%, and average permeability 19.4 md. The reservoir rock is characterized as highly heterogeneous, and short circuit or unwanted communication paths have resulted in serious sweeping problems and operational problems caused by excessive production of CO_2.

Particle Gel Treatment. Superabsorbent Polymers (SAP) were injected in multiple wells to remediate their short circuits and reduce CO_2 production. The properties of injected particle polymers are listed as follow:

- 100% Cross-linked, synthetic (sodium acrylate based)
- Links created from identical acrylic acid monomers neutralized with caustic acid
- Swell 300 to 800 times (various solutions)
- Swelling time relative to size, smaller creates more surface area and faster swelling; general range 30 minutes to 3 hours
- Solutions: fresh water (use caution), produced oil, diesel, brines, produced water (salinity), sodium silicate solutions
- Multiple size grades – solid material
  Sizes: ground 300-400 mesh, 0.5 mm, 1 mm, 2 mm, 4 mm, and 14 mm diameter
- Does not absorb on rock (wettability unaffected)
- Environmentally friendly
- Acid resistant
- Confined to fractures

- Resistant to degradation by CO_2, bacteria and temperatures below 275 °F

Treatment Results. SAP particles with size up to 4 mm (0.157 inch) were successfully injected into all selected wells. The injection profiles were improved and gas production was reduced with the increase of oil production. The field application results showed that the particle treatment is a cost-effective profile modification option for CO_2 Flooding oilfields.

2.3.6. Plug Void Conduit in Anton Irish Field

Reservoir Description (Pyziak and Smith, 2006; Smith, 2006): The Anton Irish field, a carbonate reservoir located in West Texas was discovered in 1945. The field was then utilized for a produced gas pressure maintenance project in 1950 and converted to a waterflood in 1969. CO_2 Flooding began in 1997 and currently accounts for approximately 85% of the unit production. The rapid breakthrough of injection fluids (CO_2 or water) leads to excessive cycling of the injection fluid through conduits rather than sweeping the reservoir matrix. The downhole video inspection of the wellbore (injection #63) indicated that the well has a larger fracture similar to image in Figure 2-13.

Particle Gel Treatment: To fill the void conduit in the well, a swelling polycrystalline material (similar to PPG) was used. They injected 30,000 lbs of the swelling polycrystals at a mixed ratio of 0.25 lbs/gal which was carried by a 9.5 lbs/gal brine. The swelling ratio of the particle gel in the brine is around 35. It was estimated the product would occupy a void volume of appropriately 3,000 bbls when they were fully expanded. The pumping flow rate was 4-5 BPM. The injection continued for more than 10 hrs. Figure 2-14 showed the real-time pressure change during the particle injection. A steady flow was observed, possibly indicating the void or conduit feature was filling.

Results: After initial completion of the treatment and 36 hours of shut-in, the well could not be injected. The well was cleaned out with coil tubing. Injectivity is shown in Figure 2-15.

2.3.7. Large Volume PPG Injection in Daqing Oilfield

Reservoir Characterization: The pilot project is located in one block of Lamadian, Daqing. Lamadian is an unsymmetrical, short-axial anticlinal oilfield, and it has three major intervals including Gaotaizi (G), Putaohua (P) and Saertu (S) from top to bottom.

The reservoir rocks are middle early –Cretaceous lacustrine and fluvio-deltaic sandstone and siltstone with muddy rock intercalated. The reservoir temperature is about 45 ºC (113 ºF) and formation water salinity is about 4,000 mg/l (ppm). The oil-bearing area of the selected pilot is 2.43 km^2 (600 acres) with an initial-oil-in-place of 5.94×10^6 tons (4.354×10^7 barrels). The major production zones are PI4 to GI4+5, and each individual zone is thick and very heterogeneous The block was produced for more than 30 years with an average water cut of above 95.4%. Large volume of PPG treatments were carried out from the year 2003 to 2004, with the target zone being PII.

Criteria to Well Candidate Selection: Selection of treatment wells is based on a good understanding of the reservoir geology, wellbore and near wellbore conditions, reservoir surveillance results, and reservoir static and dynamic data. The well criteria to select a candidate for a large volume of PPG treatments were set as follows in Daqing:

- The well must be located in the main sand body of the fluvial depositional reservoir with thick oil pay zones and good connectivity with adjacent producers.
- The well must have strong injectivity; the water injection pressure is lower than the average water injection pressure in the block and the starting pressure is also lower than the average starting pressure in block
- The connected producers have relatively high average water cut comparing to other well groups.
- Vertical or areal heterogeneity is very serious, and the inner-layer permeability contrast is large, and both injection profile and the production profiles of connected production wells are extremely heterogeneous.
- The degree of water-flooded regions is different; there exist middle, low and unflushed zones.

Based on the above criteria, four injection wells, 7-1827, 7-1927, 8-1827 and 9-1927, were. Figure 2-16 shows the location of the selected wells. The distance of each injection well and its connected edge producer is 300 m (984 ft). Forty-six production wells were connected to the four treated wells. Twenty-three of them only produced from PII and the other 23 produced from the interval PII and other intervals. Table 2-9 gives the basic parameters for the selected four wells. In the table, the maximum permeability refers to the permeability of the most permeable portion of the specified interval, derived

from well logging. The starting pressure refers to the minimum wellhead pressure that water starts to enter the formation. That is, water cannot enter the formation if the injection pressure is smaller than the starting pressure. PI is the pressure index, which is from the pressure drawdown test for a period of 90 minutes after an injection well is shut down. The PI(90) is calculated from the following equation:

$$PI(t) = \frac{\int_0^T P(t)dt}{T} \quad (2\text{-}1)$$

where *PI (t)*---pressure index, MPa or psi;

P(t)---pressure at the time t after a well is shut in, MPa or psi;

T---shut in time, min, usually T is set as 90 minutes.

PPG Characterization and Selection: The selected PPG is an improved super absorbent polymer (SAP). The selection of this PPG mainly considered its compatibility with the formation water, its thermo-stability at reservoir temperature, the swelling ratio, strength after swelling and particle size (Bai, et al, 2004; Liu, 2010). Six samples were evaluated for the best PPG candidate for the pilot. Results showed all PPGs had good capability with produced water from the pilot and they were thermally stable at reservoir temperature for more than 2 years. Table 2-10 showed the evaluation results for PPG particle size, swelling ratio, pressure resistance, and breakthrough pressure. All PPG dispersions were prepared by produced water from the pilot. PPG sizes were sieved by screens with proper mesh sizes. The swelling ratio was the mass ratio of the PPG after and before swelling. The pressure resistance is defined as the minimum pressure that swollen particle can pass through the holes with a diameter of 0.3 mm (0.012 inch). The breakthrough pressure is defined as the minimum pressure that water can be injected after PPG is placed in a core. The minimum pressures in Table 2-10 were measured using the cores with the permeability of 3-3.5 μm^2 (3-3.5 darcy), which were injected using 1,000 mg/l (ppm) of 250 mesh (61 μm) PPG particles. The WT product was selected for the pilot because it had relatively high swelling ratio and enough strength.

PPG Treatment Design:

PPG Suspension Volume Determination: Reservoir simulation was run to optimize PPG dispersion volume in terms of the profit-to-investment ratio. It was assumed that PPG dispersion only entered the fully flushed areas with only residual oil

rather than the low- and none-flushed areas. After PPG was placed, the permeability of the areas where PPG entered was equal to that of low permeability areas. This assumption is based on the gel property of which gel can reduce permeability to same level (Bai, 1997). The equation to calculate profit-to-investment ratio is as follow:

$$R = \frac{e_3 Q_p + e_4 + e_5 + e_6}{e_1 \Delta Q_o + e_2 \Delta Q_w} \tag{2-2}$$

where e_1 ---oil price, $/t;

e_2 ---produced water treatment cost, $/bbl;

e_3 ---PPG price, $/t;

e_4 ---operation cost for PPG injection, $;

e_5---well service cost due to PPG treatment, $;

e_6 ---well testing costs, $;

Q_p---dry PPG particle cost, $/t;

ΔQ_o---incremental oil, t;

ΔQ_w---decreased oil, t;

R--- profit-to-investment ratio.

PPG Concentration: The designed concentration was based on previous successful field experience and laboratory coreflooding testing results. Field applications and our lab coreflooding results have demonstrated that a large volume of low concentration PPG injection may be the key for the widely successful application of PPG. Before 1999, when the large volume of low concentration PPG treatment was first implemented in Zhongyuan oilfield (Bai, et al, 2007), small volumes of high concentration PPG had been injected in a number of wells but most of them failed. Two reasons come to mind. One reason was realized from the extensive core flooding test results, where it was found that the injection pressure of high concentration PPG particles was much higher than that of low concentration PPG particles. Low concentration particles were much easier to propagate deeply into the reservoir and thus low concentration PPG treatment was not limited to near wellbore (Bai, et al, 2007). The other reason was identified from the field application practices of high concentration PPG treatments. It was found that the wellhead injection pressure oscillated widely through a large range of pressure variances if a high concentration PPG was injected. The water injection pressure after treatments

often did not increase and even reduced sometimes. The unexpected pressure reduction might have resulted from newly-generated hydraulic fractures which were induced by the more fluctuating bottom-hole pressure during PPG injection. Since 1999, almost all PPG treatments in China have used PPG suspensions with concentrations below 5,000 mg/l (ppm).

The average PPG concentration was designed to be in a range of 2,000-3,000 mg/L (2,000-3,000 ppm) with an average of 2,500 mg/L (2,500 ppm). To make PPG transport as deeply into the reservoir as possible, the sizes of injected PPG particles were designed to start from the smallest sizes of 0.06 mm (0.0024 inch), and the actual sizes would be adjusted according to the increase of monitored real-time pressure during PPG injection. For example, a larger size of particle will be used if the injection pressure does not increase as expected during PPG injection. PPG suspension injection rate was designed to be the same as the previous water injection rate of each individual well, to aid in minimizing PPG damage in low-permeability oil zones. The density of swollen PPG particles is higher than that of formation water used to prepare PPG suspension; therefore, PPG could not suspend in formation water very well. We designed the treatment using 200 mg/L (ppm) polymer to carry the PPG particles. Table 2-11 shows the optimized PPG dispersion volume, PPG weight and other designed injection parameters for each treated well.

Pilot Execution:

The pilot site was close to polymer flooding area and it was easy to obtain the polymer solution. A total volume of 56,268 m^3 (1,987,085 ft^3) suspension, which was prepared from a total 132 tons (291,010 lbs) of dry PPG, was injected into the four wells. Compared to initial treatment design, 6 more tons (13,228 lbs) of PPG was injected with an additional suspension volume of 3,939 m^3 (139,104 ft^3). Table 2-12 shows the practical injection parameters and compares them with the initial design. The PPG amount was increased for the wells 7-1937 and 7-1827 because the PPG injection pressure did not increase as expected when the designed amount was injected. The injected PPG suspension volume for the well 9-1827 increased about 2,922 m^3 (103,147 ft^3) because the well was difficult to inject using the designed concentration of 2,000-

3,000 mg/l (ppm) and thus a reduced PPG concentration (1,920 ppm) was used to prevent the injection pressure from becoming too high.

Wells 7-1937 and 7-1827 started to inject PPG in September 5, 2003 and were completed in Jan 10 and Jan 31, 2004, respectively. Both 8-1827 and 9-1827 started in September 26, 2003 and completed in Feb 3, 2004. The real-time pressure was monitored for each well during PPG injection and was used to adjust PPG particle sizes and concentrations. Figures 2-17 to 2-20 show the monitored injection pressure for the four treatments separately. Each well was treated with three to five slugs. The information shown in each figure also includes the dry PPG weight, particle size, PPG suspension volume, swollen PPG volume for each slug. The swollen particle volume refers to the total particle volume after swelling, which is calculated using the swelling ratio of 70 and dry PPG density of 1.8 g/cm^3 (15.0 lb/gal). One slug is distinguished from others in particle sizes. One major advantage of PPG treatment is that PPG injection pressure can be adjusted by particle sizes. If the injection pressure does not reach the target pressure, particle sizes can be adjusted. For the all four treatments, the particle sizes in latter slugs are smaller than those in preceding slugs. This is because we planned to use small particles to make PPG transport as deep as possible, but initial injection pressure increases did not reach our expectation. Thus the particle sizes were gradually increased. As shown in each figure, the injection pressures did not increase very fast nor very much, even though the injected particle sizes were fairly large (up to 0.9 mm (0.035 inch) (wells 8-1827 and 9-1827) or 3 mm (0.118 inch) (wells 7-1937 and 7-1827)). Obviously, there was no any injectivity problem for any of the treatments. In addition, no particles were produced from connected adjacent production wells during PPG injections.

Project Results:

Reservoir Performance after PPG injection: Two methods were used to evaluate the reservoir performance after PPG treatment. One method was to measure the injection profile, which would reflect the plugging effect of PPG on different zones near the wellbore. Another method was to perform a well test, including starting pressure, injection pressure at the same injection flow rate as that before treatment, and pressure drawdown test for pressure index PI(90). These parameters reflect the PPG plugging

slightly farther from the wellbore. The pressure gauge was set at a depth of 500 m (1,640 ft) below the wellhead when drawdown pressure was measured.

Well test results: The pressure drawdown test was performed after PPG treatment. Figures 2-21 to 2-25 show the pressure drawdown test curves before and after treatments for each well. Table 2-13 compared PI(90)s and injection pressures before and after treatments. PI(90)s and injection pressures were significantly increased for each well.

Water injection profiles: The water injection profile was also measured for each well after PPG treatments. Figures 2-25 to 2-28 show the injection profiles for each well before and after PPG treatments. All injection profiles, both inner-layer and inter-layers, were significantly improved after treatments.

Production Performance and Economics: The treatments resulted in increased oil production and decreased water cut. The four treated wells had six center production wells; five of which were effected with an oil increase of 5.8 tons/day (42.5 bbl/day) and an average water cut reduction of 3%, as shown in Table 2-14. Table 2-15 showed the results of 26 comparable wells which connected to treated wells and had no other well services or operations. After treatments, oil production rate increased 34.8 tons/day (255 bbl/day) and water cut reduced 0.94% for the 26 wells at the condition without considering production decline. The accumulative incremental oil is about 15,000 tons (109,950 barrels) until March 2005, which means 51.3 barrels oil increase per 1,000 pounds of PPG injection. The profit-investment ratio can be calculated as follow:

- PPG costs: 291,010 lbs × ($1.04/lb) = $3.03×10^5
- PPG injection costs: 4 wells × ($2.83×10^4/well) = $1.132×10^5
- Injection profile measurement: $1.57×10^4
- Pressure drawdown test: $1.5×10^4
- Total investment: $4.47×10^5
- Oil price: $80/bbl
- Profit from oil sales: 109,950 barrels × ($80/bbl) = $8.8×10^6
- Profit-investment ratio: 19.68

2.4. Conclusions

1. Preformed gels overcome some distinct drawbacks inherent in in-situ gel systems. Millimeter-sized preformed particle gel (PPG) is unique due to its advantages in certain situations over other particle gels.
2. A variety of literature studies show that PPG has been successfully injected into reservoirs both with and without initial fractures, and no significant injectivity problems were found.
3. PPG has been successfully used in reservoirs with different conditions, including high salinities, high temperatures, thick heterogeneous zones, reservoirs with severe sand production, reservoirs with previous polymer flooding, and reservoirs with CO_2 flooding.
4. A detailed study of a large volume PPG treatment showed that:
    - There is no injectivity problem for large volume of mm-size PPG treatment for most wells in mature oilfields. All four wells in the case were successfully injected more than 10,000 m^3 (62,898 barrels) of PPG suspension without abrupt pressure increase.
    - Real-time PPG injection pressure response can be used to adjust PPG particle size concentration to better fit the reservoir. Real-time monitoring data can be used to adjust previous design for better gel treatment results.
    - PPG treatment is a cost-effective method to control conformance. The four treatments successfully resulted in improved oil production, reduced water production, and better injection profile.
    - Simple calculations do not indicate the existence of fractures in these wells, but coreflooding tests indicated there should exist super-high permeability channels otherwise such large amounts of PPG could not be steadily injected into these wells.

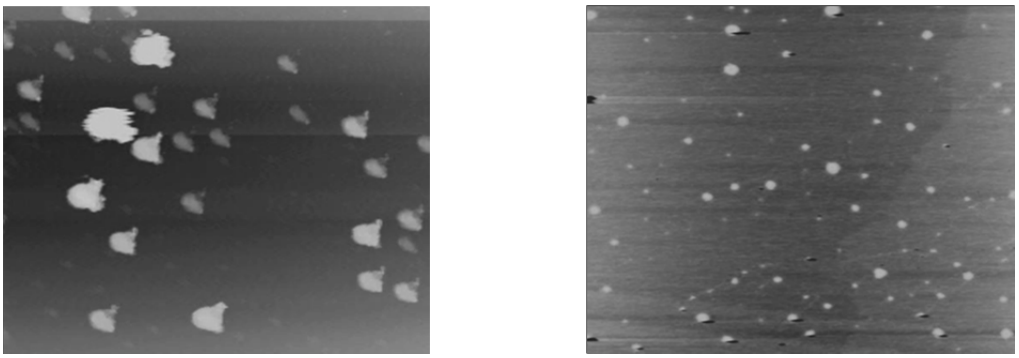

Figure 2-1 Dispersed gel particles from porous media.

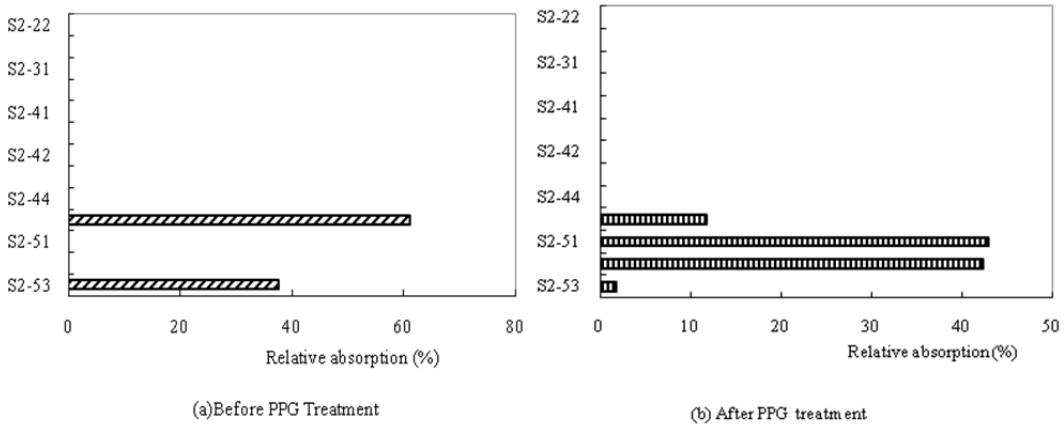

Figure 2-2 Injection profile comparison of well M11-23 before and after PPG treatment.

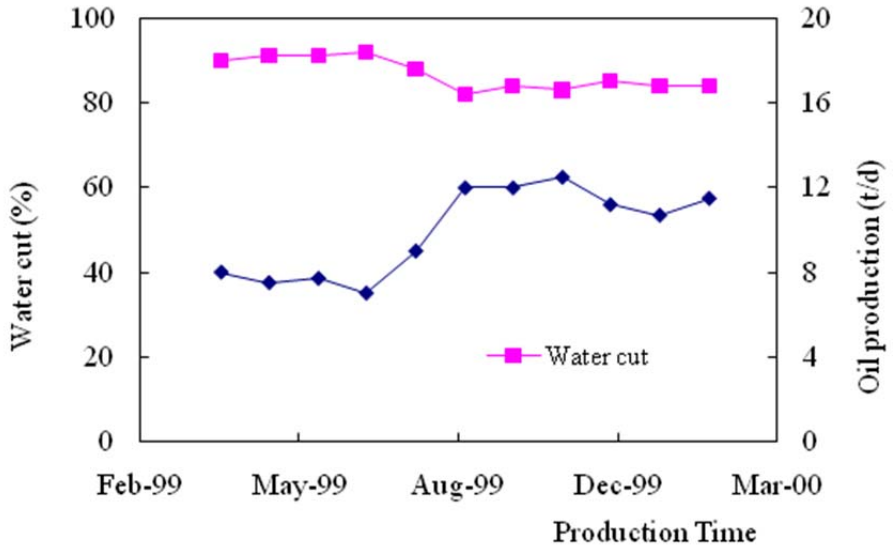

Figure 2-3 Production curve before and after PPG treatment.

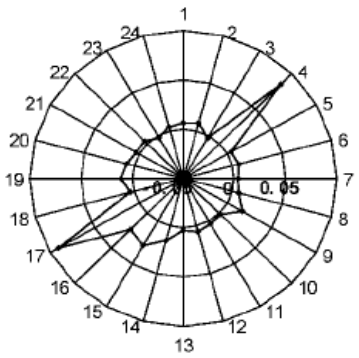

Figure 2-4 Areal heterogeneity of well group.

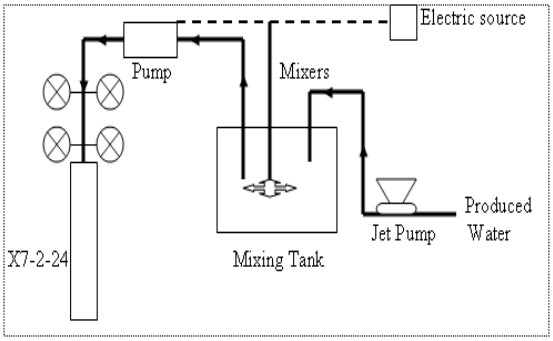

Figure 2-5 Flow chart of PPG injection.

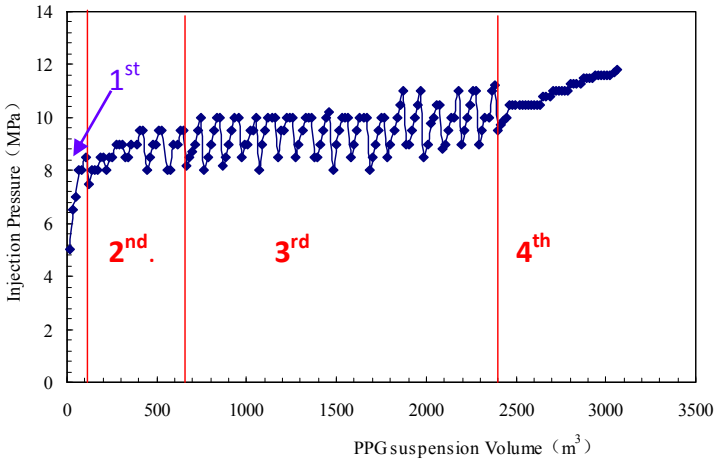

Figure 2-6 Pressure change during PPG suspension injection.
(1 MPa = 145.0377 psi; 1 m = 3.28 ft)

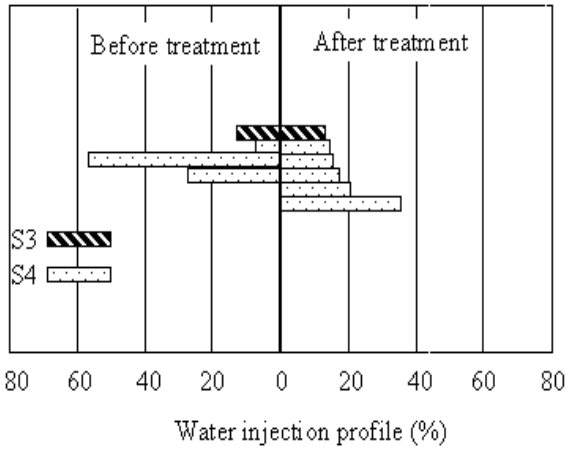

Figure 2-7 Water injection profile of well Bin-24.

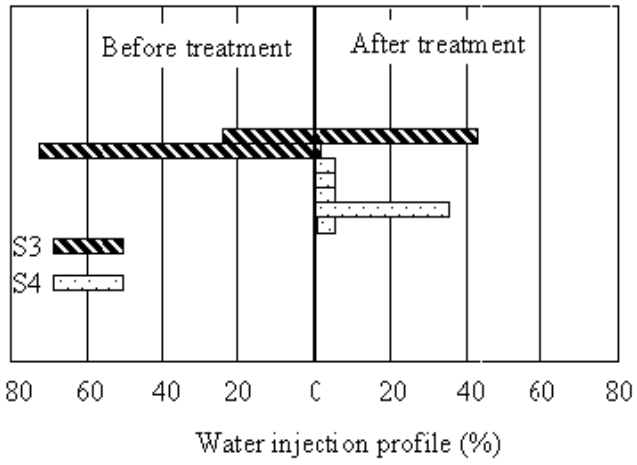

Figure 2-8 Water injection profile of well Bin24-17.

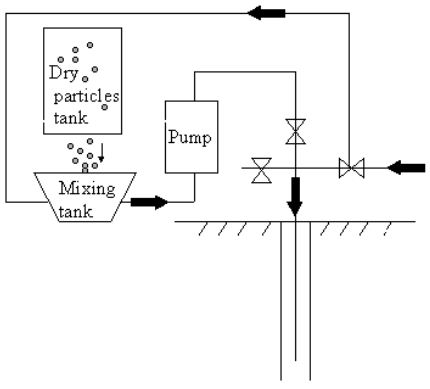

Figure 2-9 Schematic of surface facility for PPG injection.

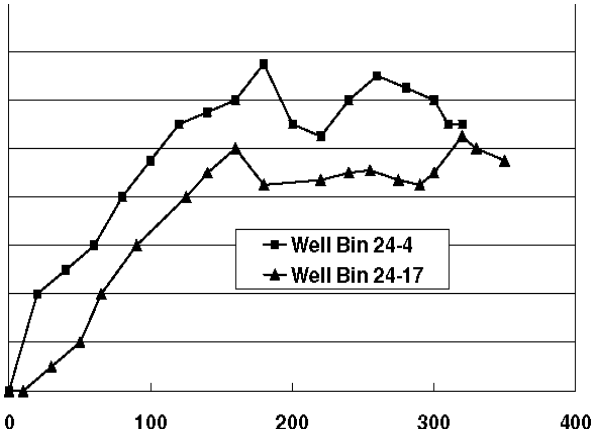

Figure 2-10 Real-time pressure results for PPG injection.

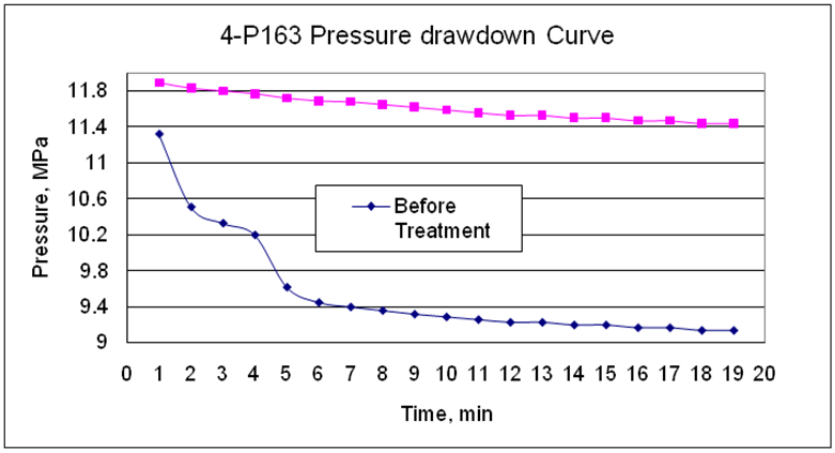

Figure 2-11 Well 4-P163 pressure drawdown comparison before and after treatment.
(1 MPa = 145.0377 psi)

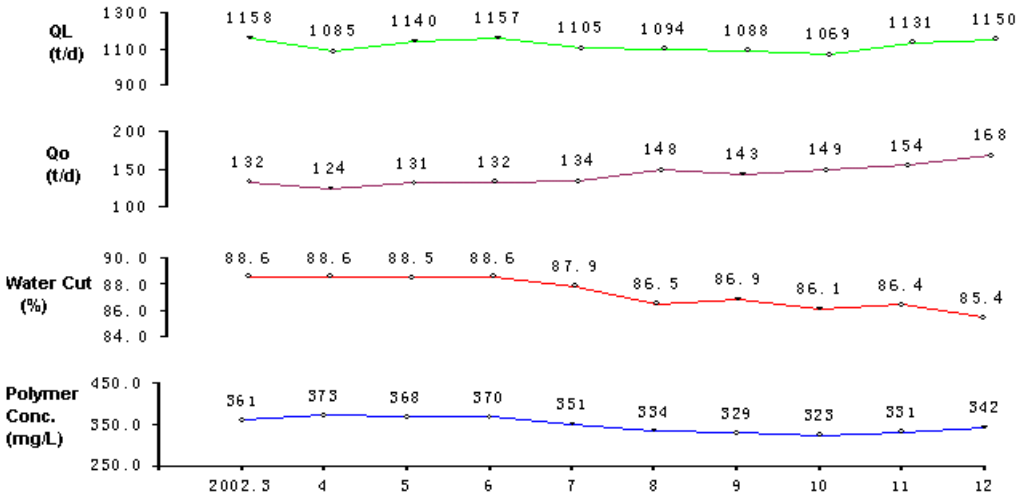

Figure 2-12 Production curves of the production wells connected to the four treated wells.
(1 metric ton = 7.33 barrels)

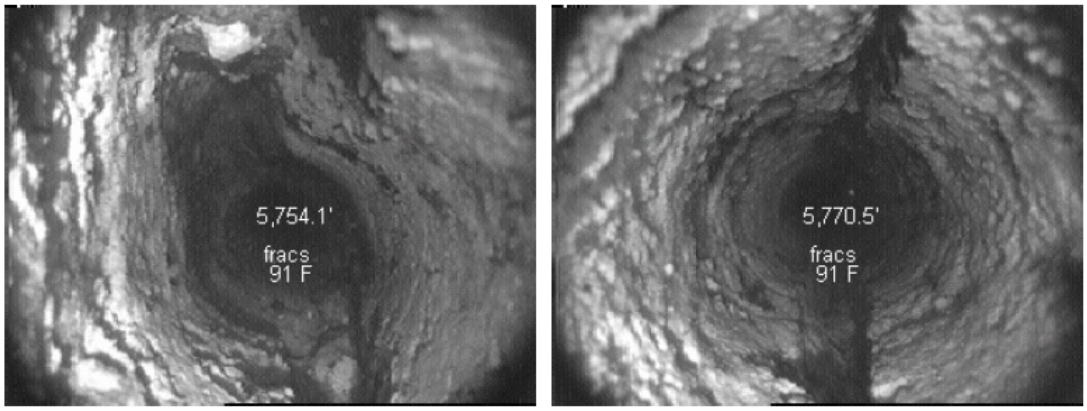

Figure 2-13 Fractures in AICU 63 wellbore (Courtesy, Pyziak and Smith, 2006).

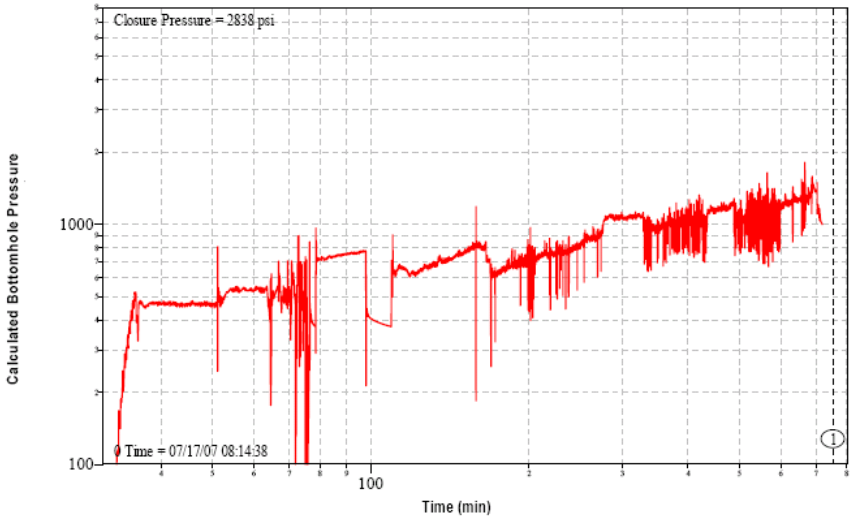

Figure 2-14 Real time pressure monitoring results during particle gel injection for the well AICU63.

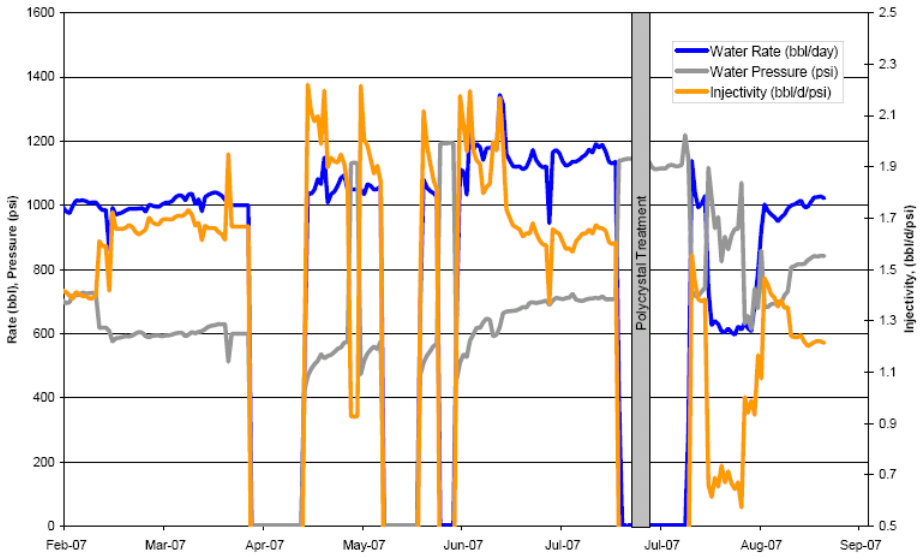

Figure 2-15 The injectivity of AICU 63.

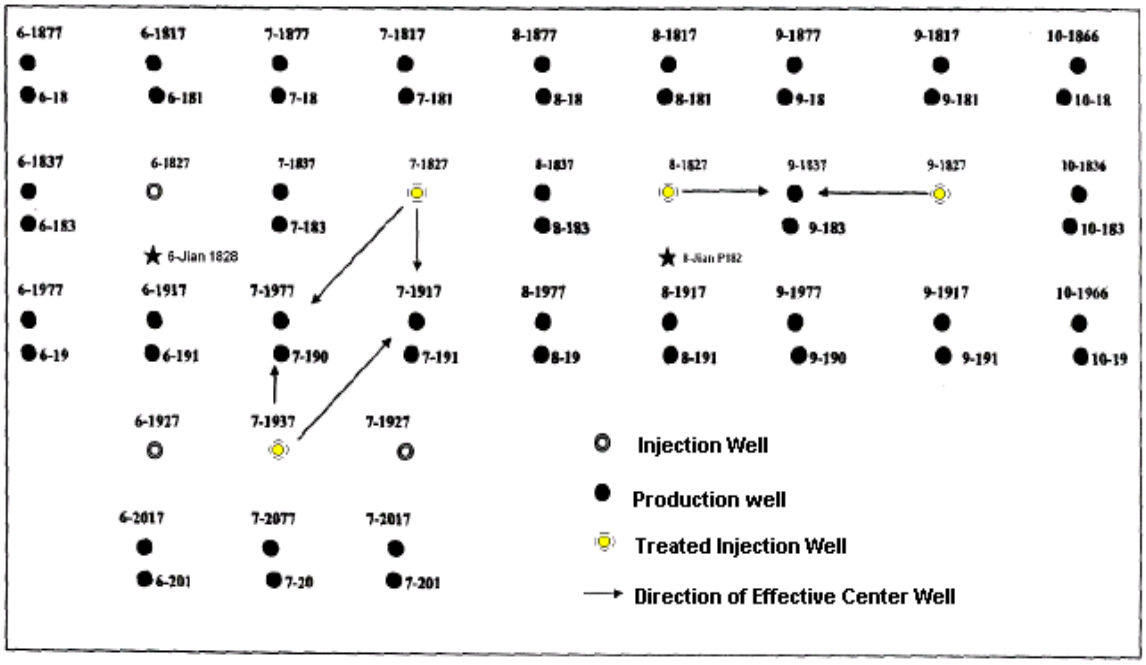

Figure 2-16 Well location map for the PPG treatment pilot.

	1st slug	2nd slug	3rd slug	4th slug	Total
Particle size (mm)	0.16-0.45	0.45-0.90	0.90-2.0	2.0-3.0	0.16-3.0
Dry particle weight (kg)	6,000	25,350	11,300	350	43,000
Swollen particle volume (m^3)	233	986	439	31	1,689
PPG Suspension volume (m^3)	2,261	10,162	3,678	1524	17,625

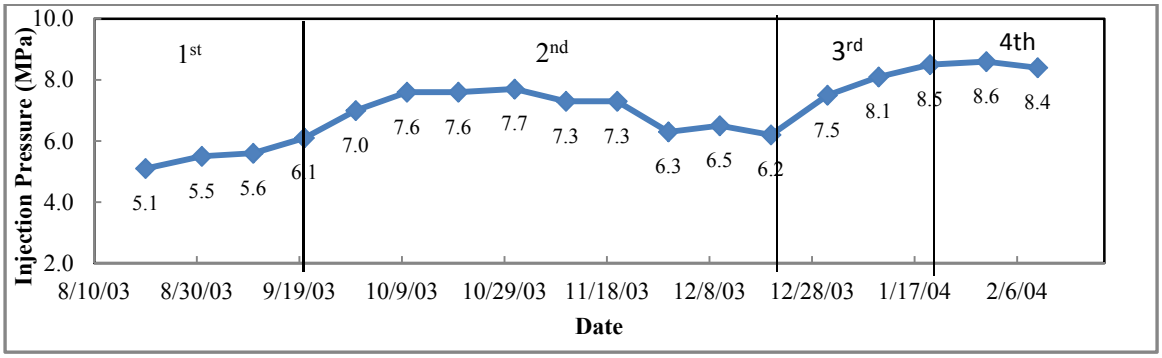

Figure 2-17 PPG injection pressure curve for well 7-1827.
(1 mm = 0.04 inch; 1 kg = 2.2 lbs; 1 m^3 = 8.386 barrels; 1 MPa = 145.0377 psi)

Slug No.	1st	2nd	3rd	4th	5th	Total
Particle size (mm)	0.06-0.16	0.16-0.45	0.45-0.90	0.90-2.0	2.0-3.0	0.06-3.0
Dry particle weight (kg)	2,312	2,925	16,252	7,473	6,038	35,000
Swollen particle volume (m^3)	90	114	632	291	235	1,362
PPG Suspension volume (m^3)	909	1,420	6,877	2,381	1,941	13,528

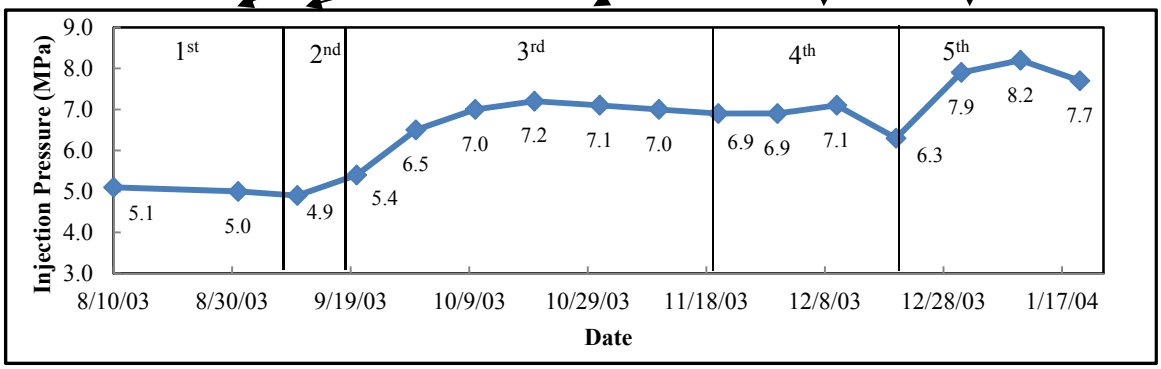

Figure 2-18 PPG injection pressure curve for well 7-1937.
(1 mm = 0.04 inch; 1 kg = 2.2 lbs; 1 m^3 = 8.386 barrels; 1 MPa = 145.0377 psi)

	1st slug	2nd slug	3rd slug	Total
Particle size (mm)	0.06-0.16	0.16-0.45	0.45-0.9	0.06-0.90
Dry particle weight (kg)	19,450	7,850	6,700	34,000
Swollen particle volume (m^3)	756	305	261	1,322
PPG Suspension volume (m^3)	9,447	2,434	1,777	13,528

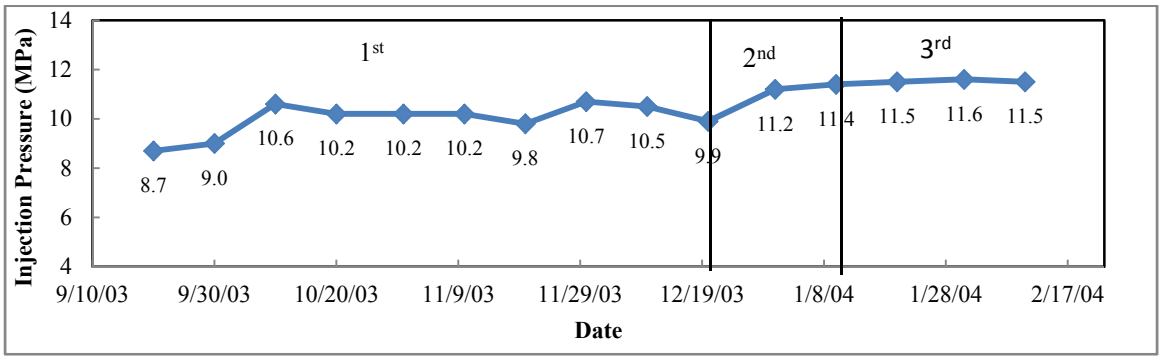

Figure 2-19 PPG injection pressure curve for well 8-1827.
(1 mm = 0.04 inch; 1 kg = 2.2 lbs; 1 m^3 = 8.386 barrels; 1 MPa = 145.0377 psi)

Slug	1st	2nd	3rd	Total
Particle size (mm)	0.06-0.16	0.16-0.45	0.45-0.90	0.06-0.90
Dry particle weight (kg)	10,290	5,710	6,000	22,000
Swollen particle volume (m^3)	400	222	233	855
PPG Suspension volume (m^3)	7,586	1,977	1,895	11,458

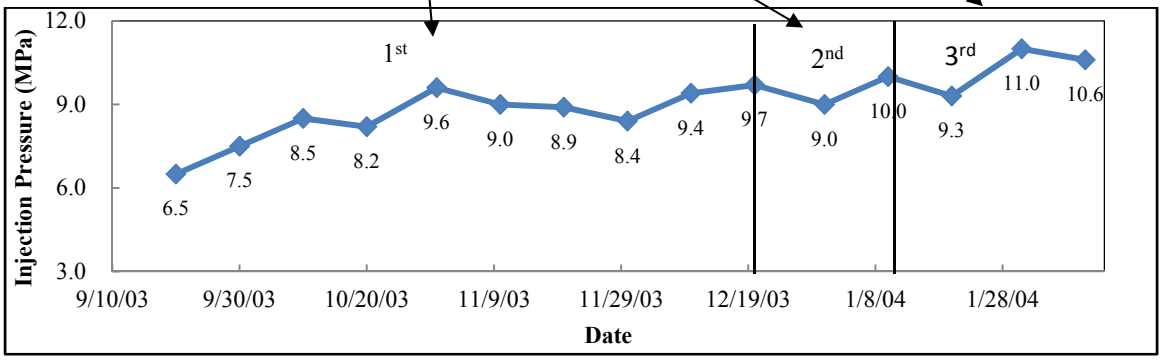

Figure 2-20 PPG injection pressure curve for well 9-1827.
(1 mm = 0.04 inch; 1 kg = 2.2 lbs; 1 m^3 = 8.386 barrels; 1 MPa = 145.0377 psi)

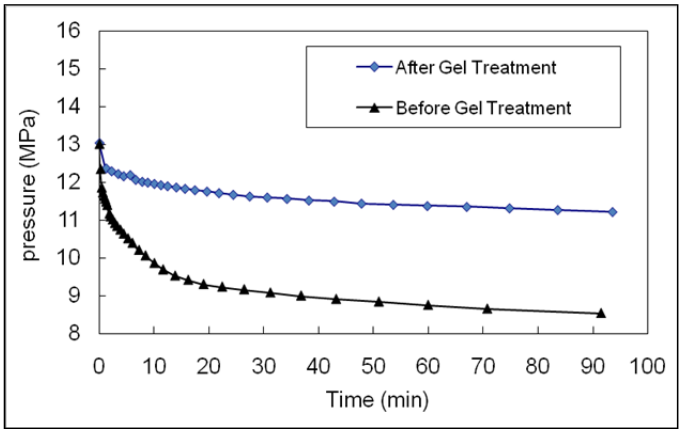

Figure 2-21 pressure drawdown test curve for well 7-1827.
(1 MPa = 145.0377 psi)

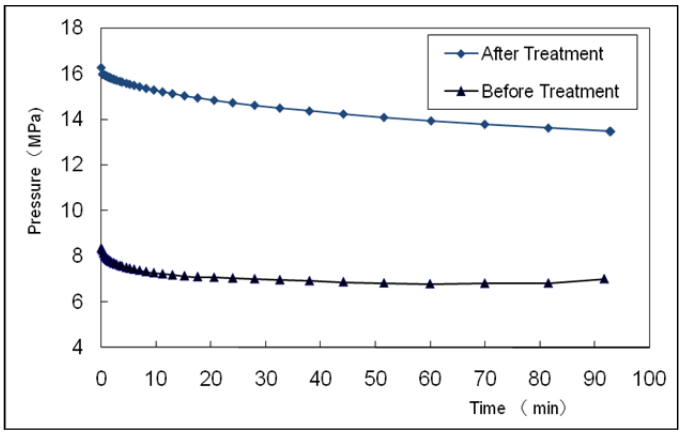

Figure 2-22 Pressure drawdown test curve for well 7-1937.
(1 MPa = 145.0377 psi)

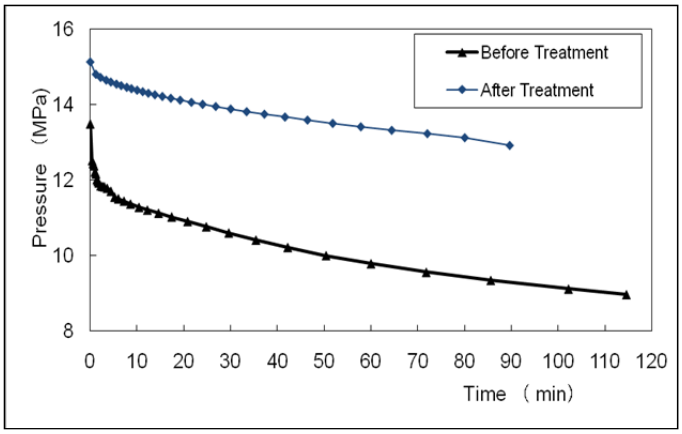

Figure 2-23 Pressure drawdown test curve for well 8-1827.
(1 MPa = 145.0377 psi)

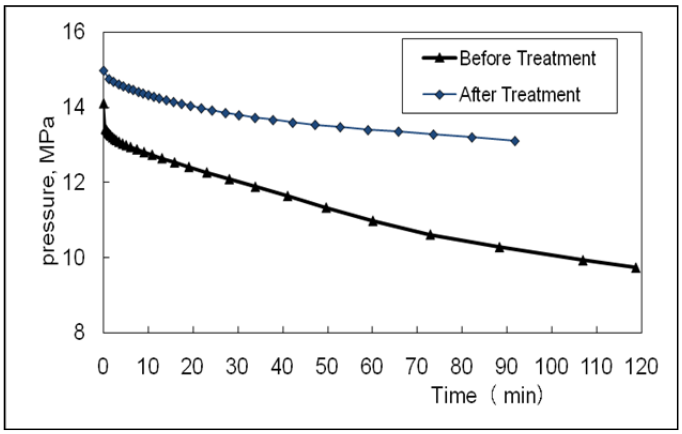

Figure 2-24 Pressure draw-down test curve for well 9-1827.
(1 MPa = 145.0377 psi)

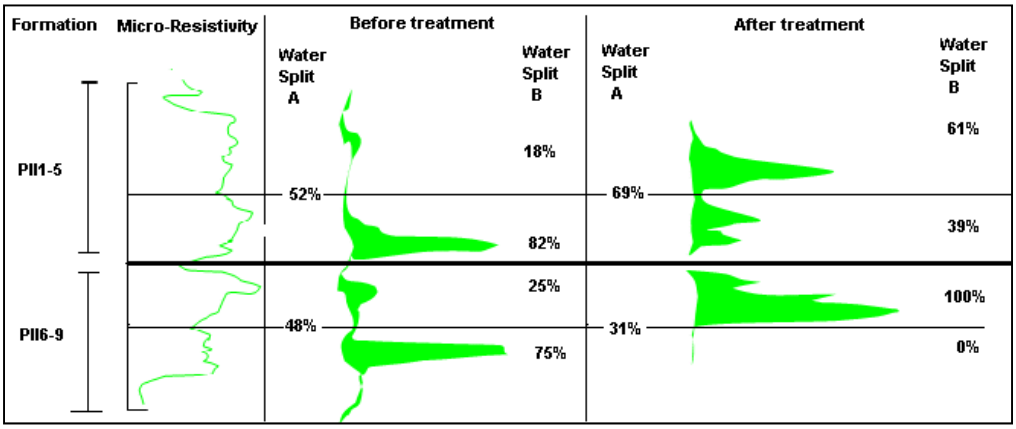

Figure 2-25 Comparison of injection profiles before and after treatment for well 7-1827.

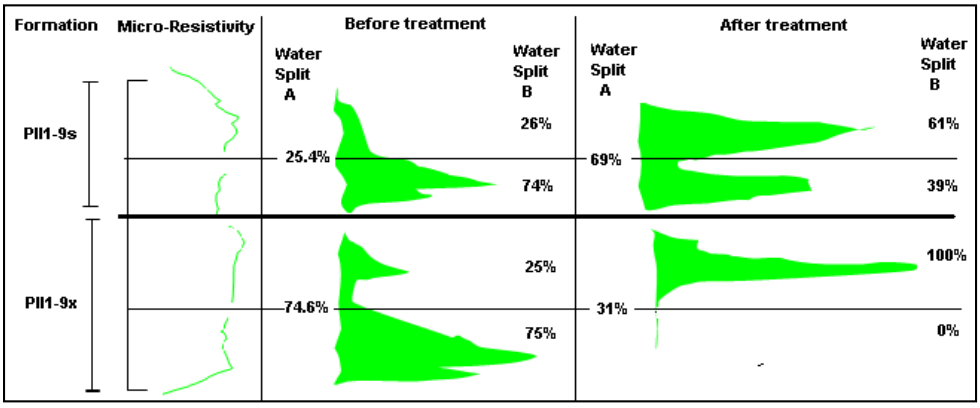

Figure 2-26 Comparison of injection profiles before and after treatment for well 7-1937.

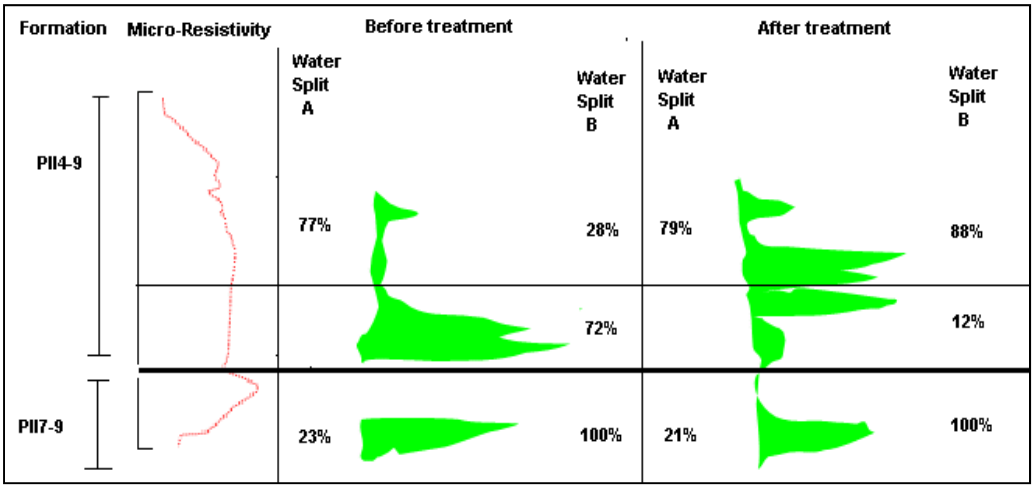

Figure 2-27 Comparison of injection profiles before and after treatment for well 8-1827.

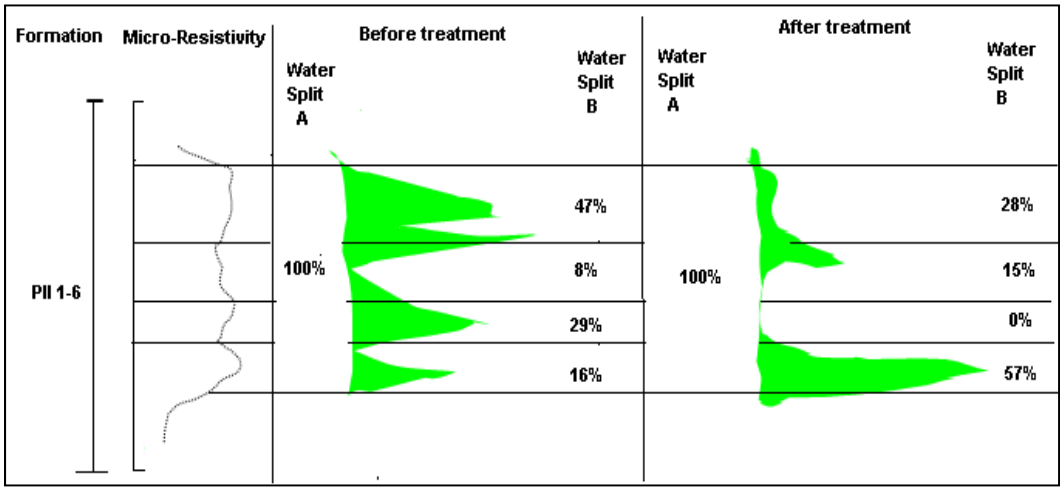

Figure 2-28 Comparison of injection profiles before and after treatment for well 9-1827.

Table 2-1 PPG Injection in Pucheng Oilfield

Well	Treated Time	Total Volume (m^3)	Concentration (mg/L or ppm)
W51-75	July 17-Sept 20, 1999	4,323	3,000
P72	July 17-Sept 20, 1999	2,503	3,000

(1 m^3 = 8.386 barrels)

Table 2-2 PPG Injection in Daqing Oilfield

Stage	PPG Size (mm)	PPG weight (kg)	Volume (m^3)	Concentration (mg/L or ppm)	Injection rate (m^3/d)
1	5.0	1,000	100	1.0	25
2	1.5	3,000	600	0.5	14-16
3	3.0	8,500	1,700	0.5	14-16
4	5.0	3,000	600	0.5	14-16
Total		15,500	3,100		

(1 mm = 0.04 inch; 1 kg = 2.2 lbs; 1 m^3 = 8.386 barrels)

Table 2-3 Parameters of Treated Two Injection Wells

Well	Depth (m)	Injecting since	Total injection interval (m)	Number of injection layers
Bin 24-4	1465	12/05/90	14.6	7
Bin 24-17	1532	3/1193	15.9	5

(1 m = 3.28 ft)

Table 2-4 Offset Production Wells of Bin24-4

Producer	Produced fluids (t/d)	Produced oil (t/d)	Water-cut (%)
B24-1	193.0	10.3	94.7
B24-3	67.7	2.3	95.8
B24-10	130.0	7.0	94.6
B24-2	53.2	8.4	84.3
B24-5	24.4	3.7	84.8

(1 metric ton = 7.33 barrels)

Table 2-5 Offset Production Wells for Bin-17

Producer	Produced fluids (t/d)	Produced oil (t/d)	Water-cut (%)
B24-9	29.7	2.8	90.4
B259	37.9	2.8	92.7
B24-15	72.1	6.2	91.4
B24-14	15.1	4.1	76.1

(1 metric ton = 7.33 barrels)

Table 2-6 Designed Parameters for both Treatments

Well	Particle size (mesh)	Particle concentration (%weight)	Injection pressure (MPa)	Treatment duration (min)
Bin 24-4	20-40	5~10	13	320
Bin 24-17	20-40	5~10	10	350

(1 MPa = 145.0377 psi)

Table 2-7 Production Results 8 Months after PPG Treatments

Producer Well	Produced fluids(t)	Produced oil (t)	Water-cut (%)	Total incremental oil (t)
B24-3	45.4	2.5	94.4	731
B24-10	167	10.3	93.8	728
B24-9	30.4	3.3	89.2	210
B24-15	107	11.2	89.6	1138
B24-14	8.6	3.9	54	62
Total	358.4	31.2		2278

(1 metric ton = 7.33 barrels)

Table 2-8 Comparison of Injection Pressure Comparion before and after PPG Treatment

Well No	PPG Suspension Volume (m^3)	Dry PPG Weight (t)	Before treatment		After treatment	
			Injection rate (m^3/d)	Injection pressure (MPa)	Injection Rate (m^3/d)	Injection Pressure (MPa)
4-P163	4400	23	200	11.0	200	11.9
6- P 173	4800	28	150	12.5	150	12.9
5- P 162	4600	24	200	12.4	200	13.1
8- P 122	4600	24	130	14.6	130	14.9

(1 m^3 = 8.386 barrels; 1 metric ton = 7.33 barrels; 1 MPa = 145.0377 psi)

Table 2-9 Parameters of the Four Treated Wells before PPG Injection

Well Name	Objective Zones	Gross Thickness (m)	Net pay Thickness (m)	Kmax (darcy)	Starting Pressure (MPa)	Injection Pressure (MPa)	Injection Rate (m^3)	Main water-absorbing zones		PI(90) (MPa)
								Thickness (%)	Absorbed Water (%)	
8-1827	PII 4-7	7.6	7.4	0.28	6.0	11.2	79	27.78	78.21	10.31
	PII 7-9	1.6	1.6	0.22	5.7	11.2	43	46.00	79.51	10.31
9-1827	PII 1-6	8.0	7.5	0.24	8.5	10.7	63	45.45	74.07	11.58
7-1827	PII 1-6	7.4	6.7	0.50	4.5	10.0	58	14.49	81.97	10.80
	PII 5-9	5.2	4.3	0.36	5.0	10.0	60	17.78	89.29	10.80
7-1937	PII 1-9u	10.8	10.5	0.46	1.0	11.5	56	28.57	56.96	6.95
	PII 1-9d				1.5	11.5	47			6.95

(1 m = 3.28 ft; 1 m^3 = 8.386 barrels; 1 MPa = 145.0377 psi)

Table 2-10 Evaluation Results for Six PPG Samples

No.	PPG Product Name	Particle Size (mm)	Swelling Ratio		Pressure Resistance (MPa)	Breakthrough Pressure (MPa/m)
			Initial (T=10 min)	Final (T=1 day)		
1	GS	3-5	5	117	Very weak	4.1
2	GS	2-3	15	153		
3	WT	3-5	10	83	1.2	10.7
4	WT	2-3	22	90	0.8	
5	SAP	3-5	3	17	2.3	17.9
6	SAP	2-3	5	31	1.9	

(1 mm = 0.04 inch; 1 MPa = 145.0377 psi)

Table 2-11 Designed Injection Parameters for Four Well PPG Treatments

Well Name	Water Injection before treatment (m^3/d)	Injection Rate (m^3/d)	PPG Weight (kg)	Particle size (mm)	PPG Suspension Volume (m^3)	Concentration (ppm)	Maximum Pressure limitation (MPa)
7-1937	116	130	32,000	0.06 – 2.00	13,445	2,000-3,000	12.5
7-1827	108	128	41,000	0.06 – 2.00	17,135	2,000-3,000	13.0
8-1827	121	133	32,000	0.06 – 0.90	13,214	2,000-3,000	14.0
9-1827	83	138	21,000	0.06 – 0.90	8,536	2,000-3,000	14.0

(1 m^3 = 8.386 barrels; 1 kg = 2.2 lbs; 1 mm = 0.04 inch; 1 MPa = 145.0377 psi)

Table 2-12 Comparison of Designed and Practical Injection Parameters

Well Name	Practical Injection			Difference from Designed Parameters	
	Dry PPG Weight (t)	PPG Suspension Volume (t)	PPG Concentration (ppm)	Dry PPG weight (t)	PPG Suspension Volume (m^3)
7-1937	35	13528	2587	3	83
7-1827	43	17625	2440	2	490
8-1827	32	13658	2343	0	444
9-1827	22	11458	1920	1	2922
Total	132	56269	2346	6	3939

(1 metric ton = 2204.62 lbs; 1 metric ton = 7.33 barrels; 1 m^3 = 8.386 barrels)

Table 2-13 Pressure Test Result after PPG Treatment

Well Name	Before PPG Injection		After PPG Treatment		Difference	
	PI(90) (MPa)	Injection Pressure (MPa)	PI(90) (MPa)	Injection Pressure (MPa)	PI(90) (MPa)	Injection Pressure (MPa)
7-1937	6.95	5.0	10.49	8.2	3.54	3.2
7-1827	9.12	5.7	11.58	8.4	2.46	2.7
8-1827	10.98	8.8	13.72	11.5	2.74	2.7
9-1827	11.12	6.5	13.71	10.6	2.59	4.1

(1 MPa = 145.0377 psi)

Table 2-14 Production Performance Comparison of Center Wells

Type	Well No.	Before Treatment			After treatment			Comparison		
		Q_L (t/d)	Q_o (t/d)	f_w (%)	Q_L (t/d)	Q_o (t/d)	f_w (%)	Q_L (t/d)	Q_o (t/d)	f_w (%)
Effective wells	8-1817	69	3	95.7	56	4.2	92.6	-13	1.2	-3.1
	9-1817	33	1	97.0	33	2.5	92.5	0	1.5	-4.5
	7-1977	42	1	97.4	35	2	94.6	-7	1	-2.8
	7-2017	73	3	96.3	71	5	93.0	-2	2	-3.3
	7-1917	50	3	94.0	34	2.4	93.0	-16	-0.6	-1.0
	Sub-total	267	11	96.0	229	16.1	93.0	-38	5.1	-3.0
Ineffective well	9-1837	53	3	94.9	57	2.7	95.5	4	-0.3	0.6
Total		320	14	95.6	286	18.8	93.4	-34	4.8	-2.2

(1 metric ton = 7.33 barrels)

Table 2-15 Performance Comparison of 26 Connected Production Well without other Operation

Well type	Producer Number	Before PPG Treatments			After PPG treatment (Aug, 2004)			Difference		
		Q_L (t/d)	Q_o (t/d)	f_w (%)	Q_L (t/d)	Q_o (t/d)	f_w (%)	Q_L (t/d)	Q_o (t/d)	f_w (%)
Wells only produced from PII	11	604	26	95.7	563	32.8	94.2	-41	6.8	-1.52
Commingle Wells	15	3717	161	95.7	3644	189	94.8	-73	28	-0.86
Total	26	4321	187	95.7	4207	221.8	94.7	-114	34.8	-0.94

(1 metric ton = 7.33 barrels)

3. Screen Experiments

3.1. Summary

This research included a series of experiments using screen models to evaluate the strength of swollen gel particles and to study the effect of the particle gel swelling ratio (depending on brine concentration), flow rate; and mesh size on the gel injection pressure and injectivity. The results show that gel injection pressure depends primarily on the swelling ratio and the mesh size. However, the injection pressure does not increase significantly with injection rates, behavior consistent with the real-time injection pressure and injection rate change observed during practical gel treatments in oilfields. These gel particles injection behaviors are completely different from conventional hard particles in that they are elastic and deformable during extrusion.

3.2. Introduction

The strength of swollen gel particles is commonly assessed qualitatively based on visual and tactile evaluation (Riccardo, 1994). The strength of a swollen particle can be determined by pressing the particles between the fingers (Ramazani-Harandi et al., 2006). They have a geometrically stable shape with sharp edges and corners (i.e., they are not soft, loose, or slimy). However, only an experienced person can discern the difference between samples. Several methods have been proposed to evaluate particle gel strength quantitatively. For instance, Riccardo (1994) proposed that gel strength be measured based on the maximum diameter of a steel ball able to settle through the swollen gel. The stronger the gel, the larger and heavier the steel ball required to settle to the bottom. Smith (1989) developed a screen model to quantify the gel strength of weak bulk gel using screen packs of 100 mesh size. However, for most commercial SAPs, which are small, sugar-like particles with irregular shapes, these methods are impractical. Thus a fast and effective method is needed to quantitatively evaluate the strength of swollen gel particles. The method mentioned in this chapter uses an apparatus designed to withstand high pressures of PPG injection to evaluate gel strength of particle gel.

The properties of specific superabsorbent polymers (SAPs) are extremely important for selecting a material for a given application, and they are highly dependent on the environmental swelling conditions. It is imperative that SAPs properties be

determined precisely under conditions that are as realistic as possible. In the experiments described here, the SAPs were allowed to swell to their maximum capacity in four concentrations of brine solution. They were then subjected to pressure in an apparatus using screens of various sizes. This chapter included a series of experiments using screen models to evaluate the strength of swollen gel particles and to study the effect of the particle gel swelling ratio (depending on brine concentration), flow rate, and mesh size on the gel injection pressure and injectivity.

3.3. Screen Model

A screen model is a long acrylic tube to which end plates are attached by two flanges using steel rods and nuts, as shown in Figures 3-1 and 3-2. The top flange has one hole connected to an ISCO pump through tubing and fitting. The bottom flange has multiple holes that allow PPG particles to flow through without the addition of extra pressure. A piston is inserted into the acrylic tube to prevent direct contact of injected water with PPG particles. Screens of various mesh sizes are placed between the gel particles and the bottom flange. The pressure from the pumped water pushes the piston, which forces the swollen PPG to pass through the wire cloth mesh at the end of tube. This model can work well under 700 psi pressure.

3.4. Experiment Materials

3.4.1. Preformed Particle Gels

A commercial SAP LiquiBlock 40K, supplied by Emerging Technologies Inc was selected as the Preformed Particle Gel (PPG) for these experiments. The main components of the PPG is potassium salt of cross-linked polyacrylic acid polyacrylamide co-polymer. Before swelling, PPG is a dry, white, granular powder. In aqueous solutions, it can absorb a large amount of water. The concentration of sodium chloride in water affect on the water absorbency. In deionized and distilled water, SAP may absorb 500 times its weight (from 30-60 times its volume), but when placed in a 0.9% saline solution, the absorbency drops to about 50 times its weight. Figures 3-3 and 3-4 show the PPG before and after swelling. Table 3-1 lists the typical characteristics of PPG, and Table 3-2 shows the size distribution of PPG as determined by a sieving test.

3.4.2. Brine

Based on the significant differences in their swelling ratios, four concentrations of sodium chloride were selected to prepare the swollen PPG: 0.05, 0.25, 1 and 10 wt %.

3.4.3. Screens

Stainless wire cloths of three different sizes were chosen: 150, 80, and 40 mesh, with 0.1041 mm (0.0041 inch), 0.1524 mm (0.006 inch), and 0.3048 mm (0.012 inch) diameter openings, respectively. Table 3-3 shows the screen parameters. The various screen sizes may represent different permeability channels or pore throats in reservoir formation. The wire cloth was cut into small circles for placement in the apparatus as described above.

3.5. Summary of Experiments

Table 3-4 summarizes the parameters of 12 experiments conducted to study the effect of brine concentration used to prepare the swollen gel particles, injection rate, and mesh size on the PPG injection pressure using various screens.

3.6. Equipment and PPG Sample Preparation

3.6.1. Equipment

The equipment used to perform these experiments included:

• Two caps made of fiber glass and attached to the pump, one with a single hole to allow water to flow into the tube, and the other with tiny holes of equal sizes distributed evenly over its surface.

• A transparent acrylic tube able to withstand a maximum pressure of 700 psi.

• A piston made of a solid block of transparent acrylic material, with a hole in the middle allowing it to be easily placed inside the acrylic tube.

• Four metal rods are used, for placing the tube with piston, top and bottom caps and tightening them.

• Nuts and washers to tighten the apparatus.

• A Teledyne ISCO Model 500D syringe pump.

• Wire cloth screens of 150, 80, and 40 mesh size.

3.6.2. PPG Sample Preparation

The PPG used in these experiments was prepared as follows unless otherwise indicated:

• An empty beaker was filled with a brine solution of the desired concentration to prepare the PPG.

• Depending on the concentration of brine used to prepare the PPG, 10-20 grams (0.35-0.70 oz) of the SAP was slowly added to the brine solution.

• The sample was allowed to swell completely, a process that required 2 to 3 hours.

• The excess brine solution was separated from the swollen PPG by allowing it to sit on the 150 Mesh.

• The PPG was then collected from the mesh and stored.

• The weight of the gel sample was measured after the removal of water.

3.7. Experiment Setup and Procedure

3.7.1. Experimental Setup

Once the swollen PPG sample was prepared with brine of the desired concentration; the apparatus was setup, as shown in figure 3-5:

• The piston was inserted into the top of the transparent acrylic tube. The tube was then packed with PPG sample of the desired brine concentration.

• A screen was placed above the holes in the bottom cap.

• Using the metal rods, the packed tube was then set on the bottom cap; and the top cap was placed on top of the transparent acrylic cylinder with the piston at the top.

• The apparatus was then tightly secured using washers and nuts.

• A pressure gauge was connected at the bottom of the transparent acrylic tube to monitor pressure changes with respect to the injection rate.

• Any air gaps in the outlet line of the ISCO pump were eliminated, and the line was connected to the top cap of the apparatus and tightened to prevent leaks.

3.7.2. Experimental Procedure

The experimental procedure was as follows:

• Gas between the piston and the top cap was released, and the gap was filled with distilled water to avoid a two phase medium.

• The pump was run at a constant injection rate of 1 ml/min (3.66 $in.^3$/hr).

• The pump pressure was observed constantly for a pressure drop to detect the movement of piston.

• The pressure noted is the minimum required pressure to move the piston.

• The pump was run at a constant injection flow rate of 0.1 ml/min (0.366 $in.^3$/hr) and the pressure response was monitored in the gauge connected to the bottom of the acrylic cylinder.

• If there was no gel or brine discharge from the apparatus, the injection flow rate was increased to 0.2 ml/min (0.732 $in.^3$/hr).

• If there was any discharge of gel after increasing the injection rate, the discharge flow rate was calculated by measuring the volume of gel collected over a specific period of time, depending on flow rate.

• For each particular injection flow rate, the pressure was monitored and when a stable pressure was observed it is noted as the constant pressure at that particular injection rate.

• The process was repeated for multiple injection flow rates, and the stable pressures for each of them are noted.

• The procedure was repeated until the pressure difference was negligible even when the increase in injection rate was significant.

The above procedure was repeated for each screen and each brine concentration, and pressure was plotted against the injection flow rate.

3.8. Results and Discussion

3.8.1. PPG Swelling Kinetics and Effect of Sodium Chloride Concentration on Swelling Capacity

The swelling ratio is defined as the ratio of the PPG particle volume before swelling to its volume after swelling. It was evaluated as a function of brine concentration. Figure 3-6 shows the change in PPG swelling ratio over time at various brine concentrations. The PPG particles swelled very fast, and the maximum swelling ratio was reached within 60 minutes for each sample. The final PPG swelling ratio depended on the brine concentration; the higher the concentration, the smaller swelling ratio, as shown in Figure 3-7. The relationship between swelling ratio and brine concentration can be fitted well using the following power equation with a R^2 of 0.96:

$$R = 65.535 \times C^{-0.296} \quad (3\text{-}1)$$

where R is the swelling ratio and C is the brine concentration in percent. Figures 3-8 through 3-10 show the particle size pictures for the original PPG particles prepared with 0.05, 0.25, and 1% brine concentration. They demonstrate that the average particle size of the swollen particles decreased as the brine concentration increased.

3.8.2. Effect of Brine Concentration on Injection Pressure of PPG

Figures 3-11 through 3-13 show the effect of brine concentration of the PPG on the PPG injection pressure for each of three screens. They indicate that at a constant injection flow rate, injection pressure increases with brine concentration. For example, at an injection rate of 0.2 ml/min (0.732 $in.^3$/hr), the injection pressures for PPG prepared with 0.05, 0.25, 1, and 10 wt% brine were 41, 70, 120, and 210 psi respectively for the 150 mesh screen model shown in Figure 3-11. The injection pressure for the sample prepared with a low brine concentration was expected to be higher than the sample prepared with a high brine concentration because the swollen particle size is larger at low brine concentrations than that at high brine concentrations. However, the experimental results showed a completely different trend: Swollen particles in a low concentration brine proved to be softer and more deformable than those in a high brine concentration. Therefore, despite their greater size the PPG swollen in low concentration brine showed higher injectivity.

3.8.3. Effect of Injection Flow Rate on Injection Pressure of PPG

Figures 3-11 through 3-13 also indicate that the injection pressure increased with the injection flow rate for all brine concentrations; however, this increase was not linear. The injection pressure increased only slightly at higher injection flow rates. For example, for PPG swollen in 10% brine concentration, the pressure increased by only 10 psi from 250 to 260 psi when the injection flow rate was doubled from 1.16 to 2.2 ml/min (4.247 to 8.055 $in.^3$/hr). This trend is consistent with those observed for practical PPG injection in oilfields.

3.8.4. Effect of Mesh Size on Injection Pressure of PPG

Three screens were chosen with mesh sizes of 150, 80, and 40. The variations in the open hole size of screens were intended to represent the pore sizes or fracture width in a channeled formation. Figure 3-14 through 3-17 show the effect of mesh size on PPG injection pressure for each swollen PPG sample. They indicate that the injection pressure

increased as the mesh size decreased. For example, with a constant injection flow rate of 0.1 ml/min (0.366 $in.^3$/hr) and a PPG sample prepared with 0.05% (figure 3-14), the PPG injection pressures for mesh sizes of 150, 80, and 40 were 32, 22, and 9 psi respectively.

3.8.5. Effect of Repacking on Injection Pressure of PPG

These experiments sought to determine whether the swollen PPG particles passed through the screen by elongating and deforming temporarily or by particle size change. This would be indicated by the change in injection pressure with respect to the injection flow rate when the PPG initially passed through the screen and when the PPG particles are repacked and passed through the screen again. The procedures followed in these experiments were similar to those described above. For each experiment the effluent PPG from the initial packing was repacked into the apparatus with the same screen and the experiment was repeated. The repacking experiments used PPG samples prepared with 0.05 and 1% brine, each tested with 150, 80, and 40 mesh screens.

3.8.5.1 150, 80 and 40 Mesh with 0.05% Brine Concentration PPG

Figures 3-18 through 3-20 show the effect of repacking on the injection pressure for each mesh size with PPG prepared in 0.05% brine concentration. Figure 3-18, indicates that the injection pressure of the repack 1 was much less than half of the original injection pressure at the same injection flow rate, suggesting that the PPG particles may have deformed and changed shape permanently on the initial pass. At lower injection rates, the injection pressure was almost the same for the first and second repacks. At higher injection rates, however the injection pressure was lower for repack 2 than for repack 1. For example, at an injection flow rate of 0.2 ml/min (0.732 $in.^3$/hr), the injection pressures for initial pass, repack 1, and repack 2 were 41, 8, and 8 psi respectively. Figure 3-19, indicates that for repack 1 and repack 2, the injection pressures were less than half that recorded during the initial pass at the same injection flow rate, suggesting that the PPG particles were permanently deformed, during the initial pass. The injection pressures for repack 1 and 2 were almost same. For example, at an injection flow rate of 0.2 ml/min (0.732 $in.^3$/hr), the injection pressures for initial pass, repack 1, and repack 2 were 29, 7, and 6.5 psi respectively. Figure 3-20 shows that the injection pressures for repack 1 and 2 were same. The injection pressure during the initial pass was more than three times the injection pressure for repack 1. For example, at an injection

flow rate of 0.2 ml/min (0.732 $in.^3$/hr), the injection pressures for initial pass, repack 1 and repack 2 are 10, 3, and 2 psi respectively.

Figures 3-21 through 3-26 show the particle size pictures for the PPG prepared with 0.05% brine concentration in each mesh for initial pass and repack 1. Compared to the original particle size of PPG swollen in 0.05% brine concentration in figure 3-8, the particles in Figures 3-21 and 3-22 appeared to be elongated and permanently deformed in shape. This could be because of the high swelling ratio of PPG in lower concentrations of brine. Figures 3-23 and 3-24 show the PPG particles passed through 80 mesh screen. As in the previous case the particle appeared to be elongated under pressure to pass through the 80 mesh. However, there was not much visible difference between particle from initial pass and repack 1. Figures 3-25 and 3-26 show the PPG passed through 40 mesh screen. Unlike the particles passed through 150 and 80 mesh, these particles appeared to be cut and in shape in order to pass through the 40 mesh. As the mesh size increased, the PPG particles were cut during passage through the mesh, but at the finer mesh size (150 mesh) they were elongated and deformed in shape during passage through the screen.

3.8.5.2 150, 80, and 40 Mesh with 1% Brine Concentration PPG

Figures 3-27 through 3-29 show the effect of repacking on the injection pressure for each mesh size with PPG prepared in 1% brine concentration. Figure 3-27 indicates that the injection pressure for repack 2 was lower than that for repack 1 at the same injection rate, demonstrating that the particles were permanently deformed and cut in both the initial pass and repack 1 and thus clearly showing that the PPG prepared with brine concentration of 1% had greater gel strength than that prepared with the 0.05% brine solution. For an injection rate of 0.2 ml/min (0.732 $in.^3$/hr), for initial pass, repack 1, and repack 2 of the PPG prepared with 1% brine concentration, the injection pressures were 120, 70, and 45 psi respectively. Figure 3-28 shows that the injection pressure for repack 2 was almost the same as that for repack 1 at the same injection rate. The injection pressures for the repack 1 and 2 were much less than the injection pressure during the initial pass. For an injection rate of 0.3 ml/min (1.098 $in.^3$/hr) and PPG prepared with 1% brine concentration, the injection pressures for the initial pass, repack 1, and repack 2 were 90, 25, and 25 psi respectively. Figure 3-29 indicates the same trend as in previous case, the injection pressure for repack 2 was less than that for repack 1 at the same

injection rate, suggesting that the particles were permanently deformed during both the initial pass and repack 1. At an injection flow rate of 0.1 ml/min (0.366 $in.^3$/hr) and the PPG prepared with 1% brine concentration, the injection pressures for initial pass, repack 1, and repack 2 were 35, 10, and 6 psi respectively.

Figures 3-30 through 3-35 show the particle size pictures for PPG prepared in 1% brine concentration passed through 150, 80, and 40 mesh. Figures 3-30 and 3-31 show that the particles appeared to be cut and permanently deformed during the passing through the 150 mesh. Figures 3-32 through 3-35 show that the PPG particles were cut and deformed in shape during the passing through the 80 and 40 mesh. As the brine concentration of the PPG increases the particles appeared to be cut to pass through the mesh under pressure. This clearly shows that the PPG prepared in higher brine concentration has greater gel strength than the PPG in lower concentrations of brine.

3.8.6. Effect of Brine Concentration on PPG Injectivity

Figures 3-36 through 3-38 show the effect of brine concentration on PPG injectivity through each of all the three meshes. They indicate that, at a constant injection flow rate, PPG injectivity decreased with increase in brine concentration. For example, at an injection rate of 0.2 ml/min (0.732 $in.^3$/hr), the injectivity for PPG prepared with 0.05, 0.25, 1 and 10% brine were 0.0048, 0.0028, 0.0017 and 0.00095 respectively for the 150 mesh screen model shown in Figure 3-36. PPG injectivity had been expected to increase as the brine concentration of the PPG increased because the swollen particles are larger at low brine concentrations than at high brine concentrations. However, the experimental results show a completely different trend, indicating that gel strength and the softness or deformability of swollen particles influence PPG injectivity more than does the size of the swollen PPG particles. Although the swollen PPG particles are smaller in high concentrations of brine, those in low brine concentrations are softer or more deformable and therefore have higher injectivity.

3.8.7. Effect of Mesh Size on PPG Injectivity

Figure 3-39 through 3-42 show the effect of mesh size on PPG injectivity for each brine concentration. These figures indicate that for any brine concentration, injectivity increases as mesh size increases. For example, as shown in Figure 3-39, for the PPG sample prepared with a 0.05% brine concentration, at a constant injection rate of 0.1

ml/min (0.366 $in.^3$/hr), PPG injectivity for 150, 80, and 40 mesh screens were 0.0031, 0.0045, and 0.0111 respectively. These results clearly show that at any given injection rate, PPG injectivity increases as mesh size increases.

3.9. Rheology Models

The results from Figures 3-11 through 3-13 are presented in a log-log plot in Figures 3-43 through 3-45. The data are a good fit for the power law rheology equation, and Table 3-5 gives the fitting equations.

3.10. Conclusions

This chapter examined the effect of gel strength and the size of the swollen PPG particles on the PPG injection pressure using screens of various mesh sizes. The results demonstrated the effect of brine concentration on PPG swelling behavior and on the injectivity characteristics of PPG:

1. The PPG swelling ratio depends on the brine concentration, and it can be fitted well using a power rheology equation.

2. PPG swelling follows a pseudo-second-order kinetics model.

3. Swollen PPG is a shear-thinning material that follows a power law rheology equation.

4. The higher the concentration of the brine used to prepare the PPG, the lower the injectivity.

5. The Gel strength is more significant than the size of the swollen PPG particles for the particle injectivity into the reservoir.

6. PPG injection pressure decreases significantly when the effluent PPG is subjected to a second test, indicating that the particles are permanently deformed in shape, after they pass through the screen.

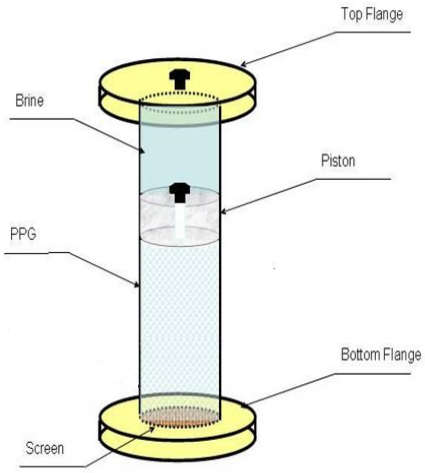

Figure 3-1 Details of screen model.

Figure 3-2 Screen model.

Figure 3-3 Dry powdered PPG.

Figure 3-4 Swollen PPG.

Figure 3-5 Screen experiment apparatus.

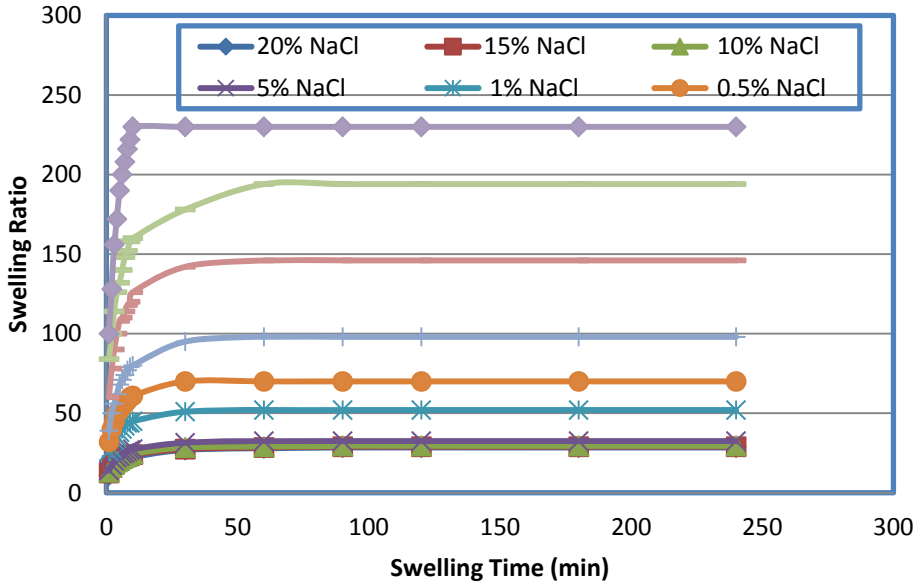

Figure 3-6 Swelling ratio of SAP-40K as a function of time and brine concentration.

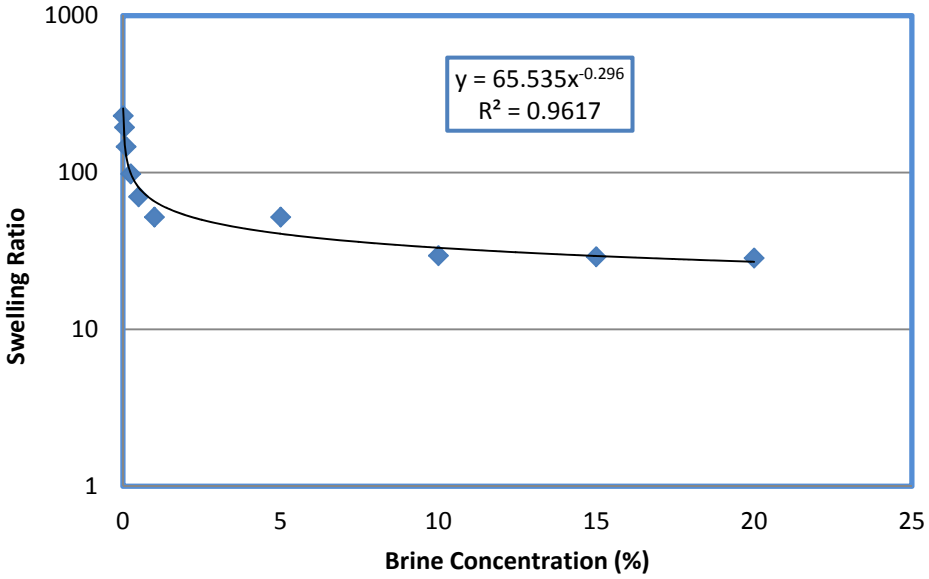

Figure 3-7 Effect of brine concentration on the final swelling ratio of PPG.

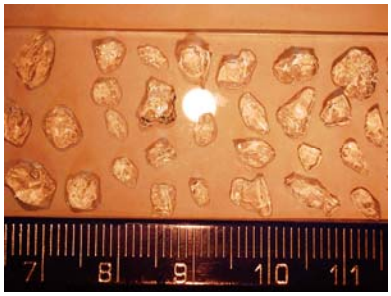

Figure 3-8 0.05% Initial PPG sample.

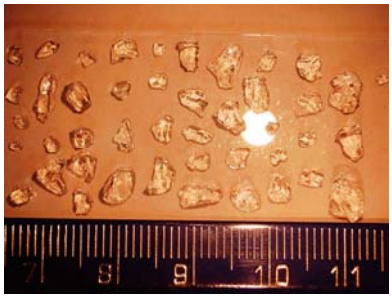

Figure 3-9 0.25% Initial PPG sample.

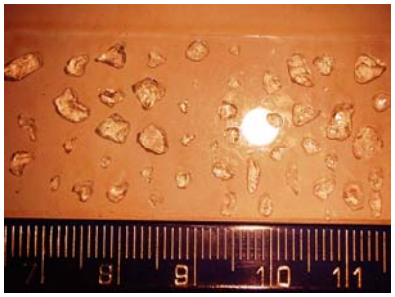

Figure 3-10 1% Initial PPG sample.

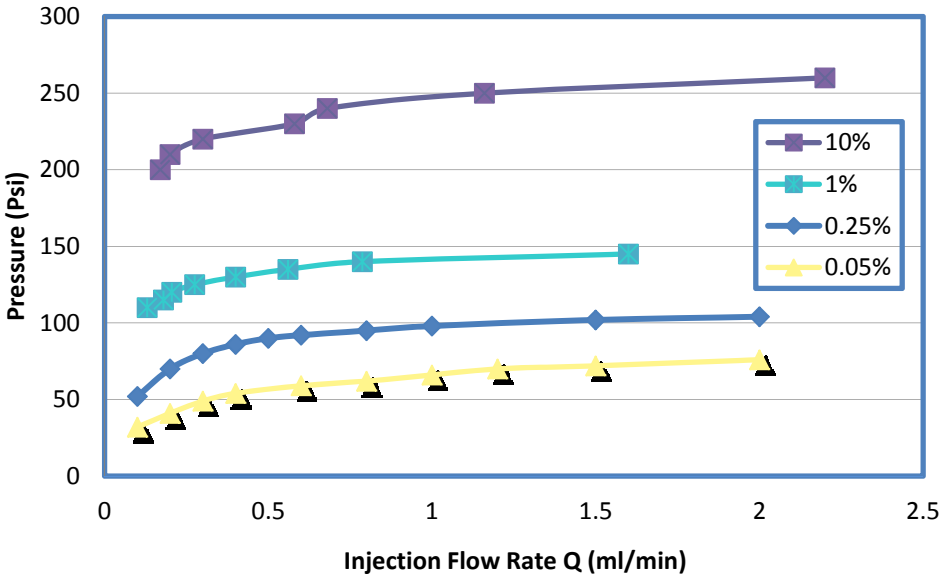

Figure 3-11 Injection pressure as a function of flow rate and brine concentration for 150 mesh screen.
(1 ml/min = 3.66 $in.^3$/hr)

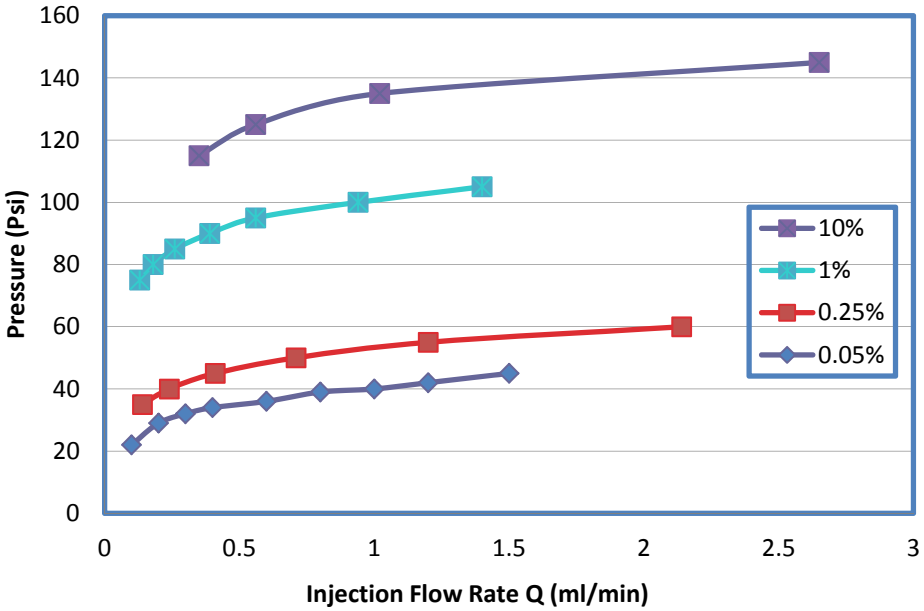

Figure 3-12 Injection pressure as a function of flow rate and brine concentration for 80 mesh screen.
(1 ml/min = 3.66 $in.^3$/hr)

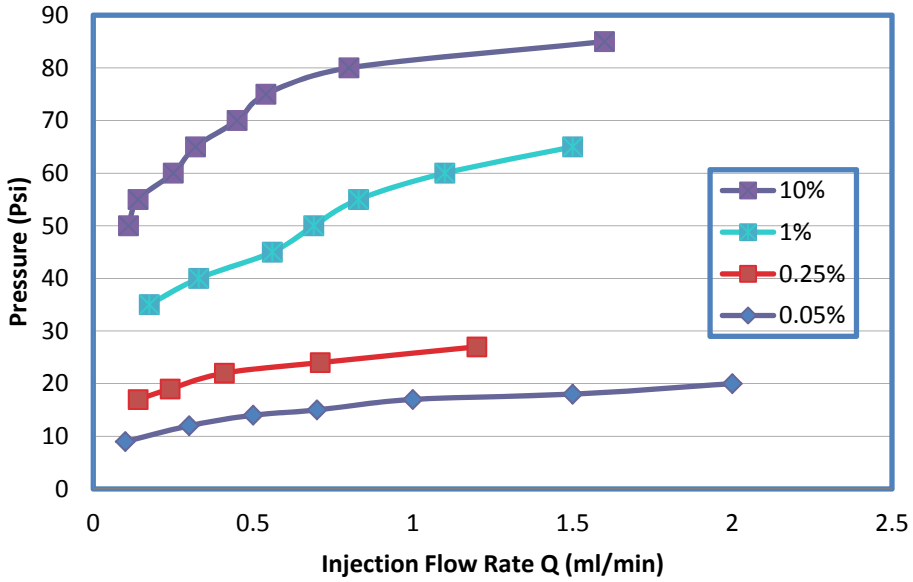

Figure 3-13 Injection pressure as a function of flow rate and brine concentration for 40 mesh screen.
(1 ml/min = 3.66 $in.^3$/hr)

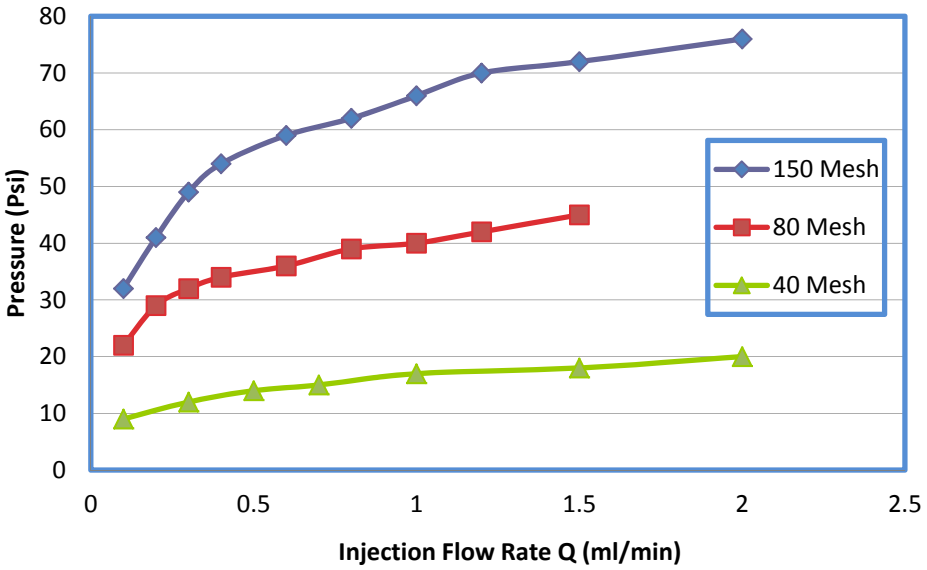

Figure 3-14 Injection pressure versus injection flow rate and mesh size for 0.05% PPG.
(1 ml/min = 3.66 in.^{3}/hr)

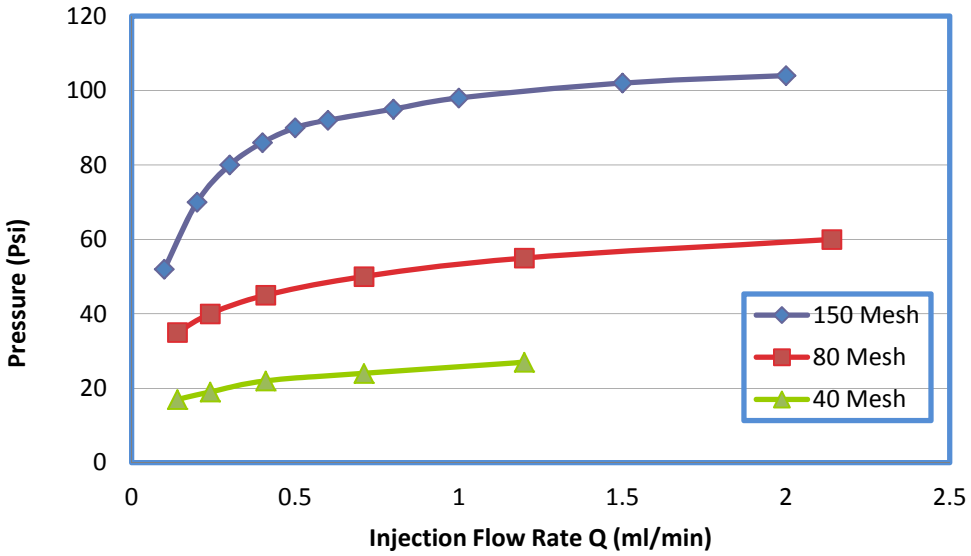

Figure 3-15 Injection pressure versus injection flow rate and mesh size for 0.25% PPG.
(1 ml/min = 3.66 in.^{3}/hr)

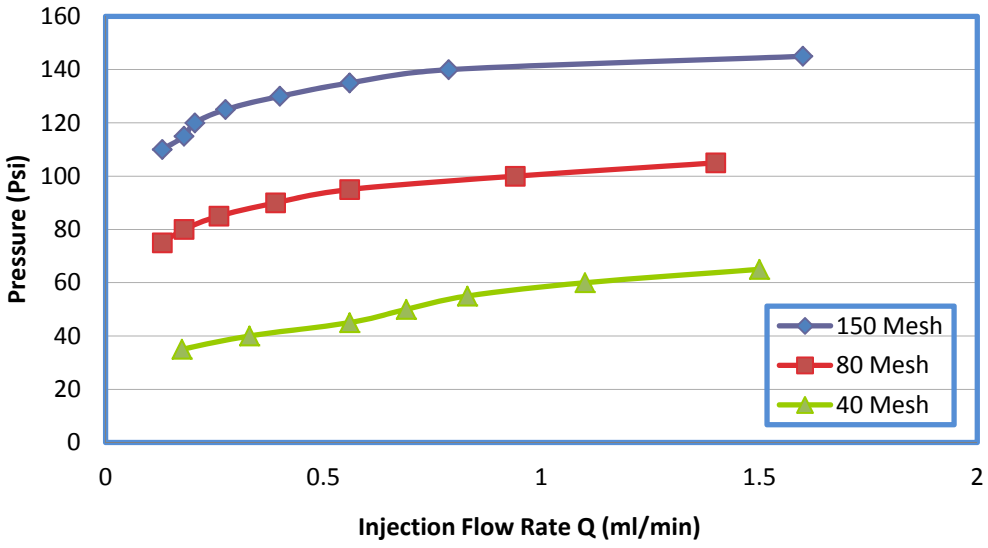

Figure 3-16 Injection pressure versus injection flow rate and mesh size for 1% PPG.
(1 ml/min = 3.66 in.^{3}/hr)

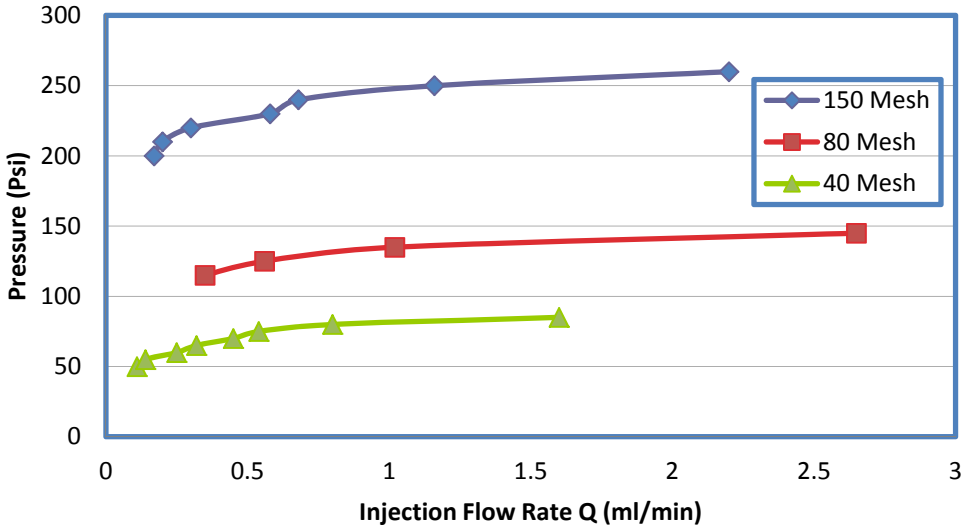

Figure 3-17 Injection pressure versus injection flow rate and mesh size for 10% PPG.
(1 ml/min = 3.66 in.^{3}/hr)

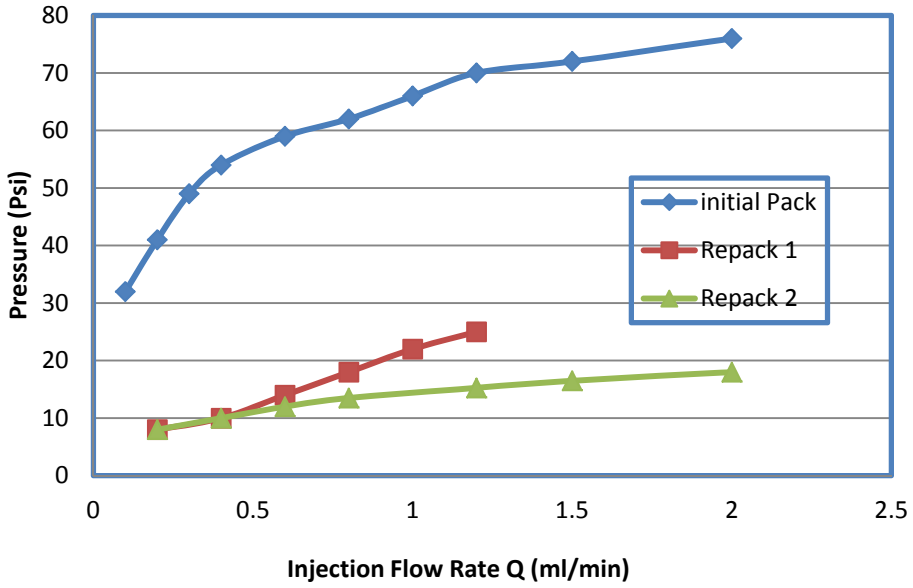

Figure 3-18 Injection pressure versus injection flow rate for 0.05% PPG in 150 mesh for two repacks.
(1 ml/min = 3.66 in.^{3}/hr)

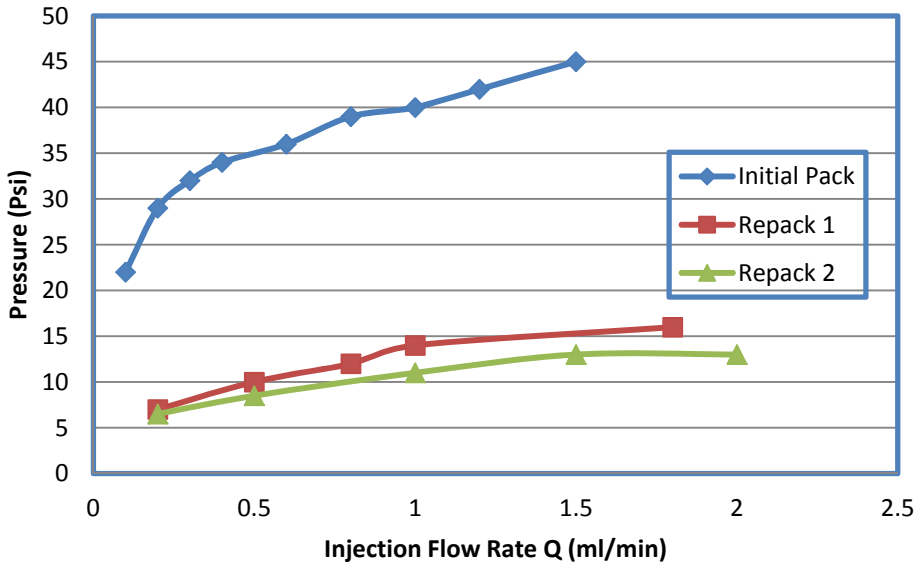

Figure 3-19 Injection pressure versus injection flow rate for 0.05% PPG in 80 mesh for two repacks.
(1 ml/min = 3.66 in.^{3}/hr)

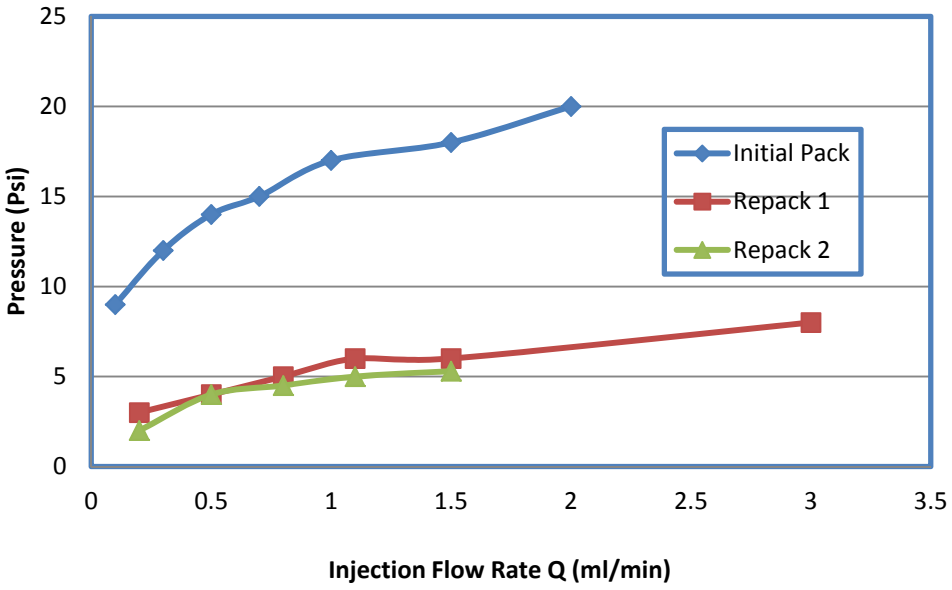

Figure 3-20 Injection pressure versus injection flow rate for 0.05% PPG in 40 mesh for two repacks.
(1 ml/min = 3.66 $in.^3$/hr)

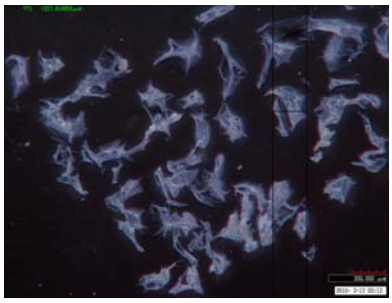

Figure 3-21 0.05% 150 mesh initial pass.

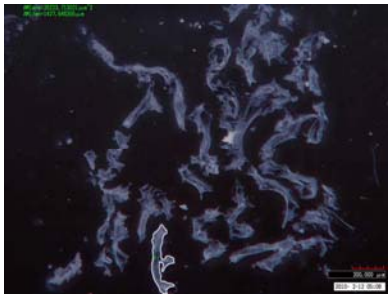

Figure 3-22 0.05% 150 mesh repack 1.

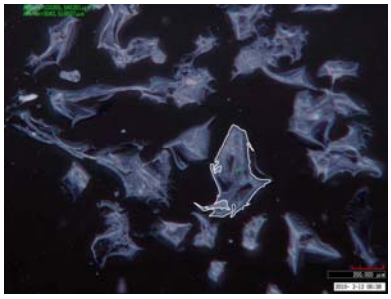

Figure 3-23 0.05% 80 mesh initial pass.

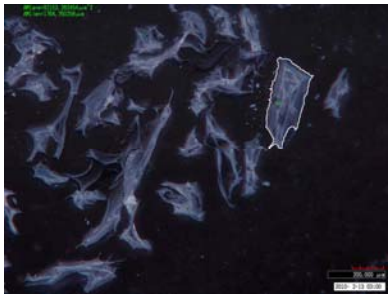

Figure 3-24 0.05% 80 mesh repack 1.

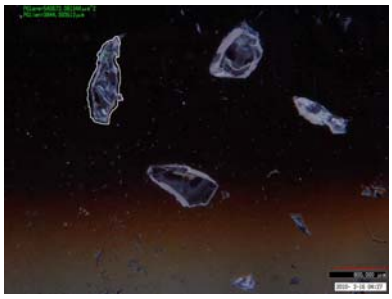

Figure 3-25 0.05% 40 mesh initial pass.

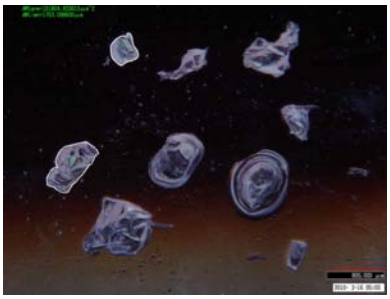

Figure 3-26 0.05% 40 mesh repack 1.

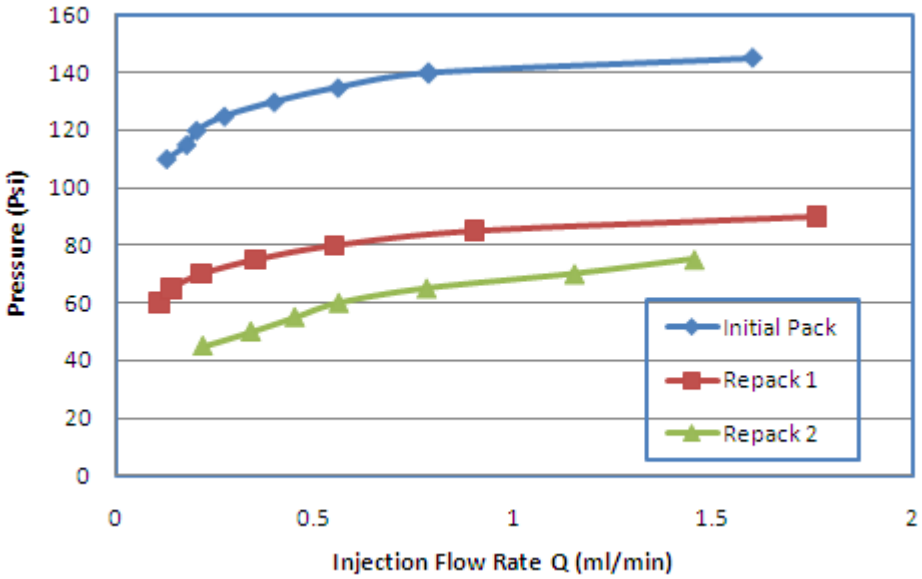

Figure 3-27 Injection pressure versus injection flow rate for 1% PPG in 150 mesh for two repacks.
(1 ml/min = 3.66 in.^{3}/hr)

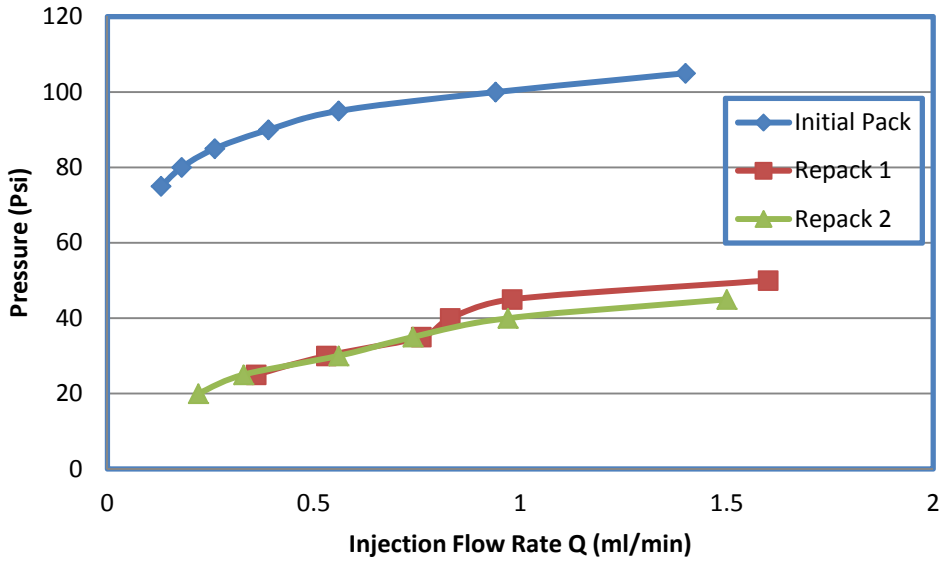

Figure 3-28 Injection pressure versus injection flow rate for 1% PPG in 80 mesh for two repacks.
(1 ml/min = 3.66 in.^{3}/hr)

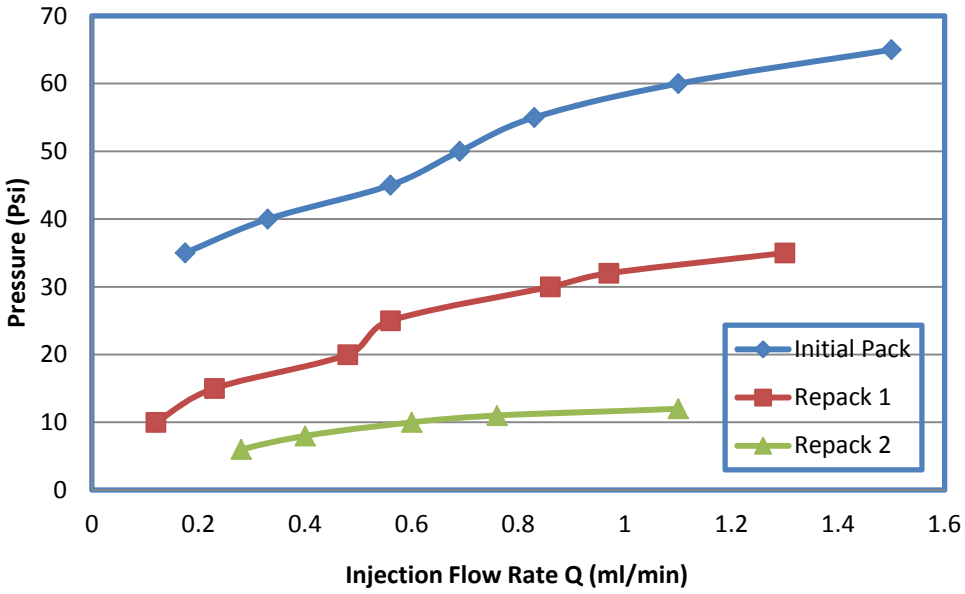

Figure 3-29 Injection pressure versus injection flow rate for 1% PPG in 40 mesh for two repacks.
(1 ml/min = 3.66 in.^{3}/hr)

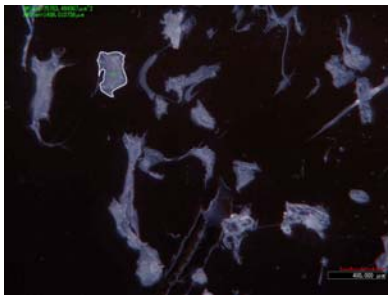

Figure 3-30 1% 150 mesh initial pass.

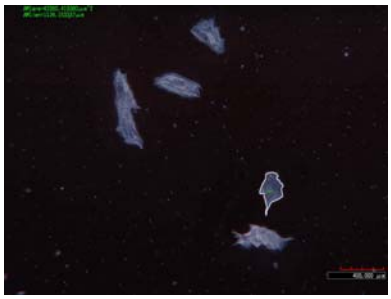

Figure 3-31 1% 150 mesh repack 1.

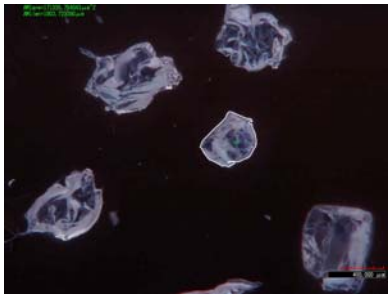

Figure 3-32 1% 80 mesh initial pass.

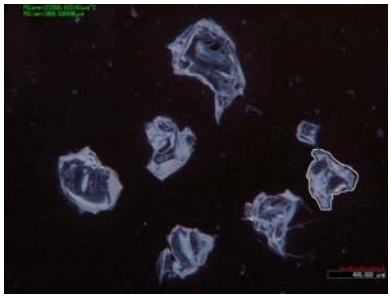

Figure 3-33 1% 80 mesh repack 1.

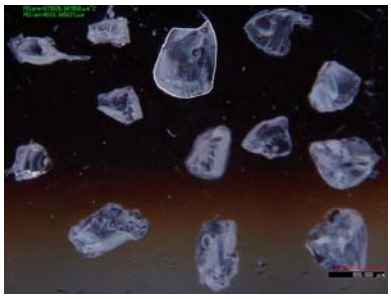

Figure 3-34 1% 40 mesh initial pass.

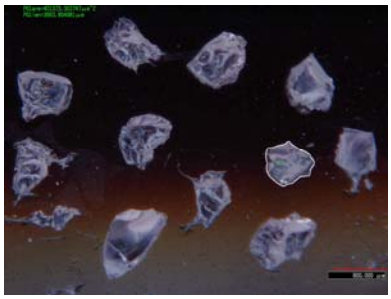

Figure 3-35 1% 40 mesh repack 1.

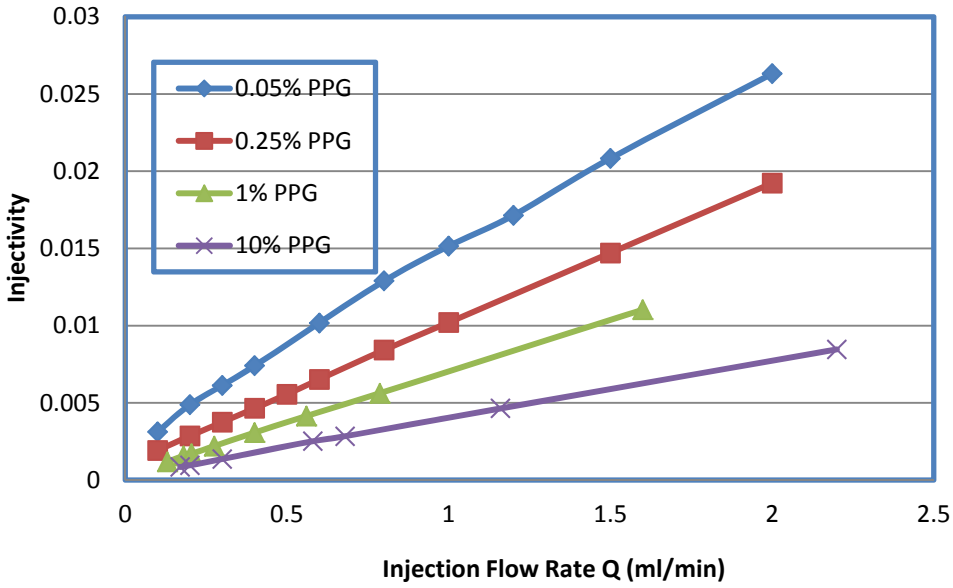

Figure 3-36 Injectivity as a function of flow rate and PPG brine concentration for 150 mesh.
(1 ml/min = 3.66 in.^{3}/hr)

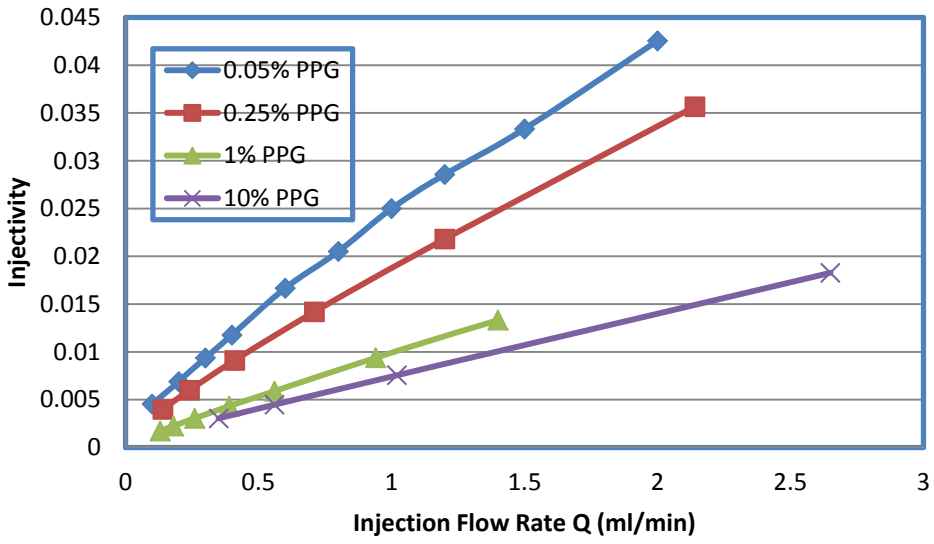

Figure 3-37 Injectivity as a function of flow rate and PPG brine concentration for 80 mesh.
(1 ml/min = 3.66 in.^{3}/hr)

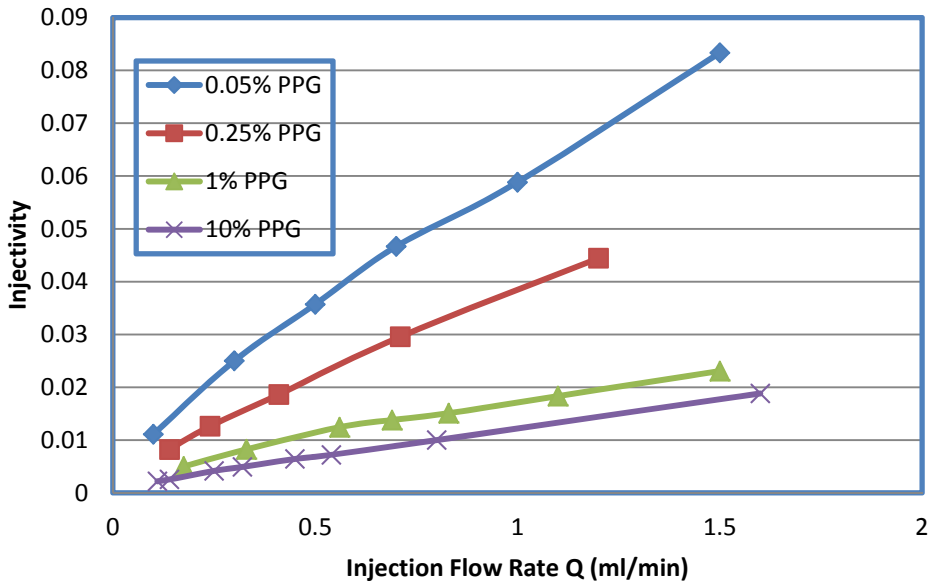

Figure 3-38 Injectivity as a function of flow rate and PPG brine concentration for 40 mesh.
(1 ml/min = 3.66 in.^{3}/hr)

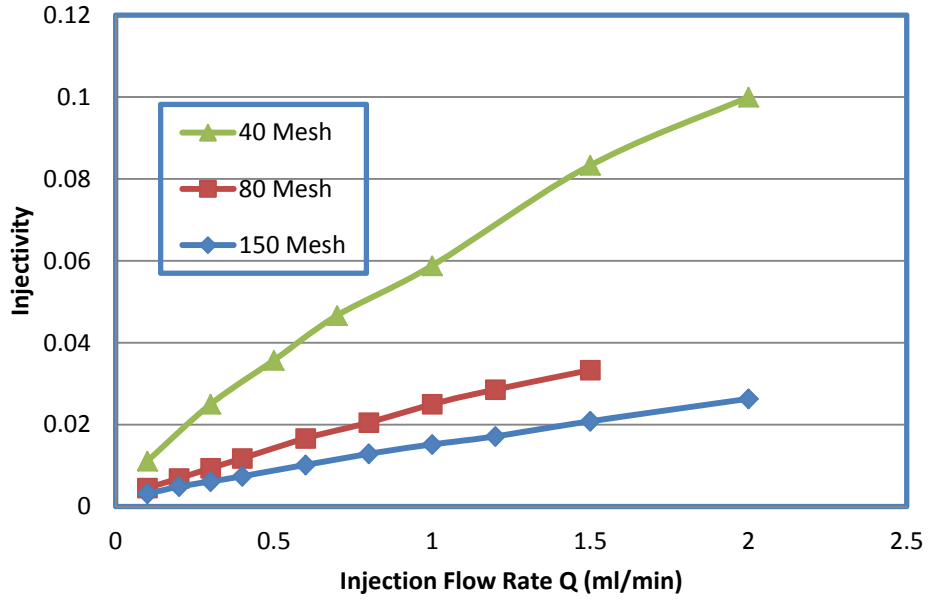

Figure 3-39 Injectivity versus injection flow rate and screen size for 0.05% PPG.
(1 ml/min = 3.66 in.^{3}/hr)

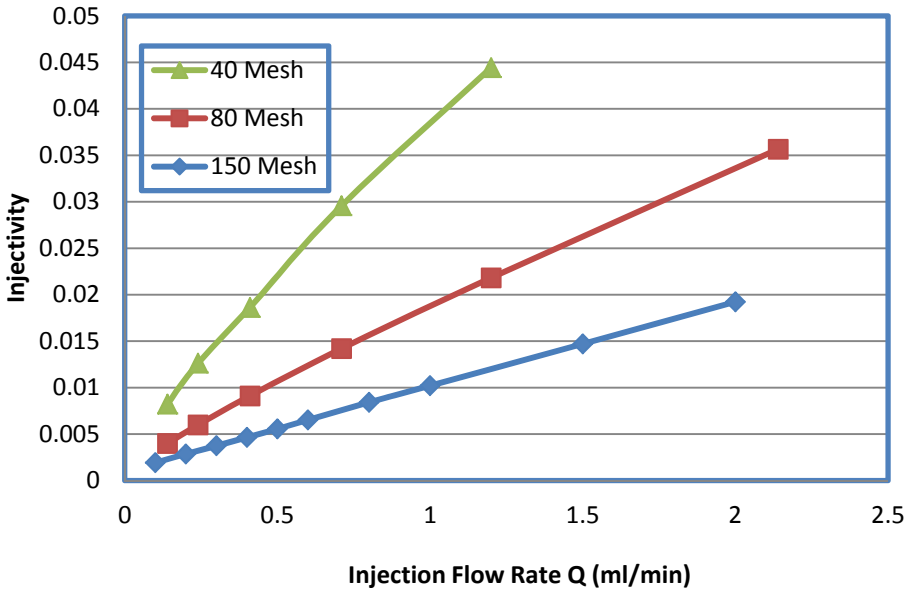

Figure 3-40 Injectivity versus injection flow rate and screen size for 0.25% PPG.
(1 ml/min = 3.66 in.^{3}/hr)

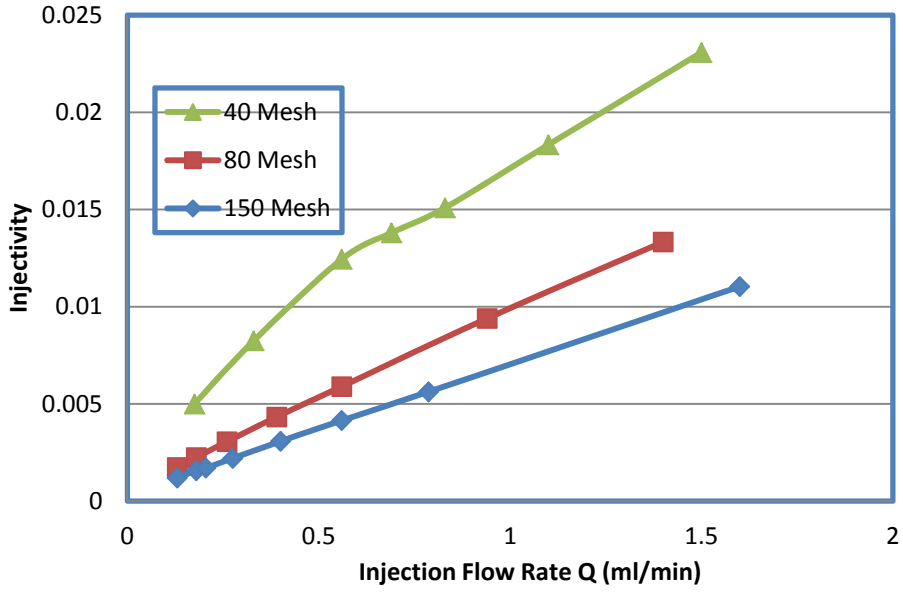

Figure 3-41 Injectivity versus injection flow rate and screen size for 1% PPG.
(1 ml/min = 3.66 in.^{3}/hr)

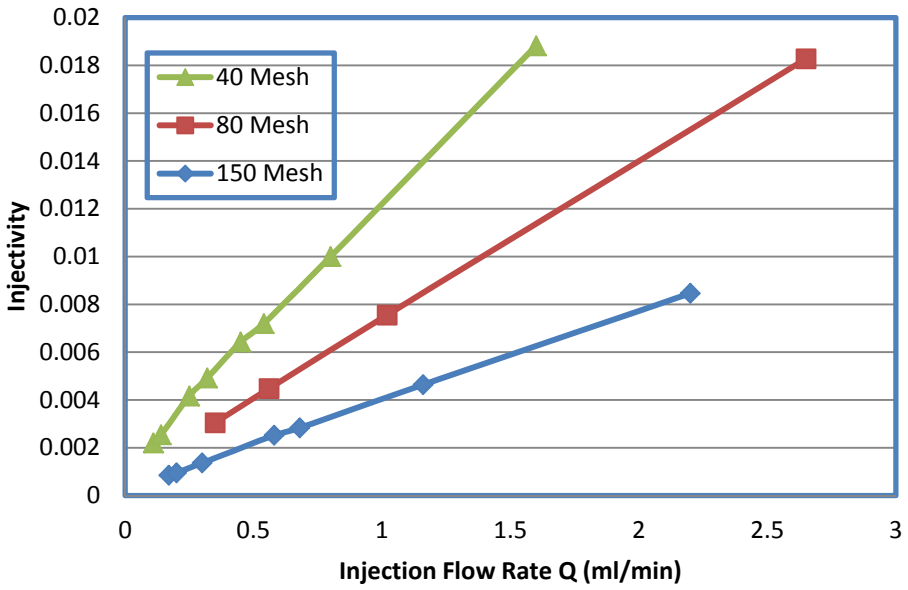

Figure 3-42 Injectivity versus injection flow rate and screen size for 10% PPG.
(1 ml/min = 3.66 in.^{3}/hr)

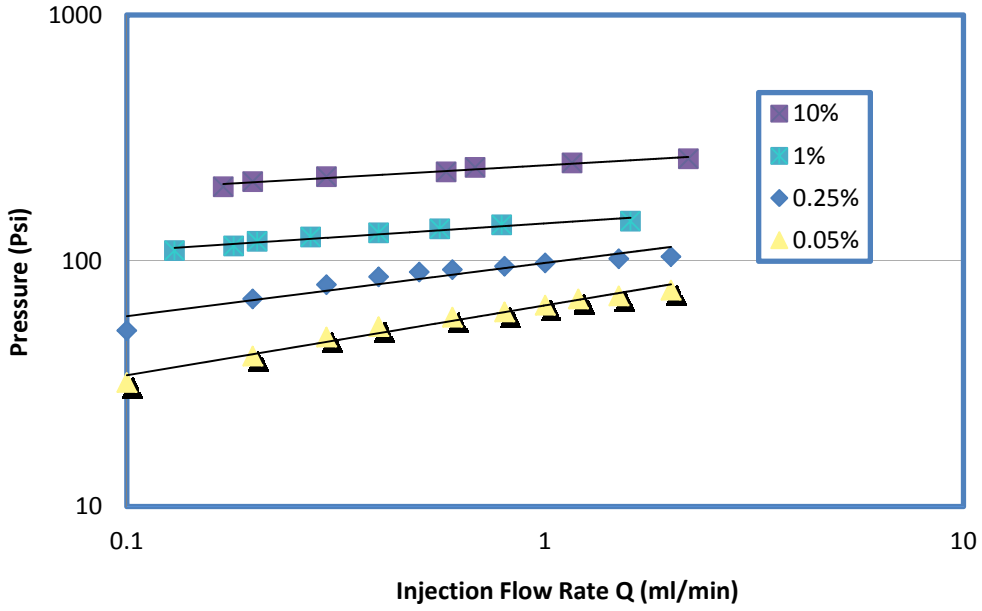

Figure 3-43 Fitting result for injection pressure as a function of injection flow rate using power rheology equation (150 mesh screen).
(1 ml/min = 3.66 in.^{3}/hr)

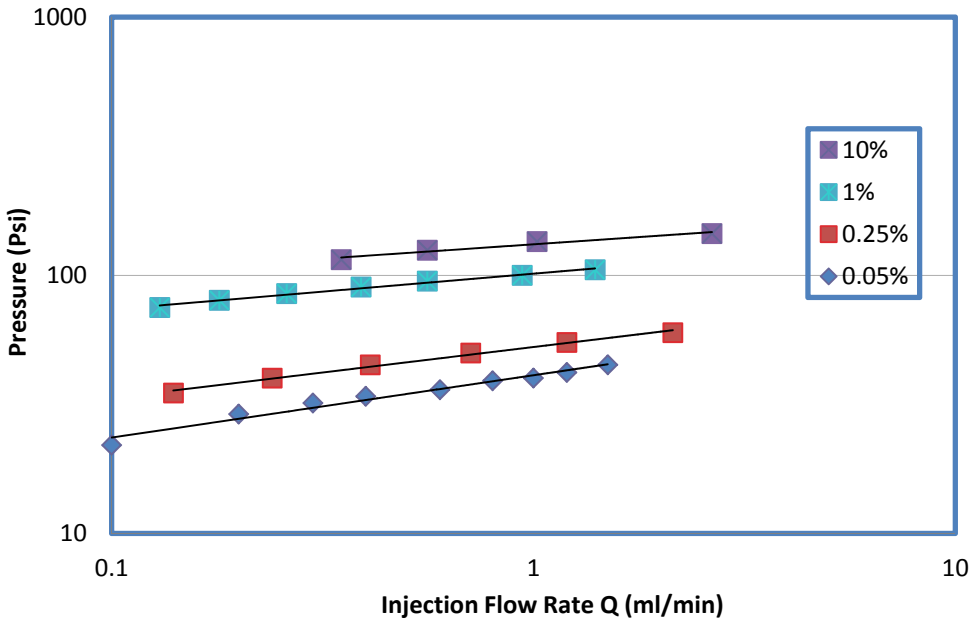

Figure 3-44 Fitting result for injection pressure as a function of injection flow rate using power rheology equation (80 mesh screen).
(1 ml/min = 3.66 in.^{3}/hr)

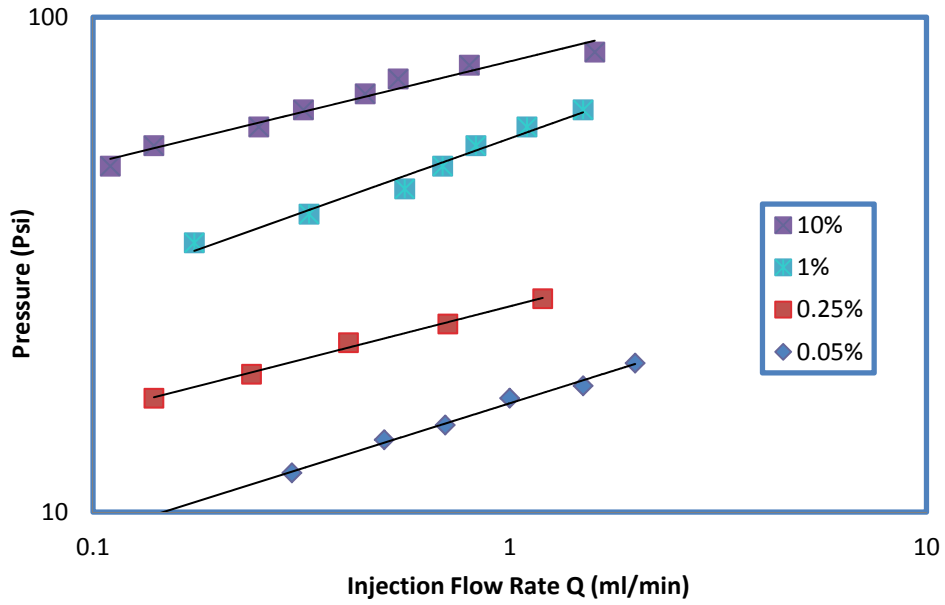

Figure 3-45 Fitting result for injection pressure as a function of injection flow rate using power rheology equation (40 mesh screen).
(1 ml/min = 3.66 in.^{3}/hr)

Table 3-1 Typical Characteristics of PPG

Properties	Value
Absorption De-ionized Water (g/g)	>200
Apparent Bulk Density (g/l)	540
Moisture Content (%)	5
pH Value	5.5-6.0 (+/- 0.5; 1% gel in 0.9% NaCl)

(1 g/l = 0.00835 lb/gal)

Table 3-2 Size Distribution of PPG

Sieves (Mesh)	Size (microns)	Content (percent)
20	>830	12.01
40	380~830	75.32
60	250~380	12.46
80	180~250	0.20
100	150~180	0.01
120	120~150	0
>120	<120	0

Table 3-3 Screen Parameters

Screen Type	Wire Diameter (Inch)	Mesh Per Linear Inch	Width Opening (Inch)
Small	0.0026	150 * 150	0.0041
Medium	0.007	80 * 80	0.0060
Large	0.013	40 * 40	0.0120

Table 3-4 Summary of the Screen Experiments

Screen size	0.05% Brine PPG	0.25% Brine PPG	1% Brine PPG	10% Brine PPG
150 mesh	x	x	x	x
80 mesh	x	x	x	x
40 mesh	x	x	x	x

Table 3-5 Fitting Equations for Pressure versus Injection Flow Rate

Screen (Mesh)	Brine Conc. (%)	Fitting Equations	R^2
150 Mesh	10	$p = 244.48\ q^{0.0991}$	0.9691
	1	$p = 141.87\ q^{0.1123}$	0.9538
	0.25	$p = 97.943\ q^{0.2166}$	0.8907
	0.05	$p = 65.825\ q^{0.2843}$	0.9767
80 mesh	10	$p = 131.84\ q^{0.112}$	0.9613
	1	$p = 101.46\ q^{0.139}$	0.9888
	0.25	$p = 52.737\ q^{0.1974}$	0.9926
	0.05	$p = 41\ q^{0.2414}$	0.9733
40 Mesh	10	$p = 81.394\ q^{0.2054}$	0.9683
	1	$p = 56.874\ q^{0.3002}$	0.9765
	0.25	$p = 26.048\ q^{0.2153}$	0.9949
	0.05	$p = 16.591\ q^{0.2642}$	0.9965

4. Tubing Experiments

4.1. Summary

This chapter addresses experiments using tubes of various internal diameters to study the PPG propagation and extrusion behavior through tubes. Experiments were designed to consider several factors that influence PPG behavior during extrusion, including particle gel swelling ratio (brine concentration), and internal diameter of tube through which particle gel is injected. Effect of gel flow resistance factor on the tube internal diameter and the brine concentration of the PPG are also discussed. Contrary to common understanding, experimental results have shown that the particle gel flow resistance factor increases as tube diameter increases. Particle gel injectivity decreases as the brine concentration increases and as the tube internal diameter decreases.

4.2. Introduction

The common method to study PPG behavior would be to inject the gels into real sandstone cores, but this process is both expensive and time consuming. The alternative method is to inject the swollen gels through stainless steel tubes of various internal diameters (Seright, 1997). This process mimics the injection of gels into a fracture. In actual sandstone fracture models, however, the water produced from gel dehydration leaks into the rock matrix. In tubes, on the other hand, the water front produced by gel dehydration flows ahead of the gel front in the tube. Our experiments used tubes of various internal diameters to study the PPG propagation and extrusion behavior.

4.3. Tubing Experiments

Fifteen experiments were conducted as shown in Table 4-1. Four concentrations of sodium chloride brine were used to prepare the PPG: 0.05, 0.25, 1, and 10%. The brine concentrations were carefully chosen so that the swelling ratio of the gel in each would be significantly different. Five stainless steel tubes of various internal diameters were selected; their internal radii were 0.06, 0.0345, 0.0275, 0.02025, and 0.01525 inch. Each tube was cut into 5 ft long equal lengths.

The swollen PPG was packed into the injection apparatus, and the effluent outlet was connected to the tubes. Initially, the apparatus was run at a constant maximum injection rate for that tube as shown in Table 4-3. The pressure buildup data for that

injection rate were recorded against time. Once the pressure had stabilized for at least 30 minutes, the injection rate was lowered to the next highest value, and the pressure decline data were recorded until pressure was again constant for a minimum of 30 minutes. This process was continued for at least four injection rates. The data recorded were plotted in various ways to analyze gel propagation behavior through the tubes.

4.4. Tubes

This work used stainless steel tubes of various internal diameters (ID) supplied by Swagelok® Fluid system Technologies. The tubes were originally 20 ft long, but they were later cut to 5 ft lengths for the experiments. Table 4-2 summarizes the parameters of the tubes.

4.5. Calculation of Injection Flow Rate

Tube #2 represents the standard, and the flow rates for other tubes were calculated based on the ratio of the internal area of each tube to that of the standard tube. Table 4-3 shows the flow rate for each tube.

4.6. Calculation of Resistance Factor

The superficial velocity of injection for each tube was calculated from the flow rate for that tube. For a given velocity, the resistance factor was calculated by dividing the pressure drop during gel injection by the pressure drop during water injection, at a constant injection flow rate:

$$F_r = \frac{\Delta P_g}{\Delta P_w} \tag{4-1}$$

where:

F_r is the resistance factor,

ΔP_g is the pressure drop during the gel injection at the injection rate Q, and

ΔP_w is the pressure drop during the water injection at the same injection rate Q.

The pressure during the gel injection was recorded; the pressure drop during water injection was calculated using the Poiseuille's law: The equation is as follows

$$\Delta P = -(6.22 * 10^{-8}) * \frac{(\mu * L * V)}{r^2} \tag{4-2}$$

where:

ΔP is the pressure drop in psi,

r is the internal radius of the tube in inch,

V is the velocity in feet per day,

L is the length of the tube in feet, and

μ is the viscosity of liquid in centipoises.

Tables 4-4 through 4-8 show the superficial velocity of gel injection and the pressure drop caused by water injection for each flow rate.

4.7. Experimental Setup and Procedure

4.7.1. Experimental Setup

Figure 4-1 shows the experimental apparatus, which is as follows:

• The PPG particles were placed in the brine concentration and left overnight to swell completely.

• The swollen particle gel was allowed to sit on a 150 mesh to separate it from the excess brine solution.

• The swollen PPG was packed in one end of the transparent acrylic tube with the piston in place at the other end.

• Rods were used to set the packed tube on the bottom cap, and the top cap was placed on top the cylinder.

• The apparatus was tightly secured with washers and nuts.

• The entire apparatus was connected at the top to the ISCO pump and at the bottom was connected to the tube on which the experiment was to be performed.

• A pressure gauge was connected to one end of the tube to record the pressure data over time.

4.7.2. Procedure for Tubing Experiment

Once the apparatus was setup, the following experimental procedure was performed:

• Initially, the pump was run at the maximum injection rate designed for that particular tube.

• To avoid a two phase flow, the gap between the top cap and the piston was filled with water so that there was no air left.

• Run the pump at a maximum constant injection rate for the tube, there was water discharge from the gel because of gel dehydration.

• Maintaining the pump at the maximum constant flow rate, the gel flows in to the experimental tube.

• As the gel was injected, the pressure build up data were recorded every 5 to 10 minutes.

• When the gel was extruded from the other end of the tube initially, the gel breakthrough pressure was recorded.

• Pressure data were recorded until pressure stabilized for at least 30 minutes.

• Once the pressure had stabilized, the pump injection rate was lowered to the next lower injection rate.

• The pressure decline data were recorded every 5 minutes, until the pressure had stabilized for at least 30 minutes.

• This procedure was repeated for at least five different injection rates.

• At the conclusion of the experiment, brine solution of the same concentration as the gel was injected into the tube.

4.8. Results and Discussion

4.8.1. Effect of Tube Internal Diameter

Experiments with PPG prepared in 0.05% brine concentration were performed with all the five tubes. Four tubes were used to perform experiments with PPG prepared in 0.25% brine concentration; these had the following internal radii 0.06, 0.0345, 0.0275, and 0.02025 inch. Three tubes were used to perform experiments with PPG prepared with brine concentrations of both 1 and 10%; these had internal radii of 0.06, 0.0345, and 0.0275 inch. Because the swelling ratio of the PPG decreases as brine concentration increases, the 0.02025 and 0.01525 inch tubes could not withstand the injection pressures of PPG prepared in these higher brine concentrations.

4.8.1.1 Pressure Build-up over Time

The pressure build-up data were recorded over time, and Figure 4-2 shows those data for 0.05% PPG for all five tubes. For each injection flow rate stable pressures increased as tube internal radii decreased. As the tube radii decreased, the slope of the pressure build-up curve increased, indicating that the rate of pressure build-up was faster in smaller radius tube. The gel breakthrough pressure was defined as the injection pressure at which the gel front comes out of the tube. The gel breakthrough occurred

early and at lower pressures for larger tubes. The gel breakthrough pressures for 0.06, 0.0345, 0.0275, 0.02025, and 0.01525 inch tubes were 10, 23, 52, 60, and 94 psi respectively.

Figures 4-3 through 4-5 show the pressure build-up data over time for PPG prepared with 0.25, 1, and 10% brine PPG concentrations. As indicated by the steep slope of the curves in these figures, the rate of pressure build-up for tubes with small internal radii was high. The smaller the internal radius of the tube, more was the time needed to reach a stable pressure for each injection rate. For PPG prepared with 0.25% brine concentration, the gel breakthrough pressures for 0.06, 0.0345, 0.0275, and 0.02025 inch tubes were 15, 40, 74, and 160 psi respectively. For PPG prepared with 1% brine concentration, the gel breakthrough pressures for 0.06, 0.0345, and 0.0275 inch tubes were 25, 60, and 155 psi respectively. For PPG prepared with 10% brine concentration, the gel breakthrough pressures for 0.06, 0.0345, and 0.0275 inch tubes were 33, 97, and 226 psi respectively. The gel breakthrough pressure values for each of the tubes clearly indicate that the gel injectivity decreased as tube radii decreased.

4.8.1.2 Constant Pressure versus Superficial Velocity

Once the pressure build-up data was obtained, for each of the four brine concentrations tested for all the tubes, the constant stable pressure for each injection flow rate was recorded and plotted against the superficial velocity of each injection flow rate.

Figure 4-6 through 4-9 plot the constant stable pressures for each injection rate versus the superficial velocities for all four brine concentrations. For all the tubes, the injection pressure clearly increased as superficial velocity increased. At low superficial velocities, the increase in injection pressure was high with increase in superficial velocity, as the tube radii decrease (Seright, 1997). Irrespective of tube size, at higher injection rates injection pressure increased insignificantly with the increase in superficial velocity. This phenomenon was particularly apparent in the case of tubes with larger internal radii, perhaps because the gel “slips” (Seright, 1999) along the walls of the tube. The gel propagated through the tube as a plug (Seright, 1999); that is, gel plugs were formed as a result of temporary pressure build-up. When the pressure became too high, the gel plug broke and the pressure dropped until a new plug formed. For a fixed volumetric injection rate, the average pressure varied inversely with tube radii.

The data in figures 4-6 through 4-9 were then plotted on a log-log plot in figures 4-10 through 4-13, and the data fit very well with power rheology model. Table 4-9 lists the fitting equations. PPG extrusion through tubes exhibited shear thinning or pseudoplastic behavior (Seright, 1995). At a constant velocity, the injection pressure decreased as tube radius increased. For example at around 1,950 ft/d, the stable pressures for injection of a PPG prepared with 0.05% brine concentration into tubes with radii of 0.06, 0.0345, 0.0275, 0.02025, and 0.01525 inch were 48.5, 120, 184.3, 326, and 405psi respectively.

At around 1,950 ft/d, the stable pressures for injection of PPG prepared with 0.25% brine concentration into tubes with radii of 0.06, 0.0345, 0.0275, and 0.2025 inch were 61.8, 153, 248, and 375 psi respectively. For injection of PPG prepared with 1% brine concentration, at a superficial velocity of 1,950 ft/d, the stable pressures for tubes with radii of 0.06, 0.0345, and 0.0275 inch were 81, 218, and 339.5 psi respectively. At a superficial velocity of 1950 ft/d, the stable pressures for injection of PPG prepared with 10% brine concentration into tubes with radii of 0.06, 0.0345, and 0.0275 inch were 110, 255, and 440 psi respectively.

4.8.1.3 Resistance Factor versus Superficial Velocity

Figure 4-14 through 4-17 plot the gel flow resistance factors versus the superficial velocities for propagation of PPG prepared with 0.05, 0.25, 1, and 10% brine concentrations through the corresponding tubes. For a given superficial velocity, the gel flow resistance factor was calculated by dividing the pressure drop during gel injection by the pressure drop during water injection.

Figure 4-14 shows the log-log plot for the resistance factor and the superficial velocity for propagation of PPG prepared with 0.05% brine concentration through the five tubes. The resistance factor curves for the 0.0345 and 0.0275 inch tubes are similar, as are the curves for the 0.02025 and 0.01525 inch tubes. This similarity may be because the difference in their internal radii was only 0.005 to 0.007 inch. For all tubes, the gel resistance factor decreased as superficial velocity increased. The trends in these curves are clearer at lower superficial velocities than at higher values. At lower superficial velocities, the gel resistance factors increased as tube diameter increased. For example, at a superficial velocity of around 250 ft/day, the resistance factors for the 0.06, 0.0345,

0.0275, 0.02025, and 0.01525 inch tubes were 975.29, 697.55, 607.44, 528.10, and 494.12 respectively. To clarify the trend in the gel resistance factor, the resistance factor was plotted against the gel volumetric injection rates, as shown in figures 4-15 through 4-17.

Figures 4-15 through 4-17 plot the resistance factors against the superficial velocities for propagation of PPG prepared in 0.25, 1, and 10% brine concentrations through the tubes. They show that the resistance factor curves for the 0.0345 and 0.0275 inch tubes move closer to one another as the brine concentration of the PPG increases. The trend may be a result of swelling ratio of the gel, which decreases as the gel strength increases. The increase in PPG brine concentration offers greater resistance to the gel flow, thus increasing the resistance factor for gel propagation through the tubes. For any given tube and brine concentration of PPG, the gel resistance factor clearly decreased as superficial velocity increased. For any given superficial velocity, the gel flow resistance factor increased as tube radius increased.

4.8.1.4 Resistance Factor versus Injection Flow Rate

The results in figures 4-14 through 4-17 were re-plotted in figures 4-18 through 4-21 as gel volumetric injection flow rate versus gel flow resistance values through the tubes. The latter figures more clearly illustrate gel flow resistance behavior during extrusion through the tubes because the curves are much more distinct than those in figures 4-14 through 4-17.

Figure 4-18 plots the injection rate against the resistance factor for the PPG prepared with 0.05% brine concentration. It indicates that, unlike the curves in figure 4-14, which were all close together, these curves are widely separated. All these graphs, demonstrate that the tube internal radius plays a very important role because for a fixed volumetric injection rate, the higher the internal radius of the tube, the higher the average gel flow resistance factor. Thus, for a pseudoplastic material, the resistance factor decreased as the gel injection rate increased (Seright, 1995) for all tubes, regardless of internal radius. At lower volumetric injection rates, the resistance factors increased significantly with increasing tube diameters. For example, at a gel volumetric injection rate of 0.1 ml/min (0.366 $in.^3$/hr), the resistance factors were 1974.82, 697.55, 428.50,

282.60, and 217.35 for tubes with radius of 0.06, 0.0345, 0.0275, 0.02025, and 0.01525 inch.

Figures 4-19 through 4-21 plot the injection rate against the resistance factor for the PPG prepared with 0.25, 1, and 10% brine concentrations. The curves in these figures are more widely separated and almost parallel to one another. The resistance factor decreased as the increasing injection flow rate increased. For PPG prepared with 0.25% brine concentration, at a gel volumetric injection rate of 0.1 ml/min (0.366 $in.^3$/hr), the resistance factors were 2478.74, 989.55, 654.18, and 404.30 for tubes with radii of 0.06, 0.0345, 0.0275, and 0.02025 inch respectively. For PPG prepared in 1% brine concentration, at a gel volumetric injection rate of 0.1 ml/min (0.366 $in.^3$/hr), the resistance factors were 4167.56, 1225.67, and 808.44 for tubes with radii of 0.06, 0.0345, and 0.0275 inch respectively. For PPG prepared with 10% brine concentration, at a gel volumetric injection rate of 0.1 ml/min (0.366 $in.^3$/hr), the resistance factors were 5011.97, 1459.99, and 1142.67 for tubes with radii of 0.06, 0.0345, and 0.0275 inch respectively. The graphs clearly indicate that the resistance factor increases as tube diameter increases and decreases as the volumetric injection flow rate increases.

4.8.2. Effect of Brine Concentration

Three tubes were used to study the PPG brine concentration effect: 0.06, 0.0345, and 0.0275 inch. The results from the experiments were analyzed to study the effect of PPG brine concentration on the injection pressure build-up over time, gel injectivity into the tubes, and the resistance factor.

4.8.2.1 Pressure Build-up over Time

Pressure build-up was recorded over time. Figure 4-22 shows the pressure build-up in 0.06 inch tube for PPG prepared in 0.05, 0.25, 1, and 10% brine concentrations. Figure 4-22 shows that the injection pressure build-up behavior for each brine concentration used to prepare fully swollen PPG. The constant pressure for each injection rate increased as the brine Concentration of the PPG increased. The greater the concentration of brine used to prepare the PPG, the more time was needed to reach the stable pressure for each injection rate. The gel breakthrough pressures also increased as the PPG brine concentration increased. The gel breakthrough pressures for PPG prepared with 0.05, 0.25, 1, and 10% brine concentration are 10, 15, 25, and 33 psi respectively.

Figures 4-23 and 4-24 show the pressure build–up over time for the 0.0345 and 0.0275 inch tubes. As the brine concentration increased, the rate of pressure build-up increased, as demonstrated by the slope of the curve. The gel breakthrough pressures in the 0.0345 inch tube for PPG prepared with 0.05, 0.25, 1, and 10% brine concentration were 23, 40, 60, and 97 respectively. Those in the 0.0275 inch tube for PPG prepared with 0.05, 0.25, 1 and 10%, brine concentrations were 51, 75, 155, and 226 psi respectively.

4.8.2.2 Constant Pressure versus Superficial Velocity

As shown in figure 4-25, at the same superficial velocity, the injection pressure required increased with the increase in brine concentration of the PPG. The stable pressure for each injection rate also increased with the increase in brine concentration of the PPG, a trend also observed in the screen experiments. For example, at a superficial velocity of 1930 ft/day for PPG prepared with 0.05%, 0.25%, 1%, and 10% brine concentration, the stable pressures were 48.5, 61.8, 81, and 110 psi respectively. These figures indicate that the PPG swollen in 0.05% brine is much softer and deformable than the PPG swollen in 10% brine concentration.

Figures 4-26 and 4-27 show a trend similar to that for the 0.06 inch tube. However, the stable pressures for each injection rate were higher than those for the 0.06 inch tube. The stable pressure for each superficial velocity rate increased as the brine concentration increased. For example, at a superficial velocity of 1940 ft/day for the PPG prepared with 0.05%, 0.25%, 1%, and 10% brine concentration, the stable pressures in the 0.0345 inch tube were 120, 153, 218, and 255 psi respectively. At a superficial velocity of about 1970 ft/day for the PPG prepared with 0.05%, 0.25%, 1%, and 10% brine concentration, the stable pressures in the 0.0275 inch tube were 184.3, 248, 339.5, and 440 psi respectively. These results clearly show that the gel swollen in 0.05% brine is much softer and more easily deformable than that swollen in 10% brine concentration. The data from the figures 4-25 through 4-27 were then plotted on a log-log plot as shown in figures 4-28 through 4-30; they fit well with power rheology model. Table 4-10 lists the fitting equations.

4.8.2.3 Resistance Factor versus Superficial Velocity

Figures 4-31 through 4-33 demonstrate that the resistance factor decreased as the superficial velocity increased, irrespective of the PPG brine concentration. Given a constant superficial velocity rate, the resistance factor increased with increasing brine concentrations. For example, for the 0.06 inch tube, for the PPG prepared with 0.05%, 0.25%, 1%, and 10% brine concentration, at a superficial velocity of 1930 ft/day, the resistance factors were 339.08, 432.06, 566.29, and 769.04 respectively. Those for the 0.0345 inch tube with PPG prepared with 0.05%, 0.25%, 1%, and 10% brine concentration, at a superficial velocity of 1940 ft/day were 252.20, 350.78, 499.81, and 584.64 respectively. For the 0.0275 inch tube, for PPG prepared with 0.05%, 0.25%, 1%, and 10% brine concentrations, at a superficial velocity of 1970 ft/day, the resistance factors were 264.05, 355.32, 486.42, and 630.41 respectively. Thus, gel resistance factor increased with increasing brine concentration of PPG, at a constant superficial velocity.

4.9. Conclusions

This chapter examined the injectivity properties of PPG in tubes with various diameters. The results characterize the gel extrusion and propagation process through the tubes, and clarify the effect of brine concentration on PPG injection.

1. Fully swollen PPGs exhibit shear thinning or pseudoplastic behavior, as indicated by the power law rheology model.

2. The gel flow resistance factor increases as the injection rate decreases.

3. The gel resistance factor increases with increasing internal tube radius, at constant superficial velocity.

4. The gel resistance factor increases with increasing brine concentration used to prepare swollen PPG, at a constant superficial velocity.

5. PPGs swollen in higher concentrations of brine have higher stable pressures, irrespective of the tube diameter.

6. For a given brine concentration of PPG, the gel's breakthrough pressure increases as the tube radius decreases.

7. Gel injectivity decreases as brine concentration increases.

Figure 4-1 Tubing experiment apparatus.

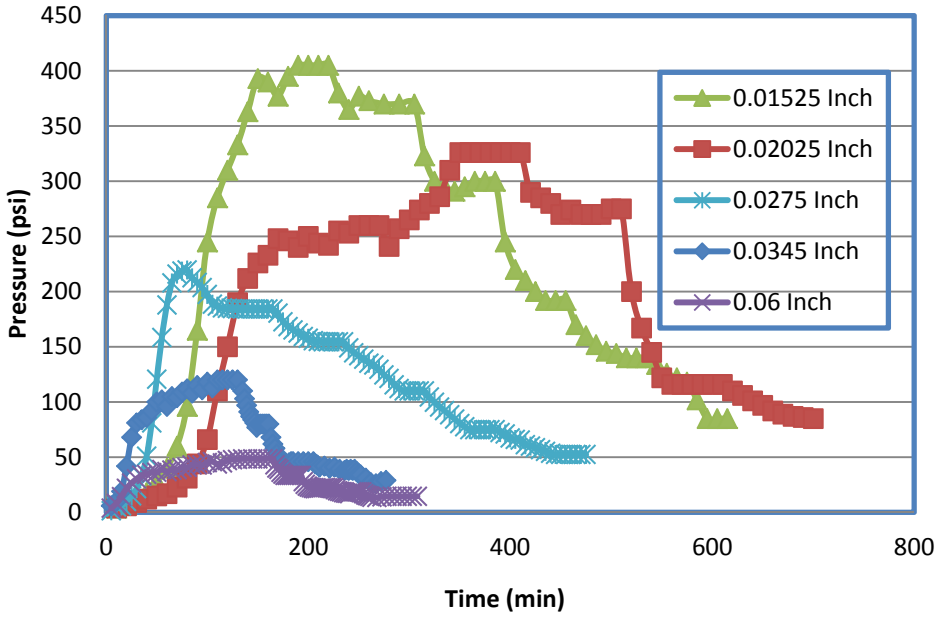

Figure 4-2 Pressure build-up over time for 0.05% PPG in various tubes.

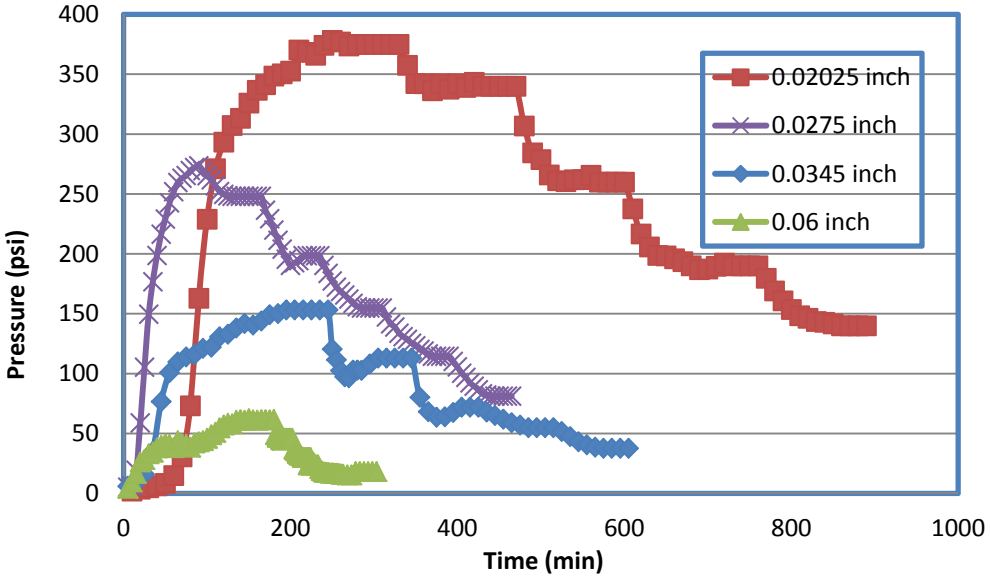

Figure 4-3 Pressure build-up over time for 0.25% PPG in various tubes.

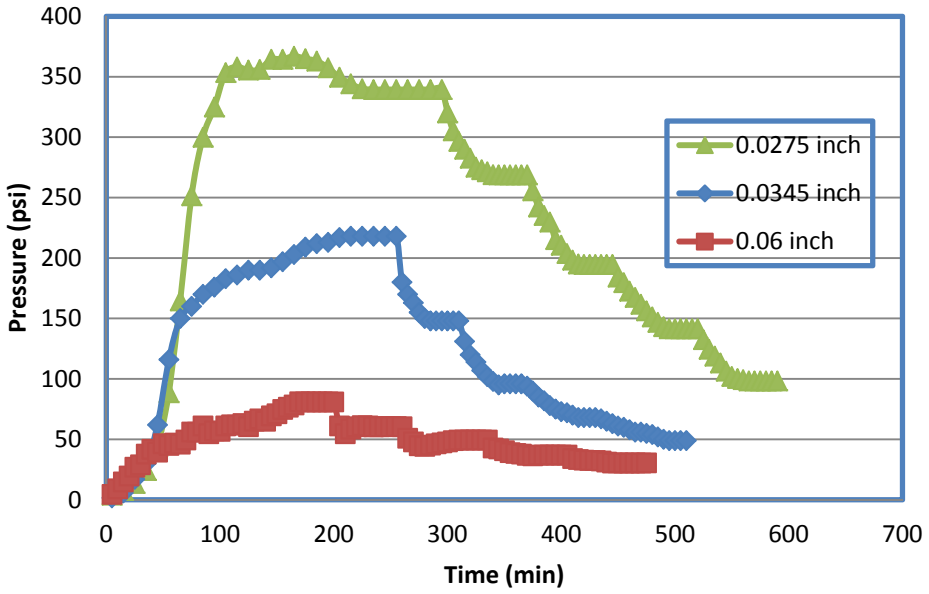

Figure 4-4 Pressure build-up over time for 1% PPG in various tubes.

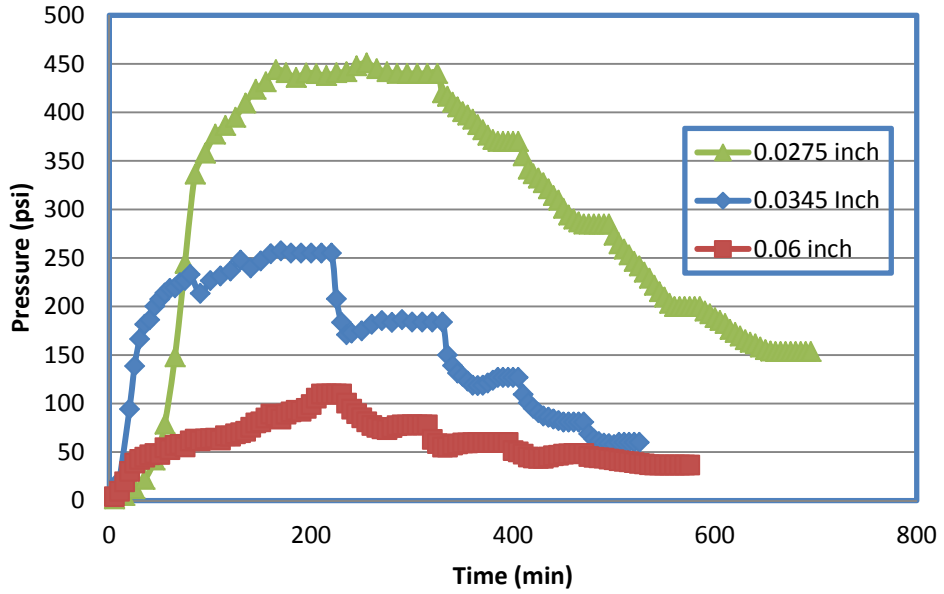

Figure 4-5 Pressure build-up over time for 10% PPG in various tubes.

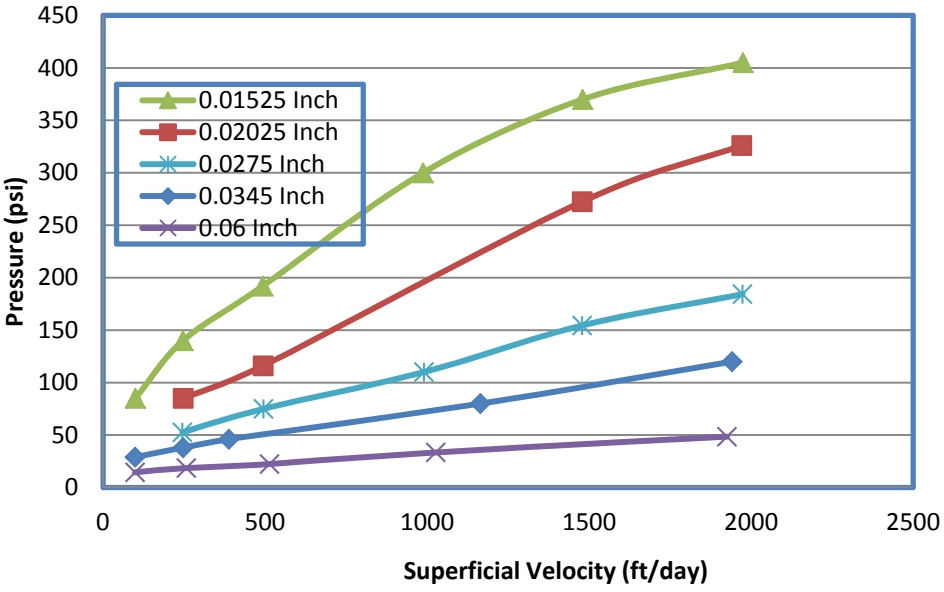

Figure 4-6 Pressure versus superficial velocity for 0.05% PPG in tubes of various internal radii.

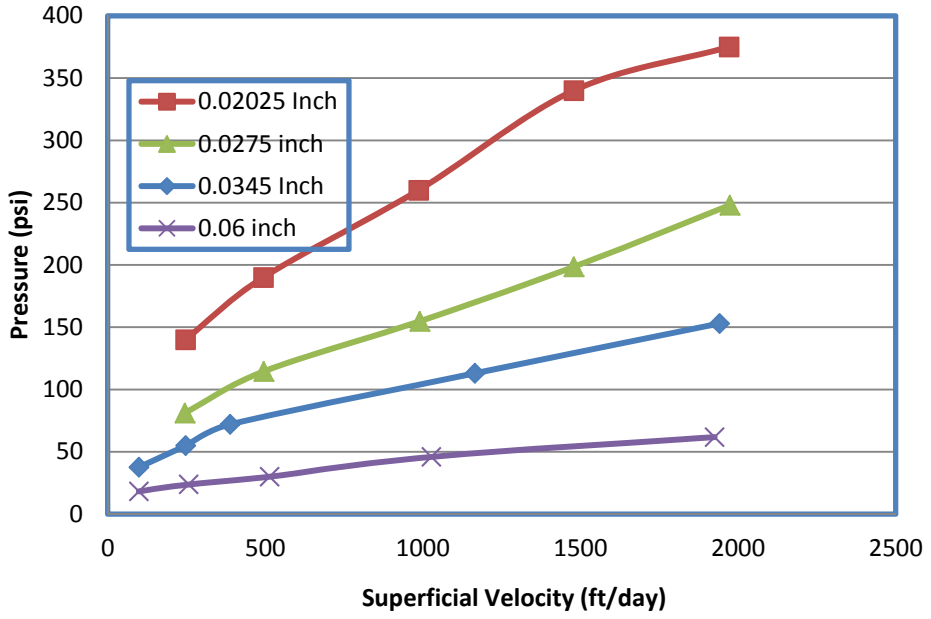

Figure 4-7 Pressure versus superficial velocity for 0.25% PPG in tubes of various internal radii.

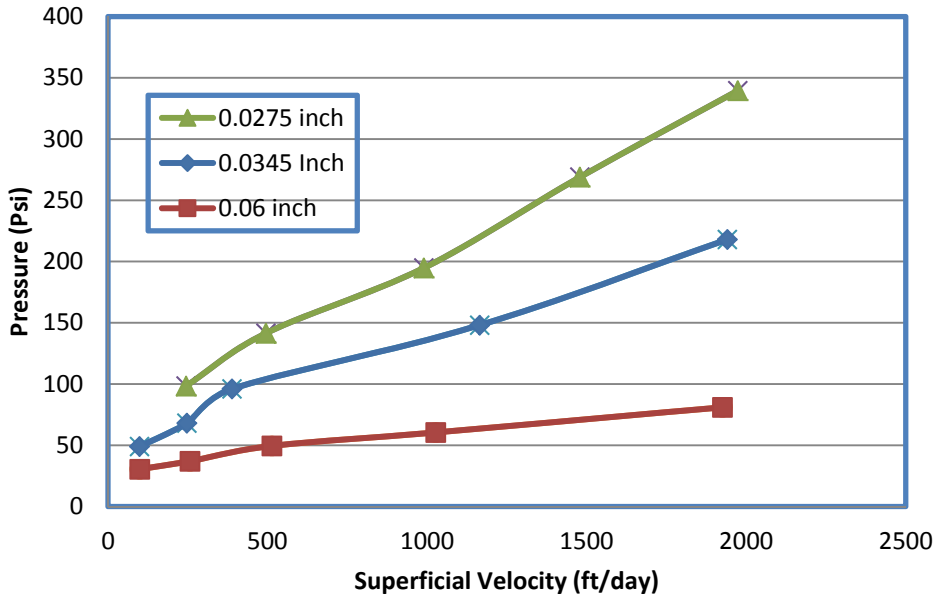

Figure 4-8 Pressure versus superficial velocity for 1% PPG in tubes of various internal radii.

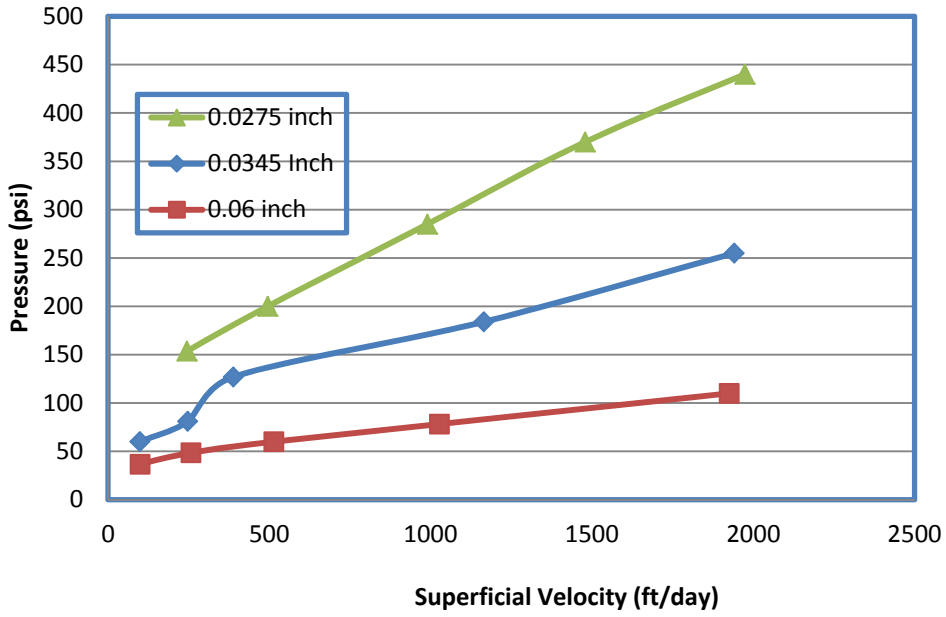

Figure 4-9 Pressure versus superficial velocity for 10% PPG in tubes of various internal radii.

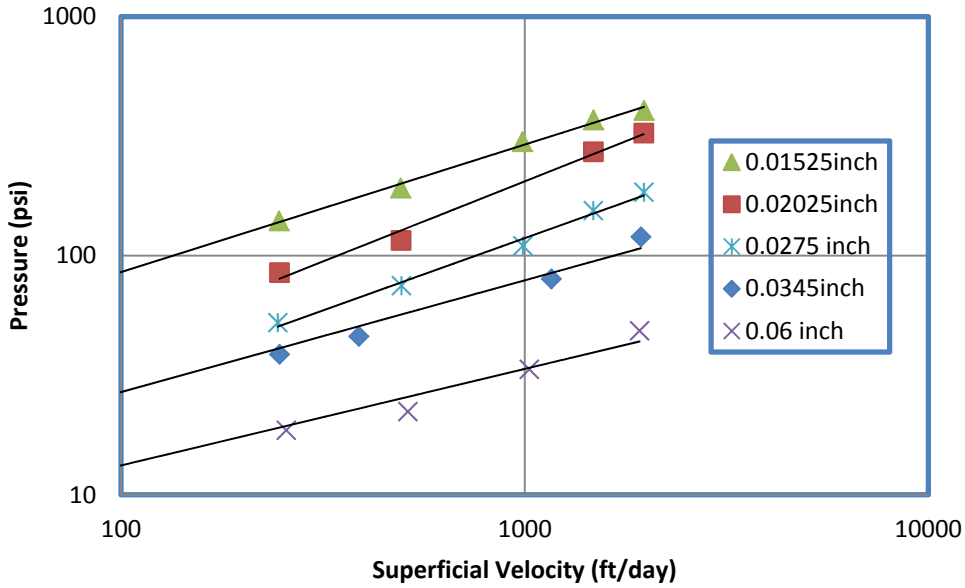

Figure 4-10 Pressure versus superficial velocity for 0.05% PPG on a log-log plot.

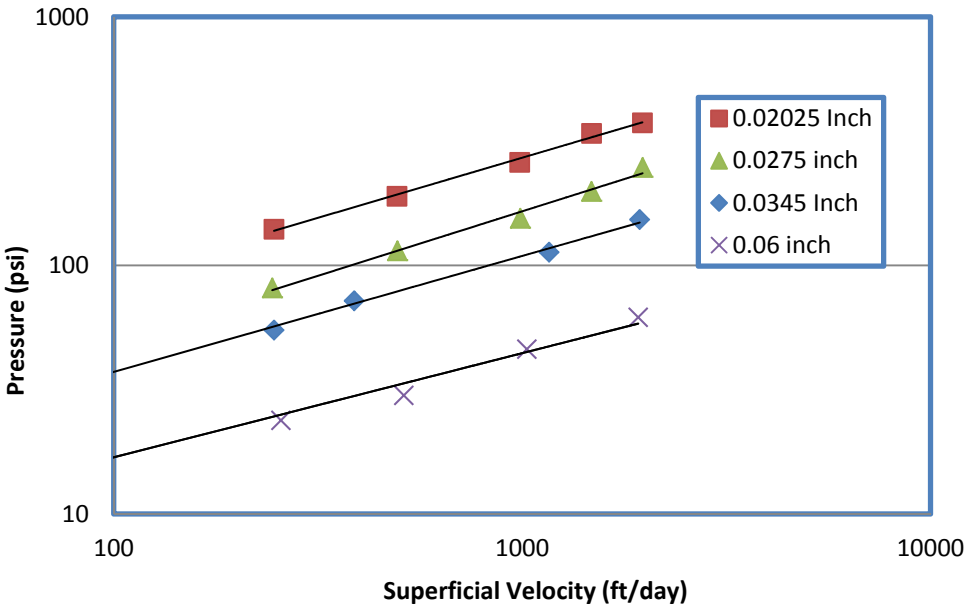

Figure 4-11 Pressure versus superficial velocity for 0.25% PPG on a log-log plot.

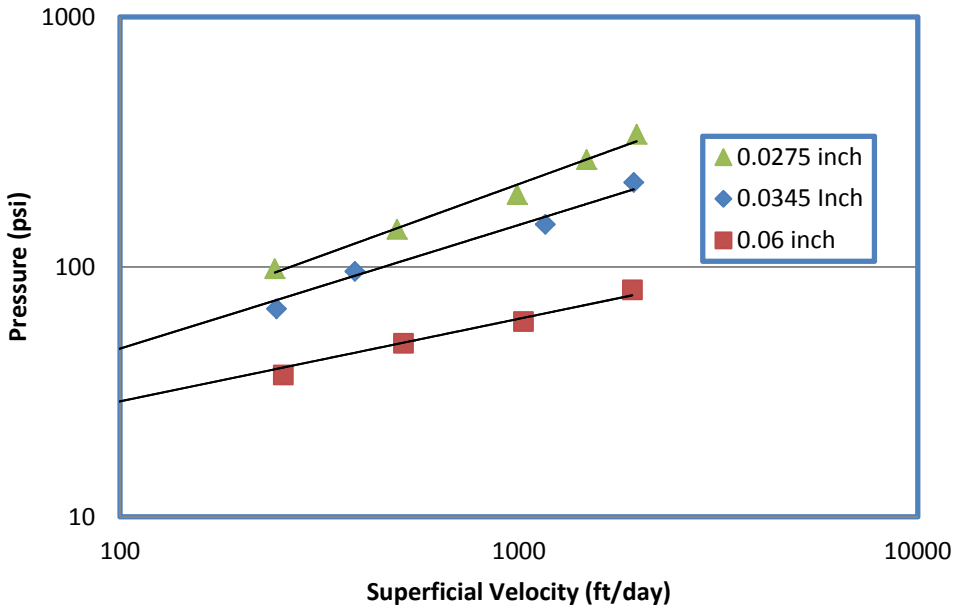

Figure 4-12 Pressure versus superficial velocity for 1% PPG on a log-log plot.

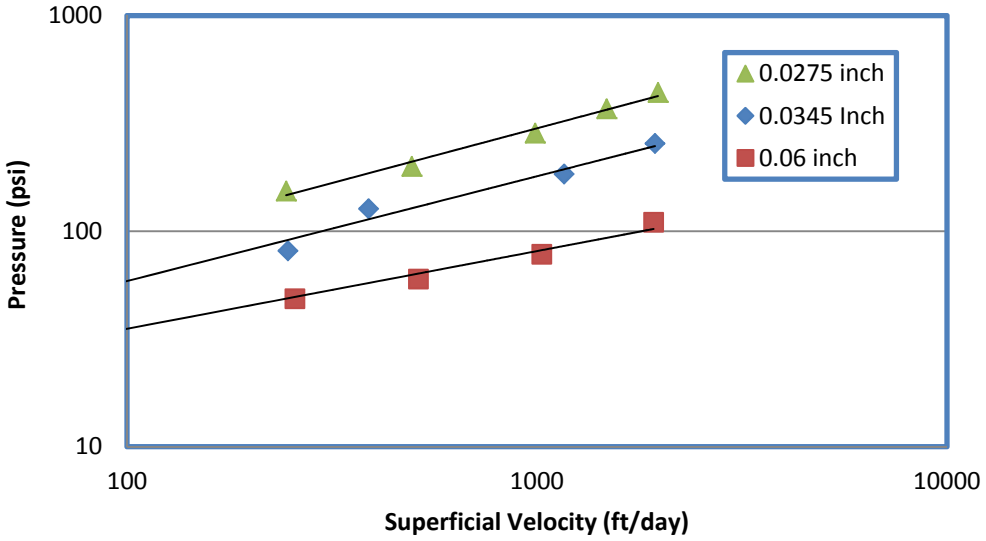

Figure 4-13 Pressure versus superficial velocity for 10% PPG on a log-log plot.

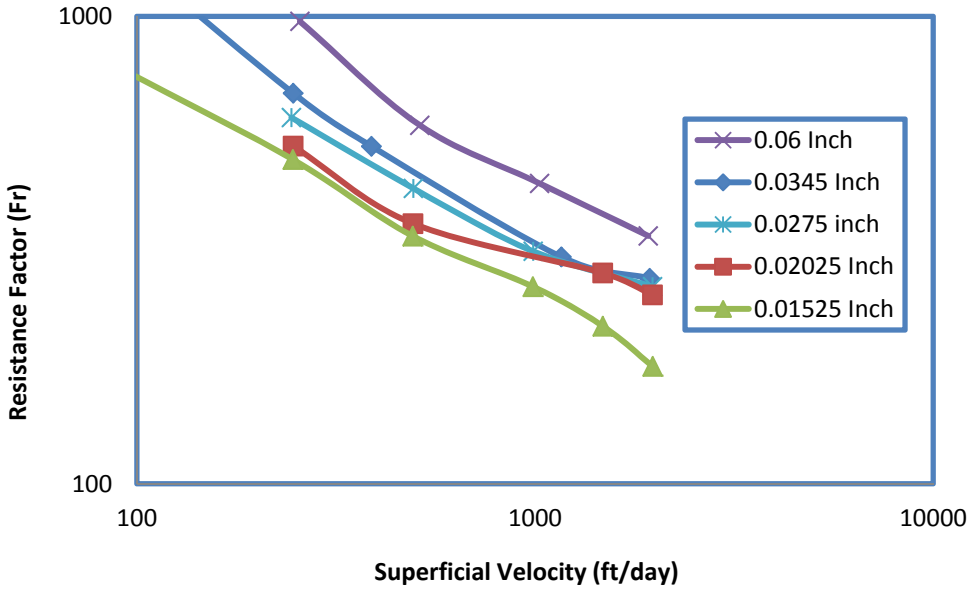

Figure 4-14 Resistance factor versus superficial velocity for 0.05% PPG in tubes of various internal radii.

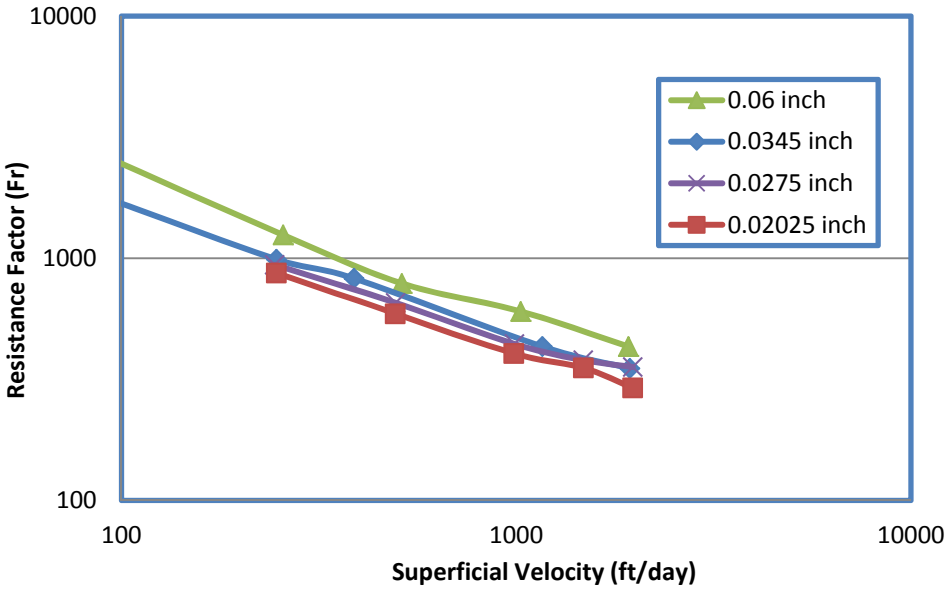

Figure 4-15 Resistance factor versus superficial velocity for 0.25% PPG in tubes of various internal radii.

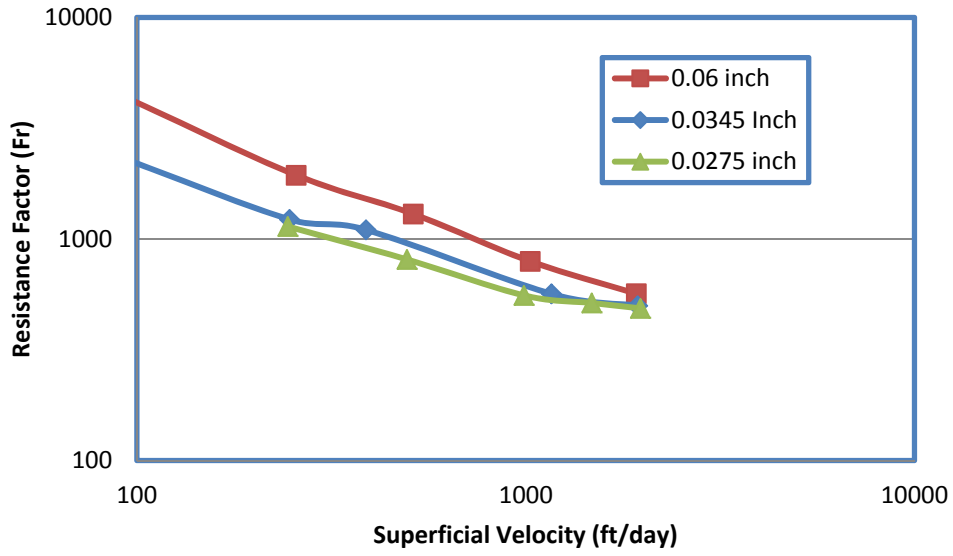

Figure 4-16 Resistance factor versus superficial velocity for 1% PPG in tubes of various internal radii.

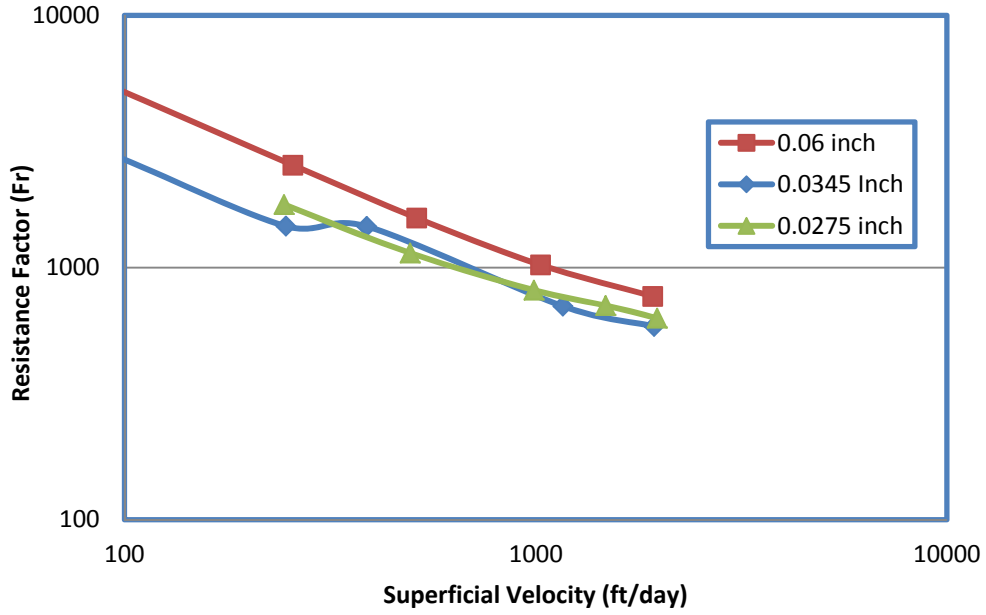

Figure 4-17 Resistance factor versus superficial velocity for 10% PPG in tubes of various internal radii.

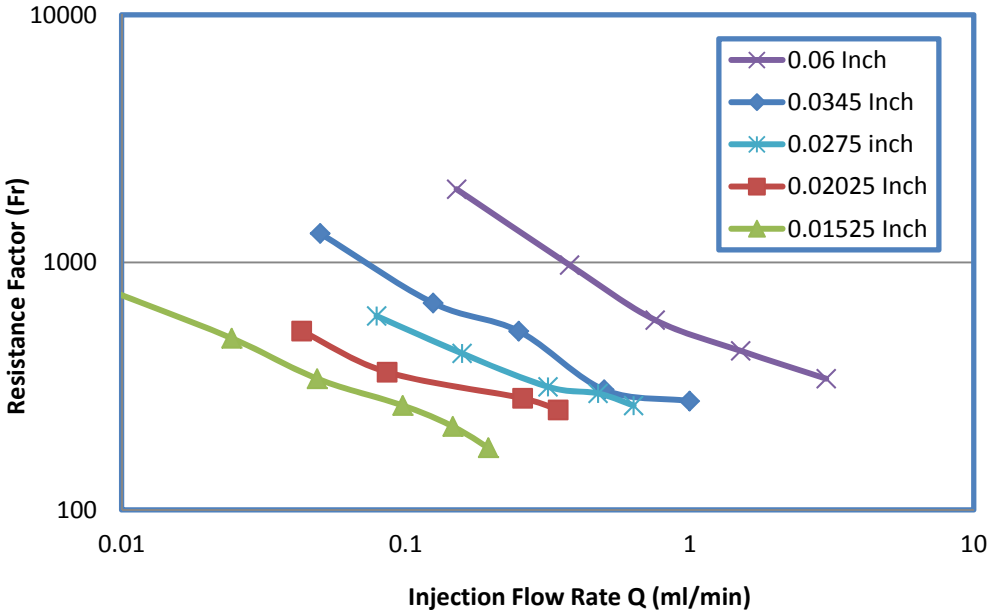

Figure 4-18 Resistance factor versus gel injection flow rate for 0.05% PPG in tubes of various internal radii.
(1 ml/min = 3.66 $in.^3$/hr)

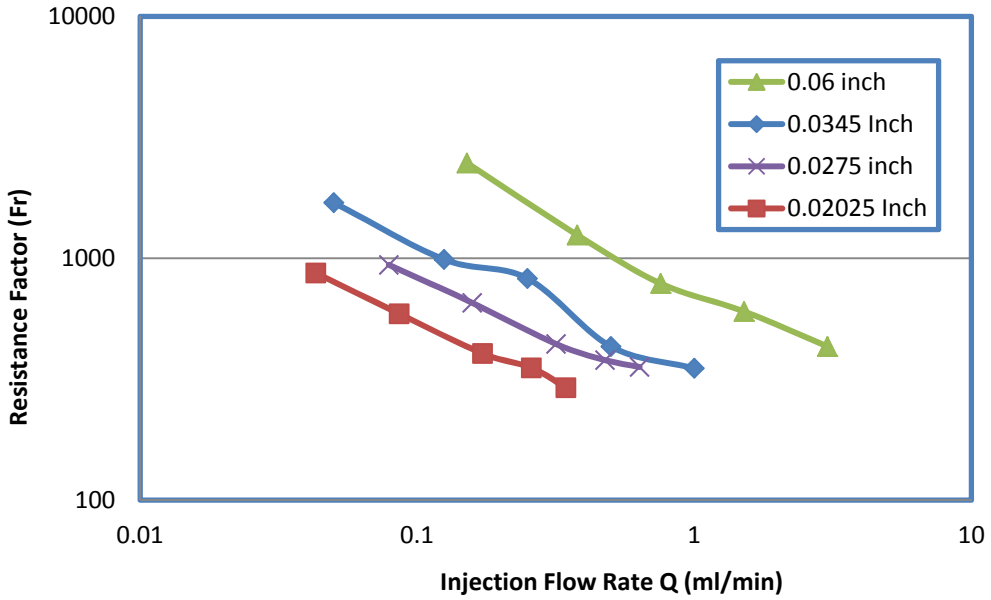

Figure 4-19 Resistance factor versus gel injection flow rate for 0.25% PPG in tubes of various internal radii.
(1 ml/min = 3.66 in.^{3}/hr)

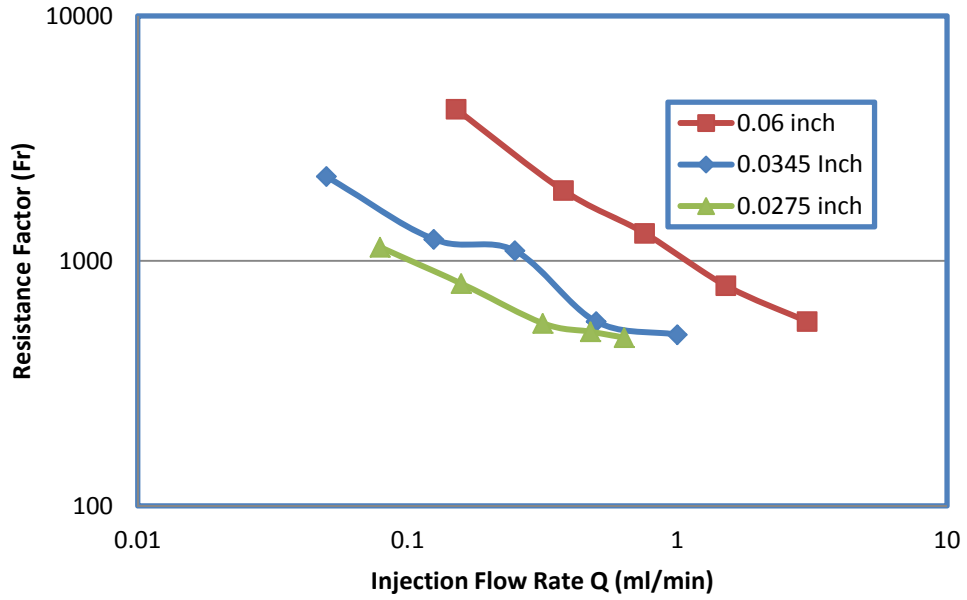

Figure 4-20 Resistance factor versus gel injection flow rate for 1% PPG in tubes of various internal radii.
(1 ml/min = 3.66 in.^{3}/hr)

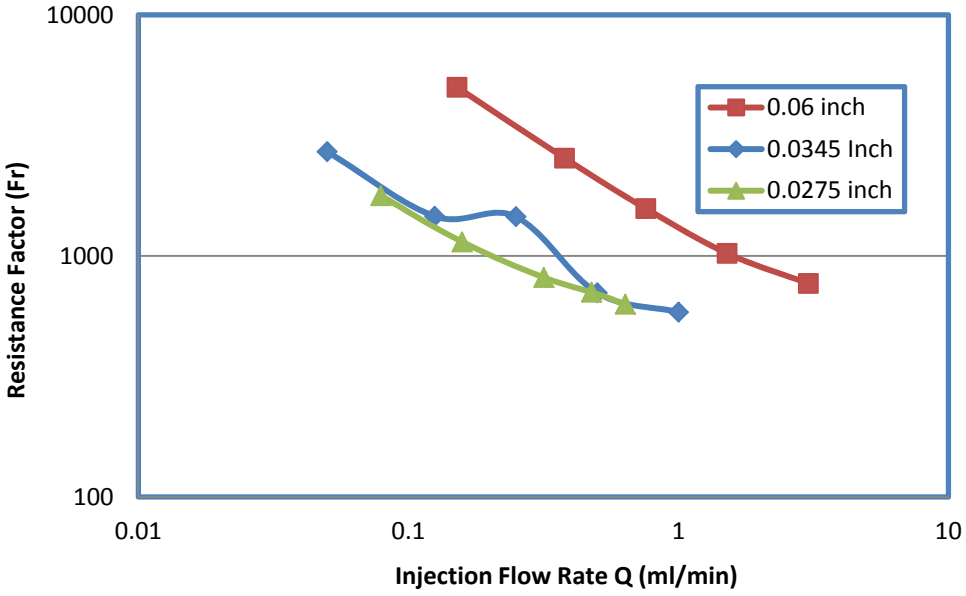

Figure 4-21 Resistance factor versus gel injection flow rate for 10% PPG in tubes of various internal radii.
(1 ml/min = 3.66 $in.^3$/hr)

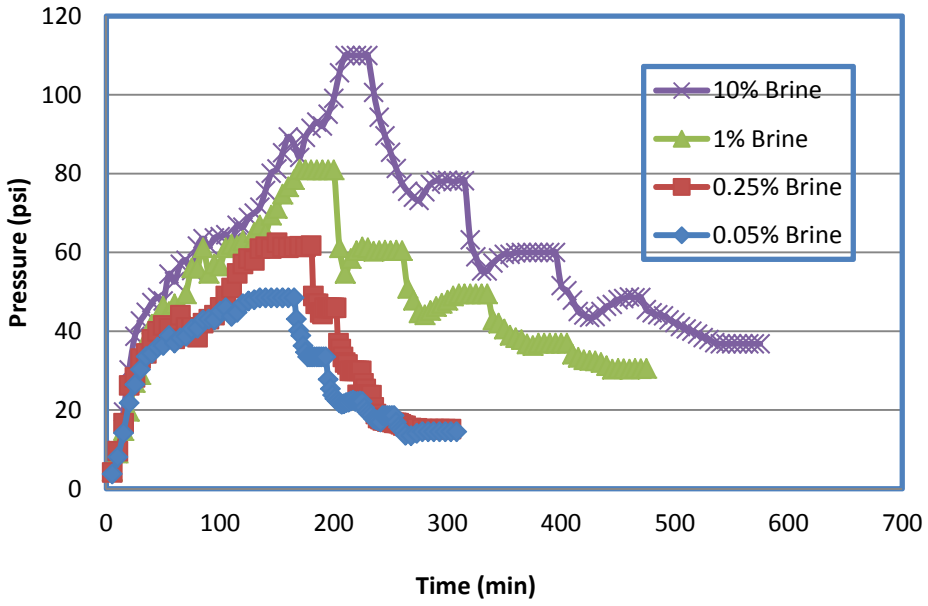

Figure 4-22 Pressure build-up over time for 0.06 inch tube.

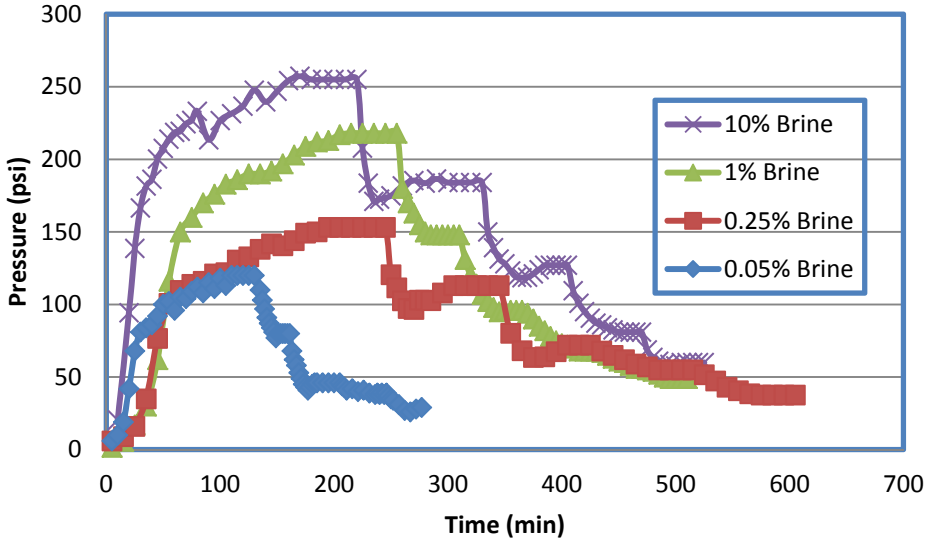

Figure 4-23 Pressure build-up over time for 0.0345 inch tube.

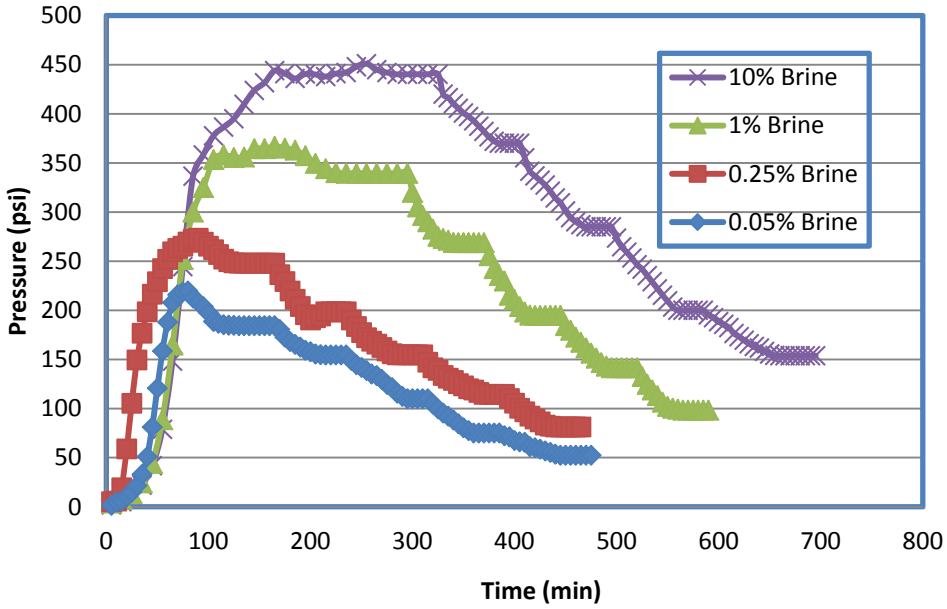

Figure 4-24 Pressure build-up over time for 0.0275 inch tube.

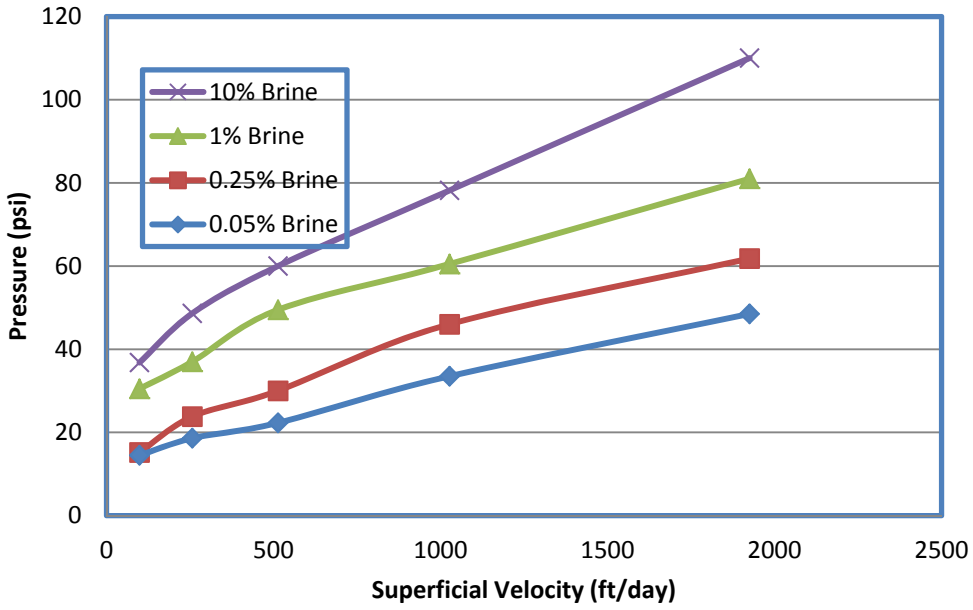

Figure 4-25 Pressure versus superficial velocity for 0.06 inch tube.

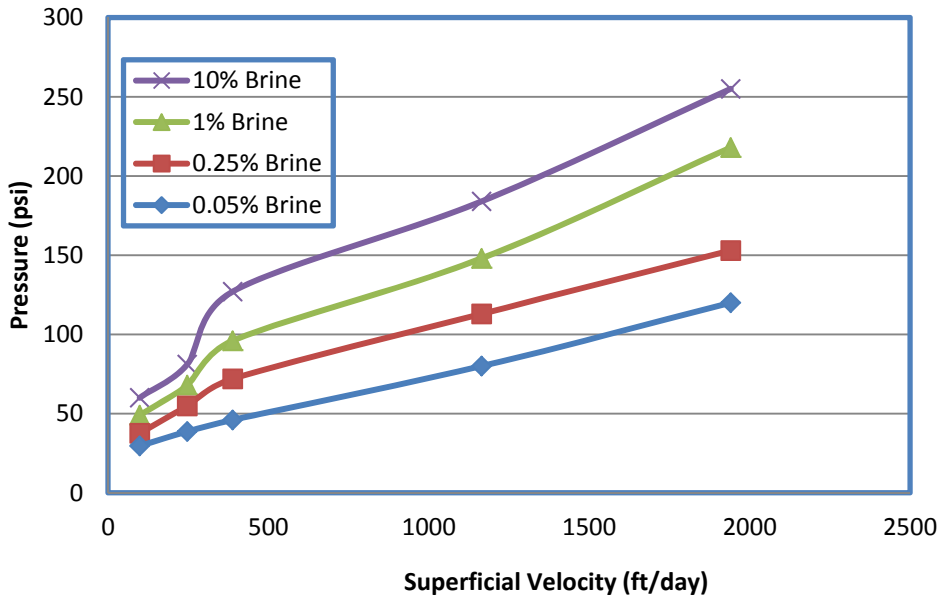

Figure 4-26 Pressure versus superficial velocity for 0.0345 inch tube.

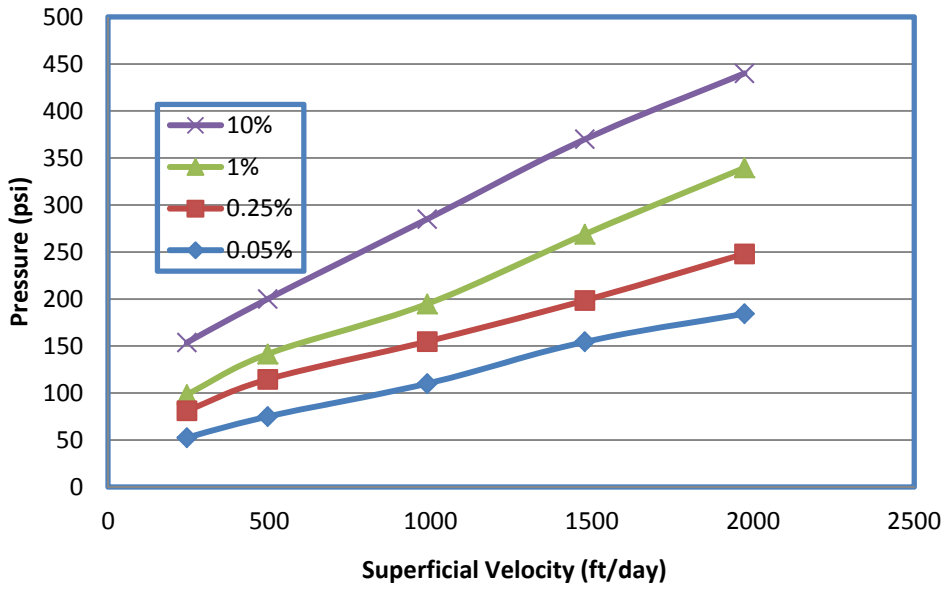

Figure 4-27 Pressure versus superficial velocity for 0.0275 inch tube.

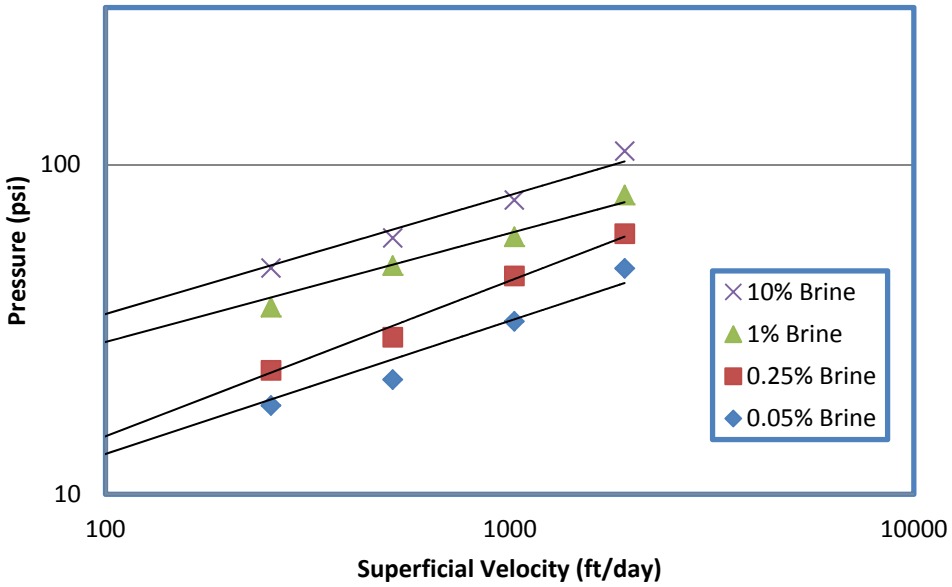

Figure 4-28 Pressure versus superficial velocity for 0.06 inch tube on log-log plot.

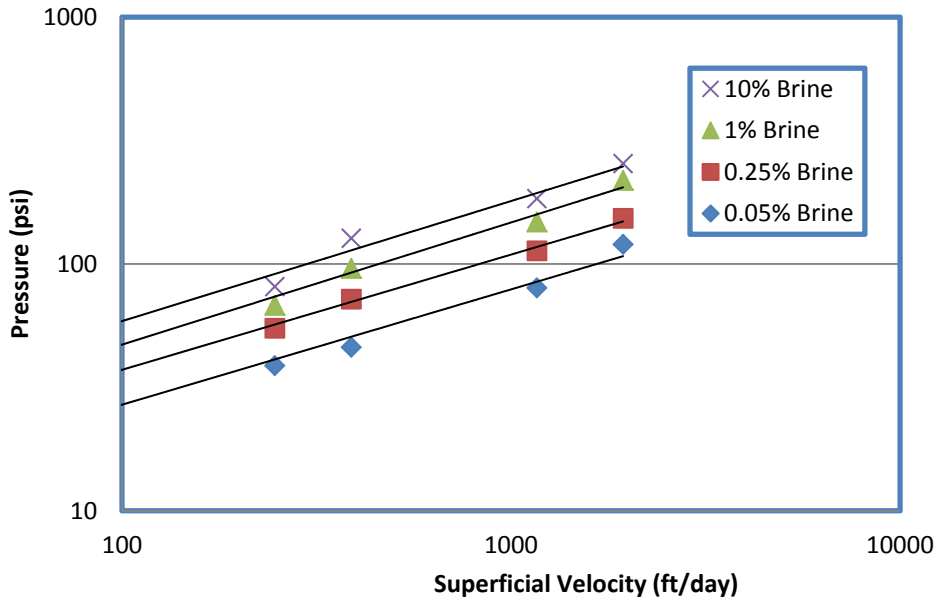

Figure 4-29 Pressure versus superficial velocity for 0.0345 inch tube on log-log plot.

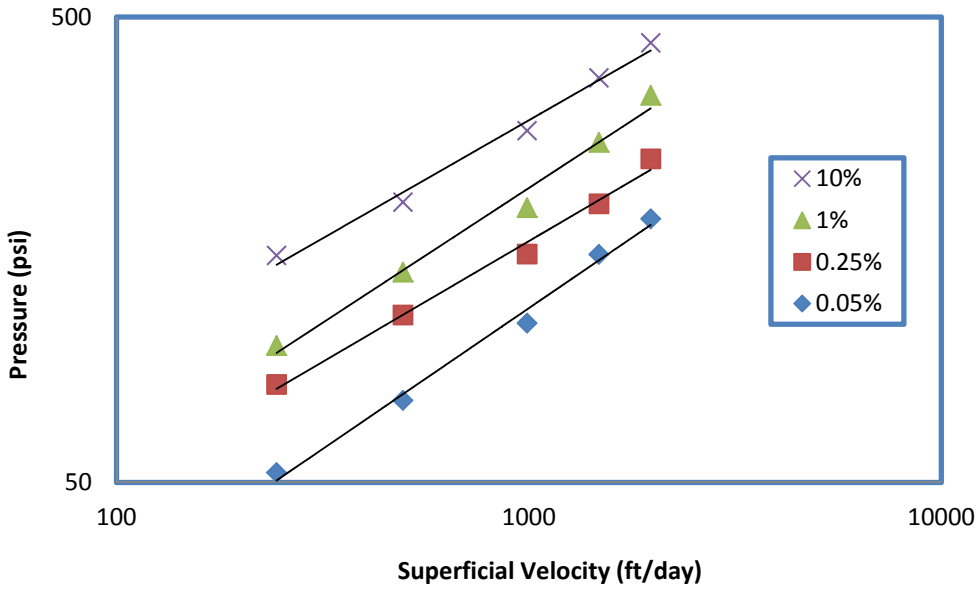

Figure 4-30 Pressure versus superficial velocity for 0.0275 inch tube on log-log plot.

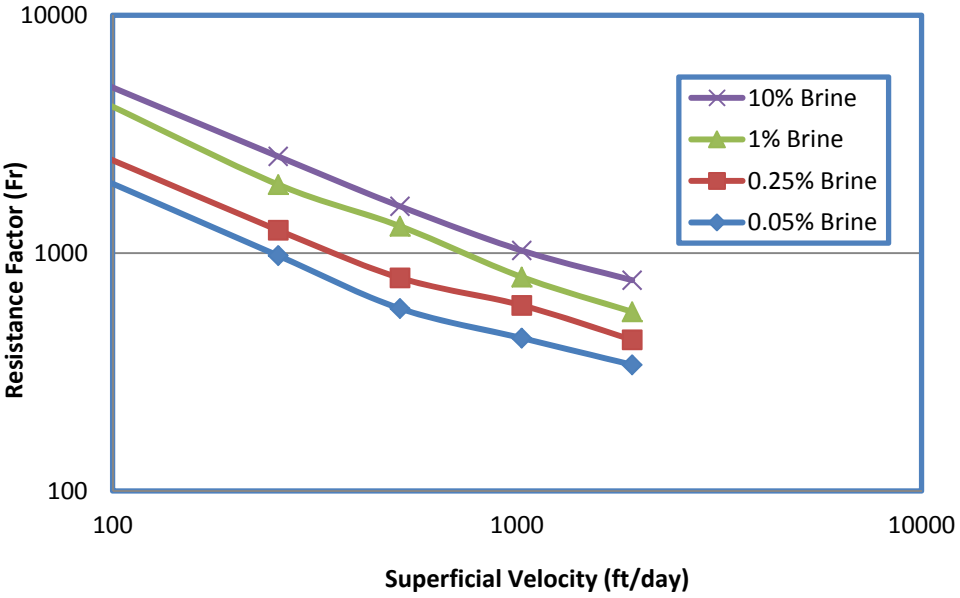

Figure 4-31 Resistance factor versus superficial velocity for various brine concentrations of PPG in 0.06 inch tube.

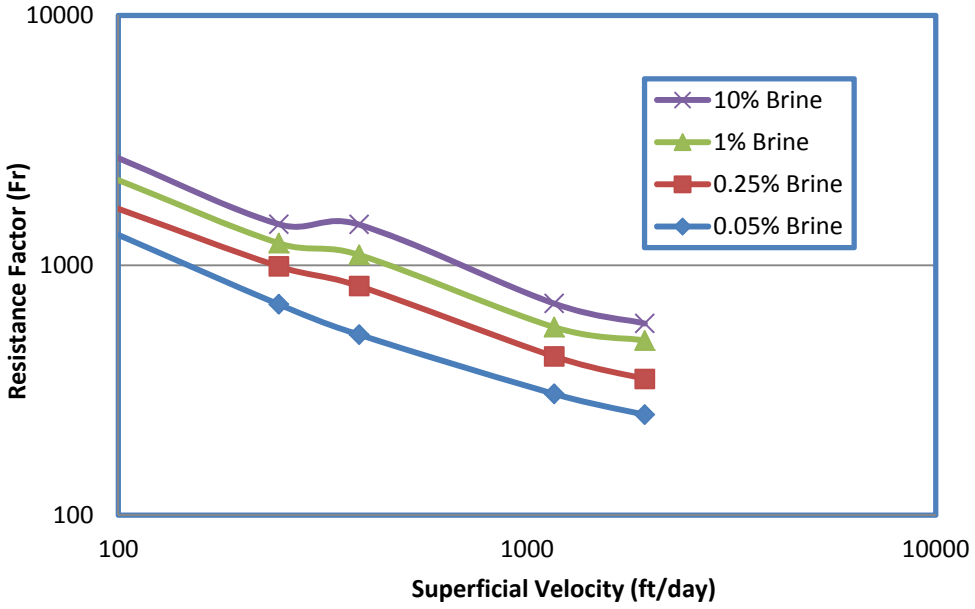

Figure 4-32 Resistance factor versus superficial velocity for various brine concentrations of PPG in 0.0345 inch tube.

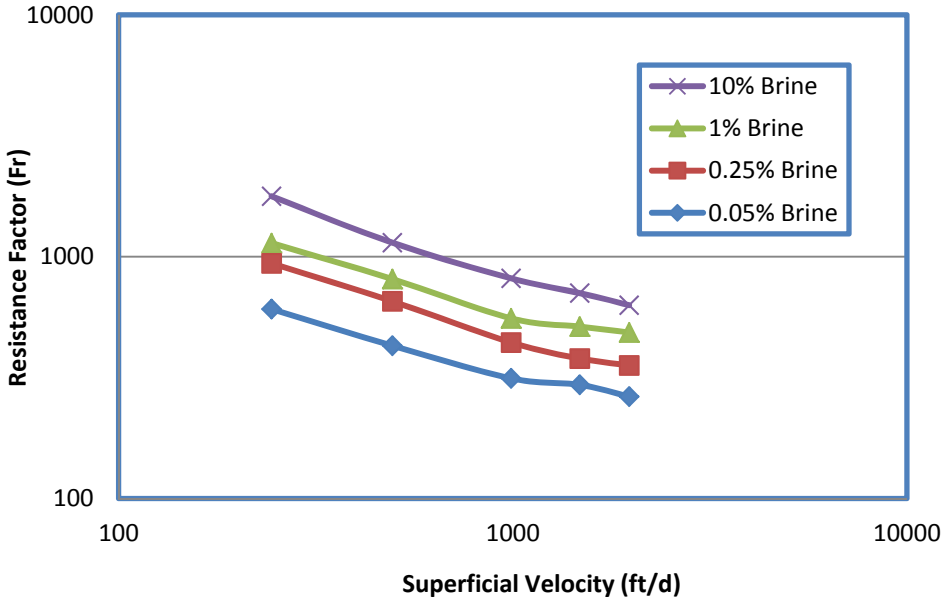

Figure 4-33 Resistance factor versus superficial velocity for various brine concentrations of PPG in 0.0275 inch tube.

Table 4-1 Summary of Experiments

Brine Concentration	SS-T4-S-065-20 (0.06inch)	SS-T2-S-028-20 (0.0345inch)	SS-T2-S-028-20 (0.0275inch)	SS-T1-S-011-5 (0.02025inch)	SS-T1-S-016-5 (0.01525inch)
0.05%	X	X	X	X	X
0.25%	X	X	X	X	*
1%	X	X	X	*	*
10%	X	X	X	*	*

* No data available. The apparatus designed for these experiments was not able to withstand pressures higher than above 700 psi.

Table 4-2 Properties of Tubes

	Tubing	Outer Diameter (inch)	Wall Thickness (inch)	Internal Diameter (inch)	Internal Radius (inch)	Area ($inch^2$)	Ai/A1
1	SS-T4-S-065-20	(1/4)	0.065	0.12	0.06	0.0113	3.0245
2	SS-T2-S-028-20	(1/8)	0.035	0.069	0.0345	0.0037	1.0000
3	SS-T2-S-035-6ME	(1/8)	0.028	0.0550	0.0275	0.0023	0.6353
4	SS-T1-S-011-5	(1/16)	0.011	0.0405	0.02025	0.0012	0.3445
5	SS-T1-S-016-5	(1/16)	0.016	0.0305	0.01525	0.0007	0.1953

Table 4-3 Flow Rates for each Tube

	Tubing	Flow Rate Q (ml/min)								
1	S-T4-S-065-20	3.0246	2.2684	1.5123	0.7561	0.3781	0.3025	0.1512	0.0756	0.0151
2	S-T2-S-028-20 (1/8)	1	0.75	0.5	0.25	0.125	0.1	0.05	0.025	0.005
3	S-T2-S-035-6ME (1/8)	0.6354	0.4765	0.3177	0.1588	0.0794	0.0635	0.0318	0.0159	0.0032
4	S-T1-S-011-5 (1/16)	0.3445	0.2584	0.1723	0.0861	0.0431	0.0345	0.0172	0.0086	0.0017
5	S-T1-S-016-5 (1/16)	0.1954	0.1465	0.0977	0.0488	0.0244	0.0195	0.0098	0.0049	0.0010

(1 ml/min = 3.66 $in.^3$/hr)

Table 4-4 Superficial Velocity and Water Injection Pressure for SS-T4-S-065-20 (0.06 inch) Tube

SS-T4-S-065-20 (0.06 inch)			
Q (ml/min)	Q (ft^3/day)	V (ft/day)	ΔP(water b)
3.0246	0.15	1925.2320	0.1430
2.2684	0.12	1540.1856	0.1144
1.5123	0.08	1026.7904	0.0763
0.7561	0.04	513.3952	0.0381
0.3781	0.02	256.6976	0.0191
0.3025	0.0154	197.6572	0.0147
0.1512	0.0077	98.8286	0.0073
0.0756	0.0038	48.7725	0.0036
0.0151	0.0008	10.2679	0.0008

Table 4-5 Superficial Velocity and Water Injection Pressure for SS-T2-S-028-20 (0.0345 inch) Tube

SS-T2-S-028-20 (0.0345 inch)			
Q (ml/min)	Q (ft^3/day)	V (ft/day)	ΔP(water b)
1	0.05	1941.0026	0.4362
0.75	0.04	1552.8021	0.3489
0.5	0.03	1164.6016	0.2617
0.25	0.01	388.2005	0.0872
0.125	0.0064	246.8955	0.0555
0.1	0.0051	197.5941	0.0444
0.05	0.0025	98.6029	0.0222
0.025	0.0013	49.3015	0.0111
0.005	0.0003	9.7050	0.0022

Table 4-6 Superficial Velocity and Water Injection Pressure for SS-T2-S-028-20 (0.0275 inch) Tube

SS-T2-S-028-20 (0.0275inch)			
Q (ml/min)	Q(ft^3/day)	V (ft/day)	ΔP(water b)
0.6354	0.0323	1973.4742	0.6980
0.4765	0.0242	1478.5782	0.5229
0.3177	0.0162	989.7920	0.3501
0.1588	0.0081	494.8960	0.1750
0.0794	0.004	244.3931	0.0864
0.0635	0.0032	195.5145	0.0691
0.0318	0.0016	97.7572	0.0346
0.0159	0.0008	48.8786	0.0173
0.0032	0.0002	12.2197	0.0043

Table 4-7 Superficial Velocity and Water Injection Pressure for SS-T1-S-011-5 (0.02025 inch) Tube

SS-T1-S-011-5 (0.02025 inch)			
Q (ml/min)	Q(ft^3/day)	V (ft/day)	ΔP(water b)
0.344	0.0175	1970.7615	1.2854
0.258	0.0131	1478.3528	0.9642
0.172	0.0088	985.9441	0.6431
0.0861	0.0044	493.5355	0.3219
0.0431	0.0022	246.7677	0.1610
0.0345	0.0018	197.1888	0.1286
0.0172	0.0009	99.1578	0.0647
0.0086	0.0004	49.5789	0.0323
0.0017	0.0001	10.1411	0.0066

Table 4-8 Superficial Velocity and Water Injection Pressure for SS-T1-S-016-5 (0.01525 inch) Tube

SS-T1-S-016-5 (0.01525 inch)			
Q (ml/min)	Q(ft^3/day)	V (ft/day)	ΔP(water b)
0.1954	0.0099	1974.8813	2.2712
0.1465	0.0075	1480.1676	1.7023
0.0977	0.0050	987.4407	1.1356
0.0488	0.0025	492.7269	0.5667
0.0244	0.0012	246.3635	0.2833
0.0195	0.0010	196.6934	0.2262
0.0098	0.0005	99.3401	0.1142
0.0049	0.0003	49.6701	0.0571
0.001	0.0001	9.9340	0.0114

Table 4-9 Fitting Equations for Stable Pressure versus Superficial Velocity for all Brine Concentrations

Brine Concentration	Tube Radius (inch)	Fitting Equations	R^2
0.05%	0.06	$y = 2.0648x^{0.4038}$	0.95
	0.0345	$y = 1.4933x^{0.5587}$	0.98
	0.0275	$y = 1.8117x^{0.6051}$	0.99
	0.02025	$y = 1.0709x^{0.7539}$	0.99
	0.01525	$y = 7.3209x^{0.5335}$	0.99
0.25%	0.06	$y = 2.4545x^{0.4189}$	0.97
	0.0345	$y = 4.3431x^{0.4667}$	0.99
	0.0275	$y = 4.5806x^{0.5188}$	0.99
	0.02025	$y = 9.5928x^{0.4838}$	0.99
1%	0.06	$y = 6.3314x^{0.3303}$	0.98
	0.0345	$y = 4.829x^{0.4947}$	0.98
	0.0275	$y = 3.9273x^{0.5792}$	0.98
10%	0.06	$y = 6.6995x^{0.3605}$	0.98
	0.0345	$y = 6.2483x^{0.4864}$	0.97
	0.0275	$y = 9.0137x^{0.5074}$	0.98

Table 4-10 Fitting Equations for Stable Pressure versus Superficial Velocity for all Tubes

Tube Radius (inch)	Brine Concentration	Fitting Equations	R^2
0.06	0.05%	$y = 2.0648x^{0.4038}$	0.95
	0.25%	$y = 1.7091x^{0.4717}$	0.99
	1%	$y = 6.3314x^{0.3303}$	0.98
	10%	$y = 6.6995x^{0.3605}$	0.98
0.0345	0.05%	$y = 3.1266x^{0.4673}$	0.97
	0.25%	$y = 4.3431x^{0.4667}$	0.99
	1%	$y = 4.829x^{0.4947}$	0.98
	10%	$y = 6.2483x^{0.4864}$	0.97
0.0275	0.05%	$y = 1.8117x^{0.6051}$	0.99
	0.25%	$y = 4.5806x^{0.5188}$	0.99
	1%	$y = 3.9273x^{0.5792}$	0.98
	10%	$y = 9.0137x^{0.5074}$	0.98

5. Preformed Particle Gel Transport through Transparent Open Fractures and its Effect on Water Flow

5.1. Summary

We constructed transparent fracture models to visually track swollen preformed-particle-gel (PPG) propagation through open fractures and water flow through PPG placed in the fractures. Results of these experiments are discussed in Chapter 5. During injection, PPG propagated like a piston along a fracture and a gel pack was formed in the fracture. When water broke through the particle-gel pack after PPG placement, several channels were created that discharged water from the outlet while water was being injected. Investigation of factors that influence PPG injectivity and plugging efficiency revealed that PPG injectivity increases with increasing fracture widths and flow rates but decreases with increasing brine concentrations (on which the PPG swelling ratio depends). PPG can reduce the permeability for fractures with different widths to the same level. Full-factorial experimental design analysis was performed to rank the influence of injection rate, fracture width, and PPG swelling ratio on pressure response, resistance factors, and injectivity.

5.2. Introduction

Optimization of the gel treatment design requires knowledge of the behavior of these gels when they extrude through fractures or channels. Seright (2001, 2004; Seright and Lee 1999) has extensively investigated the extrusion of bulk gels through fractures and tubes. He studied the effects of fracture conductivity, tube diameter, and gel-injection rates on this extrusion behavior. Researchers at the University of Kansas have also conducted extensive studies to understand the propagation of bulk gels through fractures, tubing, and high-permeability sandpack and to determine how water injected into a gel can rupture that gel and form a flow path to conduct water (Al-Assi et al. 2009; McCool and Willhite 2009; Ganguly et al. 2001). Experimental results have also been reported on deformable-particle-gel transportation through porous media. Bai et al. (2007a, 2007b) studied swollen-particle-gel transportation through porous media using sandpack and micromodels, and Rousseau et al. (2005) investigated microgel movement through

sandpacked porous media. They conducted all coreflooding tests related to particle gels in porous media without open fractures. However, no laboratory results have been reported on the transportation behavior of particle gels through fractures and their effects on water flow.

The objective of this study is to visualize PPG propagation through fractures and determine which factors affect particle gel injectivity significantly. Transparent models with open fractures were designed using two glass plates that were not permeable. Ideally, permeable materials should be used to construct fracture models. Leakage significantly affects gel propagation and distribution in fractures because of changes in gel concentration and strength caused by dehydration (Seright 2001). Although we realize the importance of leakoff, visualization was important for our current study; therefore, we could not incorporate leakoff in these experiments. The consequences of leakoff for the PPG system will be studied in next chapter.

5.3. Experiments

5.3.1. Materials

The same commercial superabsorbent polymer, LiquiBlock 40K Series, provided by Emerging Technologies, was selected as a PPG for these experiments. The main component of the PPG is a potassium salt of crosslinked polyacrylic acid or polyacrylamide copolymer. In aqueous solutions, PPG can absorb a large amount of water because of a hydrogen bond with the water molecules, although the concentration of sodium chloride affects its capacity to absorb water. Four swollen-PPG samples were prepared using four different brine concentrations (0.05, 0.25, 1, and 10%) with swelling ratios of 194, 98, 52, and 32, respectively. Fully swollen PPGs, without excess (free) water, were used for all experiments. The particle concentration varied, depending on brine concentration. The PPG concentrations were calculated using the initial weight of the dry PPG, divided by the final weight of swollen PPG, as listed in Table 5-1.

The swollen PPG, without excess water, was prepared as follows.

1. An empty beaker was partially filled with the desired concentration of brine.

2. Depending on the brine concentration, 10–20 gram (0.35-0.70 oz) of the dry PPG was slowly added to the brine solution. The mixture was then stirred for 5–10 minutes.

3. The sample was allowed to swell completely with evidence of the existence of excess water. The process took approximately 2–3 hours.

4. The excess brine solution was separated from the swollen PPG by placing the latter on a 150-mesh screen and then collecting the swollen PPG for coreflooding experiments.

5.3.2. Experimental Setup

Figure 5-1 is a flow chart of the experimental setup, which was composed of two syringe pumps, one accumulator with a piston, and one fracture model. Two Isco pumps were used, one for PPG injection and the other for brine injection. The fracture model was constructed of two acrylic plates with a rubber O-ring between them. Bolts, nuts, and shims were used to fix the two plates and control fracture width. On one side of the plate, a hole functioned as an inlet for the injection of fluids and PPG; on the other side, another hole provided an outlet to discharge fluids and PPG. The pressure transducers were connected at the inlet to record the fracture pressure. The model was transparent so that the PPG and water movement would be clearly visible. The dimensions of the model were 55 cm (21.7 in.) in length and 10 cm in height. Three fracture widths (0.5, 1.0, and 1.5 mm or 0.02, 0.04, 0.06 in.) were used to examine the effect of fracture size on gel placement. The inside diameter of the tube leading into the fracture was approximately ¼ in., and its length was 4 in. A metal connector with an internal diameter of ⅜ in. and a length of less than 1 in. was used to discharge the fluids from the outlet.

5.3.3. Experimental Procedure

Brine was first injected into the fracture model, and then fully swollen PPG was extruded into the fracture model by an Isco pump through an accumulator. Six flow rates were used for each experiment: 5, 10, 15, 20, 25, and 30 ml/min (18.3, 36.6, 54.9, 73.2, 91.5, and 109.8 $in.^3$/hr, respectively). The flow rates were tested in sequence (from lowest to highest) to obtain the corresponding stabilized pressure during gel injection. Once the gel was in place, water was injected into the gel particles packed in the fracture to test the efficiency of gel plugging on water. During these experiments, the brine-injection rates

were the same as those used during gel injection. The pressure data were recorded to check the pressure changes over time and the injection rates.

5.4. Results and Analysis

5.4.1. Swollen PPG Injection

Twelve experiments were run to study the effect of brine concentration, fracture width, and injection rate on PPG injection pressure, resistance factor, and injectivity. Particle movement through the fracture was monitored visually during PPG injection.

5.4.1.1 Observed Particle Movement during PPG injection

Figure 5-2 shows the particle movement during placement of the swollen PPG in the fracture model. The PPG propagated like a piston along the fracture. Gravity did not change the shape of the PPG front, perhaps because the fracture widths used here were smaller than, or similar to, the size of the swollen particles.

5.4.1.2 Effect on Injection Pressure

Figure 5-3 shows the effect of brine concentration and flow rate on PPG-injection pressure in three fracture models with fracture widths of 0.5, 1.0, and 1.5 mm (0.02, 0.04, and 0.06 in.).

Brine concentration effect. For a fracture model of given width, the PPG-injection pressure consistently increased with an increase brine concentration, provided the injection flow rate remained constant. The injection pressure for the sample prepared with a low-salinity brine was expected to be higher than that prepared with a high-salinity brine because swollen particles are larger with low-concentration brine than they are with high-concentration brine. However, the experimental results showed a completely different trend. The softness or deformability of swollen PPG particles proved to have a greater effect on injection pressure than did particle size because the swollen particles were softer or more deformable in low-salinity brine than in high-salinity brine, thereby promoting lower injection pressure. As seen in Table 5-1, the PPG concentrations in high-concentration brines were larger than those in low-concentration brines, which could also explain why PPG had higher injection pressures in higher concentration brines.

Flow rate effect. Figure 5-3 indicates that the PPG-injection pressure increased as the injection flow rate increased, but the degree of its increase was not as great as that of

the injection rate. For example, for the model with a fracture width of 0.5 mm (0.02 in.), the injection pressure increased only from 110 to 133 psi, while the flow rate doubled from 15 to 30 ml/min (54.9 to 109.8 in.^{3}/hr) with an injection of PPG prepared with 10% brine solution. For the model with a fracture width of 1.0 mm (0.04 in.), the injection pressure increased only from 108 to 126 psi while the flow rate doubled from 15 to 30 mL/min (54.9 to 109.8 in.^{3}/hr) with the injection of PPG prepared with a 10% brine solution. This trend is entirely consistent with the practical findings regarding PPG injections in oil fields, where injection pressure does not increase significantly with an increase in the injection pumping rate (Bai et al. 2007a). As shown in Figure 5-4, the data in Figure 5-3 were plotted on a log-log scale and, for a given brine concentration and fracture width, the relationship between the injection pressure and flow rate can be fitted well by a power-law equation:

$$P = K_1 q^{n_1} \tag{5-1}$$

where p is the PPG-injection pressure in psi, q is the flow rate in mL/min or in.^{3}/hr, and K_1 and n_1 are constants related to brine concentration and fracture width, respectively. Table 5-2 lists the 12 fitting equations and their correlation factors using the power-law model. All correlation factors are greater than 0.99.

Fracture width effect. A comparison of the three plots in Figure 5-3 indicates that, for a given flow rate and brine concentration, PPG-injection pressure decreases as the fracture width increases. The wider fracture is more conductive and, thus, reduces the injection pressure. One possible reason that the pressures are not sensitive to fracture width is that PPG particle size was larger than or similar to the fracture width in our experiments and the acrylic-plate surface was very smooth. The weak friction between the fracture wall and the particles might have led to the injection-pressure insensitivity to fracture width.

Ranking of three parameters on pressure response. This work analyzed a general full-factorial design to evaluate the influence of injection flow rate, fracture width, and PPG swelling ratio (dependent on brine concentration) on pressure response. A full-factorial experiment is one that addresses two or more factors, each with discrete values or "levels" and experimental units that take on all possible combinations of these levels across all factors. A full-factorial design may also be called a fully crossed design. Such

experiments permit the study of the effects of each factor (and interactions among factors) on the response variable. A general full-factorial design is used when any experimental factor has more than two levels because this design can determine which factors most influence the response.

Figure 5-5 shows a Pareto plot of the results of factorial design analysis. As this plot indicates, the flow rate proved to be the most influential factor on pressure. The swelling ratio was the least influential factor among the three, but its influence was similar to that of fracture width. Figure 5-5 also shows the main relationship between the factors and the response: A positive value indicates that the response will increase with an increase in a given parameter, and a negative value indicates that the response will decrease with an increase in a given parameter. Pressure increases with an increase in flow rate and decreases with an increase in fracture width or swelling ratio.

5.4.1.3 Effect on resistance factor

The resistance factor is the ratio of the particle-gel-injection pressure drop to the water-injection pressure drop at the same flow rate. It is a kind of effective viscosity of gel in porous media relative to that of water. In the experiments described here, because the outlet of the fracture was open, the recorded injection pressure could be viewed as the pressure drop for gel injection. Because the water-injection pressures in these fracture models were very low before gel injection and could not be recorded accurately, the following equation was used to calculate the water pressure drop in the fracture:

$$\Delta P_w = \frac{12\mu Lq}{hw^3} \tag{5-2}$$

where ΔP_w is the water pressure drop, μ is the viscosity of water, L is the fracture length, q is the injection flow rate, h is the fracture height, and w is the fracture width. The resistance factor was calculated from the data in Figure 5-3 and the results are shown in Figure 5-6.

Brine concentration effect. Each plot in Figure 5-6 demonstrates that the resistance factor increases with the increase in brine concentration, which indicates that the excess-water-free swollen PPG prepared with a high-concentration brine has a higher effective viscosity in porous media than that prepared with a low-concentration brine.

Flow rate effect. Figure 5-6 also shows that the resistance factor decreases with an increase in the flow rate, which indicates that the effective viscosity of PPG decreases

with an increase in injection rate. This relationship is explained by the elastic nature of PPG, which behaves as a shear-thinning fluid during its flow through a porous fracture. The relationship between the resistance factor and the flow rate can also be fitted well with a power-law equation in the following format:

$$F_r = K_2 q^{n_2} \tag{5-3}$$

where F_r is the resistance factor, q is the flow rate in ml/min or in.^{3}/hr, and K_2 and n_2 are constant coefficients. Table 5-5 lists the 12 fitting equations and their correlation factors, which clearly follow the power law equation very well.

Fracture width effect. A comparison of the three plots in Figure 5-6 demonstrates that the resistance factor increases with fracture width, which is consistent with the behavior of bulk gel in fractures and porous media (Seright 2001; Seright and Martin 1993). However, the results directly contradict the standard assumption that the narrower a fracture is the more resistance forces exist for the gel to pass through. However, a resistance factor is defined as the pressure drop of a PPG injection divided by the pressure drop of a water injection in the same fracture. The water pressure drop is inversely proportional to the cubed fracture width; therefore, the water pressure drop decreases significantly when the fracture width increases. This decrease causes a significant increase in the resistance factor of a wider fracture. It also means that the effective viscosity of the PPG increases with an increase in fracture width.

Ranking on resistance factor response. According to the Pareto plot shown in Figure 5-7, fracture width had the strongest influence on the resistance factor and the swelling ratio was the least influential factor among the three. The resistance factor increased with an increase in fracture width, but it changed inversely with regard to the flow rate and swelling ratio.

5.4.1.4 Effect on injectivity

Injectivity, defined as the flow rate divided by the pressure, is an important measure of the difficulty of injecting a gel. Higher injectivity means that injection is easier. Figure 5-8 indicates that injectivity decreases with brine concentration, meaning that excess-water-free swollen PPG prepared with a lower-concentration brine is easier to inject into a fracture than that prepared with a high-concentration brine. Because the swollen particle size is larger and more deformable in a low-concentration brine than in a

high-concentration brine, the deformability of swollen particles influences PPG injectivity more strongly than particle size. PPG injectivity is highly dependent on flow rate and increases linearly with an increase in flow rate, as shown in Figure 5-8. This relationship is totally different from water injection. According to Darcy's law, the injectivity for water should be independent of flow rate. The difference between water injection and PPG injection is caused by the fact that water is a Newtonian fluid but PPG is a pseudoplastic material. PPG injectivity increases with greater fracture width.

Ranking on injectivity response. According to the Pareto plot shown in Figure 5-9, flow rate is the factor that most strongly influences injectivity. Swelling ratio is the least influential factor among the three, but its influence is similar to that of fracture width. The resistance factor increases with increases in flow rate, fracture width, and swelling ratio.

5.4.2. Brine Injection after Gel Placement

5.4.2.1 Observed Particle Movement

Figure 5-10 shows the water flow paths in a fracture after gel placement. PPG was packed in the whole fracture after PPG injection. When water was injected, it broke through the permeable gel pack and formed several channels (or major water paths) to allow water to discharge through the outlet.

5.4.2.2 Effect of brine injection cycles and flow rates

Three cycles of brine injection were conducted to compare the pressure responses at different flow rates. Each cycle consisted of six flow rates (5, 10, 15, 20, 25, and 30 mL/min, or 18.3, 36.6, 54.9, 73.2, 91.5, and 109.8 $in.^3$/hr, respectively), used in sequence. Injection pressure was recorded during the process, and the flow rate was changed only when a steady-state pressure was achieved. Figure 5-11 shows typical examples of pressure responses for three cycles of brine injection; this represents the pressure trend over time in each cycle. The results were obtained from a 0.5-mm-wide fracture (0.02 in.) model with a 0.25%-brine injection after packing with swollen PPG that had been prepared with 0.25% brine. With the first cycle, the injection pressure rapidly increased to 48 psi then dropped steadily to 7 psi and stabilized. When the flow rate was increased from 5 to 10 mL/min (18.3 to 36.6 $in.^3$/hr), the pressure rapidly increased again, reaching 32 psi then dropping and stabilizing at 5 psi. During the first cycle, the trend in pressure

change was similar, regardless of flow rate, but the pressure increase became slower when the flow rate was increased. The trends in pressure changes in the second and third cycles were not the same as that in the first cycle. The pressure increased to a stabilized value at which the flow rate increased. The overall pressure in the second and third cycles was lower than that in the first cycle. Figure 5-12 shows the stabilized pressure at different flow rates as a function of flow rate for each of the three cycles of brine injection. In the first cycle, the stabilized pressure first decreased and then increased with the flow rate because brine broke through the particle-gel pack and formed water channels for the lowest flow rates. With an increase in flow rate, more and larger channels were formed. Eventually, enough channels had formed and brine mainly passed through the existing channels, creating few new channels even though the flow rate continued to increase. As a result, the pressure increased with the flow rate in conjunction with the last few flow rates. Pressure in the second and third cycles was less than that during the first cycle. The second and third cycles showed similar pressure trends over time; that is, pressure increased with the flow rate. The pressure in the third cycle also increased (almost linearly) with the flow rate, indicating that stationary channels had formed in the gel pack and water had passed through the solid channels. The elasticity of the gel did not affect the water flow.

Figure 5-13 shows plots of the residual resistance factor against the flow rate for three cycles. The residual resistance factor represents the reduction in the permeability of water as a result of gel. It was calculated by dividing the brine-injection pressure drop after gel placement by the brine-injection pressure drop before gel injection. For the first cycle of brine injection, the residual resistance factor initially decreased with the increase in flow rate, but it tended to be constant at higher flow rates. This trend was caused by an increasing number of water channels in the gel during the waterflooding process. With more water channels in the gel, the resistance force for brine injection should have decreased. When stable water channels formed, the resistance factors should not have been much affected by the flow rates because the reduction in water permeability caused by gel did not change much, as shown in the third-cycle curve. The three cycle curves indicate that the reduction in the permeability of water caused by PPG decreased with each cycle of brine injection until stable water channels formed in the third cycle.

5.4.2.3 Effect of Brine Concentration

Figure 5-14 shows the stabilized pressure vs. flow rates for given brine concentrations and fracture widths during the first cycle of brine injection. With a higher brine concentration, the pressure stabilized at a higher level for a given flow rate and given fracture width, indicating that PPG prepared with high-concentration brine has a higher plugging efficiency than that prepared with low-concentration brine. This can be explained by the fact that a gel concentration in high-concentration brine is higher than that in low-concentration brine, as seen in Table 5-3.

Figure 5-15 shows the residual resistance factor as a function of flow rate. This residual resistance factor increased with an increase in brine concentration, indicating a greater reduction in water permeability caused by gel prepared with high-concentration brine. With an increase in the flow rate, however, the residual resistance factor was reduced because more channels formed after the flow rate increased.

5.4.2.4 Effect of Fracture Width

Figure 5-14 compares the pressures at various fracture widths when the flow rates and brine concentrations remain the same. This demonstrates that the stabilized pressure decreased as the fracture width increased, but the difference was slight. Fig. 15 compares the residual resistance factors, indicating that resistance is much higher in a wider fracture than that in a narrower fracture. The pressure and residual resistance pressure data show that the particle gel can reduce fracture permeability to the same level, thereby mimicking the effects of in-situ gel on formations of varying permeability (Seright and Martin 1993).

5.5. Discussion and Future Work

For this set of experiments, we designed transparent models to visually observe particle-gel transport through open fractures. We also studied the effects of three key factors—brine concentration, injection rate, and fracture width—on particle injectivity and plugging efficiency. When our experimental apparatus was designed, we realized that the internal diameter of inlet and outlet tubes would have to be selected properly and their length minimized so that any pressure drop in the tubes would be negligible. Our calculations, using the Hagen-Poiseuille equation (Bird et al. 1960) and Equation 5-2, indicated that the flow capacity of our inlet line was 213 times greater than the flow

capacity of our 0.5-mm (0.02 in.) fracture and 7.7 times greater than that of our 1.5-mm (0.06 in.) fracture. Therefore, the pressure drop we obtained properly reflected the real pressure drop in the fractures.

In this study, we not only strived to understand the rheology of swollen PPG, but we also found that the particles were packed as porous media in fractures and that the permeability of the particle pack depended on the particle strength, particle size, brine concentration, and injection pressure. We expected that a particle pack with a desired permeability could be designed successfully by adjusting particle properties. This finding can significantly aid in optimizing the design of PPG treatments. Although we are reporting much new information, extensive work still needs to be performed to make our results more realistic. Additional work should include the following.

In this chapter, the swollen-particle sizes are the same as, or a little larger than, the fracture width, so the gravity segregation in our vertical fractures is negligible. Wider fractures will be used in future experiments to see how gravity changes the PPG movement and distribution. The dependence of flow rate on PPG gravity segregation in vertical open fractures also will be evaluated. In addition, models in this study were built using two pieces of acrylic plates with smooth surfaces. Plates with rough surfaces will be considered for further experiments.

New fracture models have been constructed in our laboratory using permeable sandstone. These models can be used not only to understand the effect of leakage on PPG propagation but also to evaluate whether PPGs have been damaged on a matrix. In these experiments, we injected a mixture of brine and swollen particles (at a designed ratio) to reflect different PPG concentrations. To prevent the separation caused by density differences between the brine and swollen particles, we used two pumps to deliver the brine and particles separately. The brine and particles were mixed together in the inlet tube of the fracture models and then transported to models with different fracture widths. Detailed results are reported in next chapter.

5.6. Conclusion

The following conclusions are based on our transparent-model experiment results, without considering potential leakage in real reservoirs, the smoothness/roughness of fracture surfaces, and swollen particles with excess water.

- PPG propagates like a piston along a fracture, and gravity does not change the PPG-front shape if the particle size is larger than, or close to, the fracture width.
- The injection pressure of excess-water-free fully swollen particles increases with increased brine concentration and injection flow rates but decreases as the fracture widens during PPG injection.
- PPG is a shear-thinning material that follows a power-law rheology equation during its flow through a fracture.
- The resistance factor increases with an increase in brine concentration and fracture width but decreases as the flow rate increases.
- Swollen PPG forms a gel pack after placement in a fracture, and injected brine breaks through the permeable gel pack to create several channels, allowing water to be discharged from the outlet.
- The reduction in water permeability caused by swollen PPG prepared with a high-concentration brine is much higher than that caused by a PPG prepared with a low-concentration brine.
- PPG can reduce the permeability of fractures of different widths to the same level, but more work needs to be performed to further confirm that this is true in all cases.
- Experimental design was used successfully to rank the effects of various parameters on PPG injectivity and resistance factors.

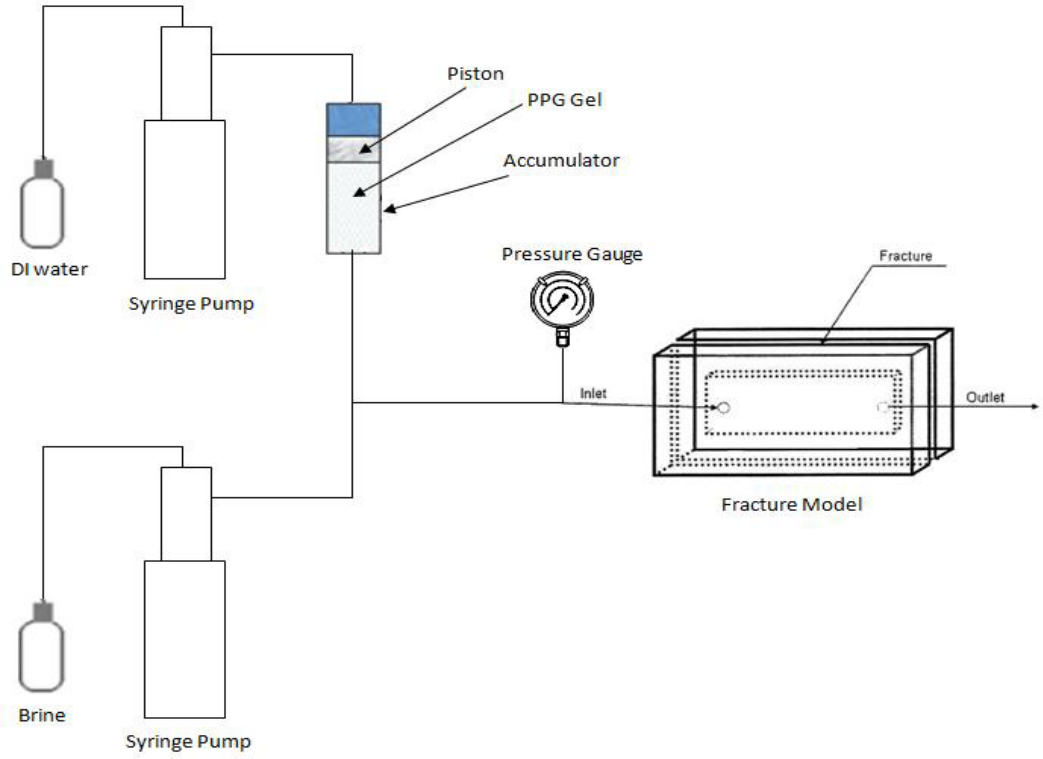

Figure 5-1 Diagram of PPG-injection setup.

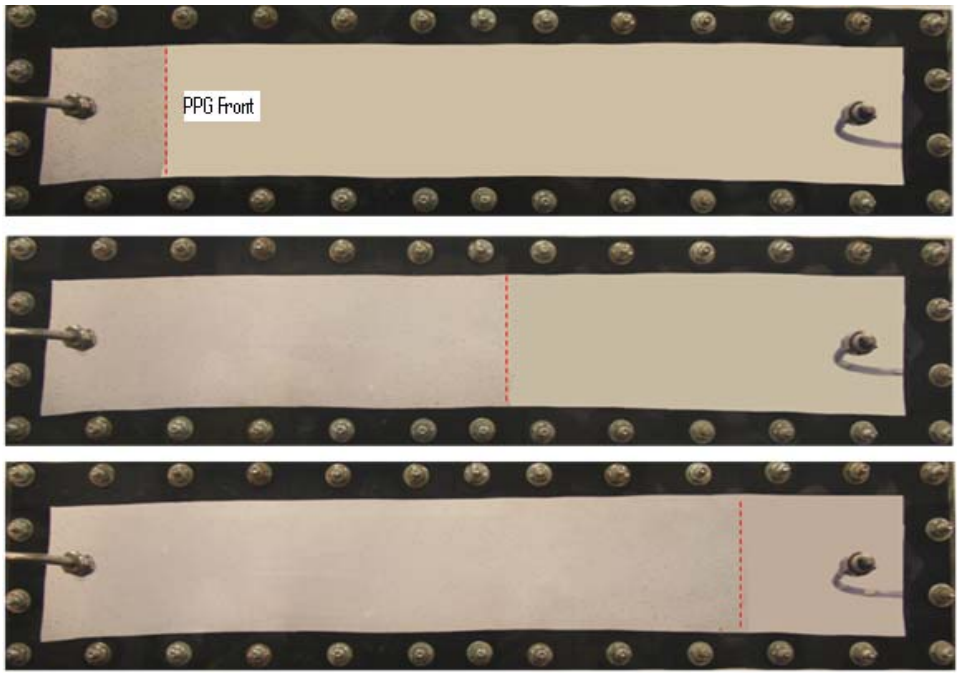

Figure 5-2 Gel movement during Gel Injection into a fracture.

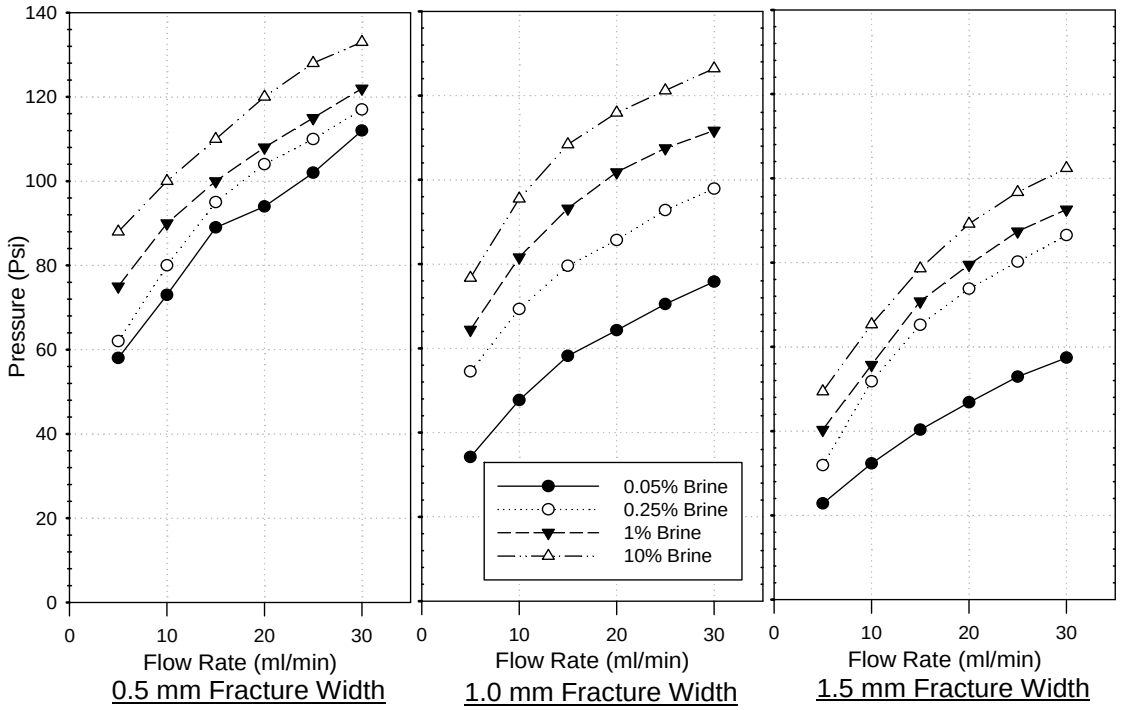

Figure 5-3 PPG injection pressure as a function of flow rate and brine concentration.
(1 ml/min = 3.66 in.^{3}/hr)

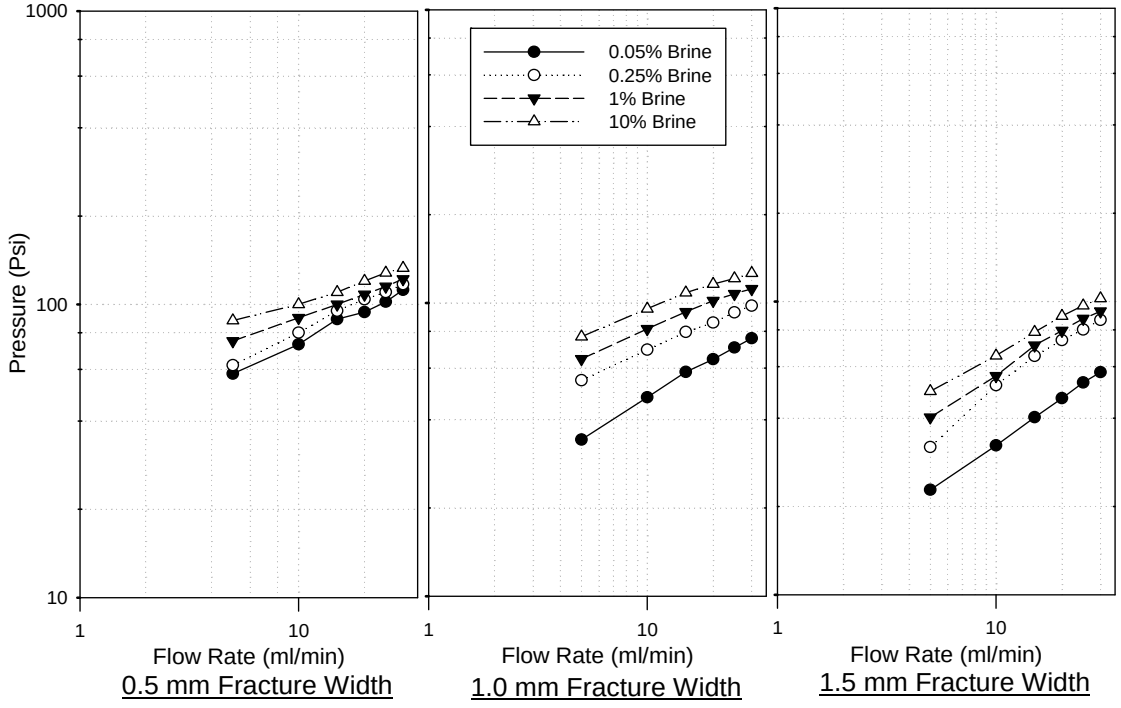

Figure 5-4 Injection pressure as a function of flow rate on log-log grid.
(1 ml/min = 3.66 in.^{3}/hr)

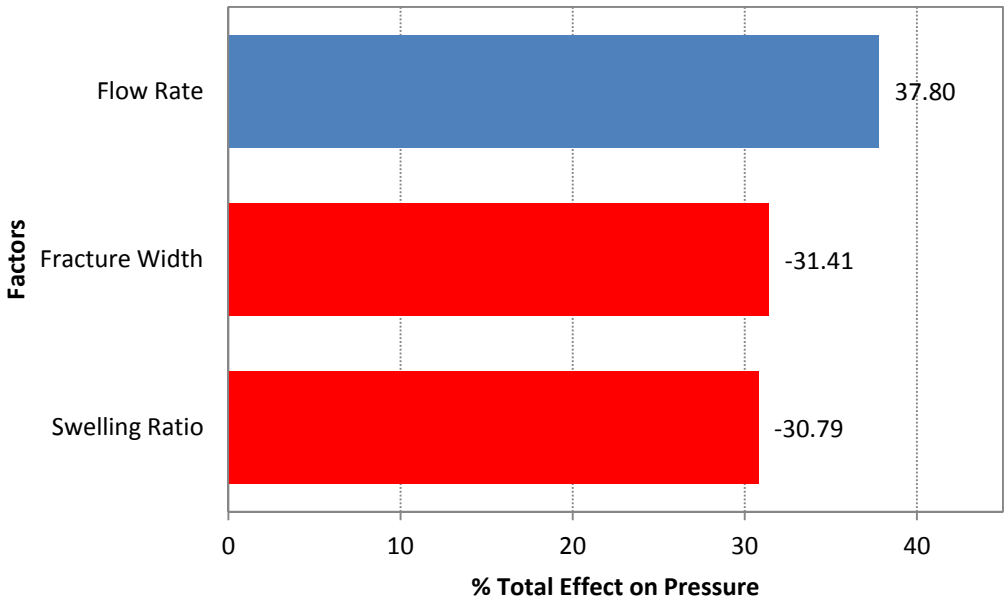

Figure 5-5 Pareto plot of injection pressure as a response.

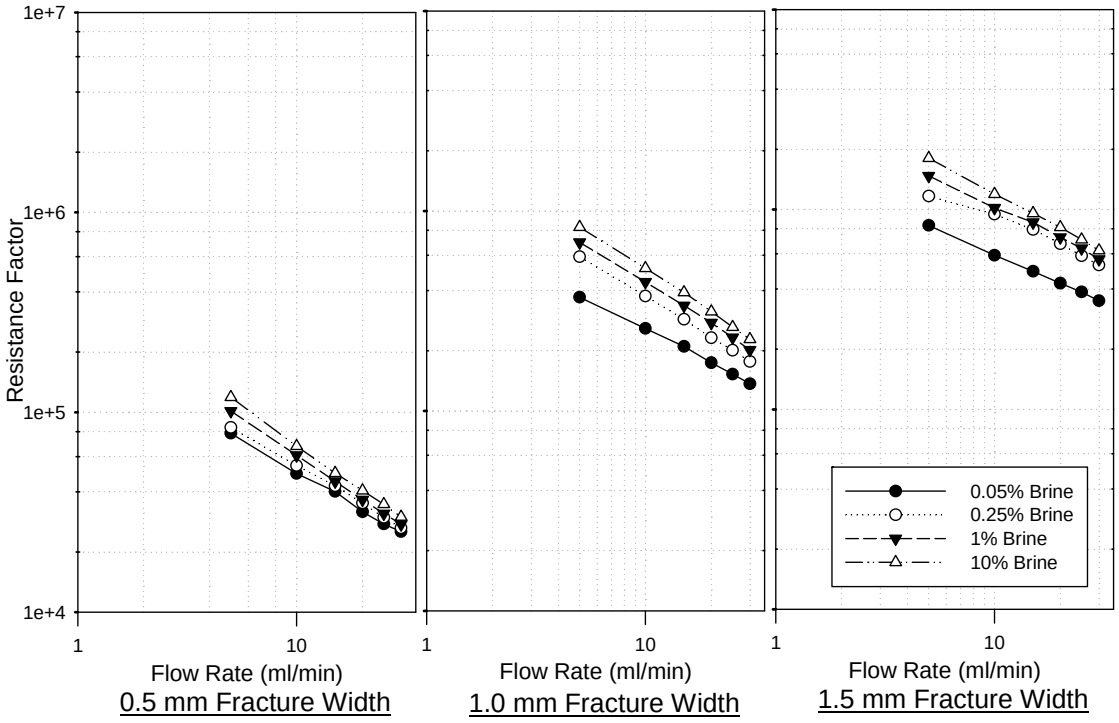

Figure 5-6 Resistance factor as a function of flow rate and brine concentration on a log-log grid.
(1 ml/min = 3.66 $in.^3$/hr)

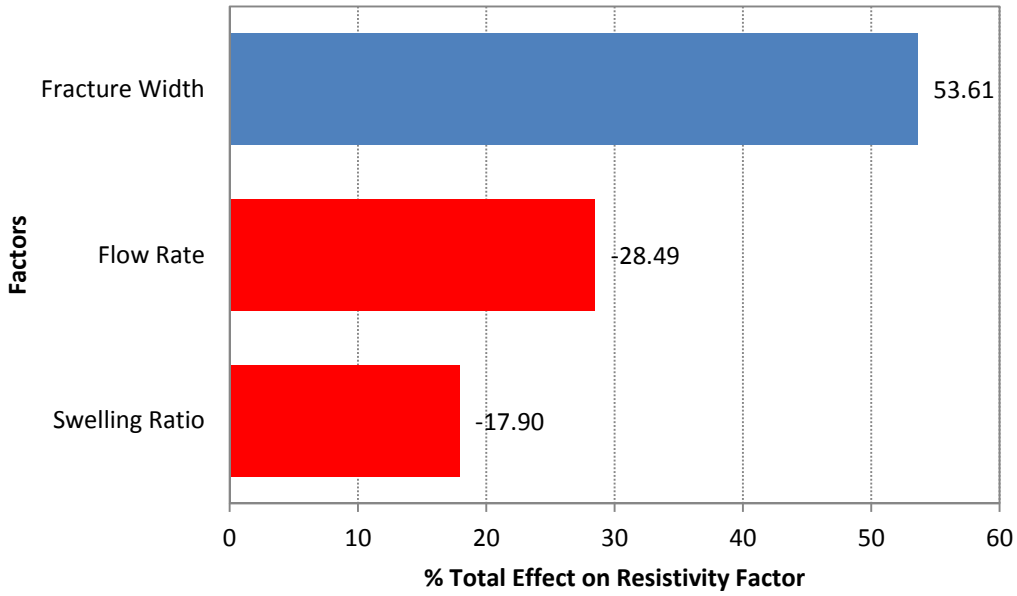

Figure 5-7 Pareto plot of the resistance factor as a response.

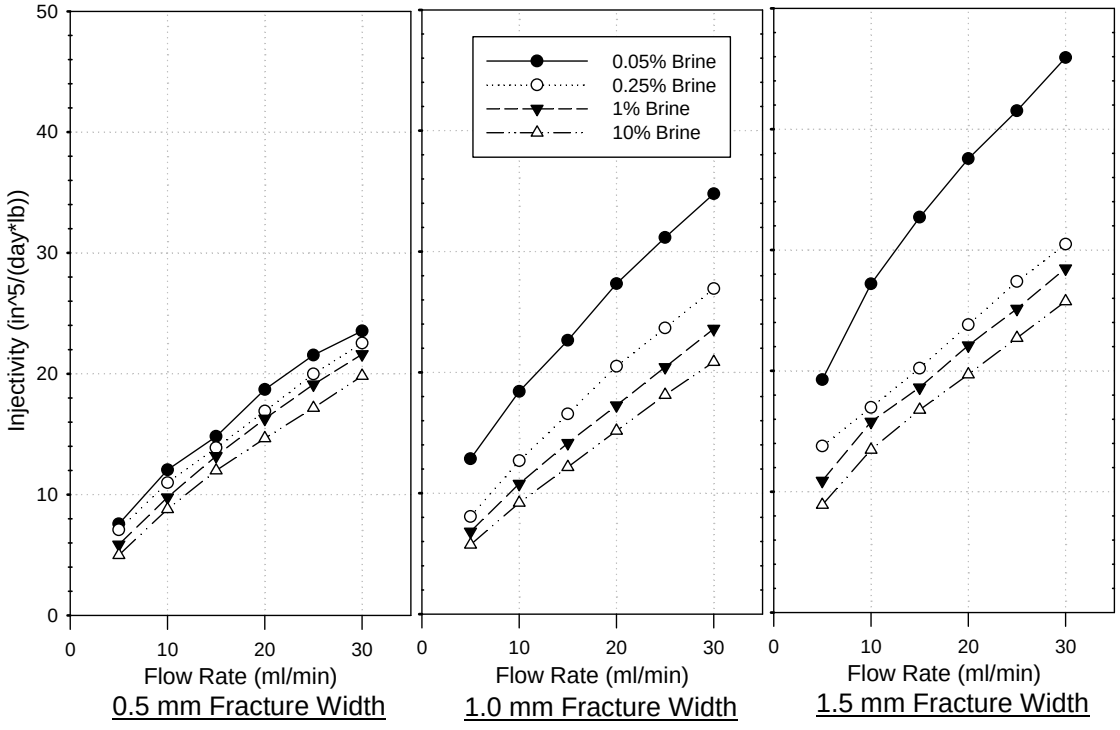

Figure 5-8 PPG injectivity as a function of flow rate and brine concentration.
(1 ml/min = 3.66 $in.^3$/hr)

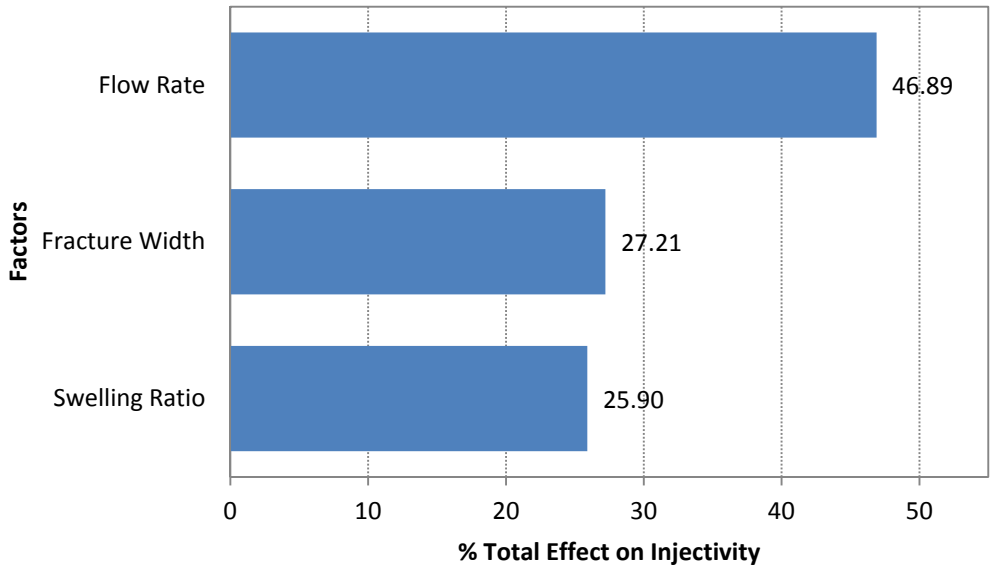

Figure 5-9 Pareto plot of injectivity as a response.

Figure 5-10 Brine movement during brine injection into a gel pack in a fracture.

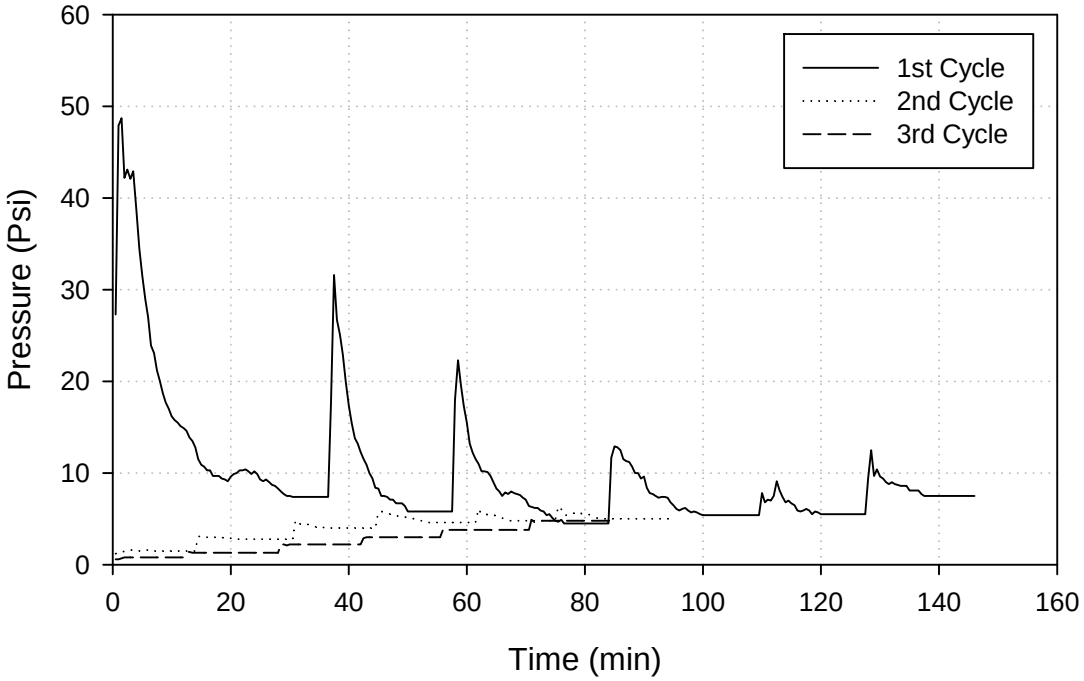

Figure 5-11 Pressure vs. time for three cycles of 0.25%-brine injection into a 0.5-mm fracture using different flow rates after PPG placement.

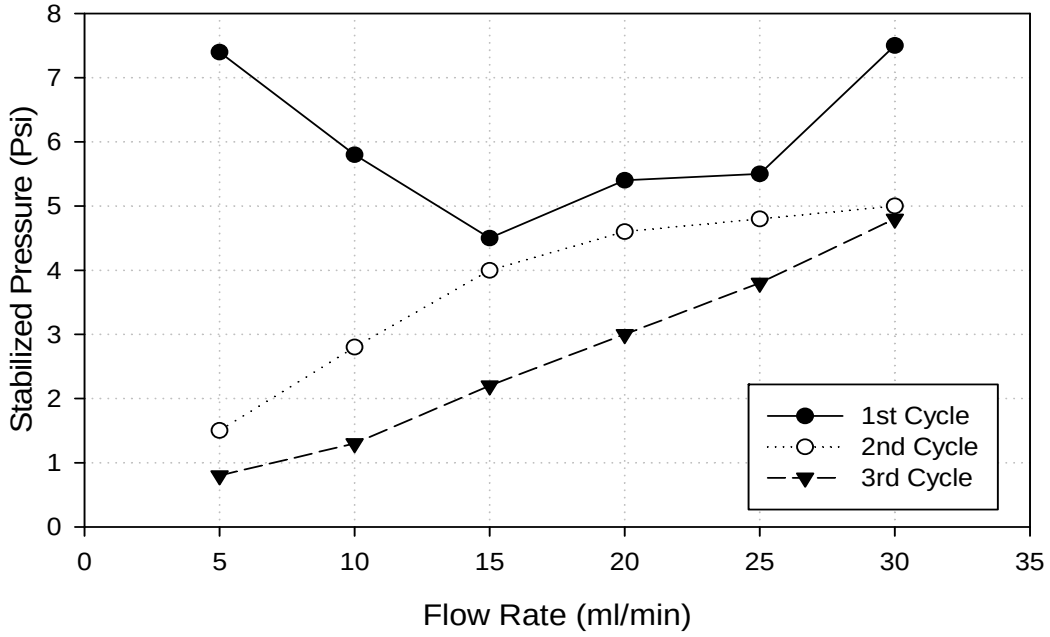

Figure 5-12 Stabilized pressure vs. flow rate for three cycles of 0.25%-brine injection into a 0.5-mm fracture after PPG placement.
(1 ml/min = 3.66 $in.^3$/hr)

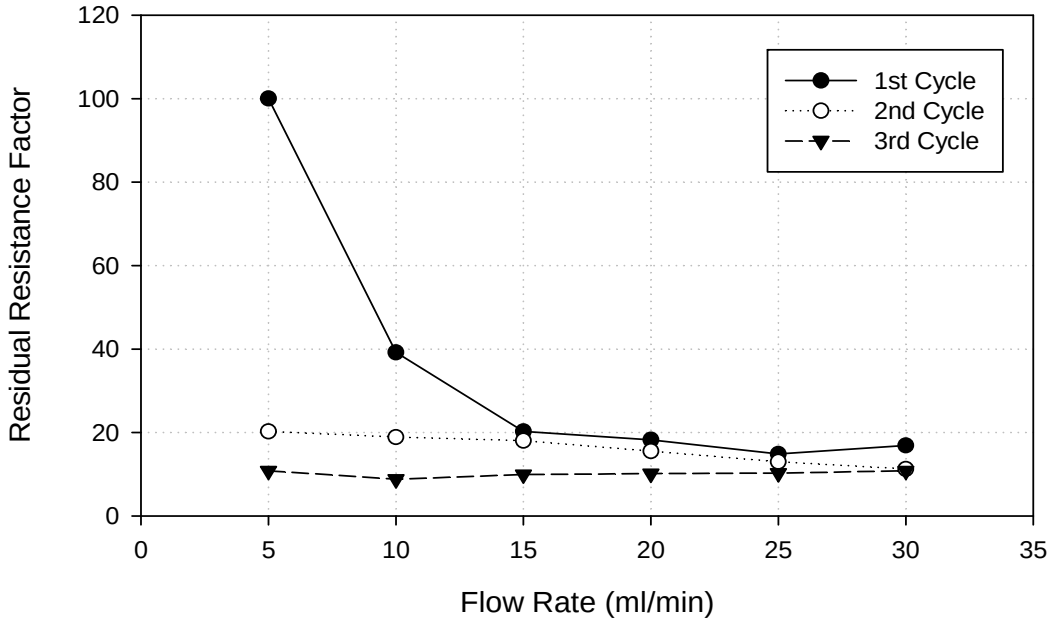

Figure 5-13 Residual resistance factor vs. flow rate for three cycles of 0.25%-brine injection into a 0.5-mm fracture after PPG placement.
(1 ml/min = 3.66 $in.^3$/hr)

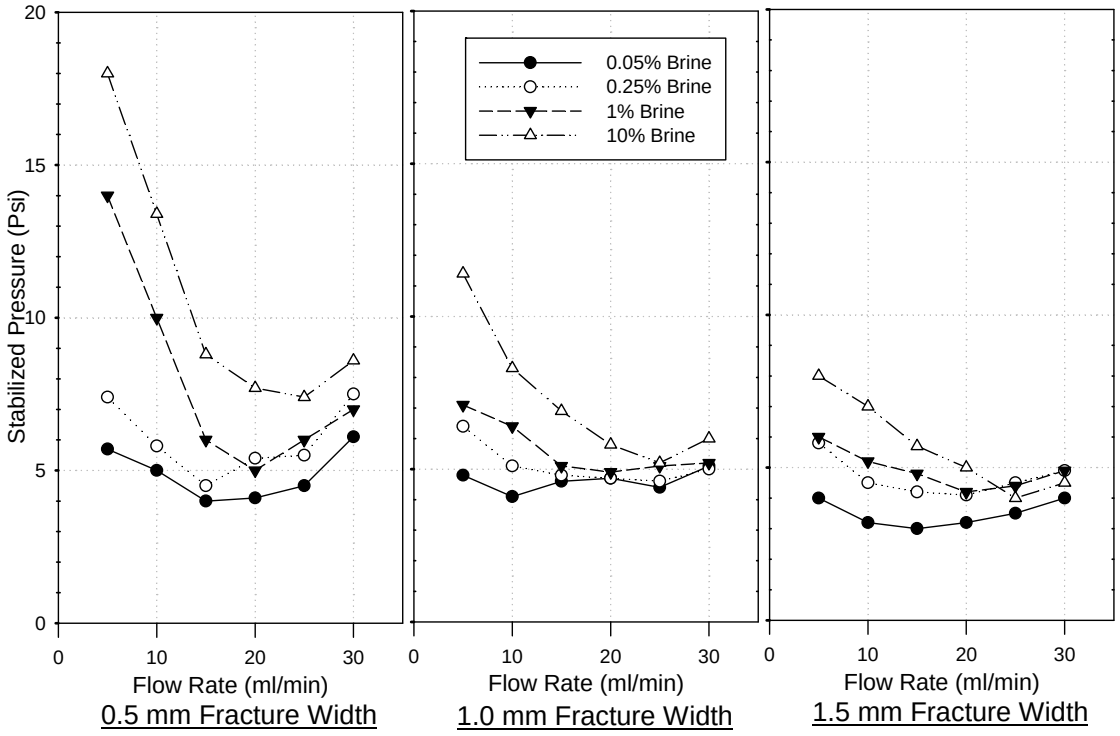

Figure 5-14 Stabilized pressure vs. flow rate for injection of brine with various concentrations after PPG placement.
(1 ml/min = 3.66 $in.^3$/hr)

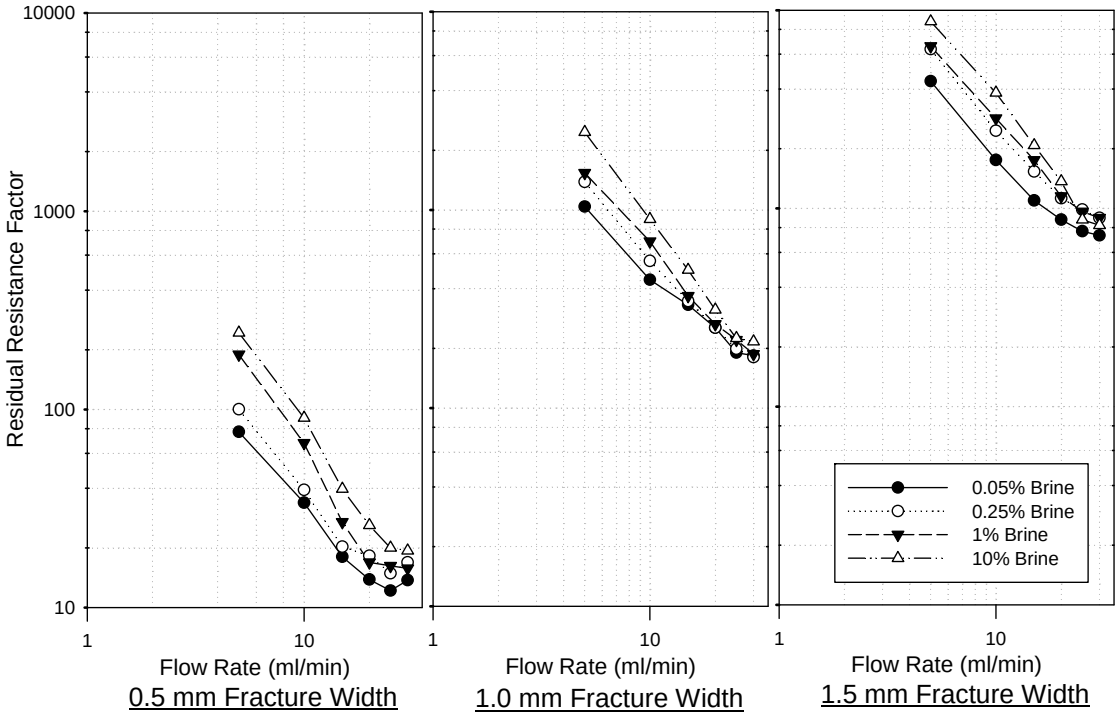

Figure 5-15 Residual resistance factor vs. flow rate for injection of brine with various concentrations after PPG placement.

(1 ml/min = 3.66 $in.^3$/hr)

Table 5-1 PPG Concentrations for Fully Swollen PPG prepared with Different Brine Concentration

Brine Concentration (%)	PPG Concentration (%)
0.25	1.597
1	2.731
10	2.961

Table 5-2 Fitting Equation for Injection Pressure as a Function of Flow Rate

Fracture Width (mm)	Brine Concentration	Fitting Equations	R^2
0.5	0.05%	$p = 32.28\ q^{0.362}$	0.992
	0.25%	$p = 35.25\ q^{0.356}$	0.995
	1%	$p = 48.49\ q^{0.268}$	0.999
	10%	$p = 59.16\ q^{0.236}$	0.990
1.0	0.05%	$p = 17.01\ q^{0.443}$	0.996
	0.25%	$p = 32.51\ q^{0.325}$	0.998
	1%	$p = 39.53\ q^{0.311}$	0.995
	10%	$p = 49.69\ q^{0.279}$	0.992
1.5	0.05%	$p = 9.830\ q^{0.520}$	0.999
	0.25%	$p = 13.79\ q^{0.553}$	0.983
	1%	$p = 18.91\ q^{0.475}$	0.995
	10%	$p = 25.35\ q^{0.414}$	0.998

(1 mm = 0.04 inch)

Table 5-3 Fitting Equation for Resistance Factor as a Function of Flow Rate

Fracture Width (mm)	Brine Concentration	Fitting Equations	R^2
0.5	0.05%	$Fr = 2182\ q^{-0.63}$	0.997
	0.25%	$Fr = 2383\ q^{-0.64}$	0.998
	1%	$Fr = 3278\ q^{-0.73}$	0.999
	10%	$Fr = 3999\ q^{-0.76}$	0.999
1.0	0.05%	$Fr = 18402\ q^{-0.59}$	0.998
	0.25%	$Fr = 32755\ q^{-0.67}$	0.999
	1%	$Fr = 45163\ q^{-0.68}$	0.997
	10%	$Fr = 53742\ q^{-0.72}$	0.998
1.5	0.05%	$Fr = 35382\ q^{-0.45}$	0.999
	0.25%	$Fr = 47553\ q^{-0.48}$	0.975
	1%	$Fr = 40353\ q^{-0.52}$	0.996
	10%	$Fr = 63884\ q^{-0.58}$	0.999

(1 mm = 0.04 inch)

6. Preformed Particle Gel Propagation through Semi-Transparent Fractures

6.1. Summary

A series of experiments has been implemented using a semi-transparent fracture model to understand the propagation of preformed particle gel along the fractures and the leakoff properties in the matrix rock. The effects of injection rate, gel concentration, gel particle size, and particle gel swelling ratio (depending on brine concentration) on particle gel intrusion were also examined in this chapter. Experimental results showed no progressive plugging was in any part of the fracture models. The required volume and time for injecting gels into a given fracture were much smaller compared to those in gelant treatments. With the use of semi-transparent models, PPG were found to propagate like a piston along the fracture when the fracture widths used were smaller than, or similar to the size of the swollen particles. But gravity dominated the PPG movement and the bottom part of the PPG front propagated faster than the top part when the fracture width was larger than the particle size. Particle gels can reduce the permeability of fractures with different widths to the same permeability. Mixed injection of PPG and brine in lower gel concentrations may achieve the same plugging efficiency while requiring lower injection pressures. These gel particle injection behaviors are different from conventional particles in that they are elastic and deformable during extrusion through fractures.

6.2. Introduction

In Chapter 5, we discuss the use of transparent fracture models to visually track swollen preformed particle gel (PPG) propagation through open fractures and water flow through PPG placed in fractures. During injection PPG propagated like a piston along the fracture. A gel pack formed in the fracture after gel placement; water broke through the particle gel pack, creating several water channels to discharge water from the outlet during water injection after PPG placement.

In Chapter 5 experiments, leakoff effects were neglected because the transparent model lacked matrix permeability, unlike a true fractured reservoir rock. More experiments are required to study PPG propagation and dehydration processes in a fracture model that combined gel movement visualization in the fracture with the fluid

leakoff effects in the matrix rock. Also, the effect of gel concentration required further investigation. Fracture widths greater than the preformed gel particle sizes examined in the first set of experiments also required more study since most of the fracture widths we used for the transparent fracture models were smaller than the swollen PPG particle size. These questions were addressed in the following set of experiments that used a semi-transparent fracture model consisting of a single wing fracture system with a transparent wall for visually tracking the PPG propagation process.

6.3. Experiments

6.3.1. PPG

The same superabsorbent polymer, LiquiBlock 40K Series, was used for this set of experiments. The main component of the PPG is a potassium salt of crosslinked polyacrylic acid or polyacrylamide copolymer. Table 6-1 lists some typical characteristics of the PPG used here, and Table 6-2 shows the size distribution of the PPG, as determined by a sieving test.

In aqueous solutions, PPG can absorb a large amount of water because of a hydrogen bond with the water molecules, although the concentration of sodium chloride affects its capacity to absorb water. Three dry PPG samples were prepared using three different screen size (40, 80, 150 mesh). Table 6-3 shows the parameters of the screens that were used. The swollen-PPG samples were prepared using three different brine concentrations (0.25, 1, and 10%) with swelling ratios of 98, 52, and 32, respectively. Fully swollen PPGs, without excess (free) water, were used for all experiments.

The particle concentration varied, depending on brine concentration. The PPG concentrations were calculated using the initial weight of the dry PPG, divided by the final weight of swollen PPG, as listed in Table 6-4.

6.3.2. Brine

To prepare the swollen PPG, three concentrations of brine were selected on the basis of significant differences in their swelling ratios: 0.25, 1, and 10 wt% sodium chloride brine.

6.3.3. Semi-Transparent Fracture Model

The semi-transparent fracture model was constructed of two acrylic plates with a rubber O-ring between them. Bolts, nuts, and shims were used to fix the two plates and

control fracture width. For one of the acrylic plates, a long square pocket (with a dimension of 2 inches wide, 10 inches long, and 1 inch deep) was drilled in the center of one side and a piece of Roubidoux sandstone slab (obtained from central Missouri) with the same dimension as the drilled pocket was placed into the acrylic plate and was casted into the pocket using epoxy. This provided a more realistic representation of a reservoir rock with matrix porosity as well as fracture porosity. The model was transparent on one side so that the PPG and water movement would be clearly visible. The fracture model had three sections of equal length that were delineated by four fracture pressure taps on the acrylic plate which was not casted with the sandstone. On one side of the plate, a hole functioned as an inlet for the injection of fluids and PPG; on the other side, another hole provided an outlet to discharge fluids and PPG. The pressure transducers were connected to the pressure taps to record the fracture pressure. The effluent from the fracture and matrix was separated and recorded through different fittings during the experiment. Figures 6-1, 6-2, and 6-3 show the schematic diagram, the cross-sectional view, and the picture of the semi-transparent model respectively in our study. Four fracture widths (0.5, 1.0, 1.5, and 5.0 mm or 0.02, 0.04, 0.06, and 0.2 in.) were used to examine the effect of fracture size on gel placement. The inside diameter of the tube leading into the fracture was approximately ¼ in., and its length was 4 in. A metal connector with an internal diameter of ⅜ in. and a length of less than 1 in. was used to discharge the fluids from the outlet.

6.4. Results and Analysis

To probe the mechanism for gel propagation and dehydration, a base case experiment was performed where a PPG gel was extruded through the ten-inch-long semi-transparent fracture model. The base case examined extrusion through a 10×2×0.04-in. fracture using 430-mD Roubidoux sandstone with 40-mesh PPG prepared in 1% brine solution. The fracture was oriented vertically during the experiments. The fracture width was 0.04 in. (0.1 cm), and the average fracture conductivity was 114 darcy-ft. The fracture volume was 0.8 $in.^3$ (13.1 cm^3), and the core pore volume was 3.1 $in.^3$ (50.8 cm^3). Before gel injection, the fractured core was saturated with brine and characterized using flow measurements. An injection rate of 7.32 $in.^3$/hr (120 cm^3/hr or estimated velocity of 240 cm/hr) was used in the experiment.

Our experiments used a fully swollen PPG which was prepared with 40-mesh dry PPG in 1% brine solution. All experiments were performed at room temperature (22 °C or 72 °F). An Isco continuous flow system coupling two pump modules to a single controller was utilized to provide non-stop, continuous feed of fluid without any interruption.

6.4.1. Observed Particle Movement during PPG Injection

Fig. 6-4 shows the particle movement during placement of the swollen PPG in the fracture model. The PPG propagated like a piston along the fracture. Gravity did not change the shape of the PPG front because the fracture widths used here were smaller than, or similar to, the size of the swollen particles. Gel arrived at the fracture outlet after injecting 3.2 fracture volumes of gel.

6.4.2. Pressure Gradients in the Fracture

We extruded 40 fracture volumes (32 $in.^3$ or 524 cm^3) of fully swollen PPG gel through the 10-inch-long semi transparent fracture model using an injection rate of 7.32 $in.^3$/hr (120 cm^3/hr). Figure 6-5 shows the pressure gradients in the fracture for the three fracture sections during swollen PPG injection. At the end of gel injection, the average pressure gradient in the fracture was about 46 psi/ft for all three fracture sections. This result suggests that all the fracture sections have the same conductivity. Also, the pressure gradients were reasonably stable during the last 35 fracture volumes of gel injection. Thus, gel injection did not show progressive plugging (continuously increasing pressure gradient) in any part of the fracture, which is consistent with our previous results in the transparent fracture model.

6.4.3. Pressure Gradients in the Porous Rock

During PPG gel injection, pressure gradient in the center of the porous rock is shown in Figure 6-6. The pressure gradient was typically between 0.1 and 0.6 psi/ft, which is much lower than the values observed in the fracture. The onset of the pressure response occurred at the similar injection volume for both the fracture pressure gradients and the matrix pressure gradients. Since there was only one matrix tap placed in our model, more matrix taps need to be designed for each section of the fracture model to confirm the results in our future experiments.

6.4.4. Produced Fluids

As mentioned earlier, the effluent from the fracture and that from the porous rock were separated and measured in our fracture model. Figure 6-7 plots the fraction of the effluent that was produced from the fracture versus that from the porous rock. During the first three fracture volumes of gel injection, virtually 100% of the flow was produced from the fracture. This result was reasonable because the calculated flow capacity of the fracture was 3,180 times greater than the flow capacity of the porous rock before gel injection. Gel arrived at the fracture outlet after injecting 3.2 fracture volumes of gel. The flow from the fracture was reduced to about 50% of the total flow for a period of about one fracture volume of gel injection. Subsequently, the fraction of flow from the fracture increased, while flow from the porous rock decreased. After injection of 40 fracture volumes of gel, flow from the fracture accounted for 75% of the total flow, while flow from the matrix accounted for 25% of the total flow.

The fluid collected from the matrix was exclusively brine and gel didn't flow through porous rock. The source of this flow was water that left the fully swollen PPG in the fracture (water from the gel dehydration process).

The Darcy equation was used to convert the pressure gradient in Figure 6-6 to flow rates. Since the total injection rate was fixed (at 120 cm^3/hr or 7.32 $in.^3$/hr), the matrix flow rates, in turn, were converted to the fraction of total flow that occurred through the rock matrix at any given time. Figure 6-8 plots the results of this conversion. The fraction of total fluid flow gradually declined after the gel front arrives at the outlet of the fracture model. After injecting 40 fracture volumes of gel, the fraction of flow in the matrix became 0.25.

At any given time, Figure 6-8 plots the average fraction of the total flow that occurred in the porous rock. For comparison, Figure 6-7 plots the measured fraction of total flow (in the matrix versus in the fracture) at the outlet of the fractured core. The two data sets were consistent in that at the end of gel injection, the final fractional flow from the matrix (25%) was the same in Figure 6-7 as that in Figure 6-8.

Figure 6-7 suggests that after 40 fracture volumes of gel placement, each new element of injected gel should be concentrated by 25% (because water produced from the matrix stabilized at 25% of the total flow). Figures 6-5 and 6-7 indicate that near the end

of the experiment, a steady state was attained. Therefore, some concentrated (dehydrated) gel appeared to propagate through propagate through the fracture. The propagating gel may be homogeneous (with a uniform concentration that was roughly 25% greater than the injected gel). Alternatively, a more convincing explanation is the propagation gel is a mixture of components with various gel concentrations. At a steady state, the pressure gradients are great enough to mobilize the dehydrated gel. Figure 6-9 compares the gel sample before and after the injection. It clearly shows the gel after the injection is more concentrated and the particle size is smaller than that before the injection, probably due to gel dehydration.

6.4.5. Effect of Injection Rate

More experiments were performed to examine the effects of injection rate on gel extrusion and dehydration. Except for the injection rate, these tests were identical to that described in the base case experiment. Specifically, in each test, we extruded 40 fracture volumes of our standard fully swollen PPG (prepared with 40-mesh dry PPG in 1% brine solution). To complement the 120 cm^3/hr (7.32 $in.^3$/hr) test that was described in previous part of this report, five new tests were performed using gel injection rates of 60, 240, 480, and 960 cm^3/hr (3.66, 14.65, 29.29 and 58.58 $in.^3$/hr), respectively. Table 6-5 summarizes the results from these tests.

Table 6-5 shows that the pressure gradients along the fracture were insensitive to injection rate. The average pressure gradients ranged from 39 to 57 psi/ft for estimated gel velocities ranging from 120 to 1920 cm/hr (3.93 to 63.0 ft./hr). At high flow rates, the pressure gradient was almost independent of gel injection rate. Figure 6-10 shows the stabilized gel resistance factors after 40 fracture volumes of gel injection at various gel injection rates. It clearly shows that gel resistance factors decreased with increased flow rate. A single power equation, shown in Figure 6-10, can fit this relationship very well. This suggests that preformed particle gels have an apparent shear-thinning behavior during extrusion through fractures, which is consistent with our previous findings in the transparent fracture model.

Comparison also reveals that the rate of gel-front propagation increased with increased injection rate. For 120 cm/hr (3.93 ft./hr), gel arrival at the end of the 10-inch-long fracture occurred after 5.3 fracture volumes of gel injection. Only 1.9 fracture

volumes of gel were required when the velocity was 1920 cm/hr (63.0 ft./hr). This result was reasonable because the swollen gel had less time to dehydrate as the injection rate increased. For a given total volume of gel injection, the gel propagates a longer distance with a lower level of gel dehydration. The result suggests that for field application, gels should be injected at the highest practical rate in order to maximize penetration into the fracture system. Compared with the data for gelant (in-situ gel) systems, the required fracture volumes of gel needed to seal the same fracture was much smaller with a given injection rate.

Consistent with earlier observations, no significant gel was produced from the matrix. And gel breakthrough decreased with increased injection rate. Figure 6-11 plots the fraction of the effluent that was produced form the porous rock with different injection rate. In each case, the peak in the fraction of matrix flow was observed when gel arrived at the end of the fracture. This is also consistent with earlier results. After gel breakthrough, the fraction of flow from the porous rock decreased in an exponential fashion. After 40 fracture volumes of gel injection, the fractions of total flow from the matrix were 34%, 25%, 20%, 17%, and 15%, for injection rates of 120, 240, 480, 960, and 1920 cm/hr (3.93, 7.87, 15.7, 31.5, and 63.0 ft./hr), respectively. Thus, for a given throughput, the final fraction of flow produced from the matrix decreased with increased injection rate. Consequently, the degree of dehydration decreased with increased injection rate. These results further support the conclusion that in field application, gels should be injected at the highest practical rate to maximize penetration into the fracture system.

6.4.6. Brine Injection after Gel Placement

Figure 6-12 shows the water flow paths after gel placement in a fracture. PPG was packed in the whole fracture after PPG injection. When water was injected, it broke through the permeable gel pack and formed several channels or major water paths to allow water discharge through the outlet.

We extruded 30 fracture volumes of the brine solution (with the same concentration as the one used to prepare the swollen PPG) into the gel particles packed in the 10-inch-long semi transparent fracture model using the same injection rate of 7.32 $in.^3$/hr (120 cm^3/hr) as the base case experiment to test the efficiency of gel plugging on water. Figure 6-13 shows the pressure gradients in the fracture for the three fracture

sections during the brine injection. The pressure gradients in all three sections first rapidly increased to a peak level then dropped and stabilized with the increasing volume of injected brine because brine needs to break through the particle-gel pack and forms water channels in the fracture. The fact that each section had the peak pressure gradient in sequence with the position along the fracture model shows that the water paths were created along the fracture. At the end of gel injection, the average pressure gradient in the fracture was about 9.5 psi/ft for all three fracture sections. This result suggests that all three fracture sections have similar conductivity after 30 fracture volumes of brine injection. And the pressure gradients were stable during the last 20 fracture volumes of gel injection. It indicates that stationary channels had formed in the gel pack and water had passed through the solid channels.

Figure 6-14 plots the fraction of the effluent that was produced from the fracture versus that from the porous rock during brine injection. The fluid collected from the matrix was exclusively brine and gel didn't flow through porous rock. The fluid from the fracture was purely gel in the beginning for the first two or three fracture volumes injected, then a mixture of gel and brine were found in the fracture outlet and the content of gel in the mixture kept decreasing over the next five or six fracture volumes injection. For the last 20 fracture volumes of brine injection, almost 100% of the effluent collected from the fracture was water. It indicated steady water channels had been formed in the gel pack and the majority of the water will go through the existing water paths. The effluent rate in the matrix first increased rapidly during the first 4 fracture volumes of brine injection, and then it dropped to a steady level in the next 5 fracture volumes. The fraction of total flow from the matrix rock remained steady for the last 20 fracture volumes of injection. After injection 30 fracture volumes of brine, flow from the fracture accounted for 64% of the total flow, while flow from the matrix accounted for 36% of the total flow. The main source of the matrix flow was brine injected in the fracture. And the response is similar to the pressure behavior of the last section in Figure 6-13. It is expected because in the early stage of brine injection, water pushed the gel pack in the fracture model and the pressure gradient kept increasing until steady water channels were created. The effluent from the matrix increased with the pressure gradient since the fraction of flow is fully dependent on the pressure difference between the fracture and the

matrix rock, and the pressure in the matrix rock is negligible compared to the fracture pressure as mentioned in the previous section.

Figure 6-15 plots the residual resistance factor behavior over time during brine injection. The residual resistance factor represents the reduction in the permeability to water as a result of gel. It was calculated by dividing the brine injection pressure drop after gel placement by the brine injection pressure drop before gel injection. The residual resistance factor in Figure 6-15 shows that the resistance force for brine injection increased before water broke through the packed gel in the beginning. After more water channels in the gel were created, the resistance force decreased until stabilized channels were achieved. This result is consistent with our previous results in the transparent fracture model.

After the water flooding test, the fracture model was opened and the core was checked visually. Figure 6-16 shows the core sample before and after the gel and brine injection. Dye was used to aid in seeing the effect of injection. The images indicate that water paths for injection were more dispersed in the center of the fracture. It may be caused by the placement of the inlet and outlet in the center of the fracture vertically. But the presence of a significant amount of dyed water in other parts of the core shows that the water flooding process could penetrate through the whole rock matrix.

The same injection rates of brine were used after each gel injection experiment as mentioned in previous discussions to check the effect of injection rate on brine injection. Table 6-6 summarizes the results. The stabilized average pressure gradient after 30 fracture volumes of brine injection increased with the injection rate. But it is also seen that at high injection rates, the average pressure gradient did not change much, implying that the stabilized pressure gradient is not sensitive with to changes in high injection rates. For example, the average pressure gradients at end of the brine injection for injection rates of 480 and 960 cm^3/hr (29.29 and 58.58 $in.^3$/hr) were 13.2 and 13.5 psi/ft, respectively. The peak and the final fractions of matrix flow decreased with the increasing injection rates. It can be explained through formation of more or larger steady water channels due to higher injection rates in the gel pack that can lead to a higher portion of the effluent flowing through the gel pack along the fracture instead of through

the matrix. For practical application, lower injection rates for water flooding should be used to maximize the recovery in the matrix.

Figure 6-17 plots the final residual resistance factor against the injection rate. The resistance force of the gel pack decreased with the increase of the injection rate. Higher injection rates will create larger water channels in the gel pack, and larger water paths will lead to smaller resistance force on the brine injection in the fracture. This result is constant with our previous findings. A simple power equation which is shown in Figure 6-17 can be used to fit the final residual resistance factor against different injection rates.

6.4.7. Effect of Fracture Width

To understand the effect of fracture width, three more experiments were performed to complement the base case experiment (performed using a fracture width of 0.04 in. (0.1 cm). The new experiments used fracture widths of 0.02 in. (0.05 cm), 0.06 in. (0.15 cm), and 0.2 in. (0.5 cm), respectively. The first three fracture widths were smaller or similar to the swollen PPG particle size, while the fracture width of 0.2 in. was larger than the particle size during the injection process. The other conditions were the same with the base case. The core was prepared using the 430-mD Roubidoux. The fracture was oriented vertically during the experiments. The fracture volumes were 0.4 $in.^3$ (6.55 cm^3), 1.6 $in.^3$ (26.2 cm^3), and 4 $in.^3$ (65.5 cm^3) for the fracture widths of 0.02 in. (0.05 cm), 0.06 in. (0.15 cm), and 0.2 in. (0.5 cm), respectively. For each test, we extruded 40 fracture volumes of our standard fully swollen PPG (prepared with 40-mesh dry PPG in 1% brine solution). The same estimated injection velocity in the fracture (240 cm/hr or 7.87 ft./hr) was used as in our base case experiment, so the gel injection rates used in the new experiments were 60, 240, 480, and 960 cm^3/hr (3.66, 14.65, 29.29, and 58.58 $in.^3$/hr), respectively. Table 6-7 summarizes the results.

From the table, the average pressure gradients along the fracture decreased dramatically with the increase in fracture width. The stabilized average pressure gradients ranged from 91 to 14 psi/ft for fracture widths ranging from 0.02 to 0.2 in. with estimated gel velocities of 240 cm/hr (7.87 ft./hr). This is expected since the smaller the fracture width is, the more “slip” effects the gel. Effects are especially obvious for the fracture width which is smaller than the gel particle size. The pressure gradient dropped from 46 to 26 psi/ft when the fracture width was increased from 0.04 to 0.06 in. When the fracture

width was changed to 0.2 in which was larger than the gel particle size, the pressure gradient was reduced to 14 psi/ft from 26 psi/ft in the fracture with 0.06 in. width. The gel "slip" effects were further reduced when the fracture width was larger than the gel particle size.

It took 4.8 fracture volumes of gel injection to break though the fracture for the fracture width of 0.02 in., while only 1.5 fracture volumes of gel was required when the fracture width increased 10 times. The result is reasonable because the pressure gradient in smaller fracture width was higher, leading to higher levels of gel dehydration. The peak and final fractions of flow produced from matrix confirmed this point since they tended to decrease with the increase in the fracture width.

Figure 6-18 shows the particle movement during placement of the swollen PPG in the 0.2-in. fracture model. The bottom part of the PPG propagated obviously faster than the top part of the gel front during the gel injection process. No piston movement was found in the pictures. This indicates that gravity affected the shape of the PPG front because the fracture widths used here were larger than the size of the swollen particles which lead to gel precipitation. Gel arrived at the fracture outlet after injecting 1.5 fracture volumes of gel.

Table 6-8 summarized the results of different fracture widths on brine injection after the gel intrusion. The brine injection rates were maintained the same as the gel injection rate for each experiment.

The average pressure gradient after the brine injection ranged between 10.1 and 9.5 psi/ft when the fracture width was increased from 0.02 to 0.06 in. It confirmed the conclusion in our transparent model that when the fracture width is smaller or similar to the gel particle size, the particle gel can reduce the permeability of fractures with different widths to the same permeability level, thereby mimicking the effects of in-situ gel on formations of varying permeability. When the fracture width was larger than the particle size in our fracture model with 0.2-in width, the pressure gradient decreased from 9.7 to 7.7 psi/ft compared to the model with 0.06-in. width. The pressure gradient didn't drop significantly (about 20%) compared to the increase in the fracture width (over 300%). The peak and final fractions of matrix flow were similar for fracture width between 0.02 to 0.04 in., while the fractions of flow for 0.2-in. fracture width were much

smaller. It indicates that larger or more water channels formed for larger fracture width. Figure 6-19 compares the residual resistance factors at different fracture widths, indicating that resistance was much higher in a wider fracture than that in a narrower fracture. Figure 6-20 shows the brine injection process in the fracture model of 0.2-in. width. Brine tended to break through the gel pack from the bottom part of the fracture, and water channels were more dispersed at the bottom half of the model after steady water paths were formed. This indicates that preformed particle gels tend to improve the sweep efficiency of the lower (deeper) part of the fracture system when the fracture width is larger than the gel particle size.

6.4.8. Effect of Gel Concentration

To evaluate the effects of various gel concentrations, two more experiments were performed to complement the base case experiment, which was performed using a gel concentration of 2.73%. The two new experiments used different gel concentrations of 1.36% and 0.91%. Mixed injections were used for these two experiments. For the base case experiment, 100% fully swollen gels (prepared with 40-mesh dry PPG in 1% brine solution) were injected into the fracture models, while in our mixed injection experiments, gel and brine were injected at the same time by using two Isco pump systems with the gel/brine ratio of 1:1 and 1:2 to create gel concentrations of 1.36% and 0.91%, respectively. The same fracture model was used in the new experiments. In each new test, we extruded 40 fracture volumes of the mixture of gel and brine. The same estimated velocity in the fracture (240 cm/hr or 7.87 ft./hr) was used as the one in our base case experiment, so the gel and brine injection rates for the experiment of 1.36% gel concentration were maintained at 60 cm^3/hr (3.66 $in.^3$/hr) each. For the experiment of 0.91% gel concentration, the rates were 40 cm^3/hr (2.44 $in.^3$/hr) and 80 cm^3/hr (4.88 $in.^3$/hr) for gel and brine, respectively. Table 6-7 summarizes the results.

From the table, the average pressure gradients along the fracture decreased dramatically with the decrease in the gel concentration. The stabilized average pressure gradients ranged from 46 to 17 psi/ft for gel concentration ranging from 2.73% to 0.91%. This result was not expected because the particle size of the gels injected was larger than the fracture width in our fracture model, so the particles should be trapped in the fracture and block the water paths. One possible explanation could be that the brine injection

created steady water paths early in the injection process and a more permeable gel pack was formed in the fracture for our mixture injection experiments.

It also took many more fracture volumes of gel injection to make the gel front arrive at the core end for mixed gel injection. Compared to the 3.2 fracture volumes for gel breakthrough in our base case, it took 8.6 and 11.3 fracture volumes of fluid injection to break though the fracture for the mixed injections with gel concentration of 1.36% and 0.91%. The gel mixture with lower gel concentration contains less fully swollen PPG particles, which should require more fracture volumes of fluid injection in order to make the gel fill in the fracture. The peak and final fractions of flow produced from matrix also decreased significantly with the decrease in gel concentration. To summarize this table, gel injection with lower gel concentration took more fracture volumes to fill out the fracture, but it also required less pressure gradient for the injection.

Table 6-10 summarized the results of brine injection after the gel intrusion. The same brine solution was used (1%) for all experiments. The brine injection rates were maintained the same as the gel injection rate (120 cm^3/hr or 7.32 $in.^3$/hr).

The average pressure gradient didn't change much when the gel concentration was reduced from 2.73% to 0.91%. The pressure gradient after brine injection ranged between 9.5 and 8.9 psi/ft for all three gel concentrations. It indicated that the mixed injection with different gel concentrations could reduce fracture permeability to the same permeability level compared to pure PPG injections. The peak and final fractions of matrix flow did not drop significantly when the gel concentration decreased. And they tend to remain steady for lower gel concentration. This result indicates that for a field application, a mixed injection with lower gel concentrations may achieve the same water blocking effects in the fracture system while requiring less injecting pressure. More fracture models with larger fracture widths should to be tested to confirm this observation because the gel particle size is larger than the fracture width used in this set of experiments.

6.4.9. Effect of Brine Concentration

Two further experiments were performed to evaluate the effects of brine concentration. These two experiments used swollen gels which were prepared in 0.25% and 10% brine solutions. The same fracture model was used in the new experiments, and

we extruded 40 fracture volumes of swollen gels. The same injection rate (120 cm^3/hr or 7.32 $in.^3$/hr) was used in the experiments. Table 6-11 summarizes the results.

Average pressure gradients along the fracture increased dramatically with the increase in the gel concentration. The stabilized average pressure gradients ranged from 28 to 73 psi/ft for brine concentration ranging from 0.25% (with swelling ratio of 98) to 10% (with swelling ratio of 32). This is due to higher gel strength in gels prepared in higher concentration of brine and is consistent with our previous findings in transparent fracture models. It took less fracture volumes of gel injection to make the gel front arrive at the core end for the gel prepared with a higher brine concentration. The higher brine concentrations lead to larger PPG swelling ratios, which also means the gel concentration is higher. In the gel intrusion process, less water will escape from the gel particles for gel samples made in higher brine concentrations, therefore it is reasonable to require fewer fracture volumes of injection to break through the fracture. The peak and final fractions of flow produced from the matrix also decreased significantly with the increase in brine concentrations. In summary, gel injection with higher brine concentration took fewer fracture volumes to fill the fracture, but it required higher pressure for the injection.

Table 6-12 summarized the results of brine injection after the gel intrusion. Corresponding brine solution was used for each experiment. The brine injection rates were maintained at the same gel injection rate of 120 cm^3/hr (7.32 $in.^3$/hr).

The average pressure gradient increased significantly with the brine concentration. It indicated fewer or smaller water channels were formed in the gel packs made in the higher brine concentration. The peak and final fractions of matrix flow also increased with the gel concentration, indicating the gel packs made in higher brine concentrations had better water blocking abilities, but the gel intrusion process required a much higher pressure gradient.

6.4.10. Effect of PPG Particle Size

Two experiments were performed to evaluate the effects of PPG particle size, complementing the base case experiment performed in the fracture model with fully swollen gels prepared with 40-mesh dry particles. The two new experiments used swollen gels which were prepared with 80 and 150-mesh dry PPG particles. The dry particle sizes

for different mesh sizes are shown in Table 6-3. The same experimental conditions were maintained. Table 6-13 summarizes the results.

From the table, it is seen that the average pressure gradients along the fracture decreased slightly with smaller PPG particle sizes. The stabilized average pressure gradients ranged from 46 to 39 psi/ft for gel samples made with 40 to 150-mesh sized dry PPG particles. One possible explanation is that smaller gel particles may experience less "slip" effects during gel extrusion through the fracture. Fewer fracture volumes of gel injection were needed to make the gel front arrive at the core end for smaller gel sizes. The peak and final fractions of flow produced from matrix decreased with the particle sizes. To summarize, gel injection with smaller PPG particle sizes took less fracture volumes to fill out the fracture while requiring lower injection pressure. Gel concentration was the same for all three experiments because the gel swelling ratio didn't change.

Table 6-14 summarized the results of brine injection after the gel intrusion. A 1% brine solution was used, and the brine injection rates were maintained at 120 cm^3/hr (7.32 $in.^3$/hr). The average pressure gradient in the end of brine flooding decreased with the gel particle size, indicating more or larger water channels were formed in the gel packs made with smaller particle sizes. The peak and final fractions of matrix flow decreased with the gel particle size. This could mean that the gel packs made with larger particle sizes had better water blocking abilities; however more fracture widths needs to be tested to confirm this point.

6.5. Conclusions

The following conclusions apply to the fully swollen preformed particle gels we used in the experiments using semi-transparent fracture models at room temperature (22 °C or 71.6 °F):

- In the gel intrusion process, the PPG propagated like a piston along the fracture when the fracture widths used were smaller than, or similar to the size of the swollen particles. When the fracture width was larger than the particle size, gravity dominated the PPG movement and the bottom part of the PPG front propagated faster than the top part. In the brine injection process after particle gel intrusion, water first broke through the center of the

packed gel then penetrated through the whole gel pack when fracture width was smaller than the gel particle size. When the width was larger compared to the particle size, water tended to sweep through the bottom part of the gel pack in the fracture. When the fracture width is smaller or similar to the gel particle size, the particle gel can reduce fracture permeability with different widths to the same level. Gel injection with smaller PPG particle sizes takes less fracture volumes to fill out the fracture while requiring lower injection pressure, but larger PPG particle sizes will reduce the fracture permeability more.

- During injection of 40 fracture volumes of swollen PPG gels, progressive plugging was not observed in any part of the fracture model. The required volume and time for particle gels to seal a given fracture was much smaller compared with conventional gelant treatments.
- During gel injection, effluent from the matrix increased to a peak level then dropped and stabilized to a lower level due to the gel dehydration process. There were no gel particles found in the fluids produced from the matrix. The degree of dehydration decreased with increased gel injection rate in a given fracture model.
- PPG injection with lower gel concentrations takes more fracture volumes to fill out the fracture, but it requires less fracture gradient for the injection. Mixed injection of PPG and brine in lower gel concentrations may achieve the same plugging efficiency in while requiring less injecting pressure the fracture system. PPG injection with higher brine concentration requires less fracture volumes to fill out the fracture, but it needs higher pressure for the injection.

6.6. Future Work for Fracture Models

In future work, additional experiments will be performed to refine our fracture model for gel extrusion. Also, using our experimental findings, analyses will be performed to predict conditions, gel compositions, and gel volumes that provide the

optimum preformed particle gel placement in fractured reservoirs. More specifically, some of the questions that we plan to address in the near future include:

1. How does a two wing fracture (consists of two pieces of sandstone slabs) model change the pressure gradient for gel extrusion compared to our semi-transparent and transparent fracture models?
2. Will different rock permeability affect PPG pressure gradient?
3. How will different fracture lengths and height change the PPG injection?
4. Will fracture surface roughness significant change the existing results?
5. How will the fracture models with various fracture width change the gel injection process?
6. How will other PPG products perform in our fracture models compared to the sample we used in previous experiments?
7. Will different reservoir conditions like different temperature or pH value change the gel injectivity?
8. Could we design different PPG products for different fractured reservoirs?

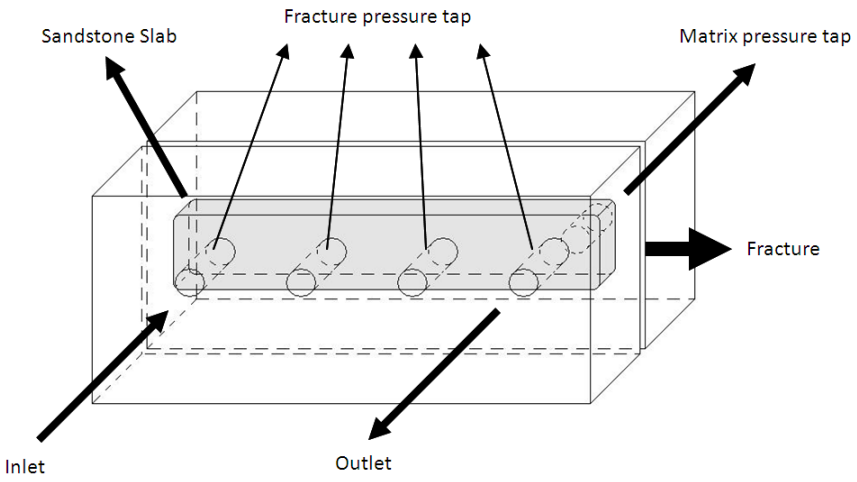

Figure 6-1 Schematic diagram of semi-transparent fracture model.

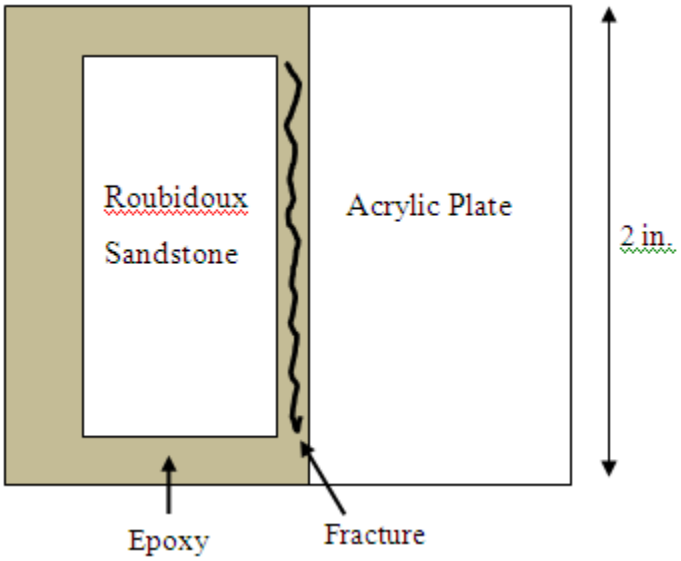

Figure 6-2 Cross-sectional view of semi-transparent fracture model.

Figure 6-3 Picture of semi-transparent fracture model.

(a)-Gel movement during PPG injection-gel started to move in the fracture (t = 0.2 PV)

(b)-Gel movement during PPG injection-gel front half way through the core (t = 1.5 PV)

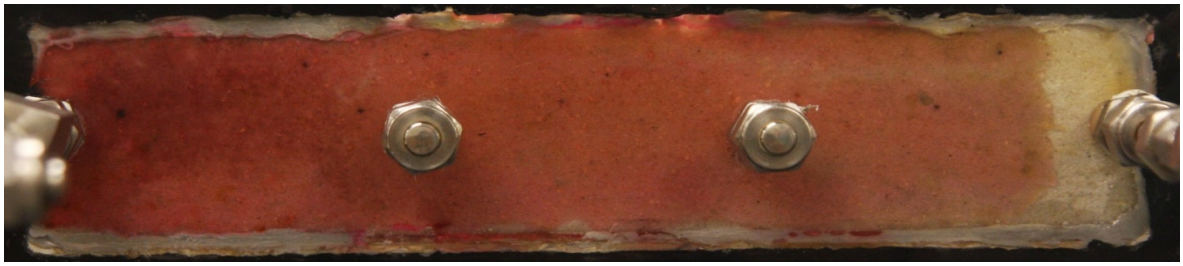

(c)-Gel movement during PPG injection-gel front close to core end (t = 2.5 PV)

(d)-Gel movement during PPG injection-gel front arrival at core end (t = 3.2 PV)

Figure 6-4 Gel movement during PPG injection.

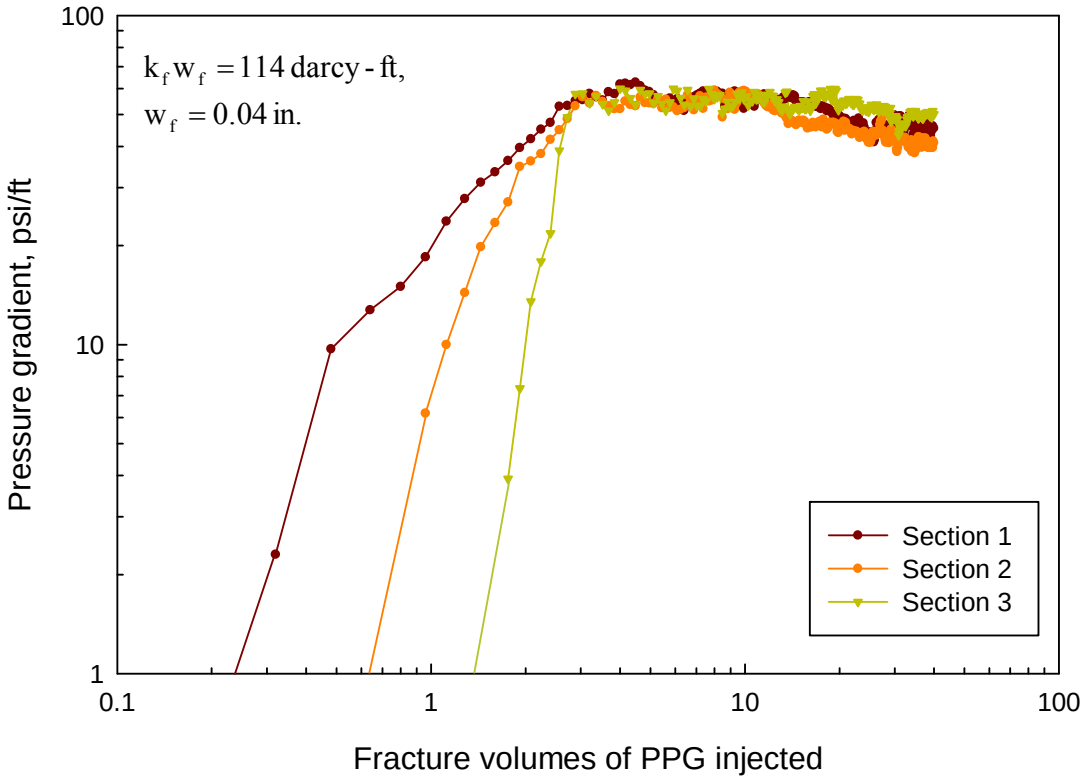

Figure 6-5 Pressure behavior in the fracture taps during swollen PPG injection.

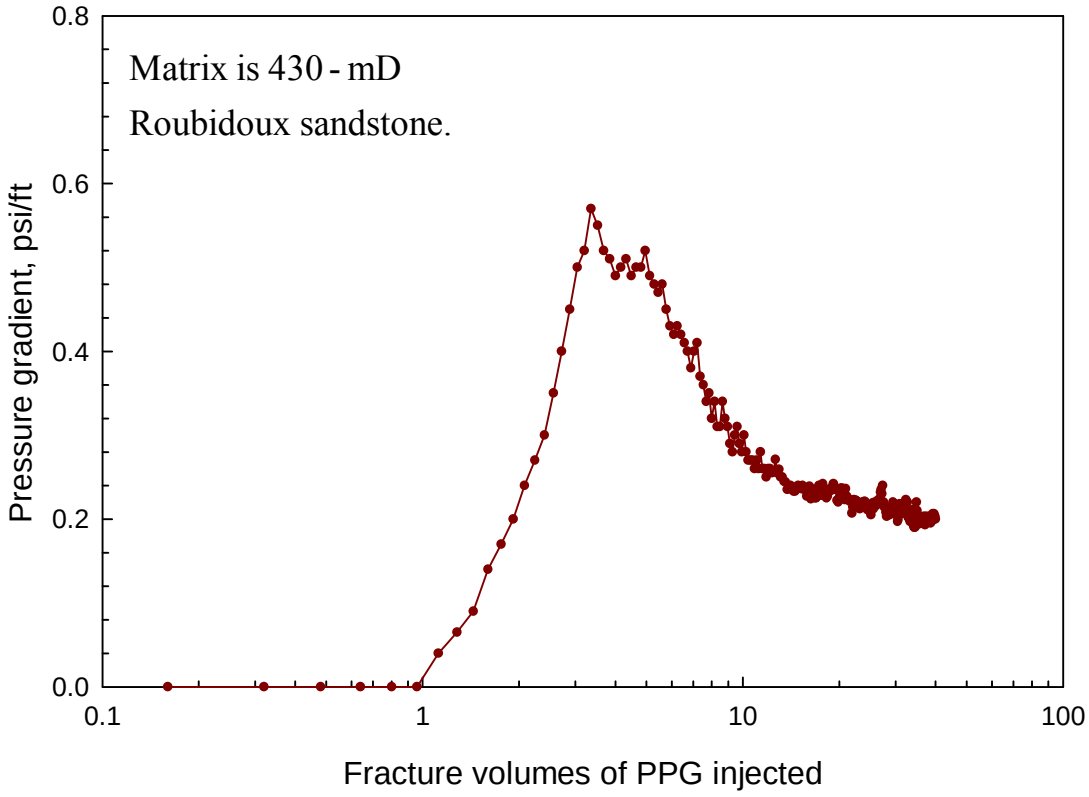

Figure 6-6 Pressure behavior in the matrix tap during swollen PPG injection.

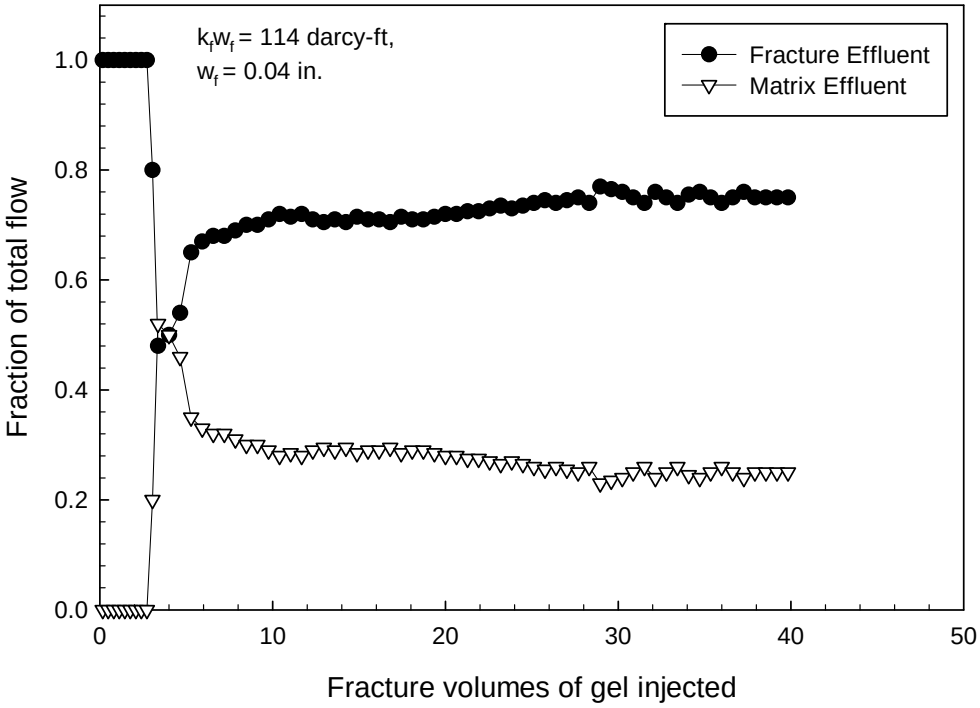

Figure 6-7 Fractional flow measured at the core outlet during gel injection (120 cm^3/hr or 7.32 in.^{3}/hr).

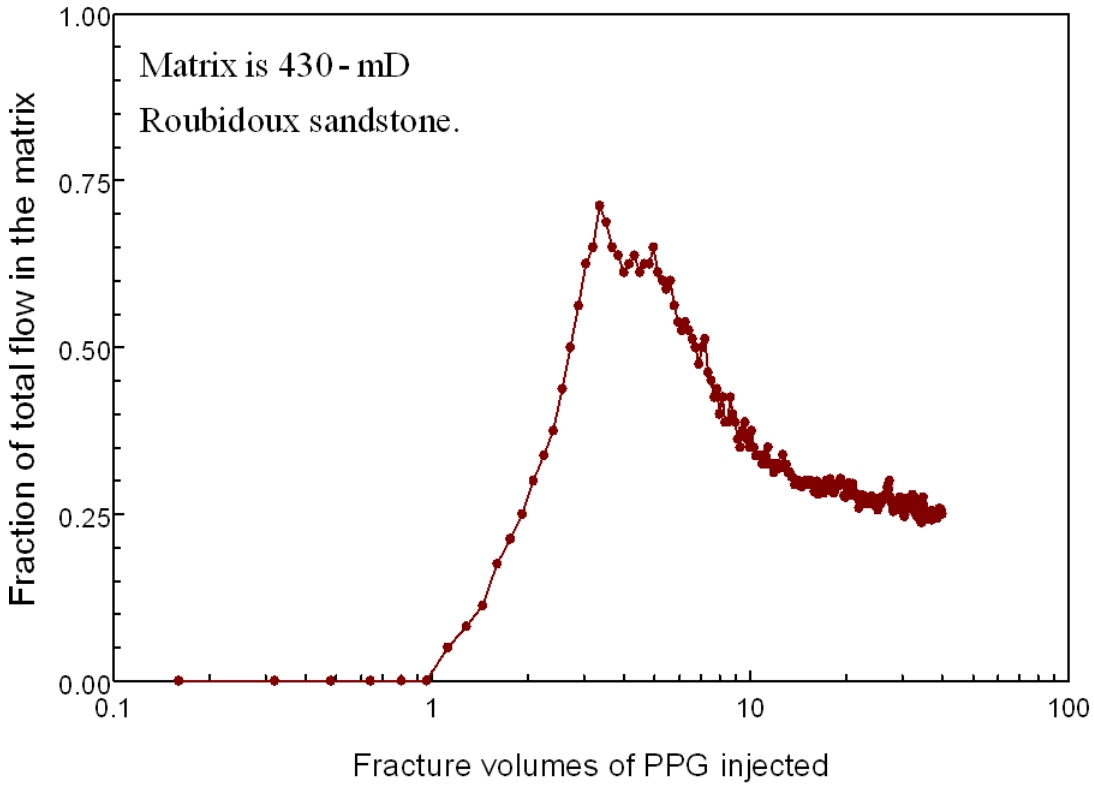

Figure 6-8 Brine flow in the porous rock during gel injection.

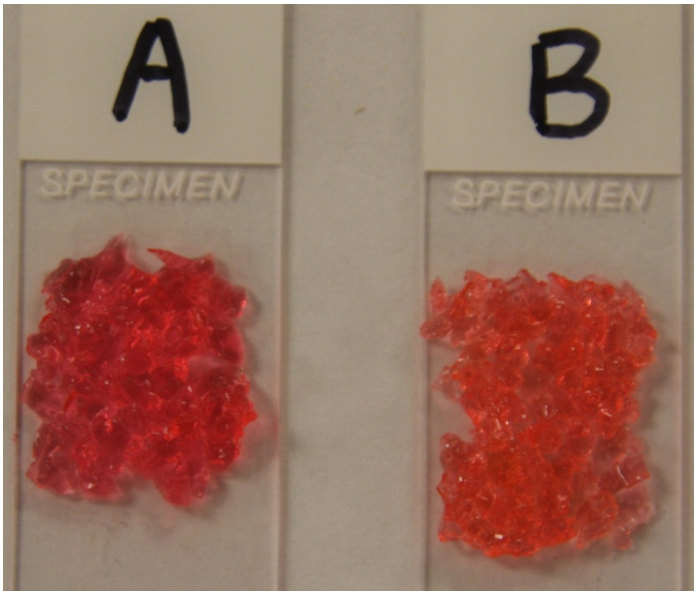

Figure 6-9 Gel samples before (Specimen A) and after (Specimen B) gel injection.

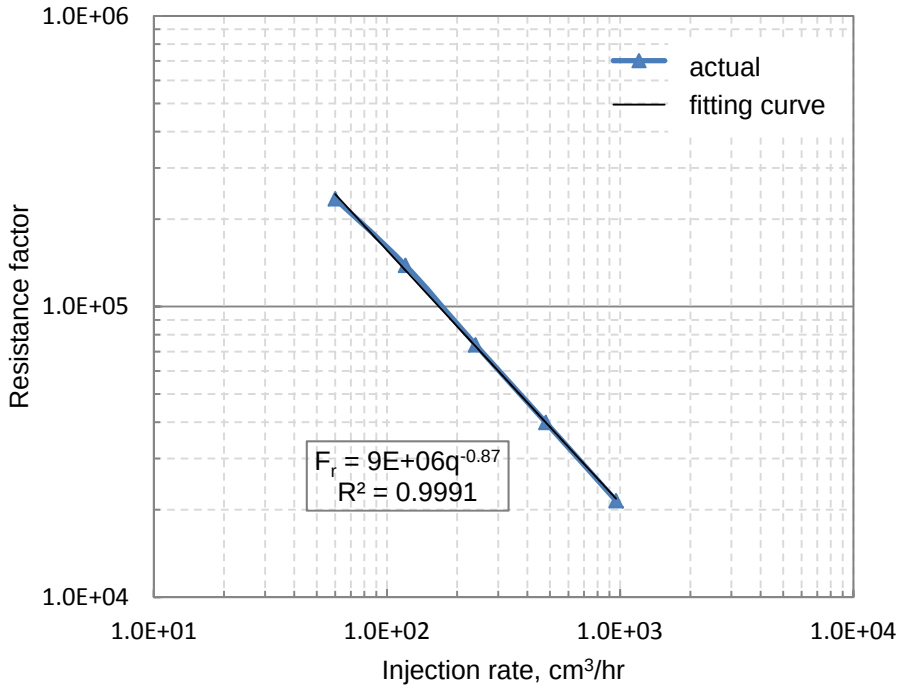

Figure 6-10 Gel resistance factor at various flow rates during gel injection.
(1 cm^3/hr = 0.061 $in.^3$/hr)

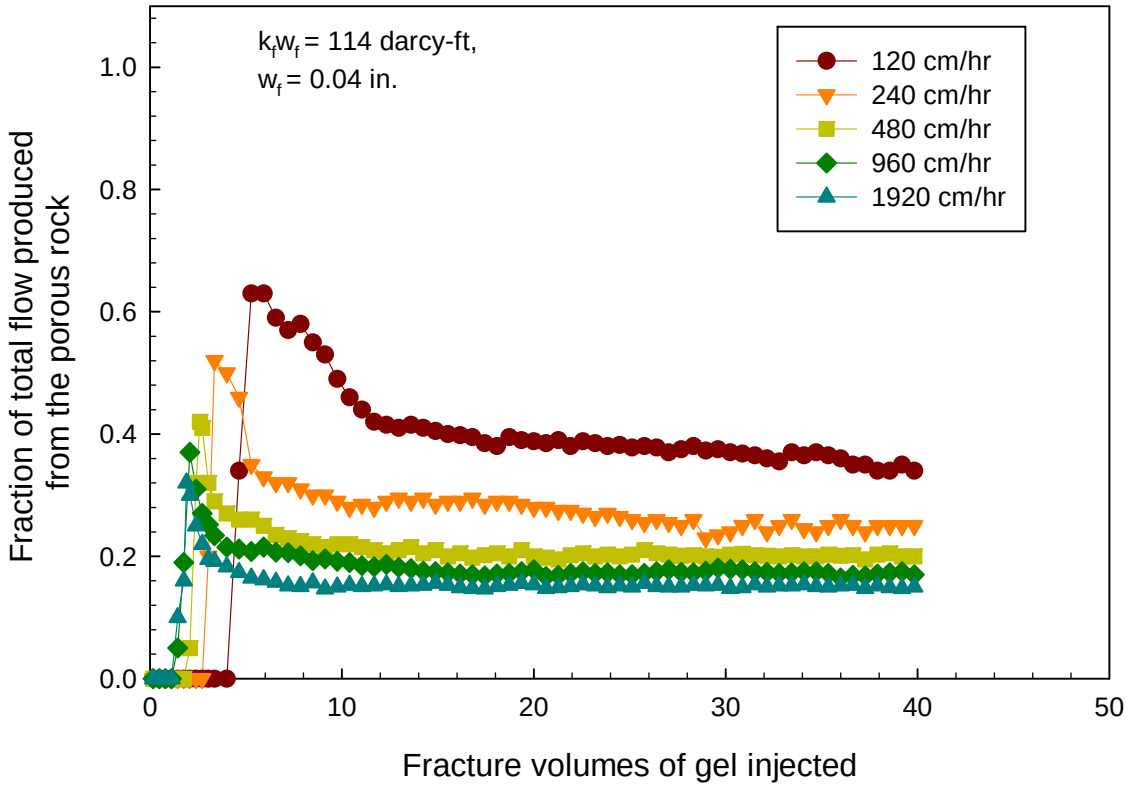

Figure 6-11 Fraction of flow produced from the porous rock during gel injection into 10×2×0.04-in. semi-transparent fracture models at various rates.

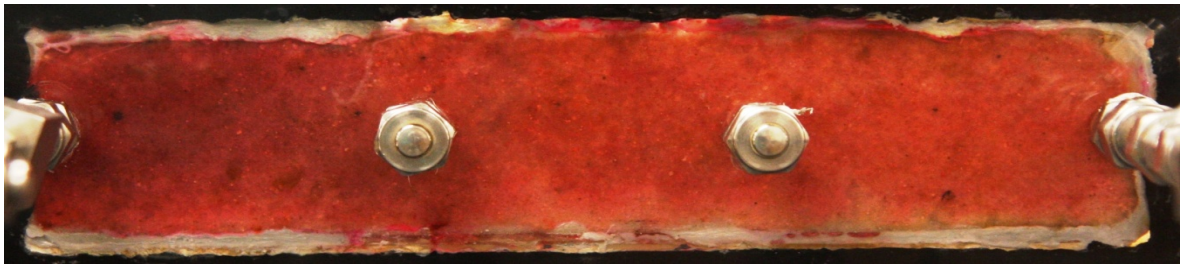

(a)-Brine movement during brine injection into gel pack in the fracture (t = 0 PV)

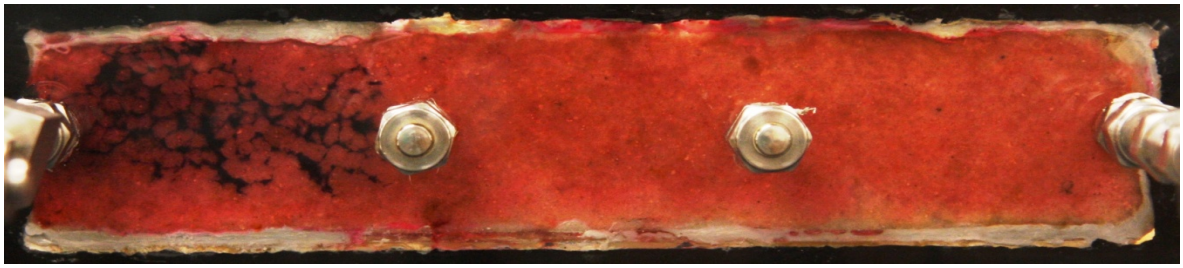

(b)-Brine movement during brine injection into gel pack in the fracture (t = 0.8 PV)

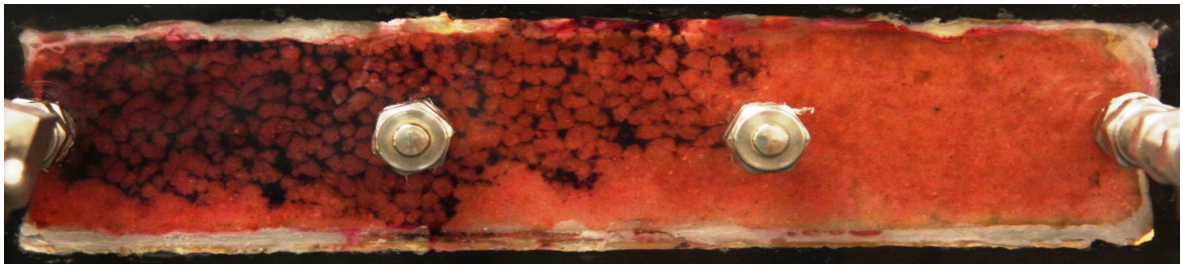

(c)-Brine movement during brine injection into gel pack in the fracture (t = 1.5 PV)

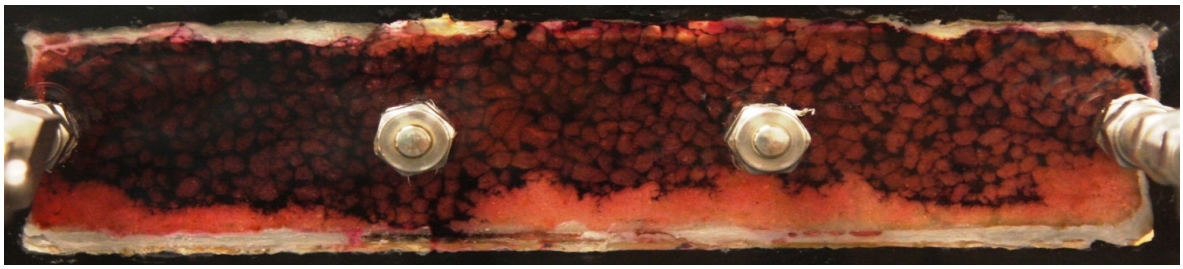

(d)-Brine movement during brine injection into gel pack in the fracture (t = 2.5 PV)

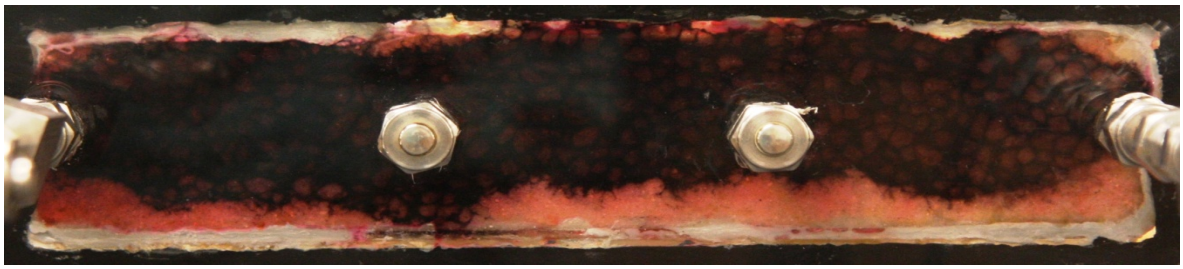

(e)-Brine movement during brine injection into gel pack in the fracture (t = 5 PV)

Figure 6-12 Brine movement during brine injection into gel pack in the fracture.

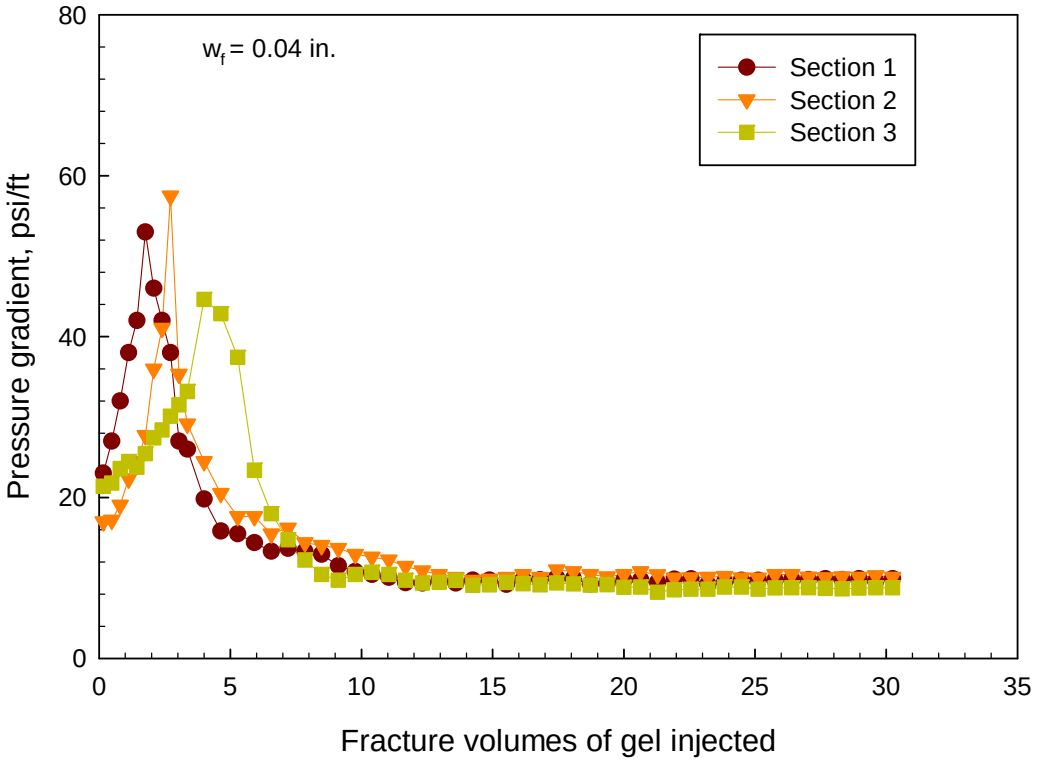

Figure 6-13 Pressure behavior in the fracture taps during brine injection.

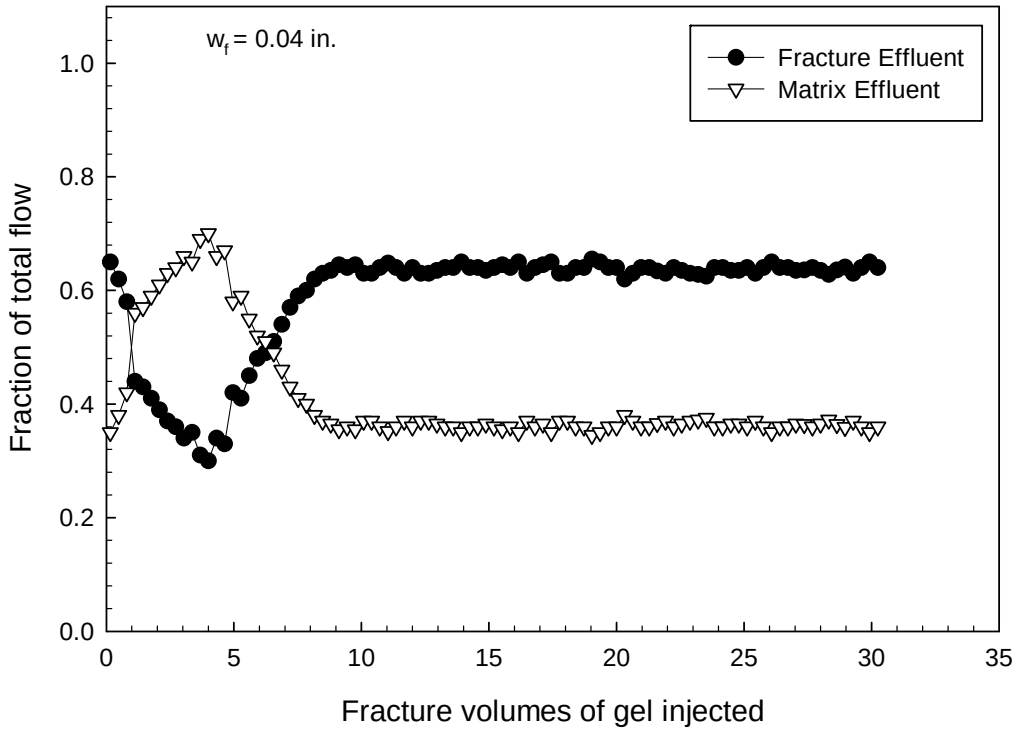

Figure 6-14 Fractional flow measured at the core outlet during brine injection (120 cm^3/hr or 7.32 $in.^3$/hr)).

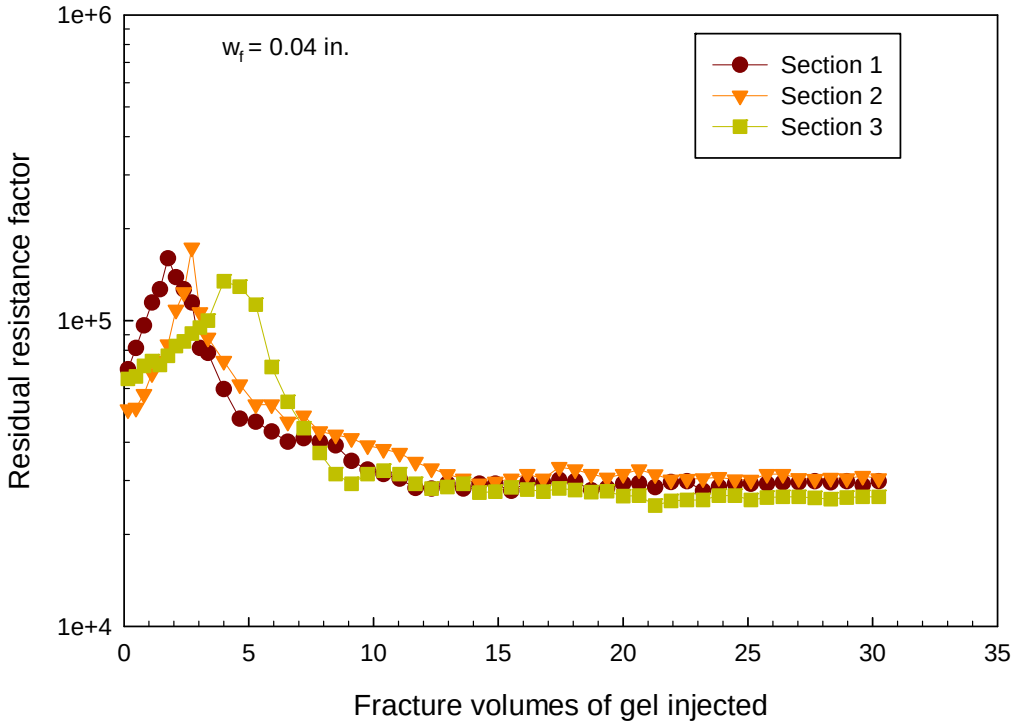

Figure 6-15 Residual resistance factor behavior during brine injection (120 cm^3/hr or 7.32 in.^{3}/hr).

(a)-Core before PPG and brine injection

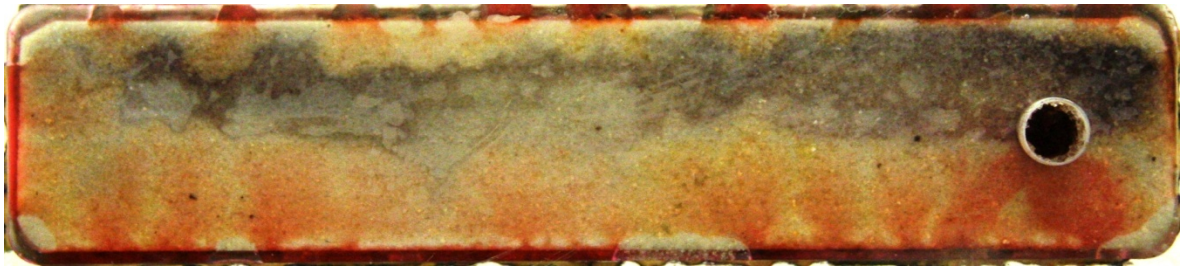

(b)-Core after PPG and brine injection

Figure 6-16 Comparison of the core sample before and after PPG and brine injection.

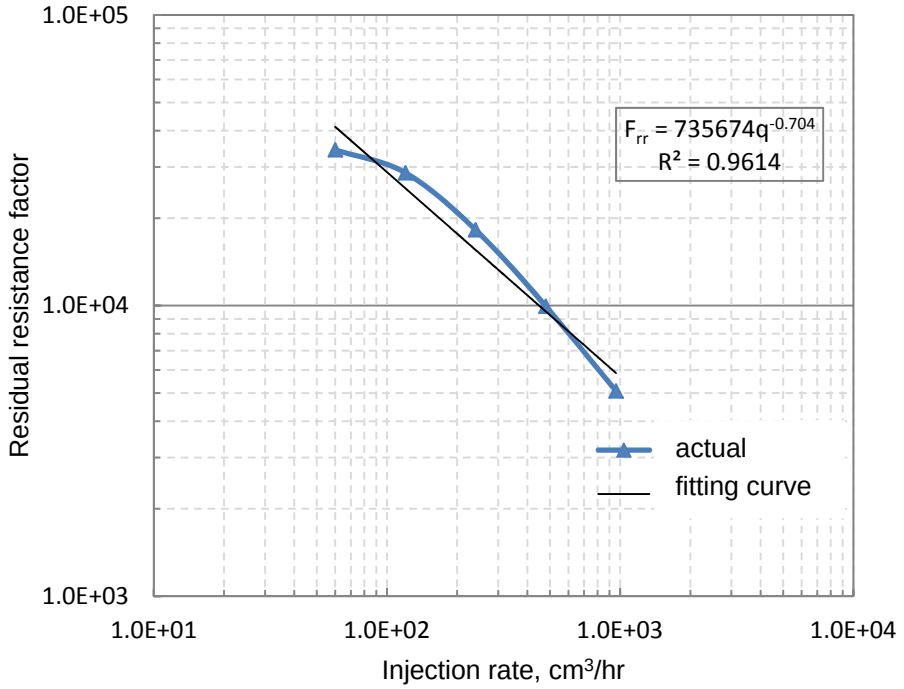

Figure 6-17 Final residual resistance factor at various injection rates during brine injection.
(1 cm^3/hr = 0.061 $in.^3$/hr)

(a)-Gel movement during PPG injection-gel started to move in the fracture (t = 0.1 PV)

(b)-Gel movement during PPG injection-gel front half way through the core (t = 0.5 PV)

(c)-Gel movement during PPG injection-gel front close to the core end (t = 1.2 PV)

(d)-Gel movement during PPG injection-gel front arrival at core end (t = 1.5 PV)

Figure 6-18 Gel movement during PPG injection in the fracture model with 0.2-in.width.

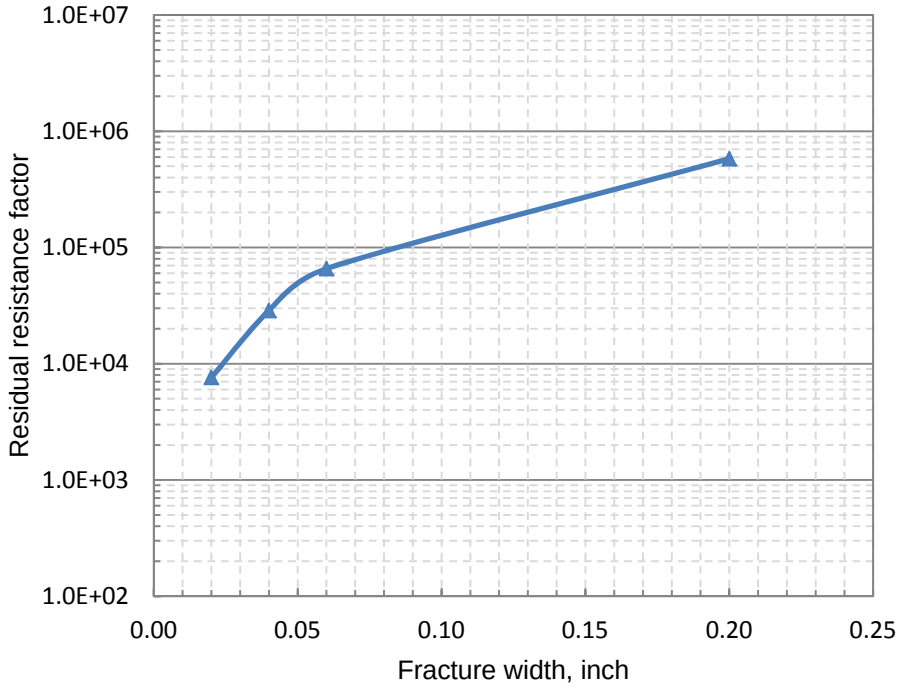

Figure 6-19 Final residual resistance factor at various fracture widths during brine injection.

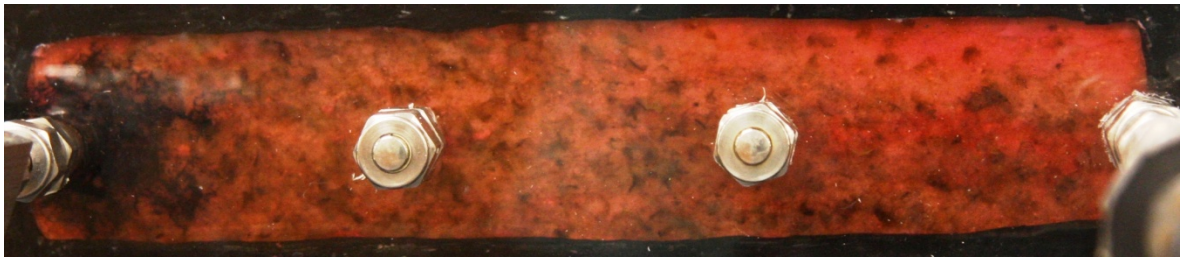

(a)-Brine movement during brine injection into gel pack in the fracture (t = 0.2 PV)

(b)-Brine movement during brine injection into gel pack in the fracture (t = 0.5 PV)

(c)-Brine movement during brine injection into gel pack in the fracture (t = 1.2 PV)

(d)-Brine movement during brine injection into gel pack in the fracture (t = 2 PV)

Figure 6-20 Brine movement during brine injection into gel pack in the fracture with 0.2-in. width.

Table 6-1 Typical Characteristics of Preformed Particle Gels

Properties	Value
Absorption Deionized Water (g/g)	>200
Apparent Bulk Density (g/l)	540
Moisture Content (%)	5
pH Value	5.5-6.0 (+/- 0.5; 1% gel in 0.9% NaCl)

Table 6-2 Size Distribution of Preformed Particle Gel

Sieves (Mesh)	Size (microns)	Content (percent)
20	>830	12.01
40	380~830	75.32
60	250~380	12.46
80	180~250	0.20
100	150~180	0.01

Table 6-3 Parameters of Screens Used for Experiments

Screen Type	Wire Diameter (Inch)	Mesh Per Linear Inch	Width Opening (Inch)
Small	0.0026	150 * 150	0.0041
Medium	0.007	80 * 80	0.0060
Large	0.013	40 * 40	0.0120

Table 6-4 PPG Concentrations for Fully Swollen PPG prepared with Different Brine Concentration

Brine Concentration (%)	PPG Concentration (%)
0.25	1.597
1	2.731
10	2.961

Table 6-5 Effect of Injection Rate on Gel Propagation

Fracture dimension ($L_f \times h_f \times w_f$)	10×2×0.04-in.				
Injection rate, cm^3/hr	60	120	240	480	960
Estimated velocity in the fracture, cm/hr	120	240	480	960	1920
Total fracture volumes of gel injected	40	40	40	40	40
Average pressure gradient, psi/ft	39	46	49	53	57
Gel front arrival at core end, fracture volumes	5.3	3.2	2.6	2.1	1.9
Peak fraction of matrix flow, %	63	50	42	37	32
Final fraction of flow produced from matrix, %	34	25	20	17	15

(1 cm^3/hr = 0.061 $in.^3/hr$, 1 cm = 0.4 inch)

Table 6-6 Effect of Injection Rate on Brine Injection

Fracture dimension ($L_f \times h_f \times w_f$)	10×2×0.04-in.				
Injection rate, cm^3/hr	60	120	240	480	960
Total fracture volumes of gel injected	30	30	30	30	30
Average pressure gradient, psi/ft	5.7	9.5	12.1	13.2	13.5
Peak fraction of matrix flow, %	78	71	65	53	46
Final fraction of flow produced from matrix, %	40	36	31	24	19

(1 cm^3/hr = 0.061 $in.^3/hr$)

Table 6-7 Effect of Fracture Width on Gel Propagation

Fracture dimension ($L_f \times h_f$)	10×2 in.			
Fracture width, in.	0.02	0.04	0.06	0.2
Injection rate, cm^3/hr	60	120	180	600
Estimated velocity in the fracture, cm/hr	240	240	240	240
Total fracture volumes of gel injected	40	40	40	40
Average pressure gradient, psi/ft	91	46	26	14
Gel front arrival at core end, fracture volumes	4.8	3.2	2.7	1.5
Peak fraction of matrix flow, %	59	50	34	8
Final fraction of flow produced from matrix, %	28	25	17	4

(1 cm^3/hr = 0.061 $in.^3/hr$, 1 cm = 0.4 inch)

Table 6-8 Effect of Fracture Width on Brine Injection

Fracture dimension ($L_f \times h_f$)	10×2 in.			
Fracture width, in.	0.02	0.04	0.06	0.2
Injection rate, cm^3/hr	60	120	180	600
Total fracture volumes of gel injected	30	30	30	30
Average pressure gradient, psi/ft	10.1	9.5	9.7	7.7
Peak fraction of matrix flow, %	75	71	65	44
Final fraction of flow produced from matrix, %	42	36	35	12

(1 cm^3/hr = 0.061 $in.^3/hr$)

Table 6-9 Effect of Gel Concentration on Gel Propagation

Fracture dimension ($L_f \times h_f \times w_f$)	10×2×0.04 in.		
Gel concentration, %	2.73	1.36	0.91
Injection rate, cm^3/hr	120	120	120
Estimated velocity in the fracture, cm/hr	240	240	240
Total fracture volumes of gel injected	40	40	40
Average pressure gradient, psi/ft	46	22	17
Gel front arrival at core end, fracture volumes	3.2	8.6	11.3
Peak fraction of matrix flow, %	50	19	11
Final fraction of flow produced from matrix, %	25	7	4

(1 cm^3/hr = 0.061 $in.^3/hr$, 1 cm = 0.4 inch)

Table 6-10 Effect of Gel Concentration on Brine Injection

Fracture dimension ($L_f \times h_f \times w_f$)	10×2×0.04 in.		
Gel concentration, %	2.73	1.36	0.91
Injection rate, cm^3/hr	120	120	120
Total fracture volumes of gel injected	30	30	30
Average pressure gradient, psi/ft	9.5	8.9	9.2
Peak fraction of matrix flow, %	71	62	57
Final fraction of flow produced from matrix, %	36	29	30

(1 cm^3/hr = 0.061 $in.^3/hr$)

Table 6-11 Effect of Brine Concentration on Gel Propagation

Fracture dimension ($L_f \times h_f \times w_f$)	10×2×0.04 in.		
Brine concentration, %	0.25	1.0	10
Injection rate, cm^3/hr	120	120	120
Estimated velocity in the fracture, cm/hr	240	240	240
Total fracture volumes of gel injected	40	40	40
Average pressure gradient, psi/ft	28	46	73
Gel front arrival at core end, fracture volumes	5.1	3.2	1.8
Peak fraction of matrix flow, %	58	50	29
Final fraction of flow produced from matrix, %	30	25	12

(1 cm^3/hr = 0.061 $in.^3/hr$, 1 cm = 0.4 inch)

Table 6-12 Effect of Brine Concentration on Brine Injection

Fracture dimension ($L_f \times h_f \times w_f$)	10×2×0.04 in.		
Brine concentration, %	0.25	1.0	10
Injection rate, cm^3/hr	120	120	120
Total fracture volumes of gel injected	30	30	30
Average pressure gradient, psi/ft	4.3	9.5	26
Peak fraction of matrix flow, %	56	71	85
Final fraction of flow produced from matrix, %	27	36	39

(1 cm^3/hr = 0.061 $in.^3/hr$)

Table 6-13 Effect of PPG Particle Size on Gel Propagation

Fracture dimension ($L_f \times h_f \times w_f$)	10×2×0.04 in.		
Mesh size, meshes	40	80	150
Injection rate, cm^3/hr	120	120	120
Estimated velocity in the fracture, cm/hr	240	240	240
Total fracture volumes of gel injected	40	40	40
Average pressure gradient, psi/ft	46	42	39
Gel front arrival at core end, fracture volumes	3.2	2.9	2.5
Peak fraction of matrix flow, %	52	47	43
Final fraction of flow produced from matrix, %	25	26	21

(1 cm^3/hr = 0.061 $in.^3/hr$, 1 cm = 0.4 inch)

Table 6-14 Effect of PPG Particle Size on Brine Injection

Fracture dimension ($L_f \times h_f \times w_f$)	10×2×0.04 in.		
Mesh size, meshes	40	80	150
Injection rate, cm^3/hr	120	120	120
Total fracture volumes of gel injected	30	30	30
Average pressure gradient, psi/ft	9.5	8.9	5.3
Peak fraction of matrix flow, %	71	58	34
Final fraction of flow produced from matrix, %	36	29	17

(1 cm^3/hr = 0.061 $in.^3/hr$)

7. Using Screen Test Results to Predict the Effective Viscosity of Swollen Superabsorbent Polymer Particles Extrusion through an Open Fracture

7.1. Summary

In this chapter, a simple method, a screen model test, was used to evaluate the rheological behavior of the swollen PPG. Results show that swollen PPG is a shear-thinning material that can be expressed using a power law equation from which an apparent consistency constant and an apparent flow index can be obtained. Considering the shear-thinning properties, we first developed a theoretical mathematical model using a general power law equation to predict the pressure gradient of swollen PPG during its extrusion through a fracture. Then we modified the model by correlating screen test results with fracture experiment results so that the apparent consistency constant and the apparent flow index obtained from screen tests were introduced to replace the consistency constant and flow index from general power law equation. These correlations correlated effective viscosity with flow rate, fracture width, apparent consistency constant and apparent flow index together. The newly developed correlations were validated and the results show that a single group of screen test measurements can be applied to determine the effective viscosity of PPG in a fracture, with limited errors.

7.2. Introduction

During gel injection, the injectivity, the ratio of flow rate to pressure drop, depends on several factors such as fracture width, gel viscosity, flow rate, and etc. Extensive efforts have been made to determine and quantify the gel viscosity and injection pressure of gel in porous media, both theoretically and experimentally, but all of the work was focused on in-situ bulk gels. Extrusion experiments using fractures can directly obtain the gel rheology properties in fractures and provide a wealth of data, but they are both expensive (for core materials and casting) and time-consuming (three to four days per experiment, with one to two weeks of setup time). Rheology measurements are often used to characterize bulk gels and gelants that are used for conformance control. The preformed gel particles that are applied for conformance control usually range in size from a few hundred micrometers to a few millimeters and are irregular in shape;

therefore, traditional methods to measure rheology properties of a material are not suitable for the swollen gel particles.

The objective of this study is to develop models that can be used to predict the effective viscosity of swollen PPG during its extrusion through a fracture. We first developed a theoretical model to predict the pressure gradient of swollen particle gel extrusion through an open fracture, assuming that particle gel is a shear-thining material and follows power-law rheology equation. However, the parameters to describe particle gel rheology in the theoretical model could not be determined by a conventional rheology measurement tool—rheometer; therefore, we used a simple screen model to see whether it could be used to determine the rheology parameters of swollen particle gel. Considering the difference between screen tests and real rheology tests, the theoretical model was modified by correlating the fracture experimental results with screen experiment results. Compared to the fracture experiment results, a screen experiment is much simpler and takes a shorter time to complete.

7.3. Theoretical Model to Calculate the Pressure Gradient of a Shear-Thinning Material through an Open Fracture

Extensive studies show that gels are shear-thinning materials that follow power-law models which are expressed as the relationship between shear rate and shear stress with viscosity. The general form of a power-law model is as follow:

$$\tau = \mathrm{K} \cdot \gamma^{\mathrm{n}} \tag{7-1}$$

where K is the consistency constant ($\mathrm{Pa \cdot s^n}$), n is the flow index, γ is the shear rate ($\mathrm{s^{-1}}$), and τ is the shear stress (Pa). The parameters n and K represent the degree of non-Nentonian behavior. The material is considered to be a non-Newtonian material if n is not equal to 1. In addition, the degree of non-Newtonian behavior increases as the flow index, n, deviates from unity.

For a steady-state flow, a momentum balance for a shell of finite thickness was first applied. As the thickness approached zero, the corresponding differential equation describing the momentum flux distribution was obtained. According to the non-Newtonian expression for the momentum flux, a differential equation for the velocity distribution could be obtained as follow:

$$\tau = \mathrm{K} \cdot \left(\frac{\partial \mathrm{v}}{\partial \mathrm{r}}\right)^{\mathrm{n}} \tag{7-2}$$

Assuming there is no potential for carrier fluid leakoff along the length and height of the fracture model, for fluids flowing between two parallel plates, the follow equation can be given:

$$\tau = (\frac{P_0 - P_L}{L})x \tag{7-3}$$

where L is the length of the fracture, x is the distance from the center of the fracture to the fracture wall, P_0 and P_L are the inlet and outlet pressures, respectively.

Comparing Equations 7-2 and 7-3, the follow equation can be obtained,

$$\mathrm{K} \cdot \left(\frac{\partial \mathrm{v}}{\partial \mathrm{r}}\right)^{\mathrm{n}} = (\frac{P_0 - P_L}{L})x \tag{7-4}$$

Integrating the differential equation, the velocity distribution along the fracture width is

$$v = \left(\frac{P_0 - P_L}{KL}\right)^{\frac{1}{n}} \frac{n}{n+1} (\frac{w}{2})^{\frac{n+1}{n}} \left[\left(\frac{2x}{w}\right)^{\frac{n+1}{n}} - 1\right] \tag{7-5}$$

where v is the velocity, and w is the fracture width.

The volumetric flow rate is

$$q = \left(\frac{P_0 - P_L}{KL}\right)^{\frac{1}{n}} \frac{h}{2} \left(\frac{n}{2n+1}\right) w^{\frac{2n+1}{n}} \tag{7-6}$$

where q is the volumetric flow rate.

The pressure gradient versus fracture width is:

$$\frac{dp}{dl} = (2K)(\frac{2n+1}{n})^n (\frac{2q}{h})^n \frac{1}{w^{2n+1}} \tag{7-7}$$

where $\frac{dp}{dl}$ is the pressure gradient.

Therefore, for a shear-thinning material following a power-law model, the pressure gradient varies inversely from the fracture width with the power of 2n+1. To calculate the pressure gradient of a shear-thining fluid flow through an open fracture, we not only need to know flow rate, fracture width and height, but we also need to know the consistency constant K and flow index n. However, K and n could not be obtained by using a conventional rheometer measurement method because the swollen PPG particles

were irregular in shape and large in size. Therefore, experiments were conducted to check if screen tests could be used to obtain the parameters which could represent the two.

7.4. Experiments

7.4.1. Materials

The same PPG samples were used in the experiments. Table 7-1 lists the main characteristics of PPG used in the experiments, and Table 7-2 shows the size distribution of the PPG as determined by a sieving test.

The swollen PPG was prepared using the procedure as mentioned in previous chapters.

7.4.2. Screen Model Experiments

A screen model consists of a long acrylic tube to which end plates are attached by two flanges using steel rods and nuts which is the same as that used in chapter 3. The top flange has one hole connected to an ISCO pump by tubing and fitting. The bottom flange has multiple holes that allow PPG particles to flow through without extra pressure. A piston was inserted into the acrylic tube to prevent direct contact between injected fluids and the PPG particles. Screens of various mesh sizes were placed between the gel particles and the bottom flange. The pressure from the pumped water pushed the piston, which forced the swollen PPG to pass through the wire cloth mesh at the end of the tube. All experiments were run at room temperature.

Three stainless wire cloths were chosen with screen meshes of 150, 80 and 40, respectively. Table 7-3 shows the parameters of the screens used here. The wire cloth was cut into small 2-inch diameter circles. A total of 12 experiments were conducted to study the effect of the brine concentration used to prepare the swollen gel particles, the injection rate and the mesh size on the PPG injection pressure.

The experimental setup for screen tests in Figure 7-1 is described as follows:

The piston was inserted into the top of the transparent acrylic tube. The tube was then packed with a swollen PPG sample prepared using a desired brine concentration. A screen was placed above the holes in the bottom cap. Using the metal rods, the packed tube was then set on the bottom cap; and the top cap was placed on top of the transparent acrylic cylinder with the piston at the top. The apparatus was then tightly secured using washers and nuts. A pressure gauge was connected to the bottom of the transparent

acrylic tube to monitor pressure changes with the injection rate. Any air gaps in the outlet line of the ISCO pump were eliminated, and the line was connected to the top cap of the apparatus and tightened to prevent leaks.

The experimental procedure for screen tests was as follows:

Distilled water was filled to release the air between the piston and the top cap; pumped distilled water into the screen model at a constant injection rate of 1 ml/min (3.66 $in.^3$/hr) until the piston started to move; switched the flow rate to 0.1 ml/min (0.366 in^3/hr) and the pressure response was monitored until a constant pressure was reached. The process was repeated with multiple injection flow rates, and the stable pressure for each injection rate was recorded. The procedure was repeated until the pressure differences were negligible, even when the increase in injection rate was significant. The above procedure was repeated for each screen and each brine concentration, and pressure was monitored during the entire process.

7.4.3. Fracture Experiments

Figure 7-2 shows the fracture model, which is also the one we used in Chapter 5 experiments. Two ISCO pumps were used, one for PPG injection and the other for brine injection. The fracture model was constructed of two acrylic plates with a rubber O-ring between them. Bolts, nuts, and shims were used to fix the two plates and control fracture width. On one side of the plate, a hole functioned as an inlet for the injection of fluids and PPG; on the other side, another hole provided an outlet to discharge fluids and PPG. The pressure transducers were connected to the inlet to record the fracture pressure. The model was transparent so that the PPG and water movement could be visibly monitored.

Brine was first injected into the fracture model, and then fully swollen PPG was extruded into the fracture model by an ISCO pump through an accumulator. Six flow rates were used for each experiment: 5, 10, 15, 20, 25, and 30 ml/min (18.3, 36.6, 54.9, 73.2, 91.5, and 109.8 $in.^3$/hr, respectively). The flow rates were tested in sequence (from lowest to highest) to obtain the corresponding stabilized pressure during gel injection. Once the gel was in place, water was injected into the gel particles packed in the fracture to test the efficiency of gel plugging on water. During these experiments, the brine injection rates were the same as those used during gel injection. The pressure data were recorded to check the pressure changes over time and the injection rates.

7.5. Results and Analysis

Figure 7-3 shows the brine concentration and flow rate effect on PPG injection pressure in the screen tests with the screen meshes of 150, 80, and 40. It can be seen that injection pressure increased with brine concentration in a given screen at a constant injection flow rate. For example, at an injection rate of 0.2 ml/min (0.732 $in.^3$/hr), the injection pressures for PPG prepared with 0.05, 0.25, 1.0, and 10 wt% brine were 41, 70, 120, and 210 psi respectively for the 150 mesh screen model. Before we conducted the experiments, it was hypothesized that the injection pressure for the sample prepared with a low brine concentration would be higher than the sample prepared with a high brine concentration because the swollen particle size was larger in the low brine concentrations. However, the experimental results showed a completely different trend. It can be inferred that the property of softness or deformability of swollen particles had a more dominant effect on PPG injection pressure than the particle size of the swollen PPG because the swollen particles in high salinity brine is much harder and less deformable than those in low salinity brine. It also can be seen that the injection pressure increased as the mesh size decreased. For example, with an injection flow rate of 0.1 ml/min (0.366 $in.^3$/hr) and a brine concentration of 0.05%, the PPG injection pressures for meshes of 150, 80, and 40 were 32, 22, and 9 psi, respectively.

Figure 7-3 also shows that the injection pressure increased with flow rate for a given brine concentration and a given screen size, and they showed straight lines in the log-log scale. A power law equation can be used to well fit their relationship as follow:

$$p = K_{a1} q^{n_{a1}} \tag{7-8}$$

where p is the PPG injection pressure in psi, q is the flow rate in ml/min, and K_{a1} and n_{a1} are constants related to brine concentration and screen size. Table 7-4 lists K_{a1} and n_{a1} with this power law equation and their correlation factors. All correlation factors are more than 0.95. The apparent flow index decreased as the brine concentration increased, whereas the apparent consistency constant increased as the brine concentration increased.

Equation 7-8 indicates that swollen PPG is a shear-thinning material. Comparing the power law model for a shear-thinning material in Equation 7-1, K_{a1} and n_{a1} in Equation 8 are quite similar to the consistency constant K and flow index n in Equation 1.

They are not exactly the same, however, so we called them as apparent consistency constant and apparent flow index, respectively.

Figure 7-4 shows the brine concentration and flow rate effect on PPG injection pressure in fracture models with fracture widths of 0.5, 1.0, and 1.5 mm (0.02, 0.04, and 0.06 in.). For fractures with given widths, it can be seen that PPG injection pressure consistently increased with brine concentration when the injection flow rate was the same. This is similar to the findings in the screen tests. The figure also indicates that the injection pressure decreased with an increase of fracture width with the same flow rate and same brine concentration. This is easy to understand because a wider fracture would be more conductive, thus the injection pressure would be lower.

Figure 7-4 also shows that PPG injection pressure increased with the injection flow rate for a given brine concentration and a given fracture width, and straight lines were shown in the log-log scale. A power law equation can be used to fit their relationship as follow:

$$p = K_{a2} q^{n_{a2}} \tag{7-9}$$

where p is the PPG injection pressure in *psi*, q is the flow rate in ml/min, and K_{a2} and n_{a2} are constants related to brine concentration and fracture width. Table 5 lists K_{a2} and n_{a2} for this power law equation and their correlation factors.

Comparing from Figures 7-3 and 7-4, it is obvious that the results from screen tests were strongly parallel to those from fracture experiments. It is more important that both experimental results showed that swollen PPG was a shear-thinning material and could be well fitted by power law equations in which the apparent consistency constant and apparent flow index can be obtained from screen tests or fracture experiments. In comparison with fracture model experiments, screen experiments usually take less time and are easier to operate. Therefore, we used the apparent consistency constant K_{a1} and apparent flow index n_{a1} from the screen models to replace the consistency constant K and flow index n in Equation 7 so that the fracture pressure gradient of swollen PPG extrusion through an open fracture model could be predicted using screen tests.

7.6. Correlations for Pressure Gradient

Because the apparent consistency constant K_{a1} and apparent flow index n_{a1} from the screen models are related to the consistency constant K and flow index n in a

standand power-law model in Equation 7-1, Equation 7-7 can be modified in the following general form:

$$\frac{dp}{dl} = aK_a{}^b\left(\frac{2n_a+1}{n_a}\right)^{c\cdot n_a}\left(\frac{2q}{h}\right)^{d\cdot n_a}\left(\frac{1}{w^{2n_a+1}}\right)^e \tag{7-10}$$

Equation 7-10 includes five given parameters, namely, the experimentally determined apparent flow index n_a, the apparent consistency constant K_a, the injection flow rate q, the fracture height h, and the fracture width w. The constants a, b, c, d, and e were determined through a regression procedure as follows:

(1) In these parameters, the experimentally determined apparent flow index n_a and the apparent consistency constant K_a were based on the screen tests, while the injection flow rate q, the fracture height h, and the fracture width w were given in the fracture experiments.

(2) The non-linear regression technique was used to generate the regression for these experimental data. The pressure gradient data in the fracture experiments were used in the regression process.

(3) The correlations developed were compared in terms of the absolute average relative errors, R^2 values, and parity charts to ensure the accuracy of the model. A parity chart is a plot with experimental value on the horizontal axis, versus one or several model predictions on the vertical axis that is used to evaluate the absolute average relative errors for each correlation. An absolute average relative error is defined as the sum of the relative difference between the experimental and calculated values of the pressure gradient, divided by the number of measurements. It is expressed as:

$$\varepsilon_a = \frac{1}{n}\sum_{i=1}^{n}\left|\frac{PG_{exp,i}-PG_{cal,i}}{PG_{exp,i}}\right| \times 100\% \tag{7-11}$$

where n is the number of data points, PG_{exp} is the experimental fracture pressure gradient (Pa/m), PG_{cal} is the calculated fracture pressure gradient (Pa/m), and ε_a is the absolute average relative error (%).

(4) Proper equations for the pressure gradient were constructed if the new correlations for the fracture pressure gradient were proved to be accurate.

(5) After the models to predict pressure gradient were obtained, validation tests were carried out to ensure its applicability for out-of-range predictions. Out-of-range

predictions are the calculated values that are not included in the data sample for the correlation procedure.

Equation 7-12 is the regressed correlation using the data from 150-mesh screen tests:

$$\frac{dp}{dl} = 39210{K_a}^{-0.0845}\left(\frac{2n_a+1}{n_a}\right)^{12.306n_a}\left(\frac{2q}{h}\right)^{1.442n_a}\left(\frac{1}{w^{2n_a+1}}\right)^{0.257} \quad (7\text{-}12)$$

Equation 7-13 is the regressed correlation using the data from 80-mesh screen tests:

$$\frac{dp}{dl} = 32154{K_a}^{-0.0942}\left(\frac{2n_a+1}{n_a}\right)^{13.475n_a}\left(\frac{2q}{h}\right)^{1.526n_a}\left(\frac{1}{w^{2n_a+1}}\right)^{0.253} \quad (7\text{-}13)$$

Equation 7-14 is the regressed correlation using the data from 40-mesh screen tests:

$$\frac{dp}{dl} = 26303{K_a}^{-0.195}\left(\frac{2n_a+1}{n_a}\right)^{14.105n_a}\left(\frac{2q}{h}\right)^{1.464n_a}\left(\frac{1}{w^{2n_a+1}}\right)^{0.246} \quad (7\text{-}14)$$

The three correlations were compared in terms of the absolute average relative errors, and R^2 values. A parity chart was generated for each correlation with the absolute average relative error as shown in Figures 7-5, 7-6, and 7-7. The absolute average relative errors for Equations 12-14 are 3.45%, 4.61%, and 5.44%, so each of the three correlations can be used to calculate the pressure gradient of the swollen PPG through an open fracture.

7.7. Determination of Viscosity

A resistance factor is often used to evaluate the flow resistance of a gel/gelant flow through porous media. It is defined as:

$$F_r = \left(\frac{k}{\mu}\right)_{brine} \Big/ \left(\frac{k}{\mu}\right)_{gel} \quad (7\text{-}15)$$

where $\left(\frac{k}{\mu}\right)_{brine}$ is brine mobility before gelant placement, md/cp; $\left(\frac{k}{\mu}\right)_{gel}$ is gel mobility during placement, md/cp. The permeability of the fracture model remains the same before gelant placement and during placement, so resistance factor can be calculated as the ratio of gel effective viscosity divided by brine viscosity. Since brine viscosity in room temperature is around 1 cp, gel effective viscosity at room temperature can be viewed as the same as the resistance factor.

The resistance factor can also be expressed as the ratio of the particle gel injection pressure drop to the water injection pressure drop at the same flow rate. The following equation is used to calculate the water pressure drop in a fracture:

$$\frac{\Delta p_w}{L} = \frac{12\mu_w \cdot q}{h \cdot w^3} \tag{7-16}$$

where ΔPw is the water pressure drop, μ is the viscosity of water, L is the fracture length, q is the injection flow rate, h is the fracture height, and w is the fracture width.

Therefore, the effective viscosity of swollen PPG flow through an open fracture can be obtained by using newly correlated pressure models Equations 7-9 to 7-11 divided by the water pressure drop equation.

For 150-mesh screen tests (Equation 7-12), the PPG effective viscosity is:

$$\mu_{PPG} = 3267.5{K_a}^{-0.0845}\left(\frac{2n_a+1}{n_a}\right)^{12.306n_a}\left(\frac{2q}{h}\right)^{1.442n_a}\left(\frac{1}{w^{2n_a+1}}\right)^{0.257}\left(\frac{hw^3}{q}\right) \tag{7-17}$$

For 80-mesh screen tests (Equation 7-13), the PPG effective viscosity is:

$$\mu_{PPG} = 2679.5{K_a}^{-0.0942}\left(\frac{2n_a+1}{n_a}\right)^{13.475n_a}\left(\frac{2q}{h}\right)^{1.526n_a}\left(\frac{1}{w^{2n_a+1}}\right)^{0.253}\left(\frac{hw^3}{q}\right) \tag{7-18}$$

For 40-mesh screen tests (Equation 7-14), the PPG effective viscosity is:

$$\mu_{PPG} = 2191.9{K_a}^{-0.195}\left(\frac{2n_a+1}{n_a}\right)^{14.105n_a}\left(\frac{2q}{h}\right)^{1.464n_a}\left(\frac{1}{w^{2n_a+1}}\right)^{0.246}\left(\frac{hw^3}{q}\right) \tag{7-19}$$

Validation tests were conducted to ensure these models' applicability for out-of-range predictions. The PPG made in 1% brine concentration and injected at 5 ml/min flow rate, was not included in the data used to generate the correlation, but was used to validate the model in Equation 7-17. The newly developed model was used to determine the PPG effective viscosity in the fracture model using the data from the 150-mesh screen tests. The corresponding effective viscosity was calculated for three different fracture widths, namely, 0.5, 1.0, and 1.5 mm (0.02, 0.04, and 0.06 in.). Table 7-6 lists the experimental effective viscosity and the value calculated using Equation 7-17. The average relative error was found to be 3.37%. This indicates that the newly developed correlation can be used to determine the effective viscosity of PPG flowing through fracture models with only a small relative error. The same procedure was repeated for the correlations in Equations 7-18 and 7-19. Tables 7-7 and 7-8 indicate that the other two

models can also be used to determine the PPG viscosity. This means that a single group of screen test measurements (e.g., 150, 80, or 40 meshes) can be applied to assess particle gel properties (effective viscosity, injection pressure) in fractures.

7.8. Conclusion

Experiments were conducted in this study to determine PPG viscosity and injection pressure using screen tests and open fracture models. The correlations are given by regression methods. The major conclusions that can be drawn from this study are as follows:

1. The rheology behavior of the preformed particle gels tested in screen tests showed a strong parallel to the results obtained from gel extrusion experiments in open fracture models.
2. PPG injection pressure increased with brine concentration when the injection flow rate was the same.
3. PPG is a shear-thinning material and can be expressed using a power law equation.
4. For a given flow rate and brine concentration, PPG injection pressure decreases as the mesh size decreases or the fracture width increases.
5. Three models were developed to determine the effective viscosity and injection pressure gradient during swollen PPG extrusion through an open fracture. The absolute average relative errors were found to be around 5%.
6. Validation results from out-of-range data showed that the tests from a single size of screen could be used to predict the pressure gradient and the effective viscosity of swollen PPG extrusion through an open fracture.
7. Screen model tests can be a good substitute for the rheology measurement of particles that vary in size at the millimeter-level and are irregular in shape.

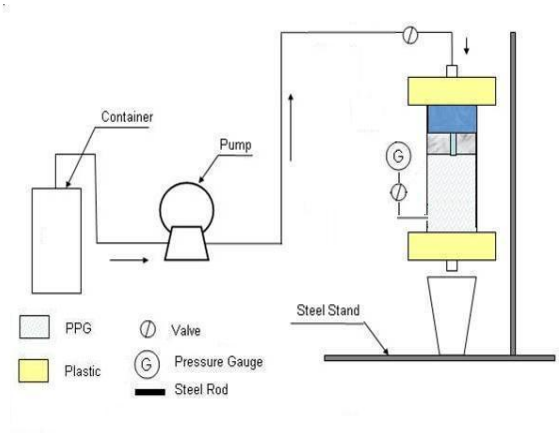

Figure 7-1 Schematic diagram of screen test model and setup.

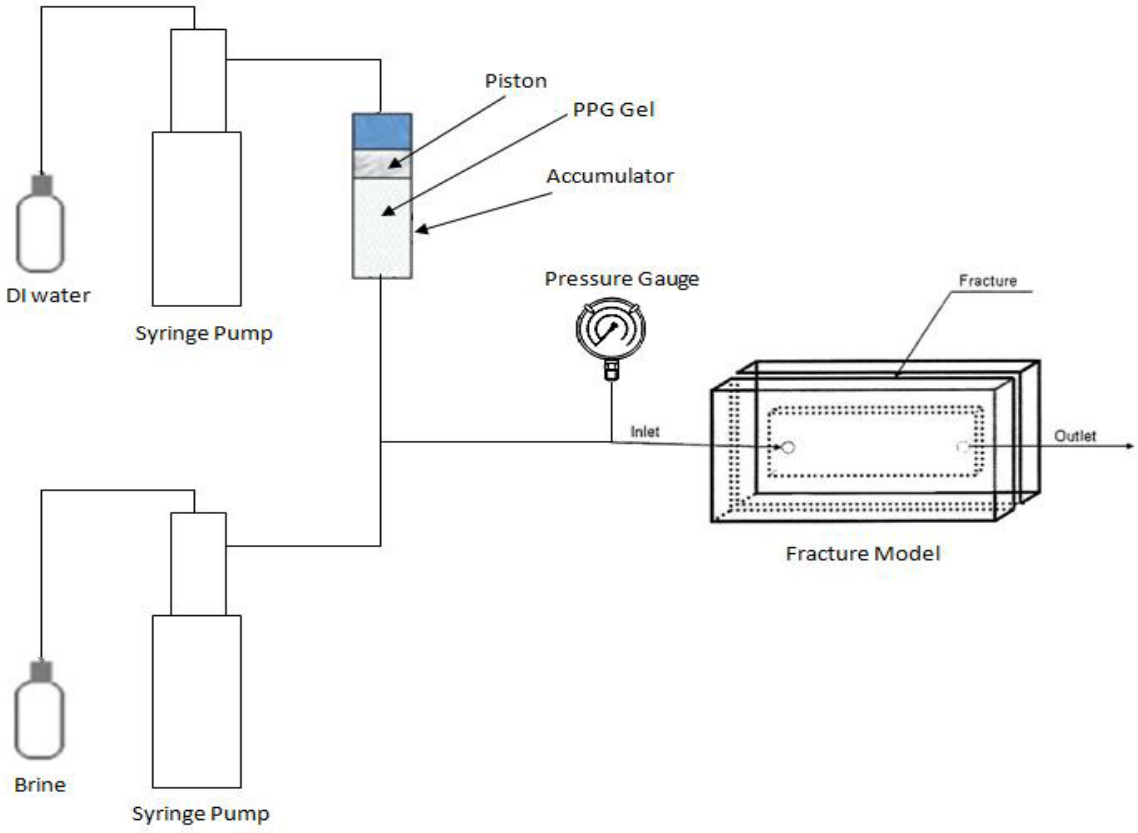

Figure 7-2 Schematic diagram of open fracture model.

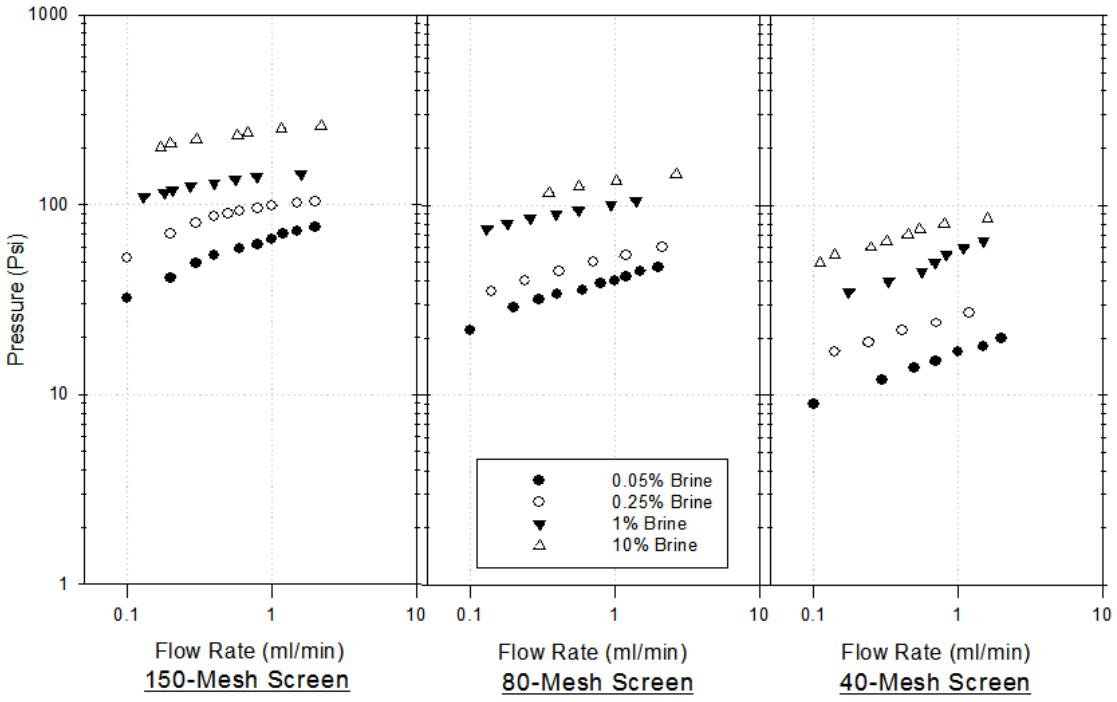

Figure 7-3 Injection pressure for screen tests as a function of flow rate in log-log scale.
(1 ml/min = 3.66 $in.^3$/hr)

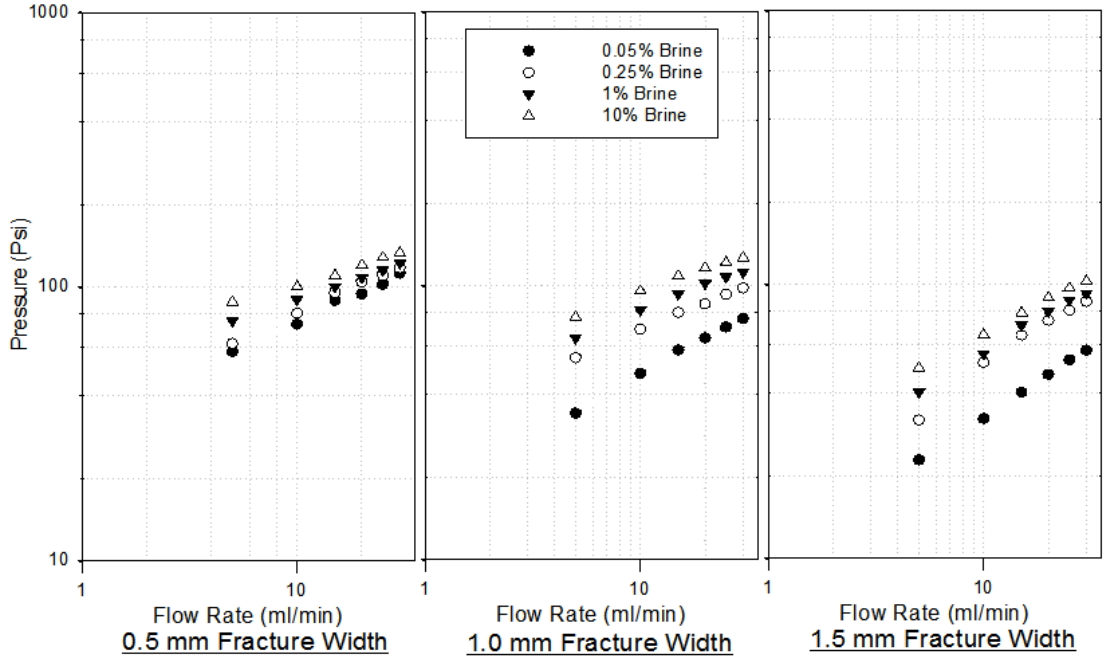

Figure 7-4 Injection pressure for open fracture models as a function of flow rate in log-log scale.
(1 ml/min = 3.66 $in.^3$/hr)

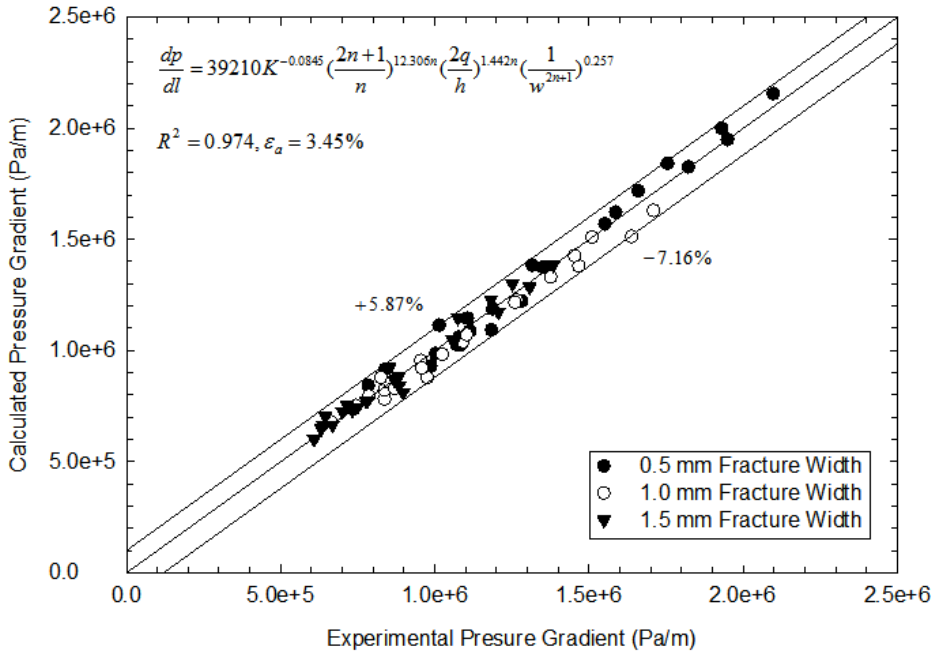

Figure 7-5 Parity chart for pressure gradient model using 150-mesh screen test measurements.

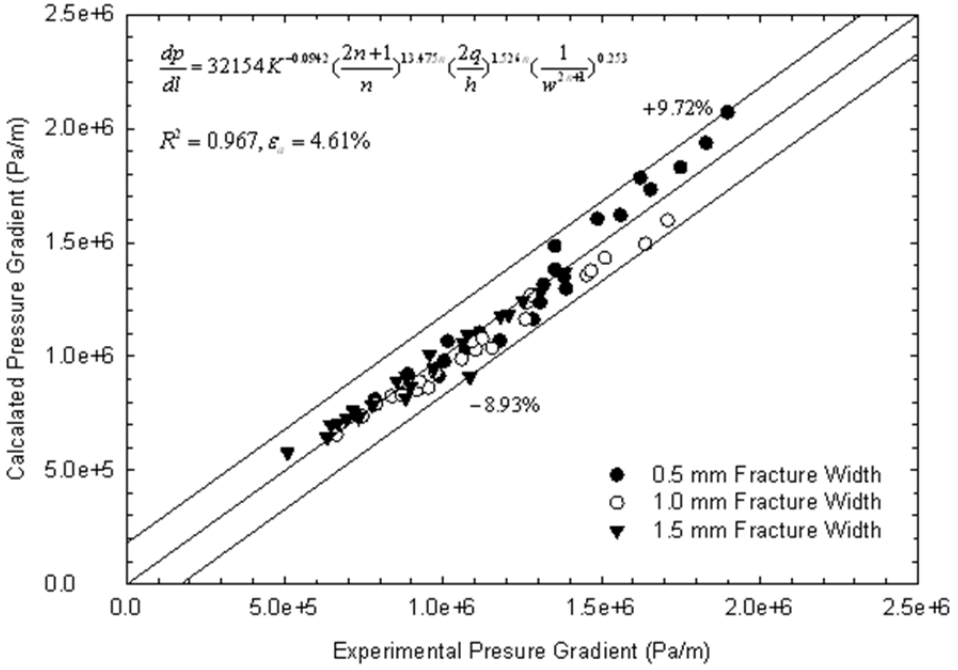

Figure 7-6 Parity chart for pressure gradient model using 80-mesh screen test measurements.

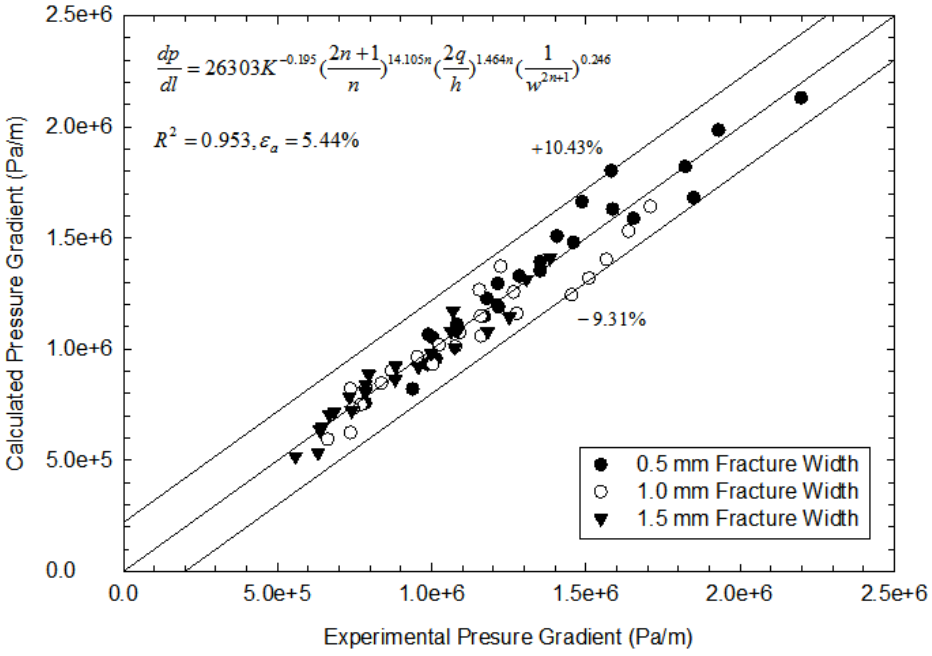

Figure 7-7 Parity chart for pressure gradient model using 40-mesh screen test measurements.

Table 7-1 Typical Characteristics of Preformed Particle Gels

Properties	Value
Absorption Deionized Water (g/g)	>200
Apparent Bulk Density (g/l)	540
Moisture Content (%)	5
pH Value	5.5-6.0 (+/- 0.5; 1% gel in 0.9% NaCl)

Table 7-2 Size Distribution of Preformed Particle Gel

Sieves (Mesh)	Size (microns)	Content (percent)
20	>830	12.01
40	380~830	75.32
60	250~380	12.46
80	180~250	0.20
100	150~180	0.01

Table 7-3 Parameters of Screens Used for Experiments

Screen Type	Wire Diameter (Inch)	Mesh Per Linear Inch	Width Opening (Inch)
Small	0.0026	150 * 150	0.0041
Medium	0.007	80 * 80	0.0060
Large	0.013	40 * 40	0.0120

Table 7-4 Fitting Results for Pressure vs. Injection Flow Rate in Screen Tests

(Using the Fitting Equation $P = K_{a1} q^{n_{a1}}$)

Screen (Mesh)	Brine Conc. (%)	Apparent Consistency Constant (K_{a1})	Apparent Flow Index (n_{a1})	R^2
150	0.05	65.86	0.2843	0.9767
	0.25	97.94	0.2166	0.8907
	1	141.87	0.1123	0.9538
	10	244.48	0.0991	0.9691
80	0.05	41.00	0.2414	0.9733
	0.25	52.74	0.1974	0.9926
	1	101.46	0.1390	0.9888
	10	131.84	0.1120	0.9613
40	0.05	16.591	0.2642	0.9965
	0.25	26.048	0.2153	0.9949
	1	56.87	0.3002	0.9765
	10	81.39	0.2054	0.9683

Table 7-5 Fitting Equations for Pressure as a Function of Flow Rate in Open Fracture Models

(Using the Fitting Equation $P = K_{a2}q^{n_{a2}}$)

Fracture Width (mm)	Brine Conc. (%)	Apparent Consistency Constant (K_{a2})	Apparent Flow Index (n_{a2})	R^2
0.5	0.05	32.28	0.362	0.992
	0.25	35.25	0.356	0.995
	1	48.49	0.268	0.999
	10	59.16	0.236	0.990
1.0	0.05	17.01	0.443	0.996
	0.25	32.51	0.325	0.998
	1	39.53	0.311	0.995
	10	49.69	0.279	0.992
1.5	0.05	9.830	0.520	0.999
	0.25	13.79	0.553	0.983
	1	18.91	0.475	0.995
	10	25.35	0.414	0.998

Table 7-6 Validation of the Newly Developed Model (Equation 14) for PPG Made in 1% Brine Concentration at 5 ml/min Injection Rate

Fracture Width (10^{-3} m)	Effective Viscosity (cp)		Relative Error (%) $[(\mu_{eff\cdot exp} - \mu_{eff\cdot cal})/\mu_{eff\cdot exp}]$
	Calculated	Measured	
0.5	2.711×10^{7}	2.512×10^{7}	-7.89
1.0	1.672×10^{8}	1.710×10^{8}	2.23
1.5	4.847×10^{8}	4.847×10^{8}	0

Table 7-7 Validation of the Newly Developed Model (Equation 15) for PPG Made in 10% Brine Concentration at 15 ml/min Injection Rate

Fracture Width (10^{-3} m)	Effective Viscosity (cp)		Relative Error (%) $[(\mu_{eff\cdot exp} - \mu_{eff\cdot cal})/\mu_{eff\cdot exp}]$
	Calculated	Measured	
0.5	6.274×10^{6}	5.711×10^{6}	-9.86
1.0	3.888×10^{7}	3.922×10^{7}	0.87
1.5	1.131×10^{8}	1.132×10^{8}	0.21

Table 7-8 Validation of the Newly Developed Model (Equation 16) for PPG Made in 10% Brine Concentration at 25 ml/min Injection Rate

Fracture Width (10^{-3} m)	Effective Viscosity (cp)		Relative Error (%) $[(\mu_{eff\cdot exp} - \mu_{eff\cdot cal})/\mu_{eff\cdot exp}]$
	Calculated	Measured	
0.5	4.147×10^{6}	3.985×10^{6}	-4.08
1.0	2.609×10^{7}	2.577×10^{7}	-1.26
1.5	7.652×10^{7}	7.165×10^{7}	-6.79

8. Interaction between Surfactant and Particle Hydrogel

8.1. Summary

In this chapter, a new technology called forced surfactant imbibition was initiated by combining PPG with surfactant. The method was developed based on a study of the compatibility of particle gels and surfactants. Results showed that most surfactants are not absorbed into particle gels. Certain surfactants can significantly reduce gel strength; however, gel strength can be recovered after the surfactants have been removed. The new technology will greatly benefit the oil industry by improving oil recovery while reducing water production.

8.2. Introduction

Gel is a solid three-dimensional network that spans the volume of a liquid medium. This internal network structure may result from physical or chemical bonds, as well as crystallites or other junctions that remain intact within the extending fluid. Virtually any fluid can be used as an extender including water (hydrogels), oil, and air (aerogel). Both by weight and volume, gels are mostly liquid in composition and thus exhibit densities similar to those of their constituent liquids. Edible jelly is a common example of a hydrogel and has approximately the density of water. Hydrogels—gels that are up to 99 percent water—have been around for some time. Unique physical properties of hydrogels such as high water affinity, high thermal and mechanical stability, biocompatibility, etc. provided them with a variety of industrial applications, such as drug delivery and contact lenses.

Recently, a novel idea to combine particle gel and surfactant has been proposed to develop a new technology that is able to enhance oil recovery from fractured reservoir while also to improve conformance control and gel particle treatment efficiency. This research studied the compatibility of PPG and surfactant. It has been found that surfactant shows significant effect on the particle gel strength in terms of storage modulus G', and lose modules G". After the surfactant solution is diluted to very low concentration or the surfactant has been washed off or removed from the gel-surfactant mixture, the gel strength can be recovered. This finding and our previous finding that PPG treatments caused no damage to porous media may result in a totally new EOR process of forced

imbibition through the combination injection of surfactant and PPG. In the process, the mixture of PPG and surfactant solution will be injected into formation at the same time. Compared to a simple PPG treatment, the process has the following distinct advantage:

1. The PPG injectivity can be greatly improved because the reduced particle gel strength will reduce the injection pressure.
2. The reduced PPG strength can be regained as water cleans the particles during water flooding after the treatment.
3. As a filtrate through the particle gel and porous matrix, the surfactant solution will be forced to enter low permeability zones/areas during the mixture injection, which solves the problem of inability to inject surfactant into low permeability zone/areas by conventional surfactant imbibition and flooding technologies. In addition, the experimental results show that surfactant concentration increased by 5~42% after mixing with PPG. This will greatly benefit the new EOR process.

Interaction between surfactant and polymer hydrogel has been a subject of considerable theoretical and practical interest, and has been extensively studied. Philippova and co-workers (1996) studied interaction of gels with ionic surfactants. They reported that absorption of anionic surfactant is governed primarily by hydrophobic interactions. Nichifor (2001) studied interaction of hydrophobically modified cationic dextran hydrogels with biological surfactants. They found that an increase in the length of the alkyl substituent of the hydrogel strongly increases the binding constants K_0 and K, but decreases the cooperativity parameter μ. This was explained by the formation of mixed micelles between pendant groups of the gel and surfactant molecules.

It is well recognized that surfactants play a critical roles in rheology. One of the results caused by addition of surfactants to hydrogel particles is the influence on the frictional behavior of gels. To date, interaction between surfactant and particle hydrogel has not been studied systematically. In this chapter, we study the influence of surfactant in aqueous solution on the dynamic modulus of water-swollen gel in 1.0 wt% NaCl. Surfactants used in this study include nonionic, anionic and cationic surfactants. Gel frictions were measured in terms of storage modulus G' and loss modulus G" under the same conditions of stress, gap, oscillation frequency and temperature for all surfactants.

The gel used in this study was synthesized from acrylamide monomer with ethylene-bis-acrylamide cross-linker.

8.3. Experiment

8.3.1. Materials

Monomer acrylamide (98.5%) and cross-linker methylene-bis-acrylamide (97+%) were purchased from Alfa Aesar Company (Ward Hill, MA) and used without further purification. Ammonium persulfate $(NH_4)_2S_2O_8$ was used as initiator for polymer gel synthesis. Cationic surfactants, n-dececylpyridinium chloride monohydrdate (98%), (1-hexadecyl) pyridinium bromide monohydrate (98%), benzalkonium chloride and anionic surfactant, sodium Sodium 4-n-octyl benzene sulfonate were also purchased from Alfa Aesar Company and used without further purification. Sodium dodecylbenzene sulfonic acid and Triton® X-40 (70% in water) were purchased from Sigma-Aldrich (St. Louis, MO) and used without further purification. Other commercial surfactants were requested from their manufacturers, Alfoterra® 23 from Sasol North America Inc.(Houston, TX), Neodol® 25-12 from Shell Chemical Company(Houston, TX), and used without further purification. NaCl (99.8%) was purchased from Fisher Scientific Inc.

8.3.2. Measurement of Concentration Change of NaCl after Gel Swelling

0.500 M $AgNO_3$ aqueous solution was used to determine NaCl concentration in free water from the test-tubes where PPG reached swelling equilibrium. To ensure accuracy of this test, a test with standard NaCl solution (1.00 wt %) was carried out at the same time. The data and results for the two experiments are listed in Table 8-2.

8.3.3. Measurement of Particle Gel Dynamic Modulus

To investigate influence of surfactant on the particle gel strength, a rheometer, HAAKE RheoScope (Thermo Scientific) was employed to measure storage modulus G' and loss modulus G" for the swollen gels. For each sample, measurements of G' and G" were taken every 30 seconds for 5 minutes. The results are shown in Table 8-4 and Figure 8-2.

8.4. Results and Discussion

8.4.1. Particle Gel Swelling Ratio

The swelling ratios for particles in different surfactant solutions at 200 ppm concentration as well as in 1% NaCl brine and distilled water are listed in Table 8-1.

Swelling ratios in surfactant solutions, distilled water and 1.0 wt % NaCl are between 22~24. The difference in the swelling ratios is in the range of experimental error and thus the swelling ratio is independent of the swelling media. This implies the neutral charge balance of the synthesized polyacrylamide gels. Therefore, the pore-size and distributions of the synthesized polyacrylamide gels do not change when the surfactants and NaCl were added. Also, the pore size of the swollen PPGs was measured and shown in Figure 8-1. The average pore size of the PPGs is around 4.1 nm, which is much less than the size of micelles formed from our tested surfactants.

8.4.2. Concentration Change of NaCl after Equilibrium of Swelling

Accuracy of the experimental results was evaluated by analysis results of a standard NaCl aqueous solution. The expected NaCl for the analyzed solution is 0.0501 grams. The mass of NaCl calculated through the precipitation of AgCl after anion metathesis is 0.0502 grams, leading to a relative experimental error of 0.2%. When PPGs were swollen in the brine solution, the equilibrium concentration of NaCl was found to be at 1.01 wt % changing from 1.00 wt %. The difference of 0.01 wt % is attributed to the experimental error. The analysis results are listed in Table 8-2, from which it can be concluded that the NaCl concentration in the excess brine is the same as the initial concentrations. After swelling equilibrium, particle gel doesn't change the concentration of NaCl in the excess solution since the sizes of sodium and chloride ions are much smaller than the pore sizes of the swollen PPGs.

8.4.3. Concentration Change of Surfactants after Equilibrium Swelling of PPGs

The initial concentration for all surfactants used in this experiment is 200 ppm. After PPGs were completely swollen, equilibrium concentration of surfactant in the excess solution was measured by the UV absorbance. The equilibrium concentrations for different surfactant solutions at PPG swelling equilibrium are listed in Table 8-3. It was been found that the concentration of most of the surfactant solutions increased after PPGs reached their swelling equilibrium (Table 8-3). Concentration change ranged from a decrease of 5%, considered to be within the experimental error of ±5% originating from the UV absorbance measurement, to as great as a 41.5% increase.

The formation of surfactant micelles in the solution is the primary reason for the dramatic increase of surfactant concentration after gel particle swelling is. Micelles have,

a much larger size than that of opening of the gel network. A single surfactant molecule has a dimension of 9 Å in diameter of hydrophilic head and about 20 Å in length of a hydrophobic tail. This size is much smaller than the average pore size of the hydrogel, 4.1 *nm* or 41 Å. On the other hand, approximate size for a rod-like surfactant micelle is about 54 Å in the rod diameter and 140 Å in the rod length, which is much larger than the average pore size of the hydrogel. When the dry PPGs contact the aqueous surfactant solution, the particles absorb water first. Other molecules and ions will diffuse into the network structure because of the concentration gradient and their much smaller size. However, surfactant micelles cannot go through the network due to their much larger size. Only unassociated single surfactant molecules can go through the opening and diffuse into the network of the swollen gel, creating a dynamic equilibrium with the micelles absorbed outside the swollen gel network. After the swelling reaches equilibrium, the gel has absorbed more water and fewer surfactant molecules can get into the gel network. As a result, the concentration of surfactant in the excess solution increases. Therefore, it is expected surfactants with low critical micelle concentrations (CMC), will have higher concentrations in the excess solution after swelling equilibrium is achieved. For a surfactant, if its CMC is high, or its initial concentration is about or lower than CMC, the concentration will change little after the gel swelling reaches.

From Table 8-4, it can be found that the change of surfactant concentration is related to the ratio of the initial concentration ($C_{init.}$) to surfactant CMC. If the ratio is less than 1.0, that means the surfactant initial concentration is lower than its CMC, the concentration change is little and in the range of experimental error. If the ratio is greater than 1.0, the equilibrium concentration increased dramatically. For example, this ratio for nonionic surfactants, Igepal® CO-530 and Tergitol® NP-10, is greater than 10, their equilibrium concentration increased from their initial concentration by 41.0% and 41.5%, respectively. This suggests that most of their molecules exist in the solution in the form of micelles for these nonionic surfactants with very low CMC. The micelles cannot go through the network of the swollen particle gel because they have a larger size than the average pore size of the PPGs. This results in the dramatic increase of their equilibrium concentration since PPGs absorbs a large amount of water during the swelling.

8.4.4. Influence of Surfactant on Friction of the Particle Gel Surface

To study the influence of surfactant on the particle gel viscoelasticity, the dry PPGs at 2 wt % were mixed with 1000 ppm surfactant solutions prepared with 1.0 wt % NaCl brine in a centrifuge tube, and the PPGs and surfactant solution mixture was shaken well to ensure complete swelling of particles. A higher concentration surfactant solution (1000 ppm) was used to ensure that all surfactants investigated in this study were aggregated in the solution. The gel viscoelasticity was measured by the HAAKE RheoScope. During the process of measurement, both G' and G" show a slow and steady increase because of the evaporation of water contained in gel samples. A blank test of the gel strength in 1.0 wt% NaCl brine without surfactant was also conducted for comparison. Measurement results for the particle gel strength (both G' and G'') in 1000 ppm and 1.0 wt % NaCl brine solution are listed and shown in Table 8-5. A typical measurement of the gel strength as a function of scan time was illustrated in Figure 8-2. It can be clearly seen from Table 8-5 and Figure 8-2 that the introduction of Alfoterra® 23 into the swelling media significantly decreased the swollen gel strength. From the data listed in Table 8-5, it can also be observed that all the tested surfactants have strong influence on viscoelasticity of the particle gel. The addition of surfactant to NaCl brine used for gel swelling can substantially reduce the gel dynamic modulus G' and G".

To understand why the dynamic modulus (G' and G") of the particle gel decreases so greatly when surfactant is introduced in the solution, one has to understand how the measurement of the dynamic modulus (G' and G'') by a plate rheometer is accomplished. The swollen particle gel sample is placed on a horizontal glass plate and another metal sensor plate is placed on top of the gel samples. Typically the top sensor plate is rotated and the torque exerted on it is measured. The movement of this plate is resisted by the frictional force, which is proportional to the frictional coefficient and the stress applied on it. Equations (8-1), (8-2) and (8-3) below describe quantitatively the relationship for torque (T), stress (N) and frictional coefficient (μ).

$$T = r \times F \tag{8-1}$$

$$F = \mu \cdot N \tag{8-2}$$

$$T = r \times F = r \times (\mu \cdot N) \tag{8-3}$$

where, T is the torque exerted on the sample; r is typically the length of the lever arm and here it is related to geometry of the rheometer sensor. For a given sensor, it is the same for all gel samples measured; F is the frictional force, it is the product of frictional coefficient (μ) between two surfaces and the force applied on the surfaces (N). In this experiment, a model of controlled stress is employed for the measurement. Therefore, the torque exerted on the sample is directly proportional to the frictional force between the particle gel and the surfaces of the plates. Furthermore, measurement results of the dynamic modulus (G' and G") are directly proportional to the frictional force coefficient between the particle gel and the plate surfaces.

We proposed a simple mechanism, shown in Figure 8-3, as a qualitative discussion of friction reduction by surfactant between the surfaces of particle gels, stainless steel sensor plate and glass plate. As shown in Figure 8-3(a) without addition of surfactant to NaCl brine for the particle gel swelling, the stainless steel sensor plate presses the particle gel and rotates on it at a constant stress mode when the dynamic modulus is measured. The original dried particle size ranges between 0.125 and 0.150 mm. Based on a volume swelling ratio of 23, the swollen particle size is between 0.355 and 0.427 mm in diameter. The gap between the sensor plate and bottom glass plate for G' and G" measurement is at 0.200 mm, which is only about half of the particle size. Therefore, the swollen gel particles experienced a remarkable deformation during the measurement. Friction between the surfaces of particle gels, the sensor plate and the glass plate is dominated by the sliding or translational motion, very similar to the case of bulk hydrogel on the solid surfaces. In Figure 8-3(b), however, with the addition of surfactant, most of surfactant molecules aggregate to form the micelles, which have a much larger size than that of the opening of the gel network and are adsorbed onto the swollen particle gel surface as discussed in the previous section of this paper. These micelles may act as many small and flexible balls between the surfaces of particle gels, the sensor plate and the glass plate in a similar way to a lubricant. In this case, friction behaviors between these surfaces may be dominated by the rolling motion of the micelles. Hence, this will dramatically reduce the frictional coefficient between the surfaces of particle gel, the sensor plate and the glass plate. Consequently, motion resistance of the sensor and the torque exerted on the instrument during the measurement will be dramatically decreased

as well. As a result, the dynamic modulus of G' and G" are decreased as compared with those measured without surfactant added.

Based on this above-mentioned mechanism, the ability of surfactants to reduce hydrogels dynamic modulus may be related to geometry of the surfactant micelles such as shape and size. Each surfactant has a critical packing parameter, *CPP*, which is related to the shape of a surfactant molecule.

$$CPP = \frac{v}{l \cdot a_0} \tag{8-4}$$

where, v is the volume of surfactant hydrocarbon core in $(nm)^3$; l is the length of surfactant hydrocarbon chain in *nm*; a_0 is effective area of surfactant hydrophilic group in $(nm)^2$. v, l and a_0 can be calculated using the following equations:

$$v = 0.027(n_c + n_{methyl}) \tag{8-5}$$

$$l = 0.15 + 0.127\, n_c \tag{8-6}$$

$$a_0 = 0.016\, m + 0.333 \tag{8-7}$$

where, n_c is the number of carbon atoms of hydrocarbon chain without methyl groups; n_{methyl} is the number of methyl groups in the hydrocarbon chain; m is the number of ethylene oxide groups.

The critical packing parameters for the surfactants investigated in this study have been calculated using Equations. (8-4)-(8-7). The results are listed in Table 8-6. From the table, it can be found that the packing parameters for all the surfactants investigated are between 0.333 and 0.423. It was known that geometry of surfactant micelle depends upon the value of *CPP*. If *CPP* is less than 1/3, the surfactant will form spherical micelles in solution; if *CPP* is between 1/3 and 1/2, it will form rod-like micelles; if *CPP* is close to 1, it will form a lamellar structure; if *CPP* is greater than 1, it will form a bi-continuous phase; and if *CPP* is much greater than 1, it will form the reversed micelles or reversed rod-like micelles in solution. It is expected that surfactants with a *CPP* less than 0.333 will be the most efficient agent to reduce the particle hydrogels dynamic modulus because they form spherical micelles in solution. For surfactants with the *CPP* between 0.333 and 0.500, the smaller the *CPP is*, the more effective on reduction it will be. The gel strength in terms of G' and G" in different surfactant solutions are plotted against *CPP* and shown in Figure 8-4. In the figure, it can be found that the particle gel strength

decreases with decrease of the surfactant *CPP* and there is a linear relationship for G'~*CPP* and G"~*CPP*. This indicates that surfactant micelles absorbed on the particle gel surface play a key role in reducing friction of the gel on the surface and the measured dynamic modules G' and G". A surfactant forming spherical micelles, such as Alfoterra® 23, would be the most effective agent to friction. The other surfactants with a *CPP* between 0.333 and 0.500 should have rod-like micelles in the solution (Table 8-6). For rod-like micelles, it is expected that both rod diameter and rod length should have effect on the hydrogel G' and G", and the micelles with greater rod diameter and less rod length should be more effective on reducing the G' and G". But this assumption of relation between micelle size and performance needs more work to get confirmed.

In order to confirm our proposed mechanism discussed above, some parallel tests were also conducted for all the surfactants listed in Table 8-6. In the parallel tests, the dry gel particle samples were mixed with surfactant solutions following the exact procedures described previously. After the particles were completely swollen, the swollen PPGs were washed and centrifuged using 1.0 wt% NaCl. The samples prepared in 1.0 wt% NaCl solution were treated with the same procedure in order to ensure all the particle gel samples were treated under the same conditions of shearing and agitation, which is believed to have significant impact on the rheological properties of the gels. The gel strength results after removing the surfactants are shown in Figure 8-5. Surprisingly, it has been found that the values of G' and G" for all the particle gels after surfactant removal increase significantly and are back to the values of the particle gel mixed with 1.0 wt. NaCl solution. This indicates that the friction behaviors between the surfaces of the particle gel, the sensor plate and the glass plate has been switched from rolling motion back to the sliding or translational motion because the surfactant micelles have been removed from the gel particle surface, leading to the recovery of G' and G''.

To provide further support of the proposed possible mechanism responsible for the dynamic modulus reduction of the particle hydrogel by surfactant, the elastic modulus G' of the synthesized particle hydrogel swollen in the surfactant solution prepared with 1.0 wt.% NaCl at the concentrations below and above their critical micelle concentration (CMC) were systematically measured. The results are shown in Figure 8-6. For the six surfactants used in this study, the G' measurement shows a substantial decrease at the

CMC for each surfactant. The very slow decrease of G' for all surfactants at the concentrations below CMC may be due to the experimental errors. However, the noticeable decrease of G' at the concentrations above CMC is due to the increase of micelle concentration for the all surfactants investigated. As surfactant solution concentration is continuously increased to a concentration above its CMC, the monomer concentration in the solution will no longer increase while the micelle concentration in the solution will continue increasing. This results in a continuous decrease in the dynamic modulus (G') of the hydrogel. Furthermore, it was found that among the surfactants investigated, Alfoterra® 23 has the lowest CMC. At 10 ppm, it can effectively reduce elastic modulus because it is the only one that can form spherical aggregates in the solution, thus it is most effective at reducing gel surface friction.

8.5. Potential Applications

Gel treatment has proven to be an effective method to reduce water production in oil industry. A new trend in gel treatments is application of preformed particle gels (PPG) that are formed at surface facilities before injection. In order to improve the gel treatment efficacy, gel particles are placed in the surfactant brine solution. When the particle gel and surfactant solution are injected into the underground reservoir, the filtrated solution can be squeezed into the matrix during the injection. As a result, the gel particles enter and stay in the fracture and large size porous media while the surfactant solutions enter into the small pores in the formation where most hydrocarbon oil is trapped by the capillary force. In this way, the surfactant solution will reduce interfacial tension at oil/brine interface and change wettability of rock surface in the formation. Based on our investigations into the interaction between the particle gel and surfactant, it has been found that surfactants have strong influence on particle gel friction. Therefore, injectivity of the particle gels can be greatly improved by the proper screening of surfactant. In other words, the gel resistance can be modified by selecting the best surfactants for the particular application.

It is also worth mentioning that the results of this investigation demonstrate a new idea of forced imbibition through the combination of particle gel injection and surfactant imbibition. Development of forced imbibition technology will enable oil producers to increase oil recovery while reducing water production.

8.6. Conclusions

- The equilibrium concentration of NaCl in excess brine remains the same after the swelling of particle gel. It is also expected that concentration of water-soluble salts such as KCl, $MgCl_2$, $CaCl_2$, Na_2CO_3, Na_2SO_4, will not change as well following the swelling of particle gels. This means that gel swelling will not increase the salinity of the underground formation water.
- The equilibrium surfactant concentration in the excess brine increases after swelling of gel particles due to the formation of surfactant micelles in the brine. The larger size of the micelles (5.4 nm x 14.0 nm) prevents them from diffusing into the small open pore size (4.1 nm) of the synthesized gel network. Surfactants with larger sizes of molecules and lower critical micelle concentration (CMC) show greater increase in equilibrium. It is expected that nonionic surfactants will show greater increase.
- Gel friction in terms of dynamic modulus G' and G" can be reduced dramatically. This might be because the surfactant micelles adsorbed on the surfaces of the particle gel change the friction between the surfaces of particle gel and solid from sliding/translational motion to a rolling motion. The latter has a much smaller friction coefficient. However, the gel resistance can be recovered after the surfactants have been removed indicating the physical absorption of the formed micelles over the surfaces of the swollen PPGs.
- Injectivity of particle gels can be significantly improved by use of the proper surfactants. Moreover, a new technology of forced surfactant imbibition can be developed by combination of the PPGs and surfactant. The new technology will greatly benefit the oil industry by improving oil recovery while reducing water production.

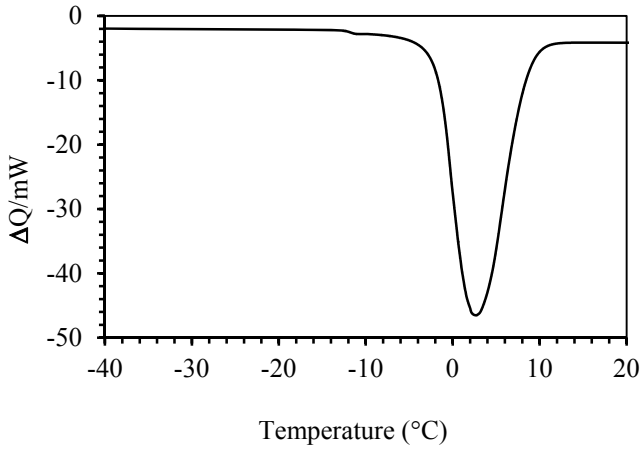

Figure 8-1 DSC curve of the swollen PPGs in the distilled water.

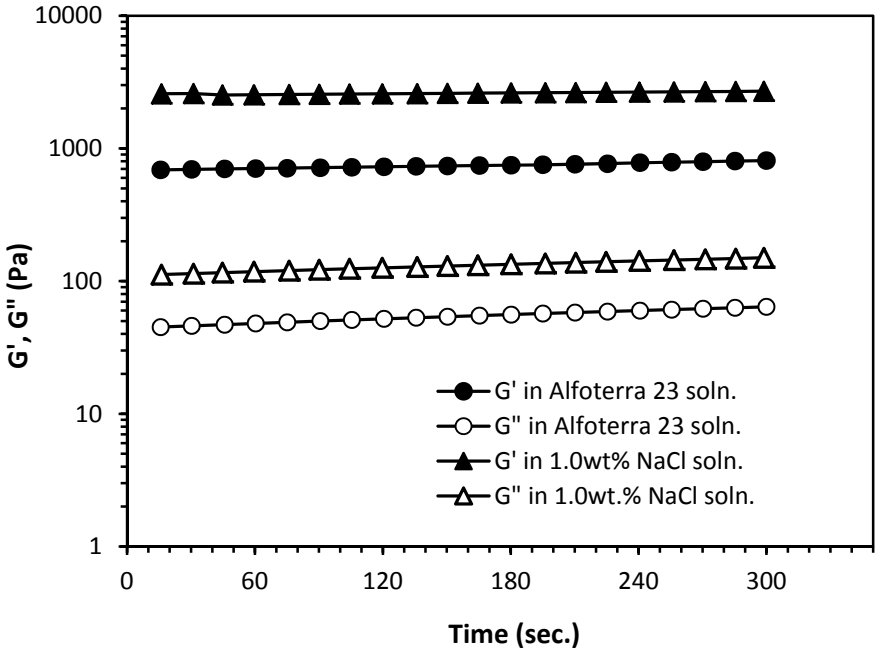

Figure 8-2 Results of G' and G" for particle gel in surfactant Alfoterra 23 solution (1000 ppm) prepared with 1.0wt.% NaCl brine and in 1.0wt.% NaCl brine only (blank test).

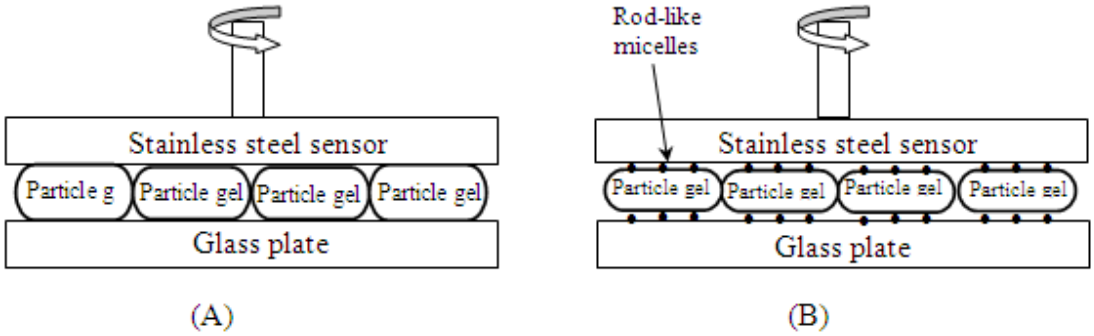

Figure 8-3 Schematic illustration of the mechanism for friction reduction between the surfaces of particle gels, stainless steel sensor and glass plate.

(A) Without addition of surfactant; (B) With addition of surfactant to NaCl brine for the particle gel swelling.

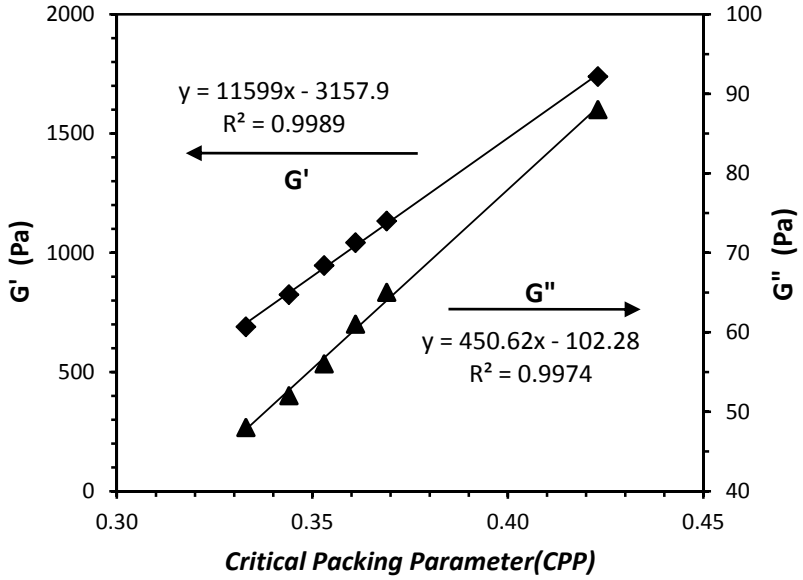

Figure 8-4 Plots of G'~ CPP and G" ~ CPP for the surfactants investigated at 1000 ppm.

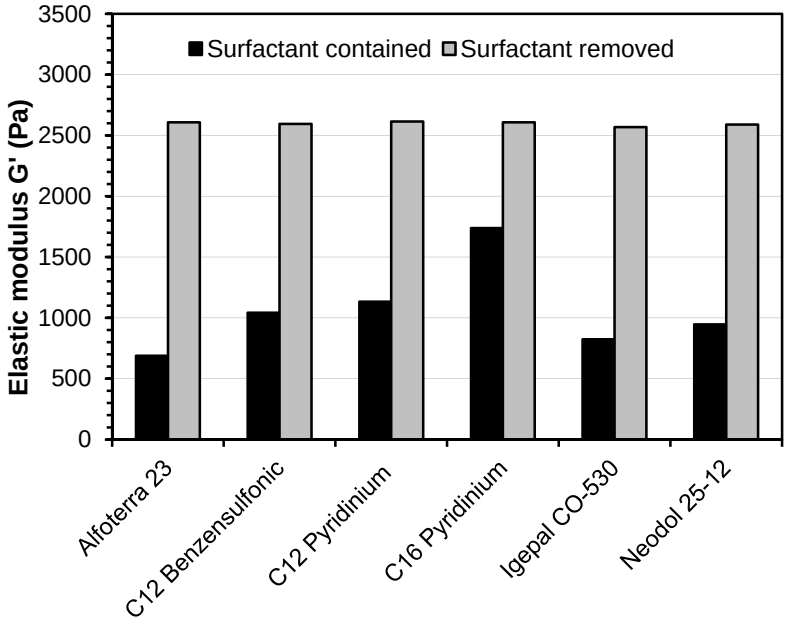

Figure 8-5 Storage modulus G'of particle gels with and without surfactant. After surfactant molecules have been washed off, the modulus G' increases to the value of the particle gel swollen in 1.0 wt.% NaCl.

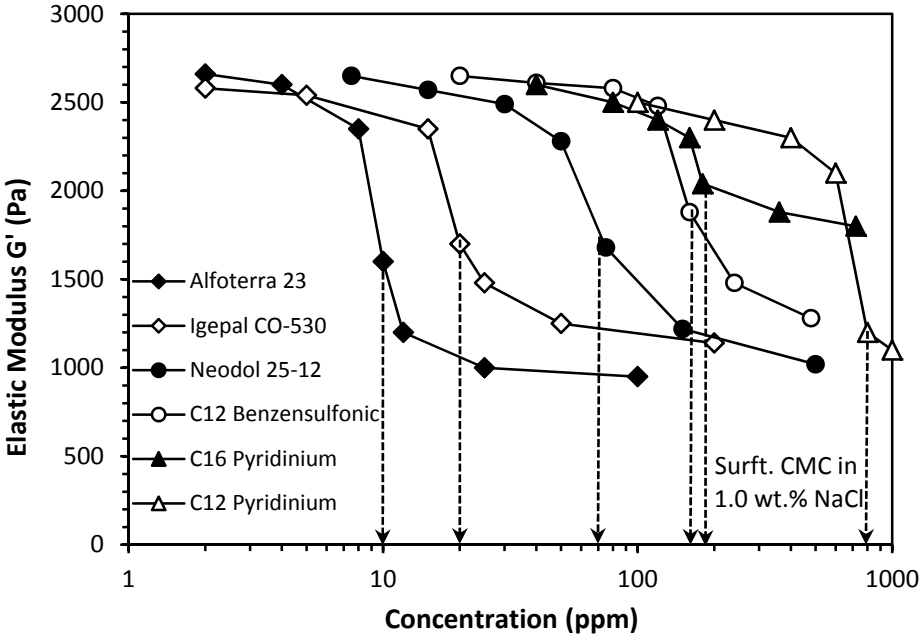

Figure 8-6 Storage modulus G'of particle gels measured with various surfactants at different concentrations shows a substantial decrease at the concentration of their critical micelle concentration (CMC).

Table 8-1 Surfactant Molecular Structure and Gel Swelling Ratio in Surfactant Solutions

Surfactant	Molecular structure	Swelling ratio
n-Dodecylpyridinium chloride	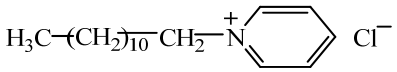	22.2~23.2
(1-Hexadecyl)pyridinium bromide	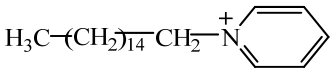	22.3~23.3
Benzalkonium chloride	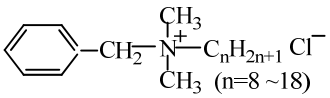	22.1~23.1
Alfoterra® 23 Sodium branched alcohol propoxylate sulfate	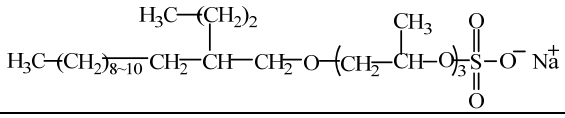	22.3~23.3
Sodium 4-*n*-octyl benzene sulfonate	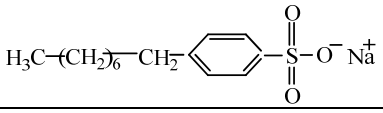	22.8~23.8
Sodium salt, dodecylbenzene sulfonic acid	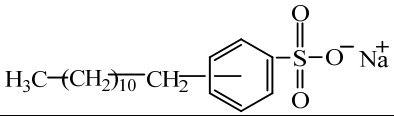	22.6~23.6
Igepal® CO-530 Nonylphenoxypoly(ethyleneoxy) alcohol	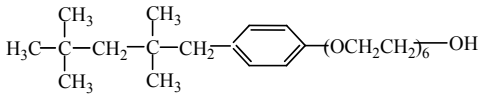	22.1~23.1
Tergitol® NP-10 Nonylphenol ethoxylated alcohol	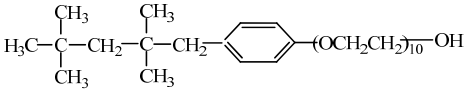	22.0~23.0
Neodol® 25-12 Linear primary alcohol ethoxylate	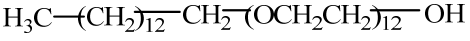	22.6~23.6
In distilled water	H_2O	22.8~23.8
In 1.00 wt.% NaCl brine	NaCl and H_2O	22.4~23.4

Table 8-2 Analysis Results of NaCl Concentration after Particle Gel Swelling

Test for Std. NaCl soln. before swelling	**Std. 1.00 wt.% NaCl solution**	**Test for unknown NaCl after swelling**	**Equili. NaCl solution**
Empty Test Tube	13.9754 g	Empty Test Tube	13.9021 g
NaCl Solution	5.0100 g	NaCl Solution	5.0081 g
NaCl Expected	0.0501 g	NaCl Mass	To be measured
Total weight after drying	14.0986 g	Total weight after drying	14.0259
Mass of AgCl (MW: 143.5)	0.1232 g	Mass of AgCl (MW: 143.5)	0.1238 g
Mass of NaCl (MW: 58.5)	0.0502 g	Mass of NaCl (MW: 58.5)	0.0505 g
Experimental Error	0.2%	Equili. NaCl Conc.	1.01 wt.%

Table 8-3 Measurement of Concentration Change of Surfactant after Gel Swelling

Surfactant Initial Concentration: 200 ppm			**At Equilibrium of Swelling**		
Surfactant	λ_{max} (nm)	Initial ABS	Net ABS	$C_{eq.}$ (ppm)	Conc. Change
n-Dodecylpyridinium chloride	257	2.451	2.326	190	-5.0%
(1-Hexadecyl)pyridinium bromide	259	2.106	2.432	231	15.5%
Benzalkonium chloride	261	0.179	0.187	209	4.5%
Sodium 4-*n*-octyl benzene sulfonate	260	0.232	0.247	213	6.5%
Sodium salt, dodecylbenzene sulfonic acid	260	0.227	0.262	231	15.5%
Igepal® CO-530	276	0.806	1.137	282	41.0%
Tergitol® NP-10	275	0.429	0.608	283	41.5%

Table 8-4 Surfactant CMC, ratio of Cinit./CMC and Concentration Change

Surfactant	M.W.	CMC* in 1.0% NaCl	$C_{init.}$ (200ppm)	$C_{init.}$/ CMC	Conc. Change
n-Dodecylpyridinium chloride	284	2.8×10^{-3} M	7.0×10^{-4} M	0.3	-5.0%
(1-Hexadecyl)pyridinium bromide	402	4.5×10^{-4} M	5.0×10^{-4} M	1.1	15.5%
Benzalkonium chloride	~410	Not a surfactant	4.9×10^{-4} M	n/a	4.5%
Sodium 4-*n*-octyl benzene sulfonate	292	1.3×10^{-3} M	6.8×10^{-4} M	0.5	6.5%
Sodium salt, dodecylbenzene sulfonic acid	348	4.6×10^{-4} M	5.7×10^{-4} M	1.2	15.5%
Igepal® CO-530	464	4.1×10^{-5} M	4.3×10^{-4} M	10.5	41.0%
Tergitol® NP-10	660	2.8×10^{-5} M	3.0×10^{-4} M	10.7	41.5%

Table 8-5 Results of Storage Modulus G' and Loss Modulus G" for Gel Particles in Surfactant Solution (1000 ppm) and in 1.0 wt.% NaCl Brine

Surfactant	Conc. in 1.0% NaCl	G' (Pa)	Change	G" (Pa)	Change
In 1.0 wt.% NaCl	brine	2582	0%	112	0%
Alfoterra® 23	1.93×10^{-3} M	689	-73%	45	-59%
Sodium salt, dodecylbenzene sulfonic acid	2.87×10^{-3}M	1042	-60%	64	-43%
n-Dodecylpyridinium chloride	3.52×10^{-3} M	1133	-56%	66	-41%
(1-Hexadecyl)pyridinium bromide	2.45×10^{-3} M	1739	-33%	87	-22%
Igepal® CO-530 (HLB=10.8)	2.16×10^{-3} M	824	-68%	51	-54%
Neodol® 25-12 (HLB=14.4)	1.35×10^{-3}M	946	-63%	56	-50%

Table 8-6 Critical Packing Parameters (CPP) of the Surfactants Investigated

Surfactant	***v* (*nm*)^3**	***l* (*nm*)**	**a_0(*nm*)^2**	***CPP***	***Micelle structure***
Alfoterra® 23	0.538	2.690	0.600	0.333	Spherical
Sodium salt, dodecylbenzene sulfonic acid	0.486	2.245	0.600	0.361	Rod-like
n-Dodecylpyridinium chloride	0.324	1.505	0.584	0.369	Rod-like
(1-Hexadecyl)pyridinium bromide	0.532	2.155	0.584	0.423	Rod-like
Igepal® CO-530	0.405	1.420	0.829	0.344	Rod-like
Neodol® 25-12	0.378	1.801	0.595	0.353	Rod-like

9. Different Samples of PPG Products and Their Swelling Characteristics

9.1. Summary

A number of PPG samples (commercial and experimental products) provided by ChemEOR were evaluated in this chapter. This group of PPG samples encompasses a range of swelling behaviors under various process conditions (different salinities of make-up brines and temperatures). The performance testing for these PPG samples focused on their swelling behavior under a matrix of salinity (sodium chloride and calcium chloride) and temperature conditions. The results indicate that the swelling ratio generally is significantly higher in sodium chloride than that in calcium chloride brine at the same salt concentration. The swelling ratio is also decidedly reduced with an increase in the salinity. There are significant differences in the swelling ratio among the twelve products tested.

In addition, the swelling behavior with an extended exposure time for a couple of experimental products was also studied. Some samples exhibit gradual swelling, taking five days to swell to maximum extent at room temperature, while some other samples showed a two-fold increase in swelled volume after fifteen days of aging at 90 °C (194 °F under lower salinity conditions.

9.2. Experimental Test Procedures

9.2.1. Synthesis of Experimental PPG Products

Five experimental PPG products (PPG-8B, PPG-9B, PPG-10B, PPG-11B, and PPG-12B) were selected for performance evaluation.

A general description of the synthesis procedure is given below:

In a 2 liter beaker in a water bath, the raw materials were added to make 500 grams sample. The mixture was stirred and purged with pure nitrogen for 30 minutes at room temperature. Then initiator was added while maintaining continuous stirring rate at 300 rpm. The mixture was polymerized at room temperature for 30 minutes to avoid sudden polymerization. After that, the temperature of the water bath was increased to 75 °C (167 °F). The reaction usually was exothermic and produces gel in relatively short time (approximately 20-30 minutes). The reaction was kept for 3-4 hours at constant temperature of 75 °C (167 °F) to achieve full polymerization.

After polymerization, the gel was first dried for 1-2 hours at 50 °C (122 °F) oven, and then they were cut into 3-mm pieces. These pieces were sent to the oven to get dried again. The dry pieces were later crushed into small particles and dried again at 50 °C (122 °F). Final grinding was performed and the resulting PPG powder was graded with a series of sieves.

These tested samples all contained predominantly acrylamide and acrylic acid. A minor amount of cross linker compound was used, such as N'N– ethylenebisacrylamide and other additives such as potassium thiosulfate. Swelling behavior in brine solution was adjusted by changing the proportions of the starting materials, adding trace components, or altering the reaction temperature or reaction time.

The commercial products (PPG-1, PPG-2, L-3, PPG-S1, SAP, and L-3), share similar elements. Some of the differences are: PPG-1 and PPG-2 share the same formula, but they have different particle size; both PPG-L-3 and PPG-S1 contain some clay material, while the others do not.

9.2.2. Swelling Tests

The purpose of these tests is to assess the swelling capability of PPG particles. Important properties include the rate and ratio of the particle swelling as a function of brine composition and temperature. Such information is used to aid in the selection of the PPG products for field applications.

9.2.3. Materials

- 50 ml plastic centrifuge tubes
- PPG powder sample

9.2.4. Procedure

1. 50 ml of test brine was added to a centrifuge tube.
2. PPG powder was weighed out.
3. The PPG powder was sprinkled gently into the centrifuge tube.
4. PPG was carefully added to avoid creating large lumps of particles.
5. Remaining PPG was added slowly.
6. After all of the PPG powder is added, the interface boundary was read between the brine portion at the bottom containing the PPG and the brine on top.

7. The interface position was read after a day at room temperature, and after heating for one day at 50 °C (122 °F) and 75 °C (167 °F).

8. The swelling ratio is reported as the ratio of the volume (ml) of brine occupied by the PPG powder to the grams of PPG sample added.

9.3. Results and Discussion

9.3.1. Expanded Swelling Data for PPG-1 and PPG-2

The Tables 9-1 and 9-2 summarize the swelling ratio in various salinity and temperature conditions. These data include a comparison to previous duplicate runs. In Figures 9-1 to 9-6, the results show normal trend for different salinity.

These results show that salinity is the most important factor to determine the swelling ratio. The sodium chloride samples had larger swelling ratios than the calcium chloride samples at the same brine concentration. In addition, increasing the salinity decreases the particle swelling ratio.

Other parameters had little effect on the particle swelling ratio. The particle size distribution has very limited effects with smaller dry particle sized PPG-1 having a slightly larger swelling ratio. The temperature has negligible impact on the particle swelling ratio in the range from 25–75 °C (77 to 167 °F).

9.3.2. Swelling Data for PPG-8B

Table 9-3 and Figures 9-7 and 9-8 indicate that for the PPG-8B sample:

- There is some delay in the swelling of the particles, but there is a noticeable increased expansion after 5 days aging at 25 °C (77 °F) compared to the samples aged only one day.
- A subsequent aging for one day at 50 °C (122 °F) shows little change for the sodium chloride solution. For the $CaCl_2.2H_2O$ solution, there is some contraction of the particles at 50 °C (122 °F).
- A rapid shrinkage at 75 °C (167 °F) suggests this product may not be suitable for high temperature applications.

9.3.3. Swelling Data for PPG-9B

Table 9-4 and Figures 9-9 and 9-10 indicate that the PPG-9 Series of samples behaves similar to the PPG-8 products. Some characteristics are as follows:

- There is some delay in the swelling of the particles, but less than that observed in the PPG-8B product we tested.
- The swelling of PPG-9B in $CaCl_2.2H_2O$ brine is a bit more robust than that in PPG-8B.
- The rapid shrinkage of the swollen particles at 75 °C (167 °F) suggests this product may not be suitable for high temperature applications.

9.3.4. Swelling Data for PPG-L3

Tables 9-5 to 9-6 and Figures 9-11 to 9-13 indicate that the PPG-L3 product exhibits the following characteristics:

- This clay-containing product has smaller swelling ratio than those in the PPG-1 and PPG-2 products.
- The PPG-L3 product has a larger swelling ratio than those in the PPG-8B and the PPG-9B samples.
- The swelling ratio of PPG-L3 increases slightly with temperature, and it becomes stable at the 75 °C (167 °F) condition. Note data in Table 9-6 indicate hardly any difference in the swelling ratio for a sample held at 75 °C (167 °F) from the initial value to Day 18.
- Like all PPG samples, there is considerable decrease in the swelling factor with an increase in salinity, and more so when there is dissolved calcium present.

9.3.5. Swelling Data for PPG-S1

Tables 9-7 to 9-8 and Figures 9-14 to 9-16 indicate that the PPG-S1 product exhibits the following characteristics:

- This clay-containing product generally has smaller swelling ratio than those in the PPG-1, PPG-2, and PPG-L3 products, also a smaller swelling ratio than seen in the PPG-8B and the PPG-9B samples.
- PPG-S1 is stable at the 75 °C (167 °F) temperature condition. Data in Table 9-8 indicate that there may be a slight increase in the swelling ratio for a sample held at 75 °C (167 °F) for a longer time.
- There is a decrease in the swelling ratio for the PPG-S1 with an increase in salinity, but not to the extent observed among other PPG samples.

9.3.6. SAP 1255 - Super Absorbing Polymer

We have identified a household commercial product that may be useful for the intended oil field application. This series of products are named as Luquasorb. They refer to these as SAP--Super Absorbing Polymers. As an example, some of these products may be used to retain water for agricultural uses or in potting soil. A product from this series, SAP 1255, was selected and evaluated with a set of swelling tests in sodium and calcium chloride brines. The data is summarized in Table 9-9 and Figures 9-17 to 9-19.

The SAP 1255 product exhibits the following swelling characteristics at different temperatures and salinities:

- The SAP 1255 has a smaller swelling ratio than the other PPG products in sodium chloride brines, and its swelling ratio is inversely related to the salinity.
- This product has a relatively small swelling ratio especially in calcium chloride brines.

9.3.7. Swelling Data for PPG-10B

The data in Tables 9-10 to 9-11 and Figures 9-20 to 9-23 verifies that the PPG-10B product has some delay in its swelling behavior. This was expected and it can be a desirable attribute.

- The PPG-10B generally has a moderate swelling ratio compared to other PPG materials tested here.
- The swelling ratio is larger at lower salinity.

9.3.8. Swelling Data for PPG-11B

Table 9-12 and Figures 9-24 to 9-25 collected for ample PPG-11B indicate:

- The PPG-11B generally has moderate swelling ratio compared to other PPG materials.
- The swelling ratio is larger at lower salinity.

9.3.9. Swelling Data for PPG-12B

Table 9-13 and Figures 9-26 to 9-29 collected for sample PPG-12B indicate

- The PPG-12B generally has moderate or large swelling ratio at low salinity, but not at high salinity.
- The swelling ratio is large at low sodium and calcium chloride salinities.

9.3.10. Swelling Data for Mixtures of PPG Products

Selected experiments were performed to observe whether the swelling ratio of the mixture of two different PPG products in equal amounts behaves like the average of the two individual components.

Two such blends are considered:

Mixture 1--50/50 blend of PPG-2 and PPG-12B

Mixture 2--50/50 blend of PPG-2 and SAP 1255

9.3.10.1 Swelling Data for Mixture 1

Table 9-14 and Figures 9-30 to 9-32 collected for the PPG Mixture 1 indicate:

- The swelling behavior of Mixture 1 can be predicted by using the swelling results observed in the individual components. For this simple 50/50 blend, the Mixture 1 swelling ratio is in the middle of those from PPG-2 and PPG-12B at the same temperature condition.
- The PPG swelling ratio is larger at the lower sodium and calcium chloride salinities.

9.3.10.2 Swelling Data for Mixture 2

Table 9-15 and Figures 9-33 to 9-34 collected for the PPG Mixture 2 indicate:

- The swelling behavior of Mixture 2 can be predicted by using the swelling results observed in the individual components. For this simple 50/50 blend, the Mixture 2 swelling ratio is in the middle of those from PPG-2 and SAP 1255 at the same temperature condition.
- The PPG swelling ratio is larger at lower sodium chloride salinities.
- This Mixture 2 is not compatible with calcium chloride brines.

9.4. Conclusions

A snapshot comparison of swelling tendency among the different PPG samples is shown in Table 9-16. Some general observations from these PPG swelling tests include:

- Sodium or calcium chloride salinities have great effects on PPG swelling ratio. The swelling ratio in lower salinity brines is always larger than that in higher salinity brines.

- The swelling ratio in a sodium chloride solution with the same concentration is larger than that in calcium chloride dehydrate. And the divalent cation has a more profound impact on the swelling tendency.
- Some products exhibit some delay before fully swelling. This feature could help to promote deeper PPG placement.
- The swelling ratio by a binary mixture of PPG is similar to the weighted average of the individual products.

9.5. Recommendations

Following recommendations can be made:

- Some static swelling tests can be performed under the conditions in field applications. The laboratory data can be used to aid rationalizing observed results in the field case.
- Additional experiments can be made using field brines to study the swelling ratio of PPG samples selected based on their behavior in simple sodium and calcium chloride solutions.
- More laboratory tests can be used to determine if the observed trend in the swelling behavior of PPG sample mixtures can be estimated from the swelling data collected from the individual samples.

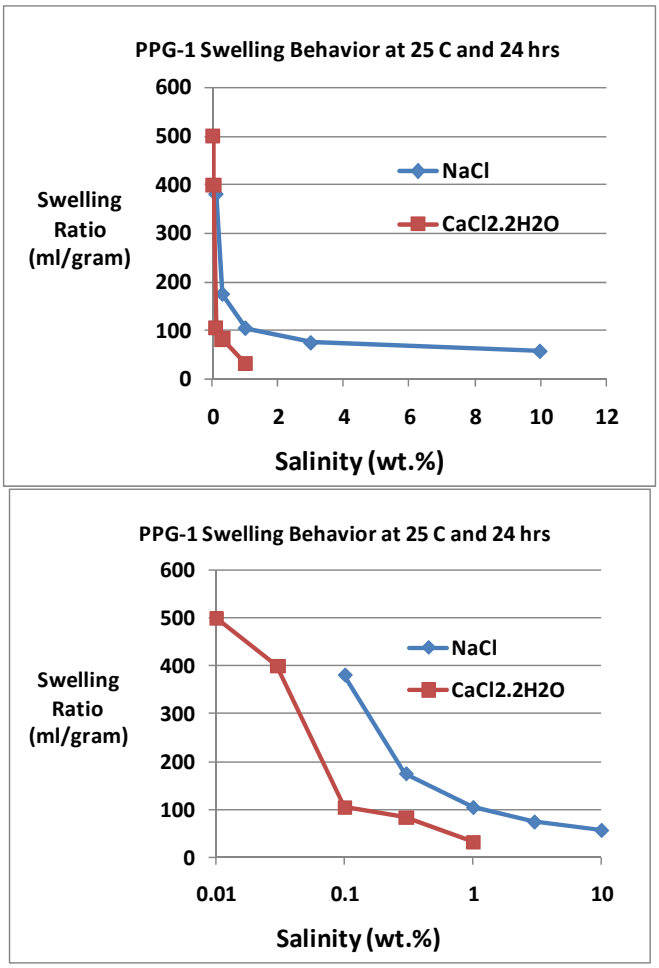

Figure 9-1 Swelling data for sample PPG-1 at 25 °C.

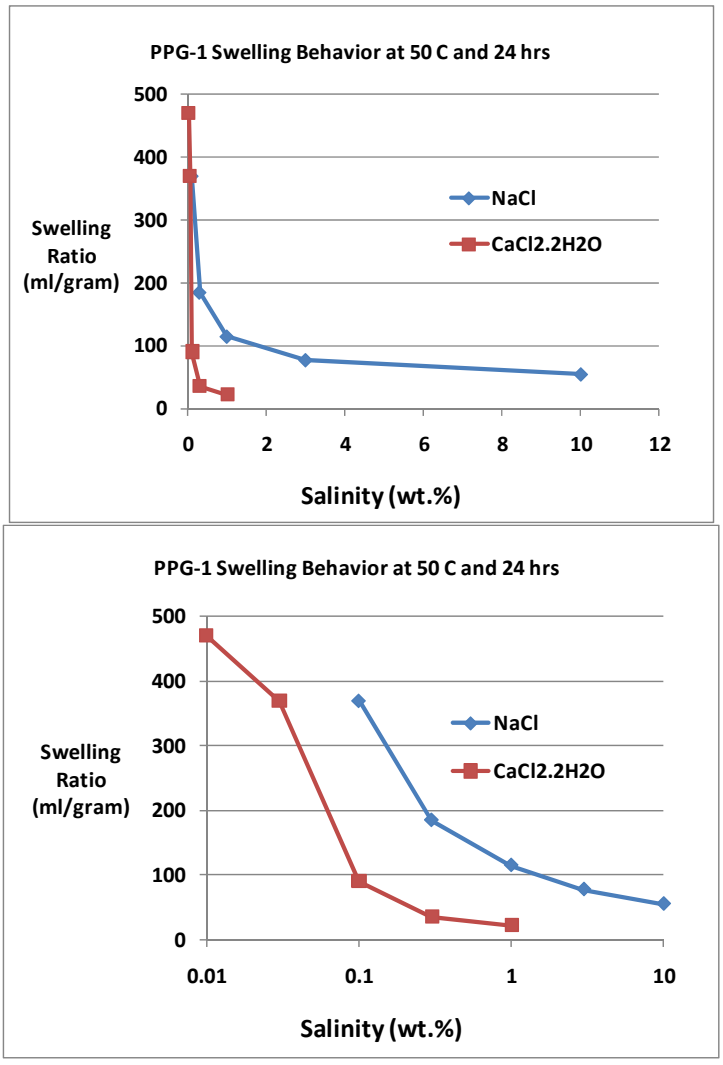

Figure 9-2 Swelling data for sample PPG-1 at 50 °C.

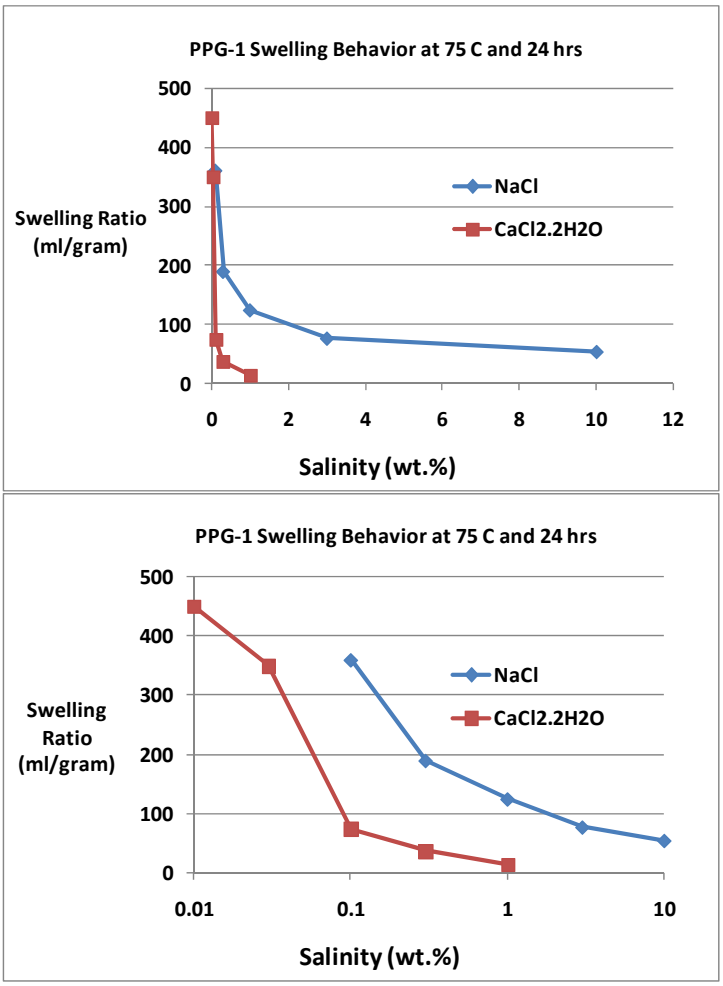

Figure 9-3 Swelling data for sample PPG-1 at 75 °C.

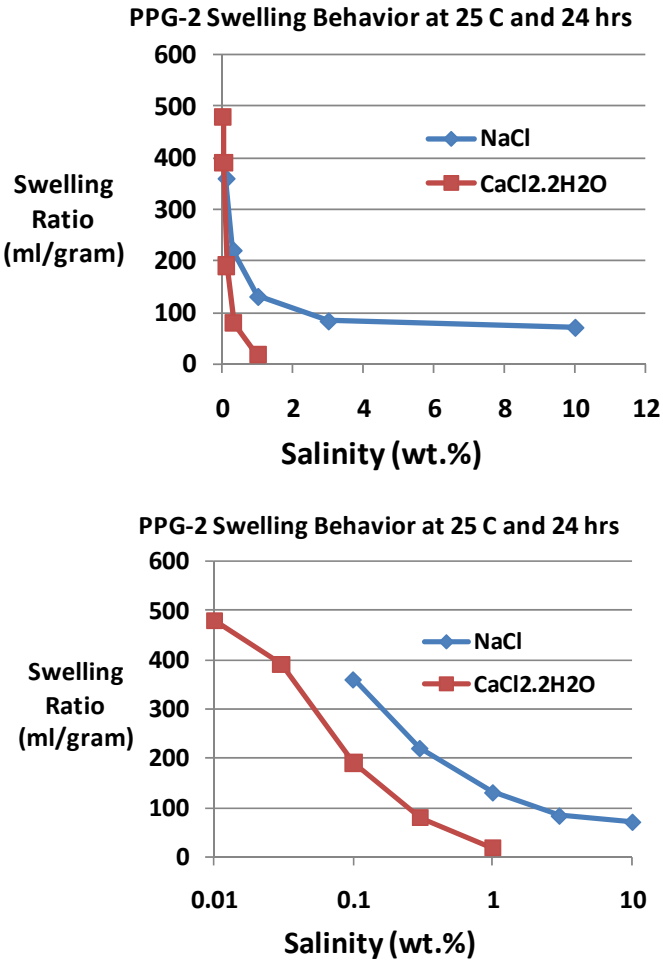

Figure 9-4 Swelling data for sample PPG-2 at 25 °C.

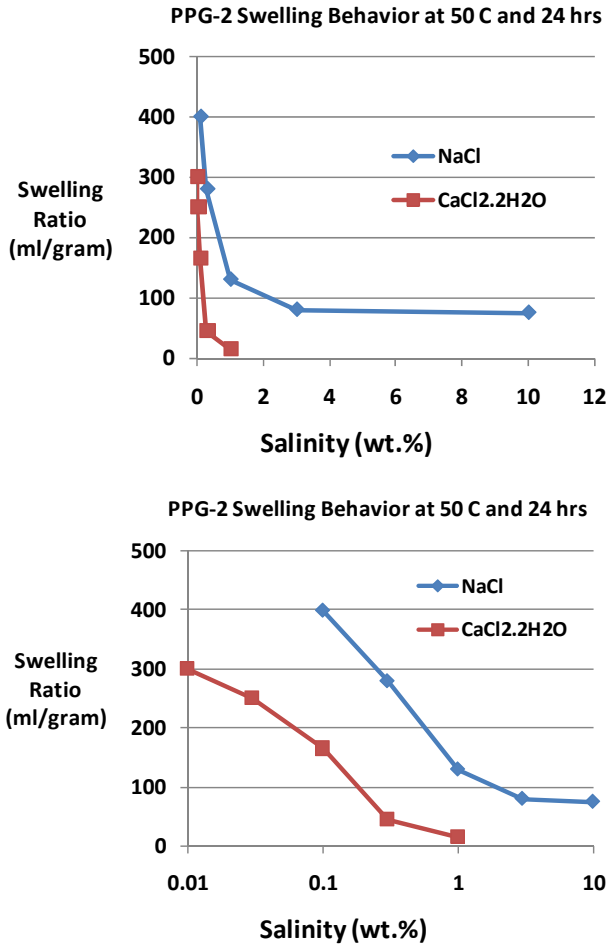

Figure 9-5 Swelling data for sample PPG-2 at 50 °C.

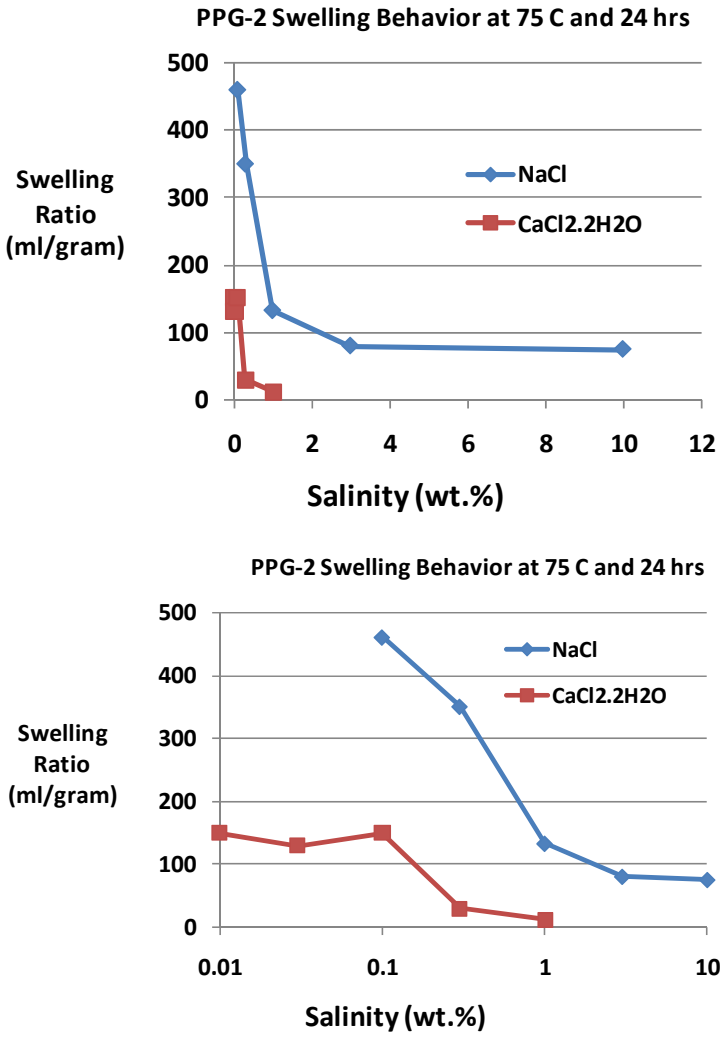

Figure 9-6 Swelling data for sample PPG-2 at 75 °C.

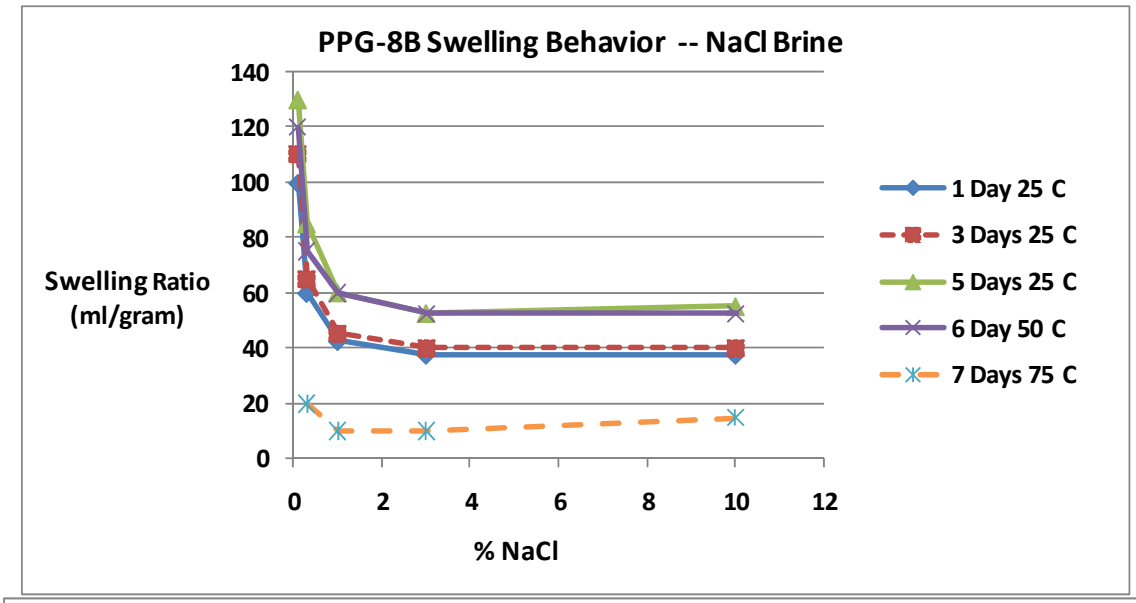

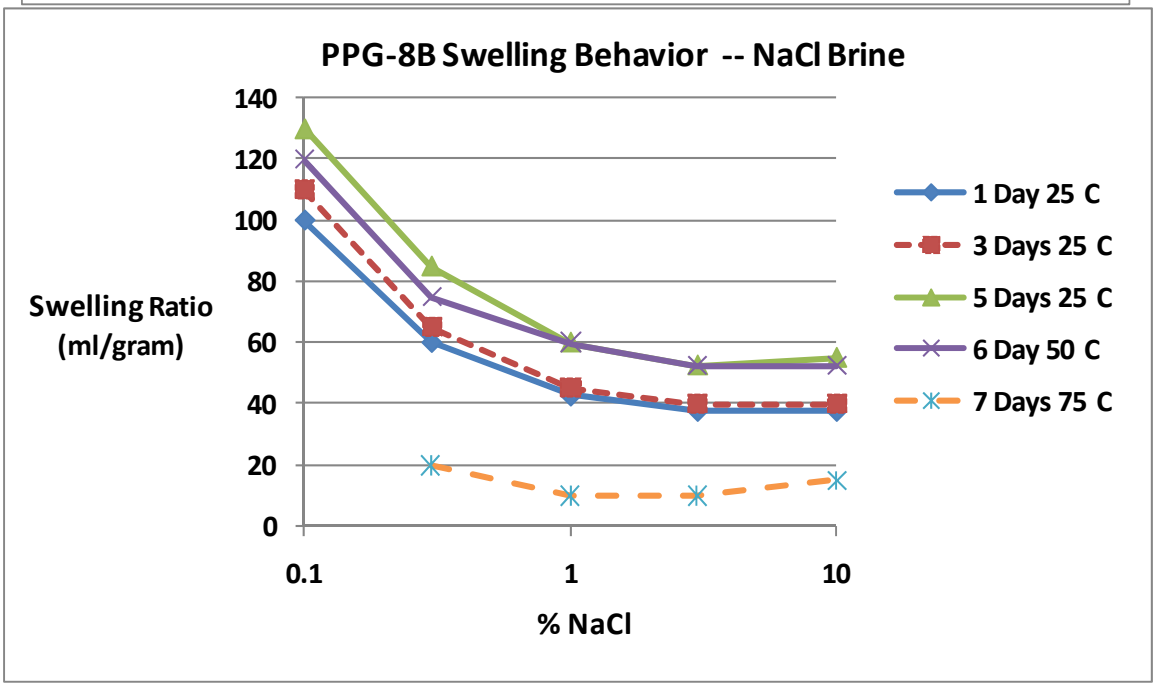

Figure 9-7 Swelling data for sample PPG-8B in NaCl brine.

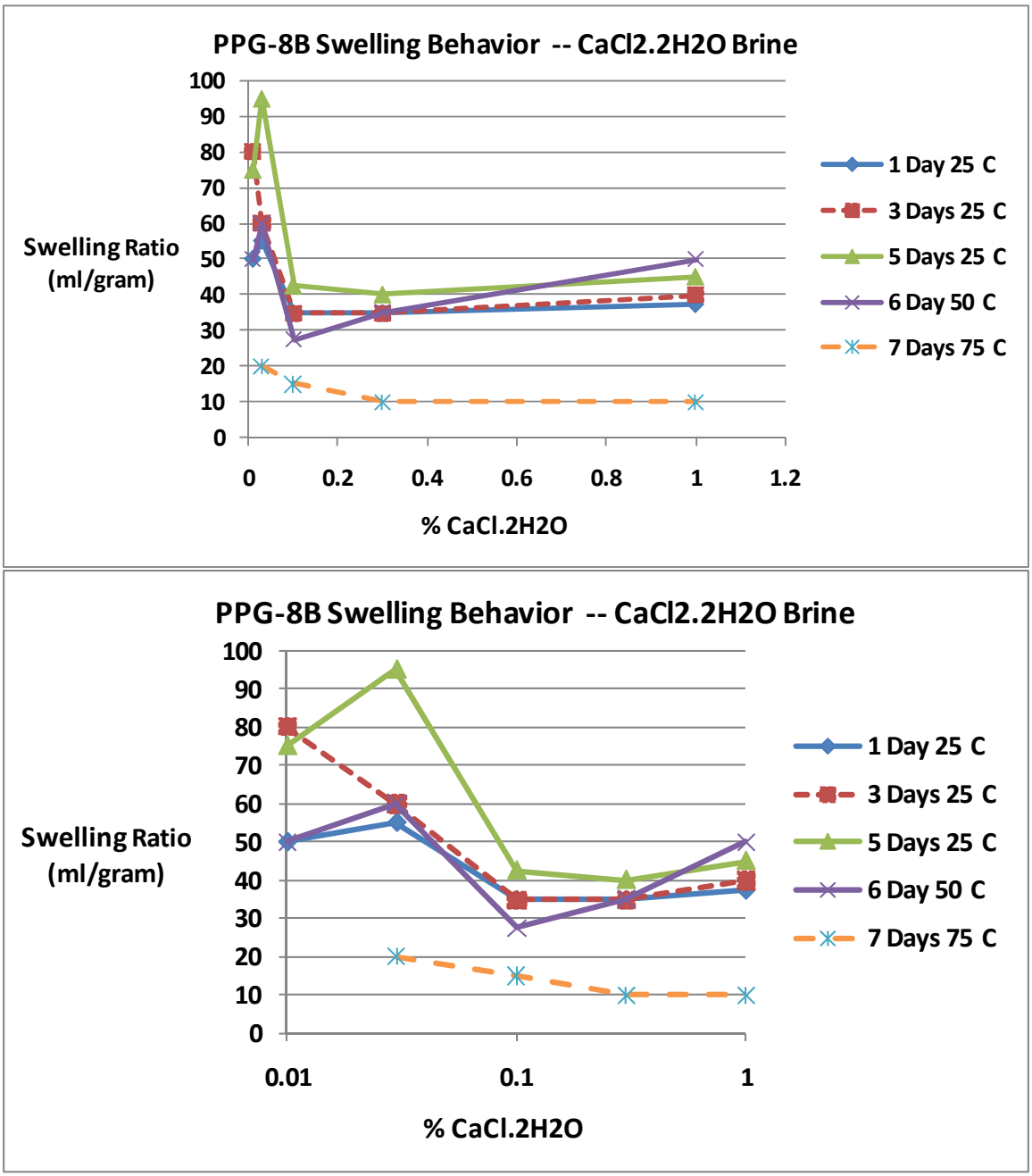

Figure 9-8 Swelling data for sample PPG-8B in $CaCl_2.2H_2O$ brine.

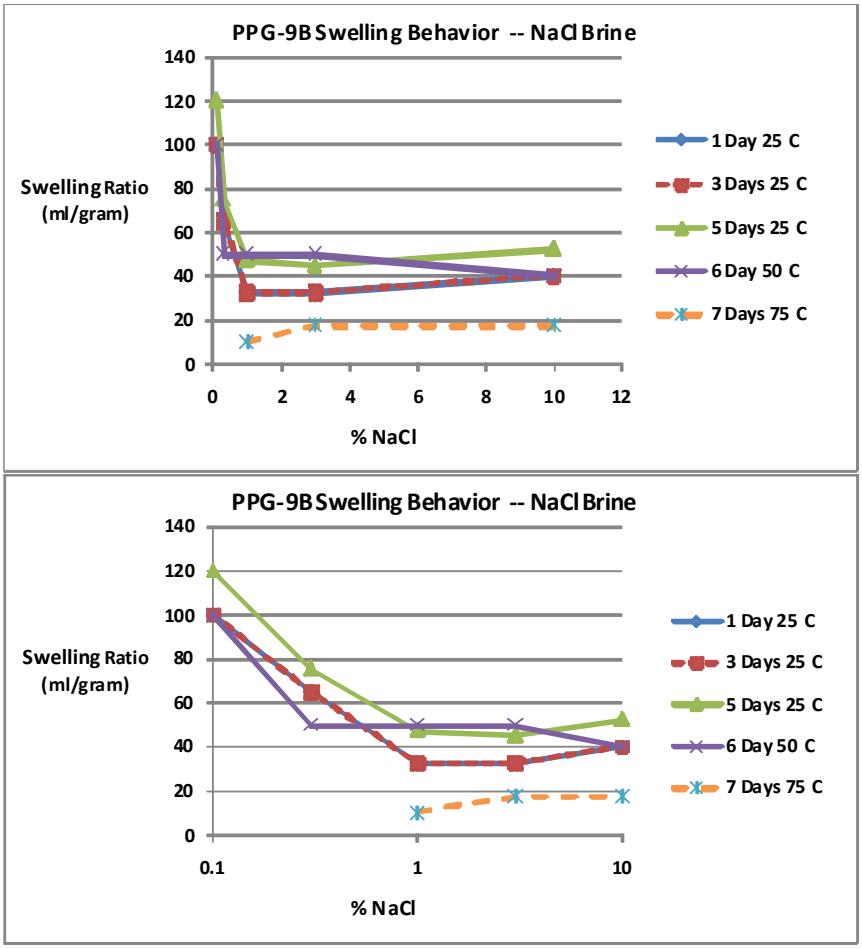

Figure 9-9 Swelling data for sample PPG-9B in NaCl brine.

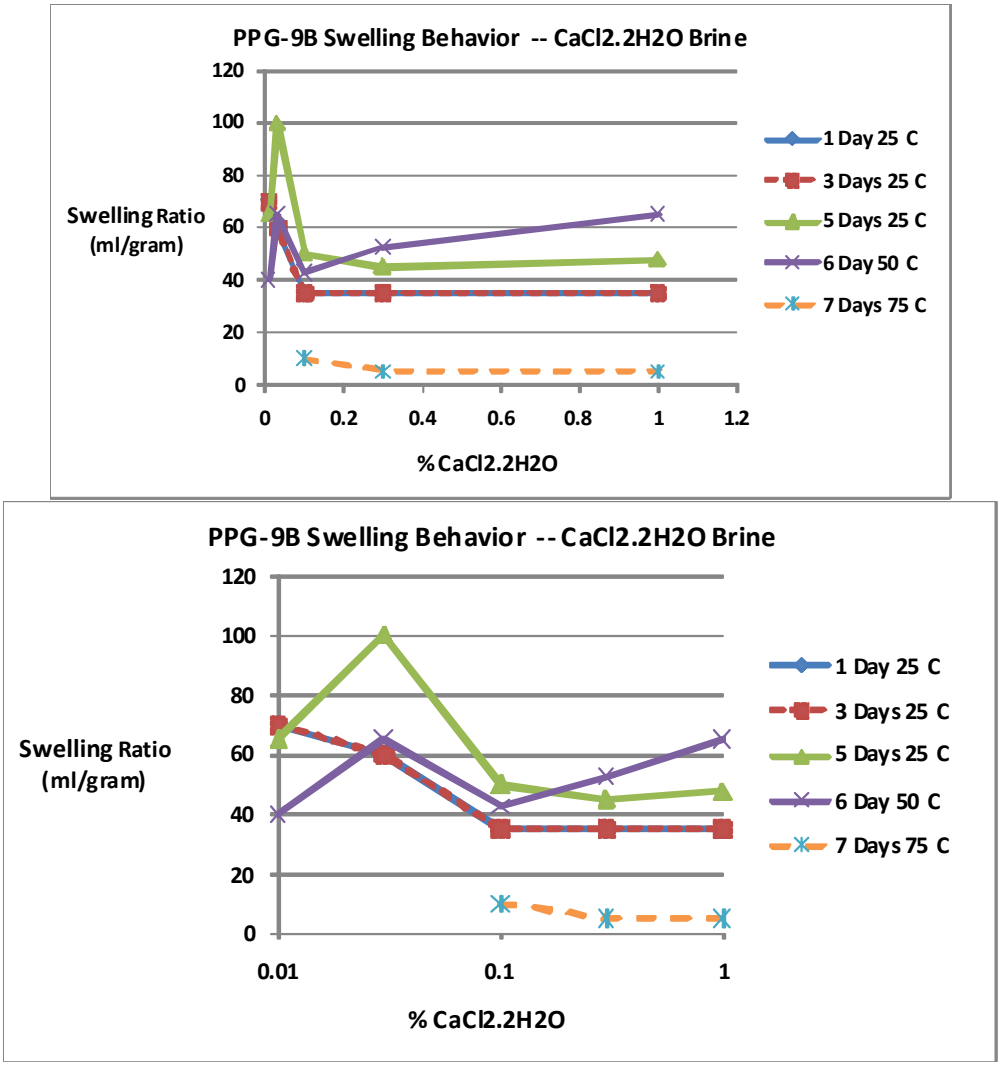

Figure 9-10 Swelling data for sample PPG-9B in $CaCl_2.2H_2O$ brine.

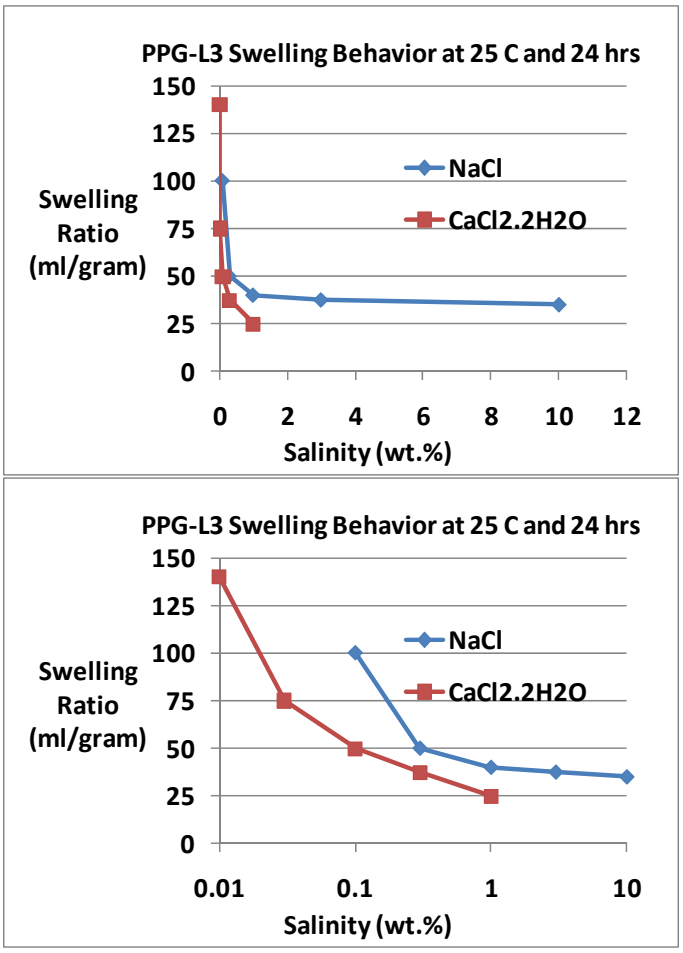

Figure 9-11 Swelling data for sample PPG-L3 at 25 °C.

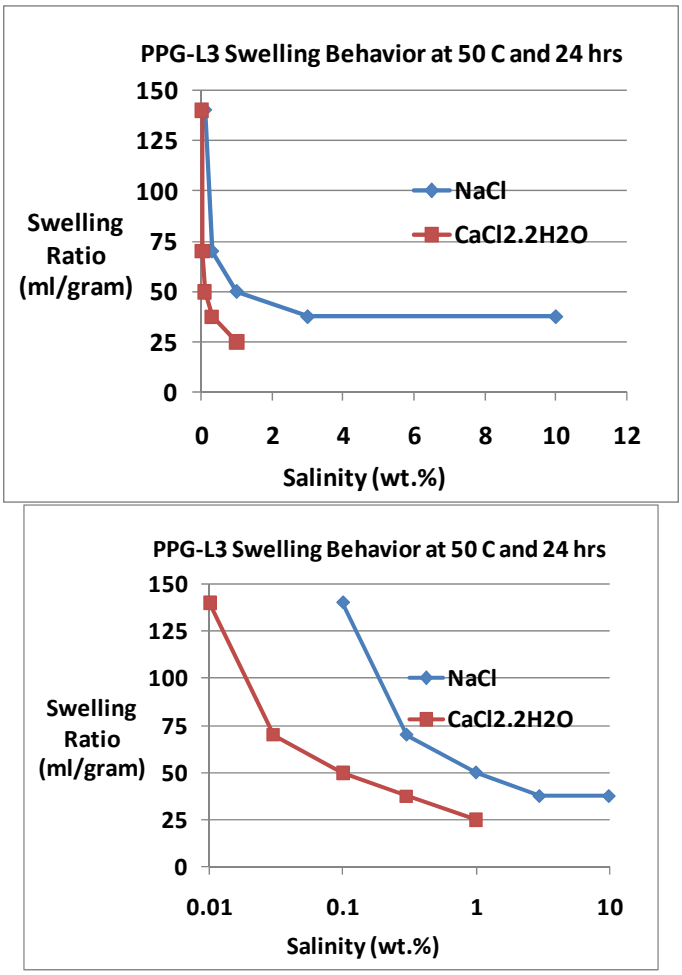

Figure 9-12 Swelling data for sample PPG-L3 at 50 °C.

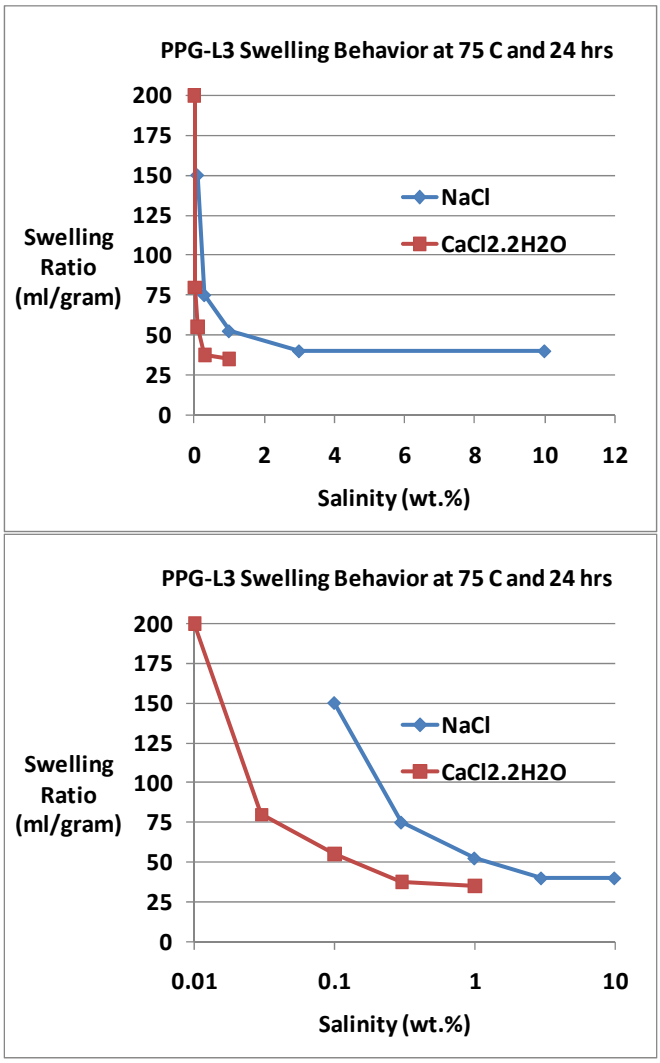

Figure 9-13 Swelling data for sample PPG-L3 at 75 °C.

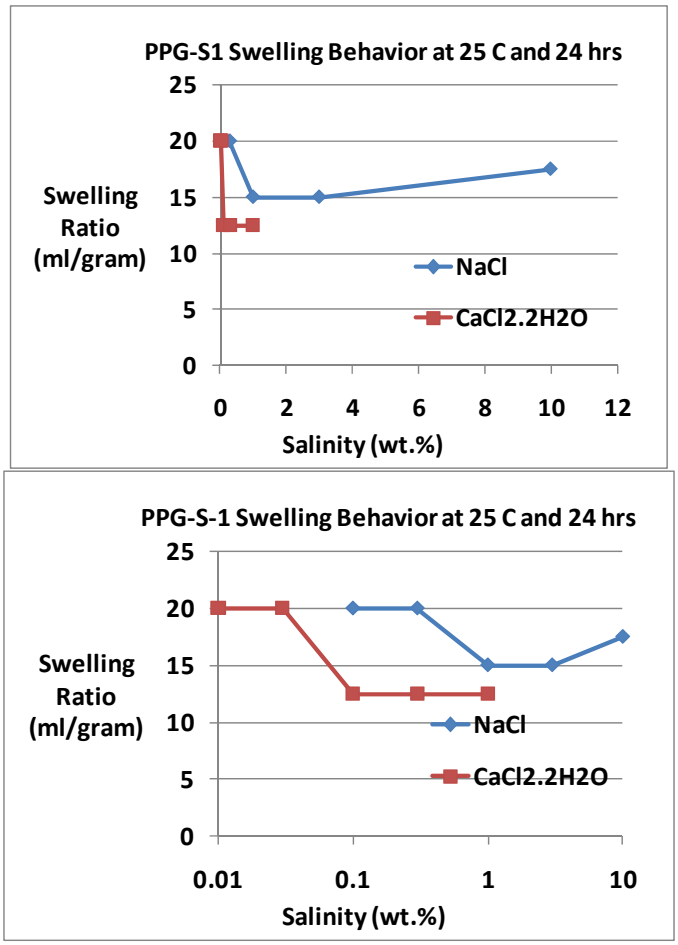

Figure 9-14 Swelling data for sample PPG-S1 at 25 °C.

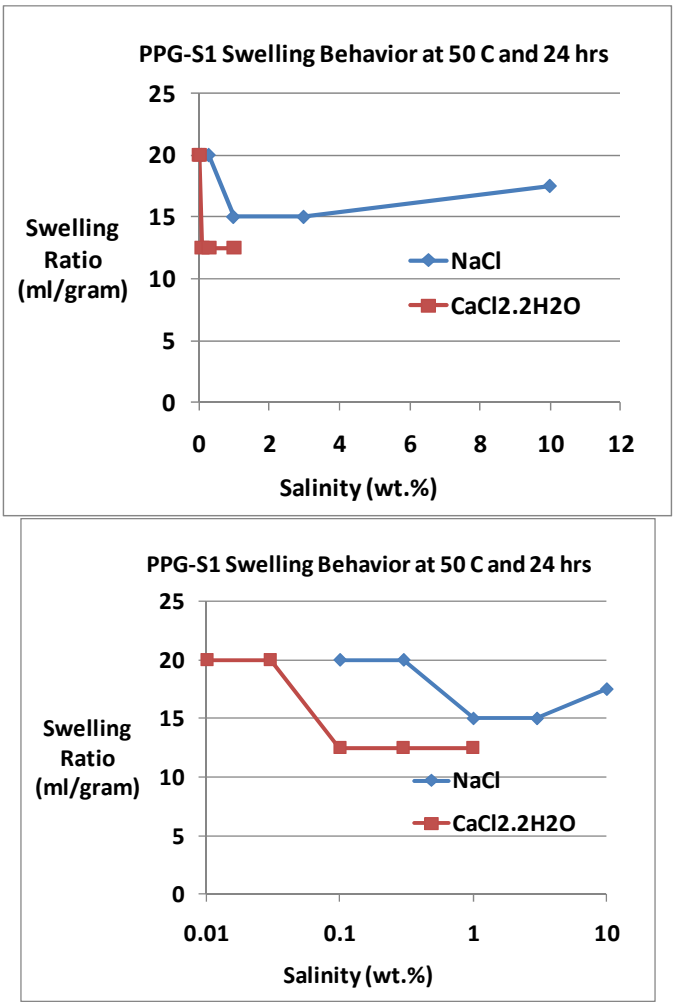

Figure 9-15 Swelling data for sample PPG-S1 at 50 °C.

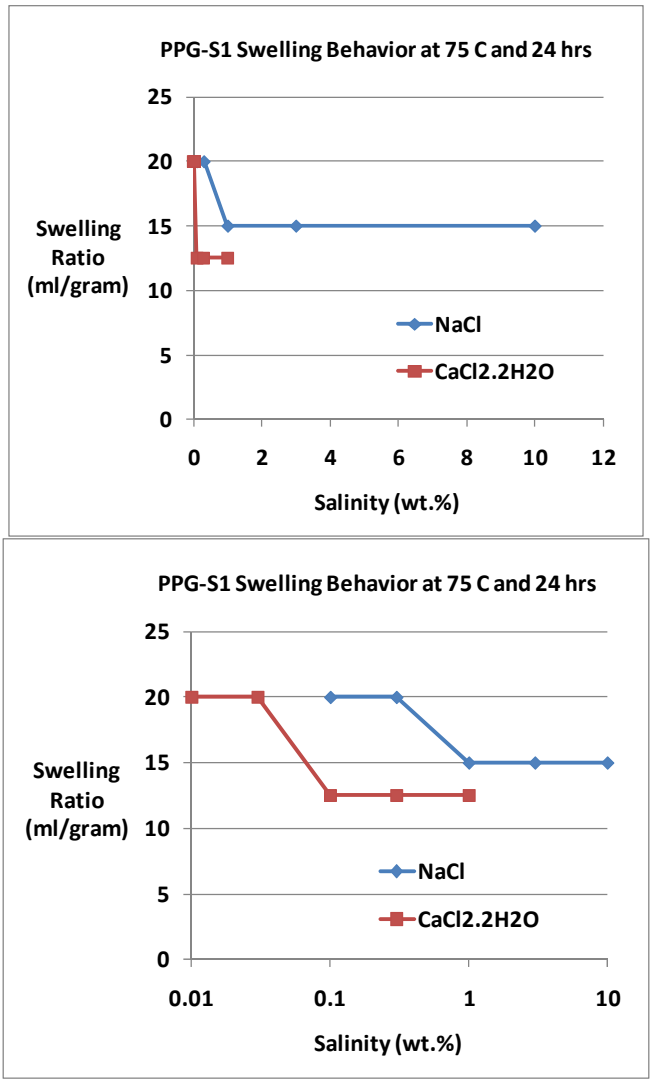

Figure 9-16 Swelling data for sample PPG-S1 at 75 °C.

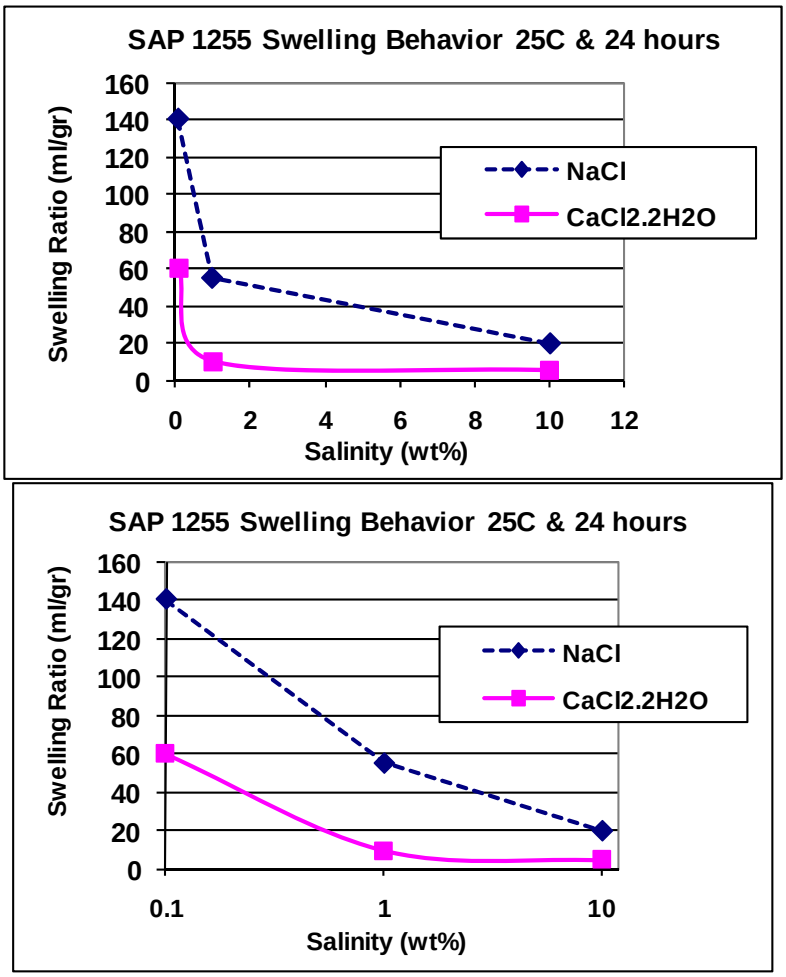

Figure 9-17 Swelling data for sample SAP 1255 at 25 °C.

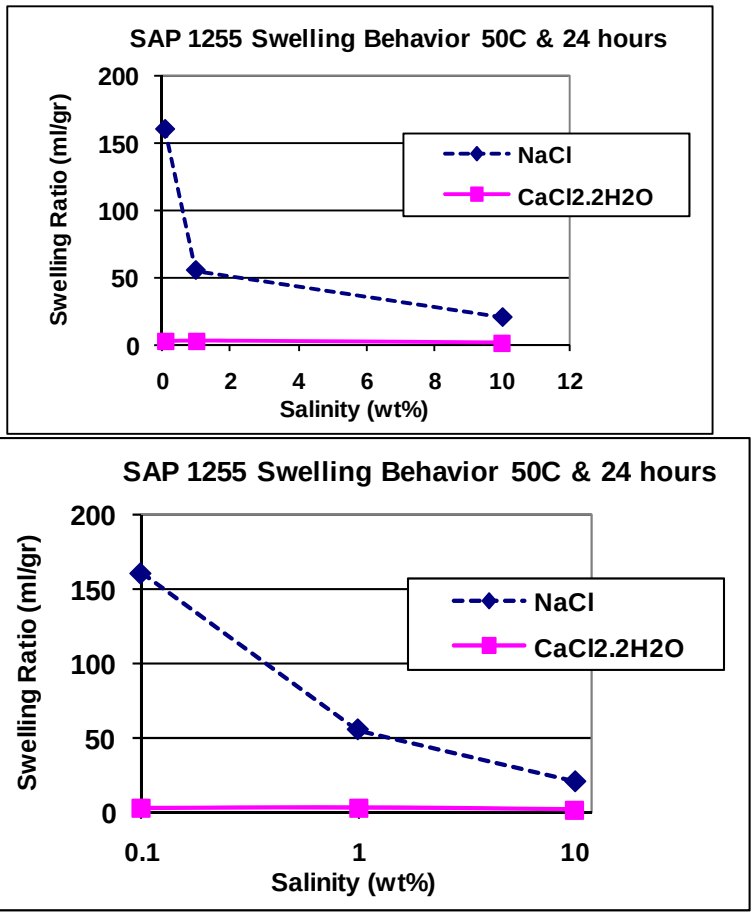

Figure 9-18 Swelling data for sample SAP 1255 at 50 °C.

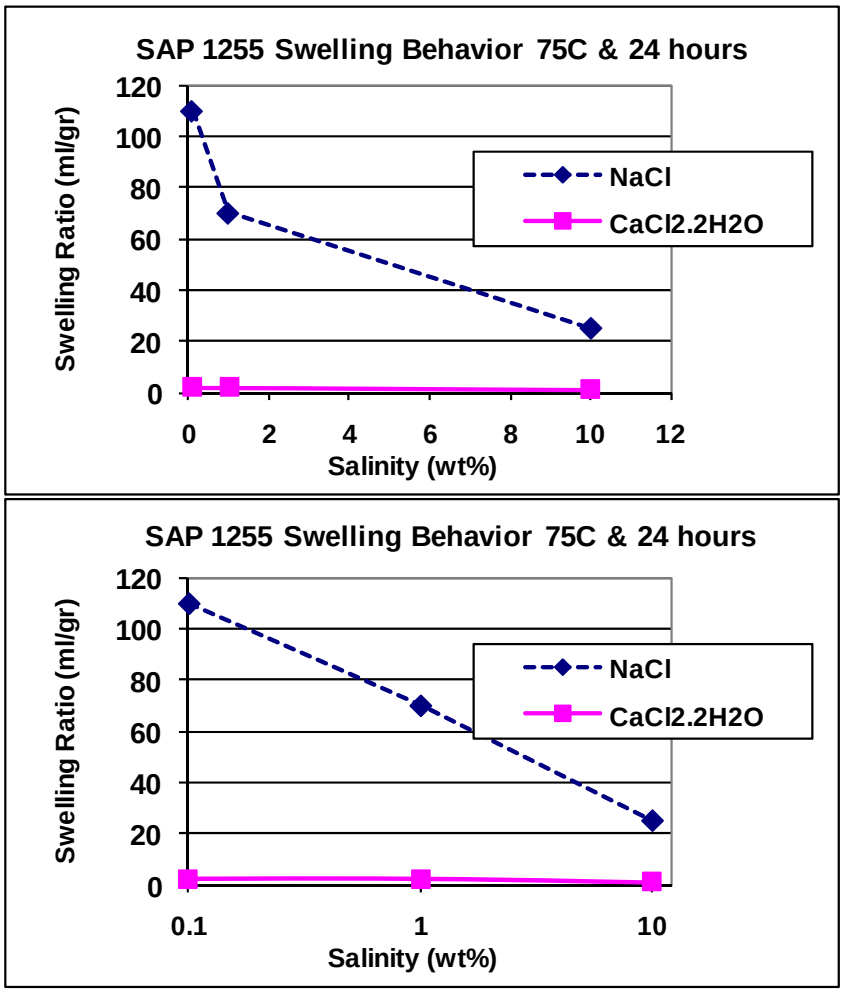

Figure 9-19 Swelling data for sample SAP 1255 at 75 °C.

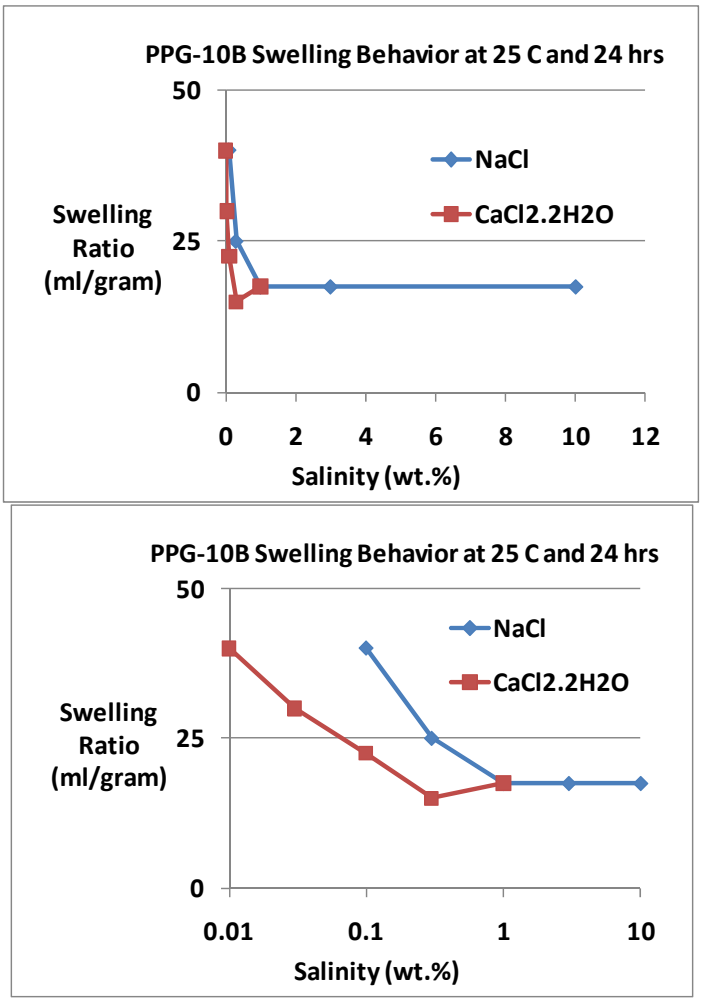

Figure 9-20 Swelling data for sample PPG-10B at 25 °C.

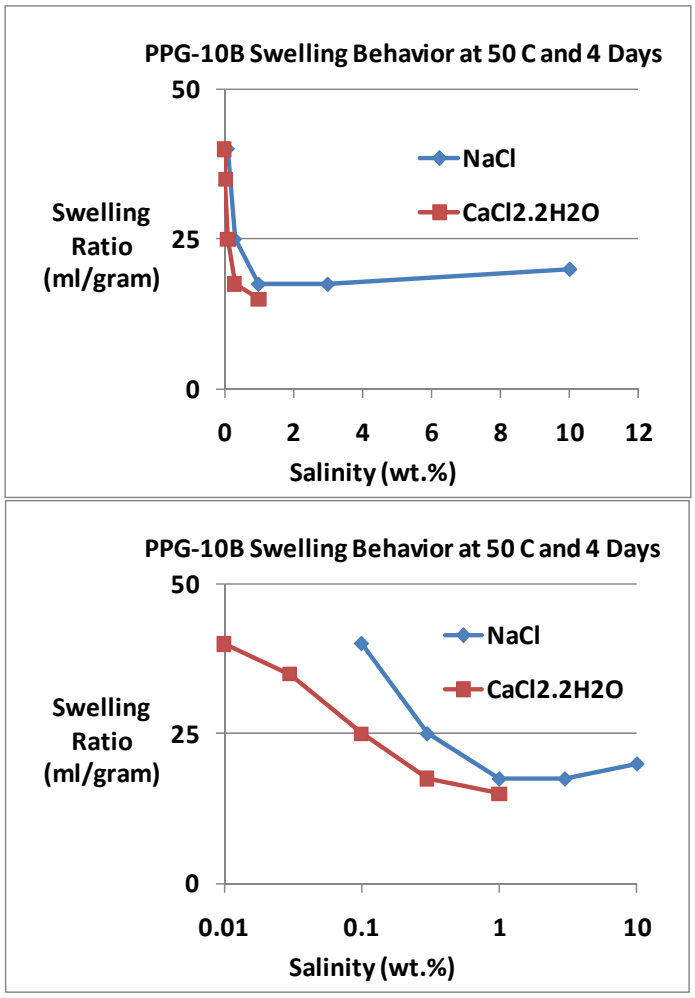

Figure 9-21 Swelling data for sample PPG-10B at 50 °C.

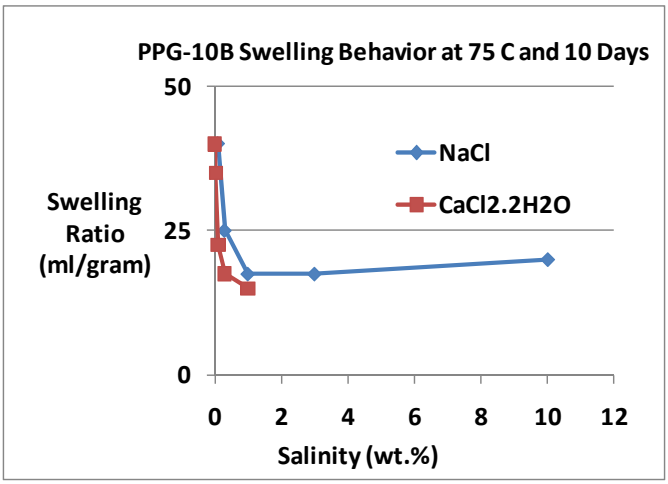

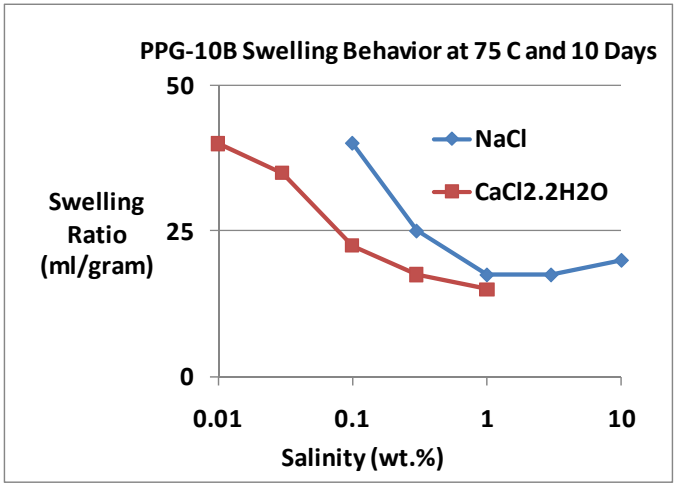

Figure 9-22 Swelling data for sample PPG-10B at 75 °C.

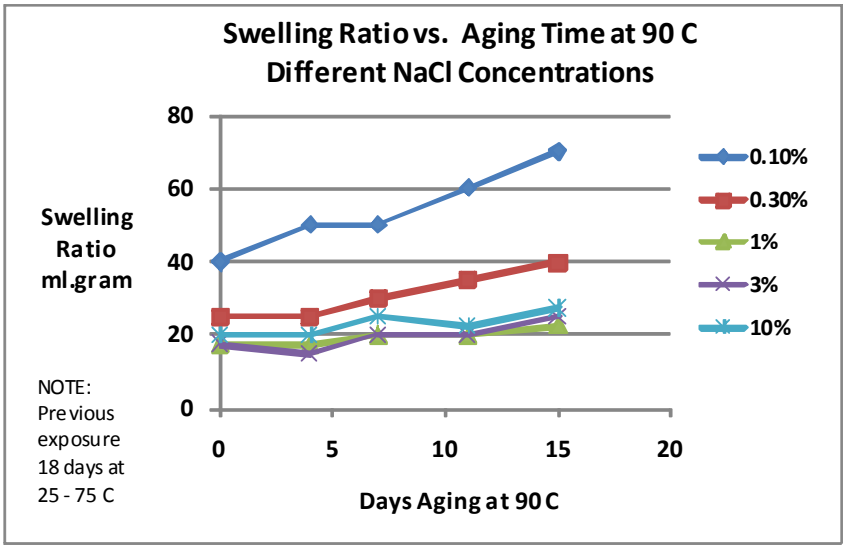

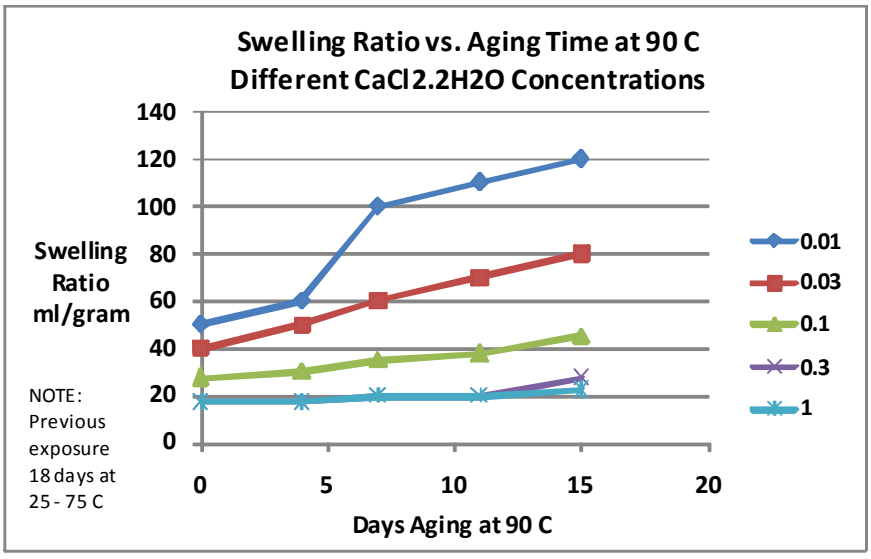

Figure 9-23 Swelling of PPG-10B versus time in sodium and calcium chloride brines.

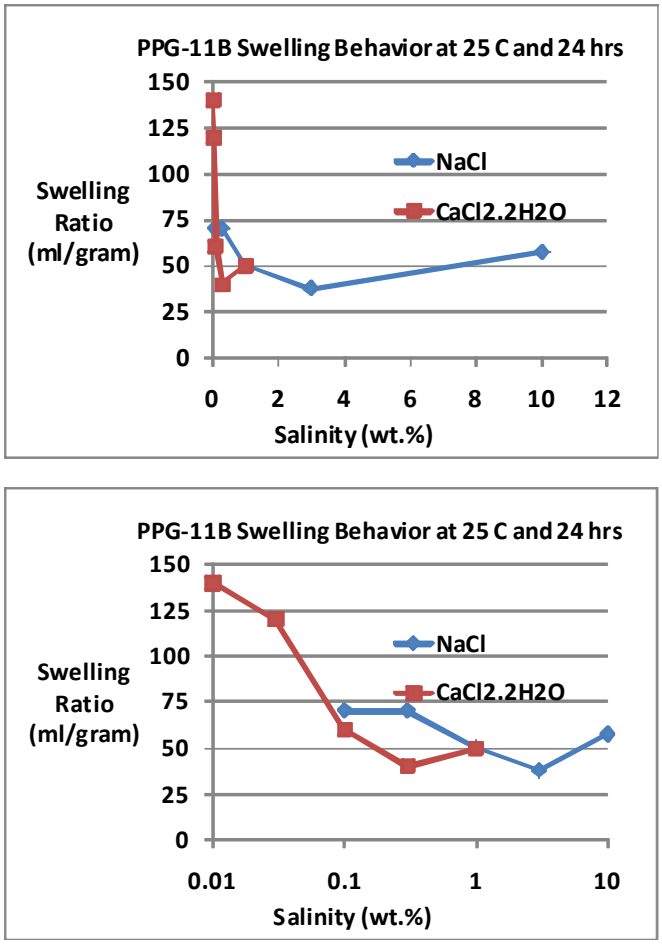

Figure 9-24 Swelling of PPG-11B versus time at salt brines 25 °C.

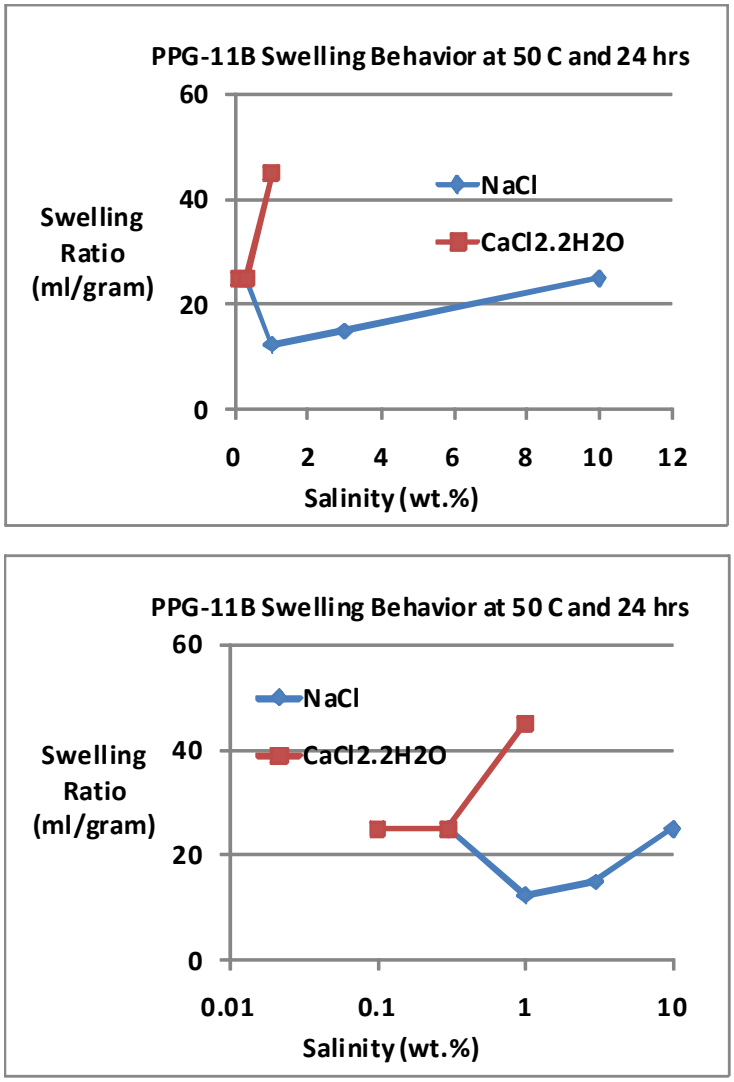

Figure 9-25 Swelling of PPG-11B versus time in brines at 50 °C.

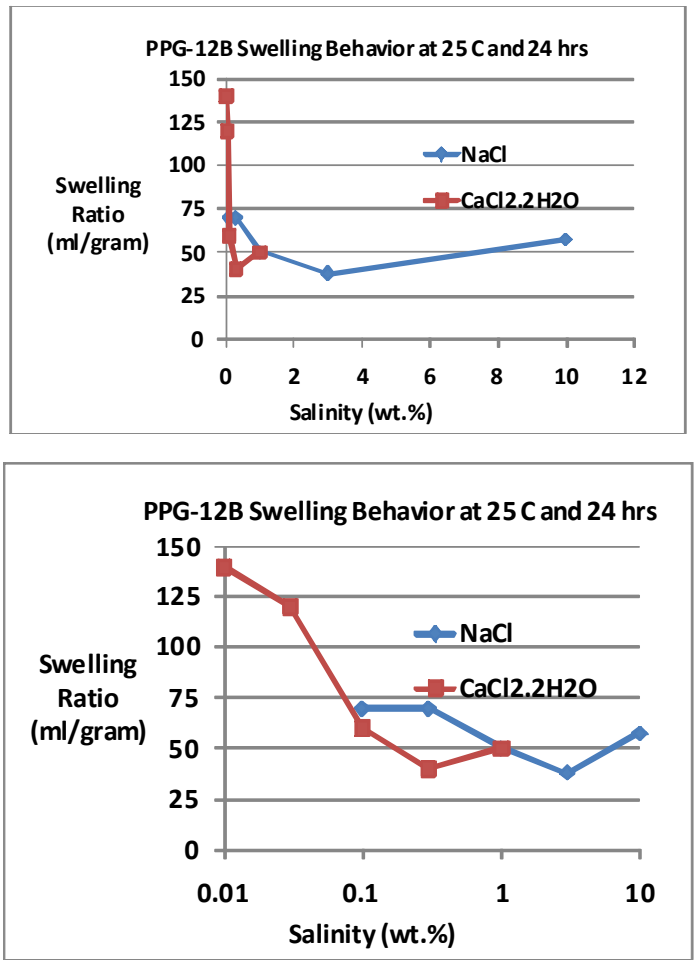

Figure 9-26 Swelling of PPG-11B versus time in brines at 25 °C.

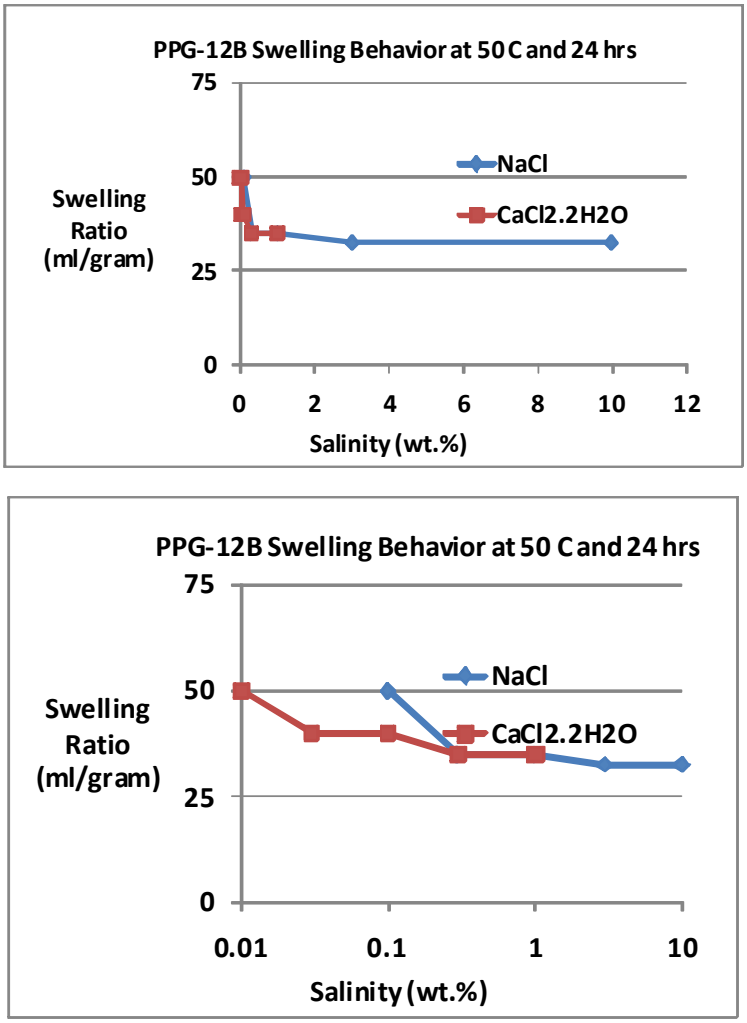

Figure 9-27 Swelling of PPG-11B versus time in brines at 50 °C.

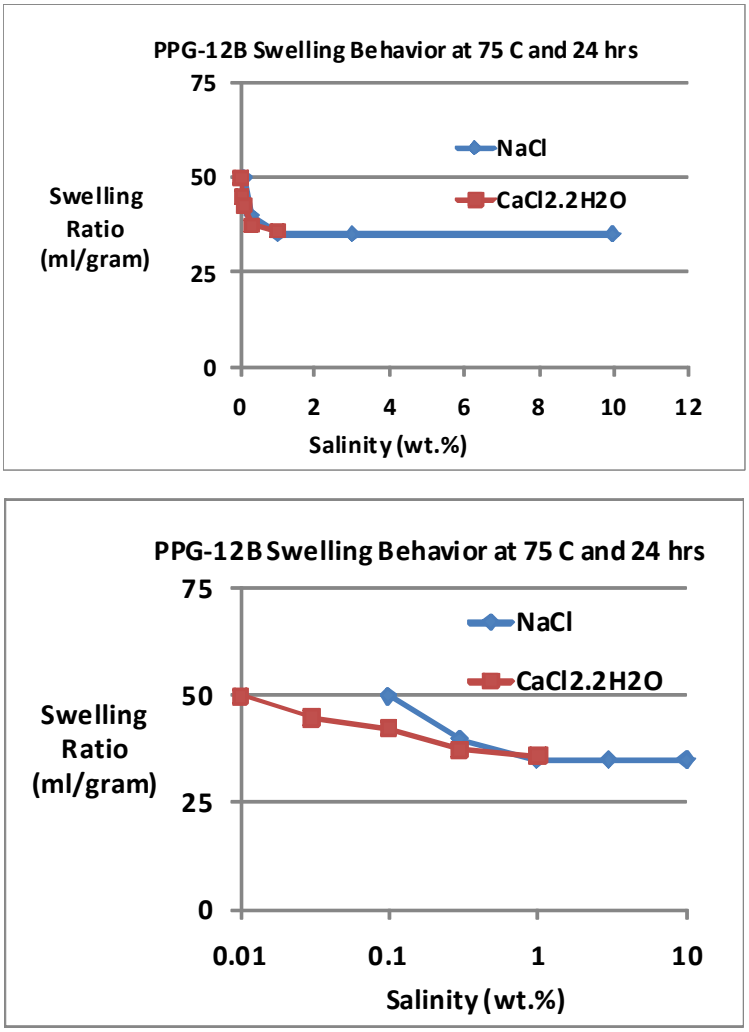

Figure 9-28 Swelling of PPG-11B versus time in brines at 75 °C.

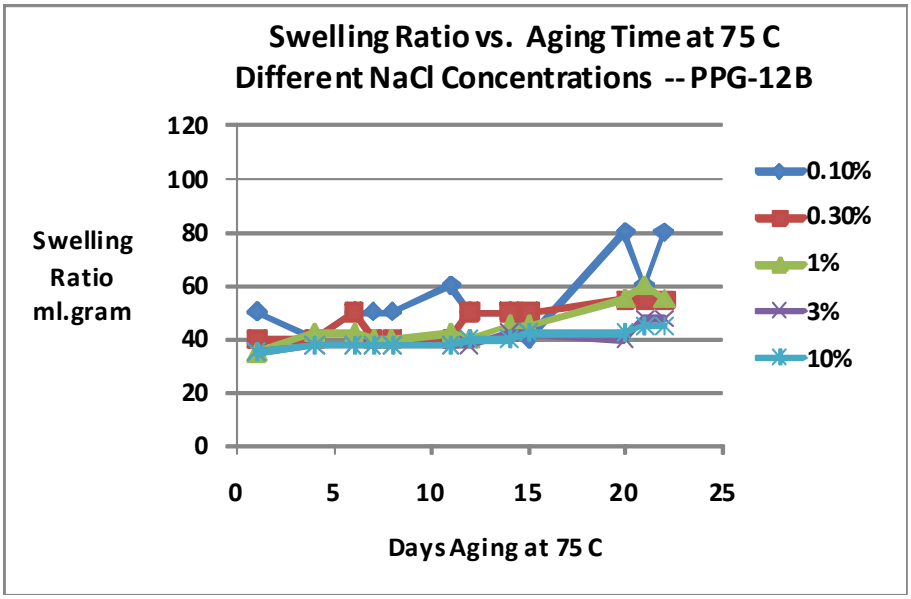

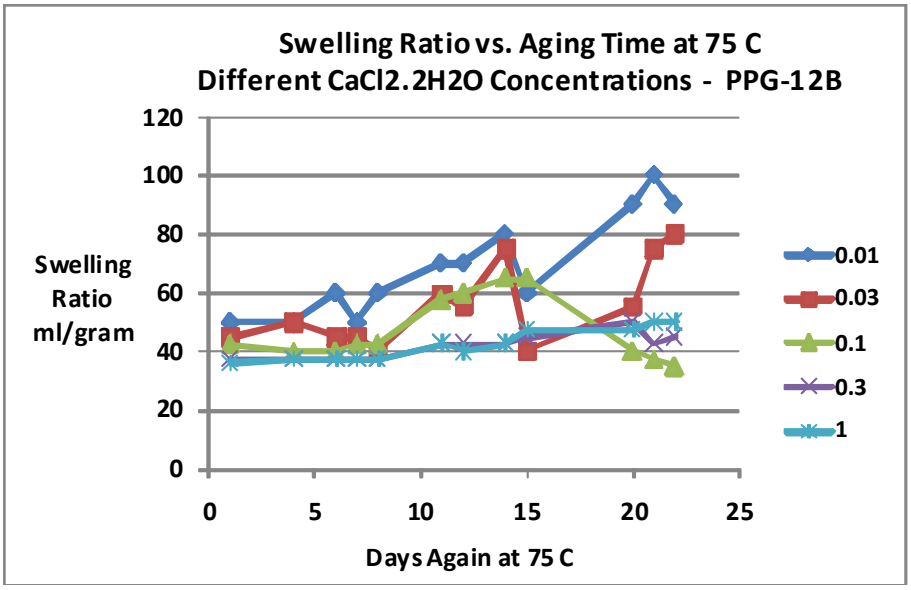

Figure 9-29 Swelling of PPG-12B versus extended time in brines at 75 °C.

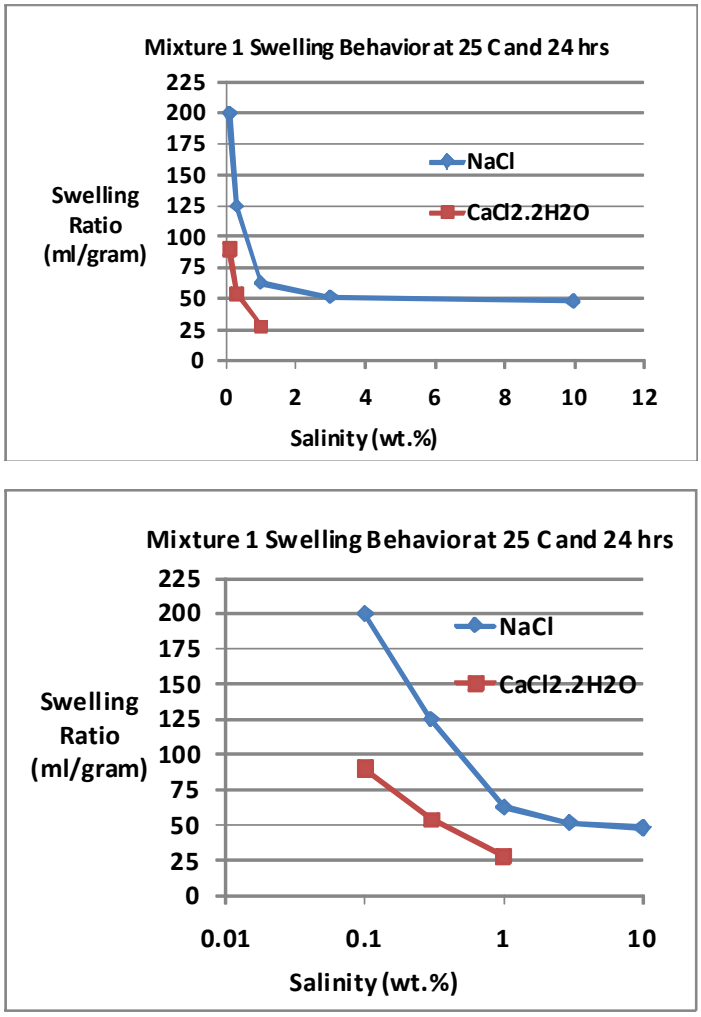

Figure 9-30 Swelling of mixture 1 PPG at 25 °C for 24 hours.

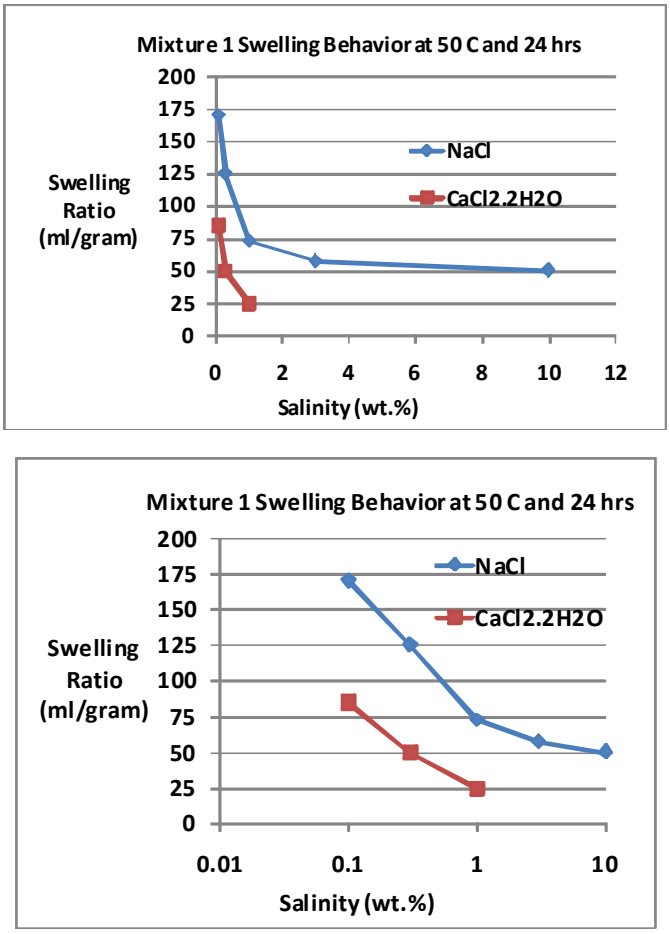

Figure 9-31 Swelling of mixture 1 PPG at 50 °C for 24 hours.

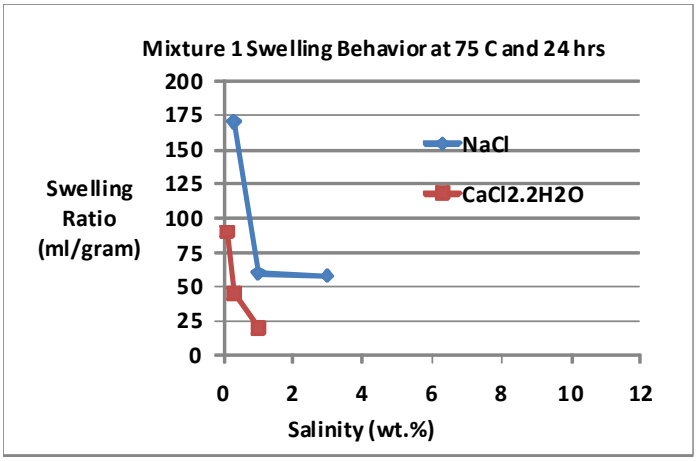

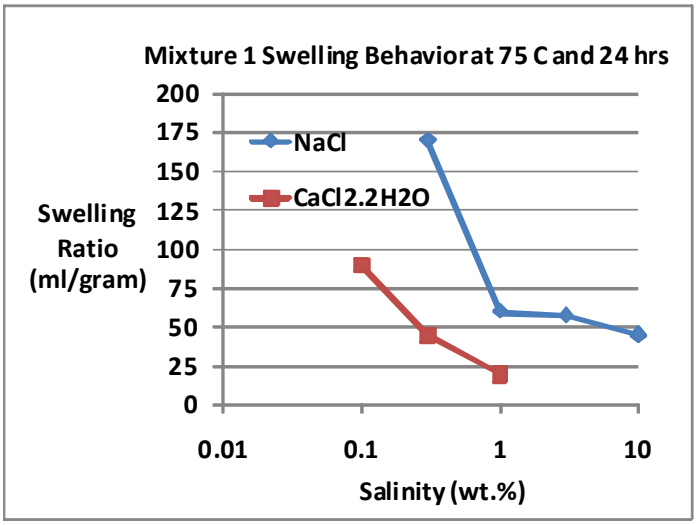

Figure 9-32 Swelling of mixture 1 PPG at 75 °C for 24 hours.

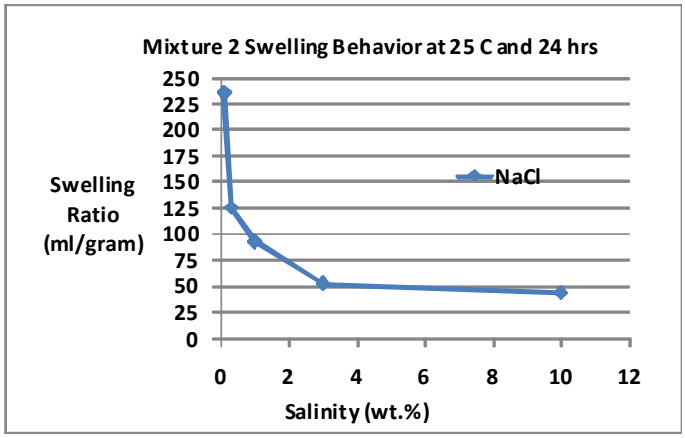

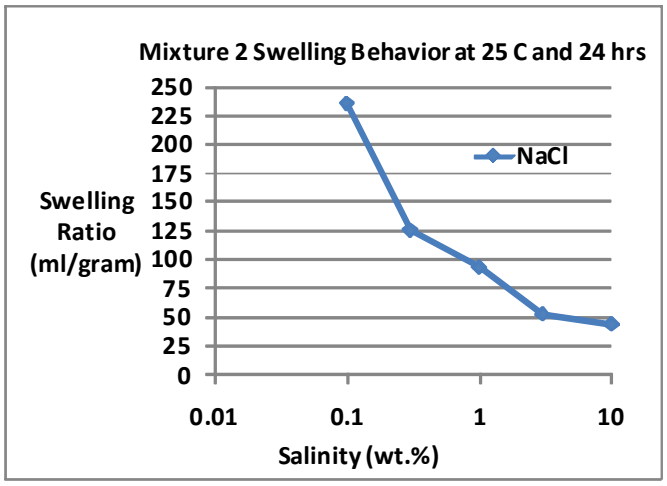

Figure 9-33 Swelling of mixture 2 PPG at 25 °C for 24 hours.

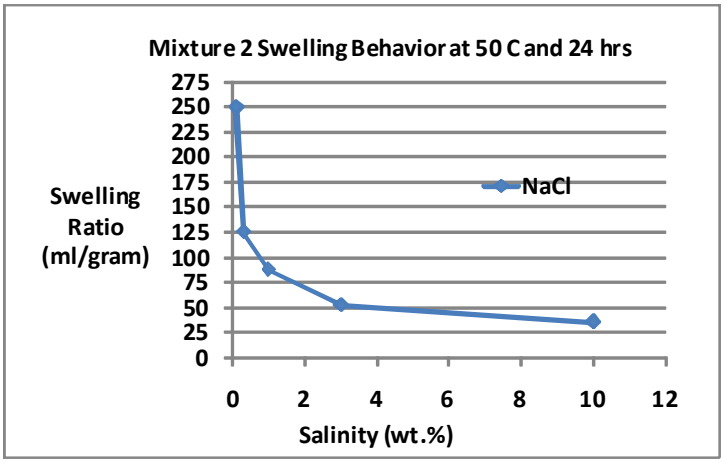

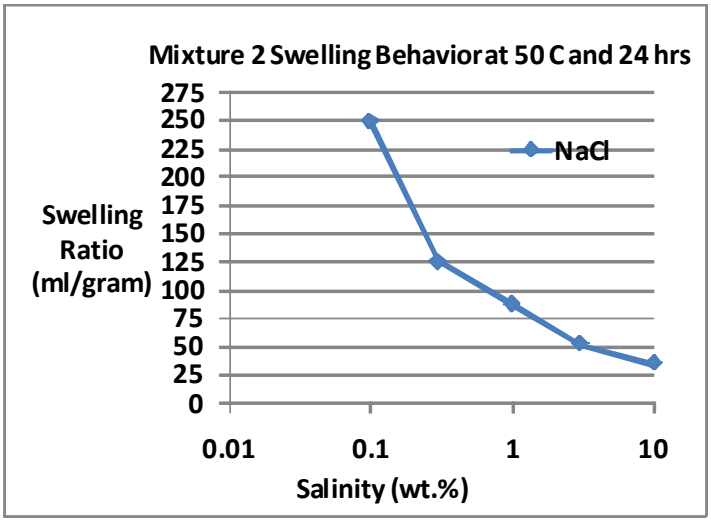

Figure 9-34 Swelling of mixture 2 PPG at 25 °C for 24 hours.

Table 9-1 Summary Swelling Data for PPG-1

UPDATED -- SUMMARY OF PPG-1 SWELLING DATA

Temp. (C.)	Salinity	Interface (ml)	Sample (gr)	Swelling - ml/gr	Previous Swelling - ml/gr
25	0.1% NaCl	19	0.05	380	300
	0.3% NaCl	17.5	0.1	175	
	1% NaCl	21	0.2	105	130
	3% NaCl	15	0.2	75	
	10 % NaCl	11.5	0.2	57.5	62.5
	0.01% CaCl.2H2O	50	0.1	500	
	0.03% CaCl.2H2O	40	0.1	400	
	0.1% CaCl.2H2O	21	0.2	105	60
	0.3% CaCl.2H2O	16.5	0.2	82.5	
	1% CaCl.2H2O	6.5	0.2	32.5	25
50	0.1% NaCl	18.5	0.05	370	290
	0.3% NaCl	18.5	0.1	185	
	1% NaCl	23	0.2	115	155
	3% NaCl	15.5	0.2	77.5	
	10 % NaCl	11	0.2	55	60
	0.01% CaCl.2H2O	47	0.1	470	
	0.03% CaCl.2H2O	37	0.1	370	
	0.1% CaCl.2H2O	18	0.2	90	55
	0.3% CaCl.2H2O	7	0.2	35	
	1% CaCl.2H2O	4.5	0.2	22.5	25
75	0.1% NaCl	18	0.05	360	400
	0.3% NaCl	19	0.1	190	
	1% NaCl	25	0.2	125	150
	3% NaCl	15.5	0.2	77.5	
	10 % NaCl	11	0.2	55	60
	0.01% CaCl.2H2O	45	0.1	450	
	0.03% CaCl.2H2O	35	0.1	350	
	0.1% CaCl.2H2O	15	0.2	75	40
	0.3% CaCl.2H2O	7.5	0.2	37.5	
	1% CaCl.2H2O	3	0.2	15	15

Table 9-2 Summary Swelling Data for PPG-2

UPDATED -- SUMMARY OF PPG-2 SWELLING DATA

Temp (C.)	Salinity	Interface (ml)	Sample (gr)	Swelling - ml/gr	Previous Swelling - ml/gr
25	0.1% NaCl	18	0.05	360	300
	0.3% NaCl	22	0.1	220	
	1% NaCl	26	0.2	130	100
	3% NaCl	16.5	0.2	82.5	
	10 % NaCl	14	0.2	70	60
	0.01% CaCl.2H2O	48	0.1	480	
	0.03% CaCl.2H2O	39	0.1	390	
	0.1% CaCl.2H2O	38	0.2	190	120
	0.3% CaCl.2H2O	16	0.2	80	
	1% CaCl.2H2O	3.5	0.2	17.5	36
50	0.1% NaCl	20	0.05	400	80
	0.3% NaCl	28	0.1	280	
	1% NaCl	26	0.2	130	100
	3% NaCl	16	0.2	80	
	10 % NaCl	15	0.2	75	57.5
	0.01% CaCl.2H2O	30	0.1	300	
	0.03% CaCl.2H2O	25	0.1	250	
	0.1% CaCl.2H2O	33	0.2	165	112
	0.3% CaCl.2H2O	9	0.2	45	
	1% CaCl.2H2O	3	0.2	15	50
75	0.1% NaCl	23	0.05	460	80
	0.3% NaCl	35	0.1	350	
	1% NaCl	26.5	0.2	132.5	100
	3% NaCl	16	0.2	80	
	10 % NaCl	15	0.2	75	57.5
	0.01% CaCl.2H2O	15	0.1	150	
	0.03% CaCl.2H2O	13	0.1	130	
	0.1% CaCl.2H2O	30	0.2	150	112
	0.3% CaCl.2H2O	6	0.2	30	
	1% CaCl.2H2O	2.5	0.2	12.5	50

Table 9-3 Summary Swelling Data for PPG-8B

PPG-8B Swelling Behavior

Salinity	Sample (gr)	1 Day -- 25 C Interface (ml)	3 Day -- 25 C Interface (ml)	4 Day -- 25 C Interface (ml)	5 Day -- 25 C Interface (ml)	6 Day -- 50 C Interface (ml)	7 Day -- 75 C Interface (ml)
0.1% NaCl	0.05	5	5.5	6.5	6.5	6	N/A
0.3% NaCl	0.1	6	6.5	8.5	8.5	7.5	2
1% NaCl	0.2	8.5	9	12.5	12	12	2
3% NaCl	0.2	7.5	8	10.5	10.5	10.5	2
10 % NaCl	0.2	7.5	8	11	11	10.5	3
0.01% CaCl.2H2O	0.1	5	8	7.5	7.5	5	N/A
0.03% CaCl.2H2O	0.1	5.5	6	10	9.5	6	2
0.1% CaCl.2H2O	0.2	7	7	9	8.5	5.5	3
0.3% CaCl.2H2O	0.2	7	7	8	8	7	2
1% CaCl.2H2O	0.2	7.5	8	10	9	10	2

Salinity	Sample (gr)	1 Day -- 25 C Swelling - ml/gr	3 Day -- 25 C Swelling - ml/gr	4 Day -- 25 C Swelling - ml/gr	5 Day -- 25 C Swelling - ml/gr	6 Day -- 50 C Swelling - ml/gr	7 Day -- 75 C Swelling - ml/gr
0.1% NaCl	0.05	100	110	130	130	120	N/A
0.3% NaCl	0.1	60	65	85	85	75	20
1% NaCl	0.2	42.5	45	62.5	60	60	10
3% NaCl	0.2	37.5	40	52.5	52.5	52.5	10
10 % NaCl	0.2	37.5	40	55	55	52.5	15
0.01% CaCl.2H2O	0.1	50	80	75	75	50	N/A
0.03% CaCl.2H2O	0.1	55	60	100	95	60	20
0.1% CaCl.2H2O	0.2	35	35	45	42.5	27.5	15
0.3% CaCl.2H2O	0.2	35	35	40	40	35	10
1% CaCl.2H2O	0.2	37.5	40	50	45	50	10

Table 9-4 Summary Swelling Data for PPG-9B

PPG-9B Swelling Behavior

Salinity	Sample (gr)	1 Day -- 25 C Interface (ml)	3 Day -- 25 C Interface (ml)	4 Day -- 25 C Interface (ml)	5 Day -- 25 C Interface (ml)	6 Day -- 50 C Interface (ml)	7 Day -- 75 C Interface (ml)
0.1% NaCl	0.05	5	5	6	6	5	N/A
0.3% NaCl	0.1	6.5	6.5	8	7.5	5	N/A
1% NaCl	0.2	6.5	6.5	8.5	9.5	10	2
3% NaCl	0.2	6.5	6.5	9	9	10	3.5
10 % NaCl	0.2	8	8	11	10.5	8	3.5
0.01 % CaCl2.2H2O	0.1	7	7	7	6.5	4	N/A
0.03% CaCl2.2H2O	0.1	6	6	10.5	10	6.5	N/A
0.1% CaCl2.2H2O	0.2	7	7	11	10	8.5	2
0.3% CaCl2.2H2O	0.2	7	7	10	9	10.5	1
1% CaCl2.2H2O	0.2	7	7	10	9.5	13	1

Salinity	Sample (gr)	1 Day -- 25 C Swelling - ml/gr	3 Day -- 25 C Swelling - ml/gr	4 Day -- 25 C Swelling - ml/gr	5 Day -- 25 C Swelling - ml/gr	6 Day -- 50 C Swelling - ml/gr	7 Day -- 75 C Swelling - ml/gr
0.1% NaCl	0.05	100	100	120	120	100	N/A
0.3% NaCl	0.1	65	65	80	75	50	N/A
1% NaCl	0.2	32.5	32.5	42.5	47.5	50	10
3% NaCl	0.2	32.5	32.5	45	45	50	17.5
10 % NaCl	0.2	40	40	55	52.5	40	17.5
0.01 % CaCl2.2H2O	0.1	70	70	70	65	40	N/A
0.03% CaCl2.2H2O	0.1	60	60	105	100	65	N/A
0.1% CaCl2.2H2O	0.2	35	35	55	50	42.5	10
0.3% CaCl2.2H2O	0.2	35	35	50	45	52.5	5
1% CaCl2.2H2O	0.2	35	35	50	47.5	65	5

Table 9-5 Summary Swelling Data for PPG-L3 at Different Temperatures

	SUMMARY OF PPG-L3 SWELLING DATA			
Temp. (C.)	**Salinity**	**Interface (ml)**	**Sample (gr)**	**Swelling - ml/gr**
25	0.1 % NaCl	5	0.05	100
	0.3 %NaCl	5	0.1	50
	1% NaCl	8	0.2	40
	3% NaCl	7.5	0.2	37.5
	10% NaCl	7	0.2	35
	0.01 % CaCl2.2H2O	7	0.05	140
	0.03% CaCl2.2H2O	7.5	0.1	75
	0.1% CaCl2.2H2O	10	0.2	50
	0.3% CaCl2.2H2O	7.5	0.2	37.5
	1% CaCl2.2H2O	5	0.2	25
50	0.1% NaCl	7	0.05	140
	0.3% NaCl	7	0.1	70
	1% NaCl	10	0.2	50
	3% NaCl	7.5	0.2	37.5
	10 % NaCl	7.5	0.2	37.5
	0.01% CaCl.2H2O	7	0.05	140
	0.03% CaCl.2H2O	7	0.1	70
	0.1% CaCl.2H2O	10	0.2	50
	0.3% CaCl.2H2O	7.5	0.2	37.5
	1% CaCl.2H2O	5	0.2	25
75	0.1% NaCl	7.5	0.05	150
	0.3% NaCl	7.5	0.1	75
	1% NaCl	10.5	0.2	52.5
	3% NaCl	8	0.2	40
	10 % NaCl	8	0.2	40
	0.01% CaCl.2H2O	10	0.05	200
	0.03% CaCl.2H2O	8	0.1	80
	0.1% CaCl.2H2O	11	0.2	55
	0.3% CaCl.2H2O	7.5	0.2	37.5
	1% CaCl.2H2O	7	0.2	35

Table 9-6 Summary Swelling Data for PPG-L3 for Extended Time at 75 °C

			EXTENDED SWELLING TEST AT 75 C FOR SAMPLE L-3					
				Interface Position (ml)				
Salinity	**Sample (gr)**	**1 day**	**3 days**	**6 days**	**8 days**	**9 days**	**10 days**	**18 days**
0.1 % NaCl	0.05	7	8	7.5	7	7.5	7.5	7.5
0.3 %NaCl	0.1	7.5	8.5	7.5	7.5	7.5	7.5	7.5
1% NaCl	0.2	10	12.5	10.5	11	10.5	10.5	11
3% NaCl	0.2	8	10	8	8	9.5	8.5	9
10% NaCl	0.2	8	8	8	9	9	9	9
0.01 % CaCl2.2H2O	0.05	7.5	10	10	10	9.5	9	9
0.03% CaCl2.2H2O	0.1	7.5	10	8	9	9.5	9	9
0.1% CaCl2.2H2O	0.2	10	11	11	11	11	10	10.5
0.3% CaCl2.2H2O	0.2	8	8	7.5	8	7	6	7
1% CaCl2.2H2O	0.2	7	7.5	7	7	7.5	7	7.5
				Calculated Swelling Ratio				
Salinity		**1 day**	**3 days**	**6 days**	**8 days**	**9 days**	**10 days**	**18 days**
0.1 % NaCl		140	160	150	140	150	150	150
0.3 %NaCl		75	85	75	75	75	75	75
1% NaCl		50	62.5	52.5	55	52.5	52.5	55
3% NaCl		40	50	40	40	47.5	42.5	45
10% NaCl		40	40	40	45	45	45	45
0.01 % CaCl2.2H2O		150	200	200	200	190	180	180
0.03% CaCl2.2H2O		75	100	80	90	95	90	90
0.1% CaCl2.2H2O		50	55	55	55	55	50	52.5
0.3% CaCl2.2H2O		40	40	37.5	40	35	30	35
1% CaCl2.2H2O		35	37.5	35	35	37.5	35	37.5

Table 9-7 Summary Swelling Data for PPG-S1 at Different Temperatures

	SUMMARY OF PPG-S1 SWELLING DATA			
Temp. (C.)	Salinity	Interface (ml)	Sample (gr)	Swelling - ml/gr
25	0.1 % NaCl	1	0.05	20
	0.3 %NaCl	2	0.1	20
	1% NaCl	3	0.2	15
	3% NaCl	3	0.2	15
	10% NaCl	3.5	0.2	17.5
	0.01 % CaCl2.2H2O	1	0.05	20
	0.03% CaCl2.2H2O	2	0.1	20
	0.1% CaCl2.2H2O	2.5	0.2	12.5
	0.3% CaCl2.2H2O	2.5	0.2	12.5
	1% CaCl2.2H2O	2.5	0.2	12.5
50	0.1% NaCl	1	0.05	20
	0.3% NaCl	2	0.1	20
	1% NaCl	3	0.2	15
	3% NaCl	3	0.2	15
	10 % NaCl	3.5	0.2	17.5
	0.01% CaCl.2H2O	1	0.05	20
	0.03% CaCl.2H2O	2	0.1	20
	0.1% CaCl.2H2O	2.5	0.2	12.5
	0.3% CaCl.2H2O	2.5	0.2	12.5
	1% CaCl.2H2O	2.5	0.2	12.5
75	0.1% NaCl	1	0.05	20
	0.3% NaCl	2	0.1	20
	1% NaCl	3	0.2	15
	3% NaCl	3	0.2	15
	10 % NaCl	3	0.2	15
	0.01% CaCl.2H2O	1	0.05	20
	0.03% CaCl.2H2O	2	0.1	20
	0.1% CaCl.2H2O	2.5	0.2	12.5
	0.3% CaCl.2H2O	2.5	0.2	12.5
	1% CaCl.2H2O	2.5	0.2	12.5

Table 9-8 Summary Swelling Data for PPG-S1 for Extended Time at 75 °C

EXTENDED SWELLING TEST AT 75 C FOR SAMPLE PPG-S1				
		Interface Position (ml)		
Salinity	**Sample (gr)**	1 day	2 days	8 days
0.1 % NaCl	0.05	1	1	1.5
0.3 %NaCl	0.1	2	2	2.5
1% NaCl	0.2	3	3	4
3% NaCl	0.2	3	3	3.5
10% NaCl	0.2	3	3	3.5
0.01 % CaCl2.2H2O	0.05	1	1	1
0.03% CaCl2.2H2O	0.1	2	2	2
0.1% CaCl2.2H2O	0.2	2.5	2.5	4
0.3% CaCl2.2H2O	0.2	2.5	2.5	3.5
1% CaCl2.2H2O	0.2	2.5	2.5	3.5
		Calculated Swelling Ratio		
Salinity		1 day	2 days	8 days
0.1 % NaCl		20	20	30
0.3 %NaCl		20	20	25
1% NaCl		15	15	20
3% NaCl		15	15	17.5
10% NaCl		15	15	17.5
0.01 % CaCl2.2H2O		20	20	20
0.03% CaCl2.2H2O		20	20	20
0.1% CaCl2.2H2O		12.5	12.5	20
0.3% CaCl2.2H2O		12.5	12.5	17.5
1% CaCl2.2H2O		12.5	12.5	17.5

Table 9-9 Summary Swelling Data for PPG product SAP 1255 vs. Temperatures

	SUMMARY OF SAP 1255 SWELLING DATA			
Temperature (C.)	Salinity	Interface (ml)	Sample (gr)	Swelling - ml/gram
25	0.1 % NaCl	7	0.05	140
	1% NaCl	5.5	0.1	55
	10% NaCl	4	0.2	20
	0.1% CaCl2.2H2O	6	0.1	60
	1% CaCl2.2H2O	2	0.2	10
	10% CaCl2.2H2O	1	0.2	5
50	0.1 % NaCl	8	0.05	160
	1% NaCl	5.5	0.1	55
	10% NaCl	4	0.2	20
	0.1% CaCl2.2H2O	0.2	0.1	2
	1% CaCl2.2H2O	0.5	0.2	2.5
	10% CaCl2.2H2O	0.2	0.2	1
75	0.1 % NaCl	5.5	0.05	110
	1% NaCl	7	0.1	70
	10% NaCl	5	0.2	25
	0.1% CaCl2.2H2O	0.2	0.1	2
	1% CaCl2.2H2O	0.4	0.2	2
	10% CaCl2.2H2O	0.2	0.2	1

Table 9-10 Summary Swelling Data for PPG-10B at Different Temperatures

	SUMMARY OF PPG-10B SWELLING DATA			
Temp. (C.)	**Salinity**	**Sample (gr)**	**Interface (ml)**	**Swelling - ml/gr**
25	0.1% NaCl	0.05	2	40
(Day 1)	0.3% NaCl	0.1	2.5	25
	1% NaCl	0.2	3.5	17.5
	3% NaCl	0.2	3.5	17.5
	10% NaCl	0.2	3.5	17.5
	0.01 % CaCl2.2H2O	0.05	2	40
	0.03% CaCl2.2H2O	0.1	3	30
	0.1% CaCl2.2H2O	0.2	4.5	22.5
	0.3% CaCl2.2H2O	0.2	3	15
	1% CaCl2.2H2O	0.2	3.5	17.5
50	0.1% NaCl	0.05	2	40
(Day 4)	0.3% NaCl	0.1	2.5	25
	1% NaCl	0.2	3.5	17.5
	3% NaCl	0.2	3.5	17.5
	10% NaCl	0.2	4	20
	0.01 % CaCl2.2H2O	0.05	2	40
	0.03% CaCl2.2H2O	0.1	3.5	35
	0.1% CaCl2.2H2O	0.2	5	25
	0.3% CaCl2.2H2O	0.2	3.5	17.5
	1% CaCl2.2H2O	0.2	3	15
75	0.1% NaCl	0.05	2	40
(Day 10)	0.3% NaCl	0.1	2.5	25
	1% NaCl	0.2	3.5	17.5
	3% NaCl	0.2	3.5	17.5
	10% NaCl	0.2	4	20
	0.01 % CaCl2.2H2O	0.05	2	40
	0.03% CaCl2.2H2O	0.1	3.5	35
	0.1% CaCl2.2H2O	0.2	4.5	22.5
	0.3% CaCl2.2H2O	0.2	3.5	17.5
	1% CaCl2.2H2O	0.2	3	15

Table 9-11 Summary Swelling Data for PPG-10B versus Time at 90 °C

SWELLING RATIO PPG-10B - VERSUS DAYS AT 90 C					
		Concentration NaCl			
Days	0.10%	0.30%	1%	3%	10%
0	40	25	17.5	17.5	20
4	50	25	17.5	15	20
7	50	30	20	20	25
11	60	35	20	20	22.5
15	70	40	22.5	25	27.5

		Concentration CaCl.2H2O			
Days	0.01	0.03	0.1	0.3	1
0	50	40	27.5	17.5	17.5
4	60	50	30	17.5	17.5
7	100	60	35	20	20
11	110	70	37.5	20	20
15	120	80	45	27.5	22.5

Table 9-12 Summary Swelling Data for PPG-11B

Temp. (C.)	Salinity	Sample (gr)	Interface (ml)	Swelling - ml/gr
25	0.1 % NaCl	0.05	3.5	70
	0.3 %NaCl	0.1	7	70
	1% NaCl	0.2	10	50
	3% NaCl	0.2	7.5	37.5
	10% NaCl	0.2	11.5	57.5
	0.01 % CaCl2.2H2O	0.05	7	140
	0.03% CaCl2.2H2O	0.1	12	120
	0.1% CaCl2.2H2O	0.2	12	60
	0.3% CaCl2.2H2O	0.2	8	40
	1% CaCl2.2H2O	0.2	10	50
50	0.1% NaCl	0.05	dissolved	N/A
	0.3% NaCl	0.1	2.5	25
	1% NaCl	0.2	2.5	12.5
	3% NaCl	0.2	3	15
	10 % NaCl	0.2	5	25
	0.01 % CaCl2.2H2O	0.05	dissolved	N/A
	0.03% CaCl2.2H2O	0.1	dissolved	N/A
	0.1% CaCl2.2H2O	0.2	5	25
	0.3% CaCl2.2H2O	0.2	5	25
	1% CaCl2.2H2O	0.2	9	45

Table 9-13 Summary Short-term Swelling Data for PPG-12B

SUMMARY OFSHORT-TERM PPG-12B SWELLING DATA				
Temp. (C.)	**Salinity**	**Sample (gr)**	**Interface (ml)**	**Swelling - ml/gr**
25	0.1 % NaCl	0.05	2.5	50
	0.3 %NaCl	0.1	4	40
	1% NaCl	0.2	7	35
	3% NaCl	0.2	7.5	37.5
	10% NaCl	0.2	7	35
	0.01 % CaCl2.2H2O	0.05	3.5	70
	0.03% CaCl2.2H2O	0.1	4	40
	0.1% CaCl2.2H2O	0.2	8.5	42.5
	0.3% CaCl2.2H2O	0.2	7	35
	1% CaCl2.2H2O	0.2	7	35
50	0.1% NaCl	0.05	2.5	50
	0.3% NaCl	0.1	3.5	35
	1% NaCl	0.2	7	35
	3% NaCl	0.2	6.5	32.5
	10% NaCl	0.2	6.5	32.5
	0.01 % CaCl2.2H2O	0.05	2.5	50
	0.03% CaCl2.2H2O	0.1	4	40
	0.1% CaCl2.2H2O	0.2	8	40
	0.3% CaCl2.2H2O	0.2	7	35
	1% CaCl2.2H2O	0.2	7	35
75	0.1% NaCl	0.05	2.5	50
	0.3% NaCl	0.1	4	40
	1% NaCl	0.2	7	35
	3% NaCl	0.2	7	35
	10% NaCl	0.2	7	35
	0.01 % CaCl2.2H2O	0.05	2.5	50
	0.03% CaCl2.2H2O	0.1	4.5	45
	0.1% CaCl2.2H2O	0.2	8.5	42.5
	0.3% CaCl2.2H2O	0.2	7.5	37.5
	1% CaCl2.2H2O	0.2	7.2	36

Table 9-14 Summary Short-term Swelling Data for Mixture 1

		Comparison of Mixture 1 and Components			
			Swelling (mg/gram)		
Temp. (C.)	Salinity	PPG-2	PPG-12B	Theoretical Mix	Actual -- Mixture 1
25	0.1 % NaCl	300	50	175	200
	0.3 % NaCl		40		125
	1% NaCl	100	35	67.5	62.5
	3% NaCl		37.5		51.5
	10% NaCl	60	35	47.5	47.5
	0.1% CaCl2.2H2O	120	42.5	81.3	90
	0.3% CaCl2.2H2O		35		54
	1% CaCl2.2H2O	36	35	35.5	27.5
50	0.1% NaCl	80	50	65.0	170
	0.3% NaCl		35		125
	1% NaCl	100	35	67.5	72.5
	3% NaCl		32.5		57.5
	10 % NaCl	57.5	32.5	45.0	50
	0.1% CaCl2.2H2O	112.5	40	76.3	85
	0.3% CaCl2.2H2O		35		50
	1% CaCl2.2H2O	50	35	42.5	25
75	0.1% NaCl	80	50		
	0.3% NaCl		40		170
	1% NaCl	100	35	67.5	60
	3% NaCl		35		57.5
	10 % NaCl	57.5	35	46.3	45
	0.1% CaCl2.2H2O	112.5	42.5	77.5	90
	0.3% CaCl2.2H2O		37.5		45
	1% CaCl2.2H2O	50	36	43.0	20

Table 9-15 Summary Short-Term Swelling Data for Mixture 2

		Comparison of Mixture 2 and Components			
		Swelling (mg/gram)			
Temp. (C.)	Salinity	PPG-2	SAP 1255	Theoretical Mix	Actual -- Mixture 2
25	0.1 % NaCl	300	140	220	235
	0.3 %NaCl		80		125
	1% NaCl	100	55	77.5	92.5
	3% NaCl		35		52.5
	10% NaCl	60	20	40	43.75
50	0.1% NaCl	80	160	120	250
	0.3% NaCl		85		125
	1% NaCl	100	55	77.5	87.5
	3% NaCl		32.5		52.5
	10 % NaCl	57.5	20	38.75	35
75	0.1% NaCl	80	110	95	100
	0.3% NaCl		85		65
	1% NaCl	100	70	85	75
	3% NaCl		40		50
	10 % NaCl	57.5	25	41.25	37.5

Table 9-16 Comparison of Swelling Tendency among Different PPG Samples

	Swelling (ml/gram) -- 50 C		
Sample	1% NaCl	0.1 CaCl2.2H2O	Other/Commenrs
PPG-1	115	90	
PPG-2	130	165	
PPG-8B	60	30	has some deayed swelling effect
PPG-9B	50	45	
PPG-L3	50	50	product contains some clay
PPG-S1	15	12.5	product contains some clay
SAP-1255	55	2	not suitable for calcium chloride brin
PPG-10B	17.5	25	most increase in swellng with time
PPG-11B	12.5	25	
PPG-12B	35	40	
Mixture 1	72.5	85	50/50 blend of PPG-2 and PPG-12B
Mixture 2	87.5	N/A	50/50 blend of PPG-2 and SAP 1255

10. Static Filtration Tests to Evaluate the Damage of Preformed Particle Gel on Non-Swept Zones/Areas during Conformance Control Treatments

10.1. Summary

Various materials have been used to decrease water production and increase sweep efficiency for mature oilfields. A new trend is using preformed particle gel (PPG) for the purpose. A filtration apparatus was designed to determine the possible penetration of PPG into low-permeability sandstone rocks. Filtration curves (the relationship between injection time versus filtration volume) were obtained, and the permeability of sandstone cores before and after PPG treatment was measured to determine whether PPGs reduce the permeability of low-permeability rocks. Two kinds of PPGs were used for our filtration experiments: Daqing (DQ) and LiquiBlock 40K. Results showed that DQ PPG formed a permeable porous media on the surface of the cores and the particles did not impair the permeability of the rock. However LiquiBlock 40K formed cake on rock surfaces and reduced rock permeability up to 60%. It was found that the damage of particle gel on unswept low-permeable zones/areas can be effectively prevented by controlling particle gel strength, particle size and the concentration of brine.

10.2. Introduction

Extensive experiments have been carried out to understand PPG transport through fractures (Bai et al 2007, Zhang and Bai, 2010). For a successful PPG treatment, it is expected that the PPG should be able to be easily injected into highly permeable streaks/channels/fractures while minimizing its penetration into previously non-swept zones/areas with low permeability. A filtration test is a simple and repeatable means for evaluating formation damage (Vetter et al., 1987, and Ershagi et al., 1986). Our work in this section sought to determine whether PPGs would damage low permeability rocks and find ways to minimize PPG damage on non-swept zones/areas.

10.3. Experimental

10.3.1. Materials

Two kinds of PPGs were used for our filtration experiments: Daqing (DQ) and LiquiBlock 40K. The particle sizes ranged from 30 to 80 meshes. DQ is a strong particle with an elastic module of more than 8000 Pa after fully swollen, while LiquiBlock 40K is

a weak gel particle with an elastic module of around 800 Pa. Both PPGs can swell to 10~100 times of the original volume. Brine concentration significantly affects the PPG swelling ratio. High salinity brine results in lower swelling ratios but higher swollen particle strength. Three brine concentrations (0.05%, 1%, and 10%) were selected to prepare the swollen PPGs.

10.3.2. Setups

The experiment setup is shown in Figures 10-1 and 10-2. It is composed of one syringe pump and one filtration model. The pump was used for brine injection. The filtration model constitutes a transparent round tube, and a core sample was fitted inside using two O-rings.

10.3.3. Procedures

The procedures are as following: (1) A core sample was vacuumed and saturated with the brine, and porosity of the core was obtained; (2) The core sample was fitted onto the bottom part of the transparent filtration model; (3) Brine was injected into the model to measure the rock permeability before gel injection; (4) Fully swollen PPG was poured into transparent tube (about half of the tube) and sat on the top of the core while the other space was filled with brine; (5) Brine was injected at the pressures of 10---50---10---100---10---200---10---400---10---500---10 psi, and each constant pressure was run for 30-minutes or until 500 mL of brine (pump capacity limitation) was pumped through the core. Accumulative effluent was recorded at 1, 2, 3, 4, 5, 7.5, 10, 15, 20, 25, and 30 minutes for the period of each pressure used; (6) PPGs were poured out from the tube, then brine was injected again to measure the rock permeability after applying PPGs.

10.4. Results and Discussion

10.4.1. Liquiblock 40K gel

Table 10-1 shows the permeability reduction of the cores for each experiment using Liquiblock 40K gel. K_b is the rock permeability before gel treatment and K_a is the permeability after gel treatment. It can be seen that all rock permeability was reduced from 40 to 60%.

Figure 10-3 shows the cumulative filtration volume as a function of time for experiment two. All filtration curves are straight lines except the one for first 50 psi. Figure 10-4 shows the filtration curves at each 10 psi. It can be seen that all curves except

the first are overlaid, which indicates that the PPG will slightly damage the core only when brine was injected at the first 50 psi, and no further damage occurred even when the injection pressure increased.

10.4.2. DQ Gel

Table 10-2 shows the permeability reduction of the cores for each experiment using DQ. It can be seen that all rock permeability does not change, which indicates DQ does not damage the rock. Figures 10-4 and 10-5 also show that there were no damages on the core samples by using this PPG.

10.5. Discussion

We calculated the effect of gel penetration depth on permeability reduction for the core used in experiment two in Table 10-1. Equations 10-1 and 10-2 were used to calculate the permeability reduction.

$$\boldsymbol{K_a = \frac{K}{F_{rr}}} \tag{10-1}$$

$$\boldsymbol{K_{avg} = \frac{L}{\sum_{j=1}^{n} \frac{L_i}{K_i}}} \tag{10-2}$$

where F_{rr} is residual resistance factor and L is the core length. K_{avg} is the average permeability of the damaged section plus non-damaged section.

Figures 10-7 and 10-8 show some calculation results. It can be seen that the rock permeability is reduced from 87.3% to 99.9% even though a weak blocking agent (F_{rr}=10) slightly penetrates into the rock. It has been frequently observed that the residual resistance factor of a block agent is more than 1000 and the permeability of the rock is reduced more than 95% while the penetration is only 1 mm. Although Liquiblock 40K gel can reduce rock permeability up to 60%, it is still much better than traditional in-situ gels which could totally block the rock.

10.6. Conclusion

Following conclusions can be drawn:

- Strong gels (DQ) do not damage the cores. The PPG neither penetrated into the cores nor formed cake on the surface of the cores.
- Weak gels (Liquiblock 40K) can form a permeable cake on the surface of cores and reduce their permeability in the range of 40% to 60 %.

- A strong PPG is a good choice for preventing formation damage because it will not penetrate into low permeability rock.
- Damage to unswept low-permeable zones/areas caused by PPG could be effectively prevented by controlling particle gel strength.

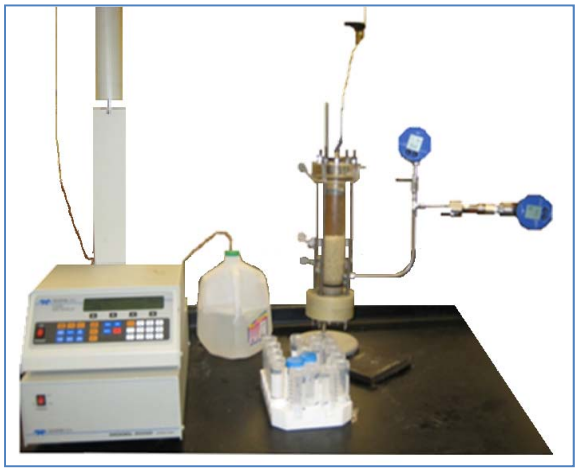

Figure 10-1 Filtration test apparatus picture.

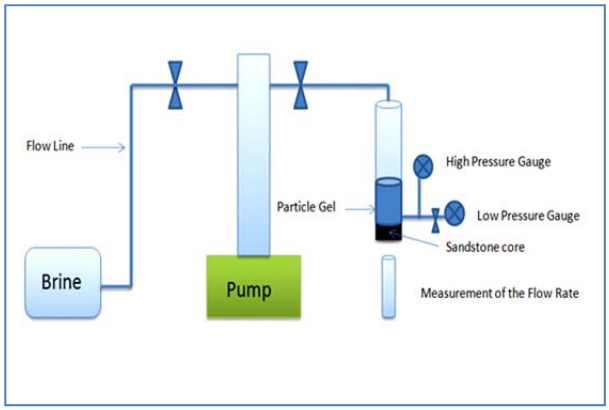

Figure 10-2 Schematic filtration test experiment.

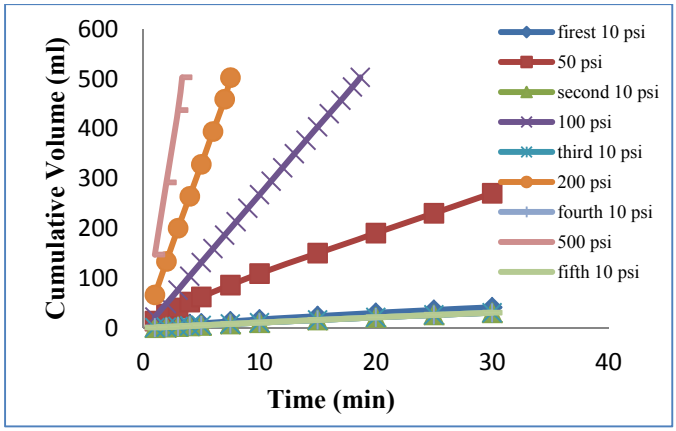

Figure 10-3 Results at 1% brine using Liquiblock 40K gel.
(1 ml = 0.061 in^3)

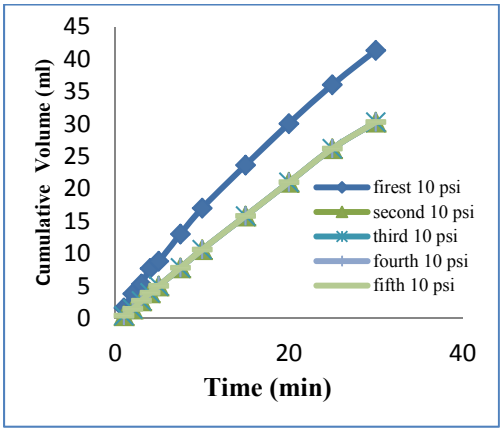

Figure 10-4 Results for each 10 psi (Liquiblock 40K gel).
(1 ml = 0.061 in^3)

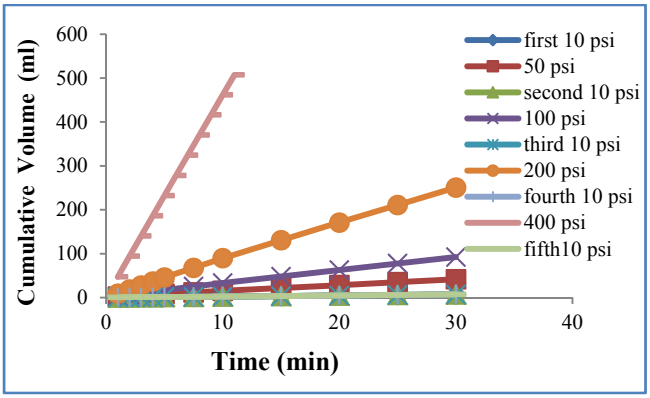

Figure 10-5 Results at 1% brine using DQ gel.
(1 ml = 0.061 in^3)

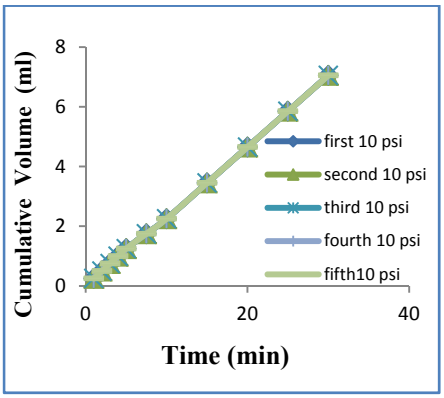

Figure 10-6 Results for each 10 psi (DQ gel).
(1 ml = 0.061 in^3)

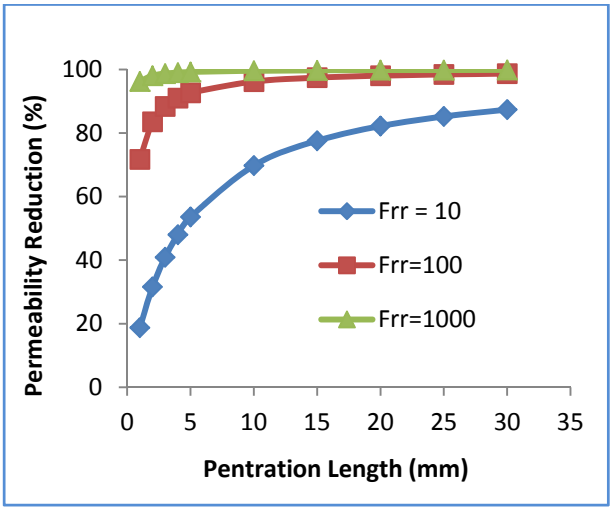

Figure 10-7 Permeability reduction results.
(1 mm = 0.04 inch)

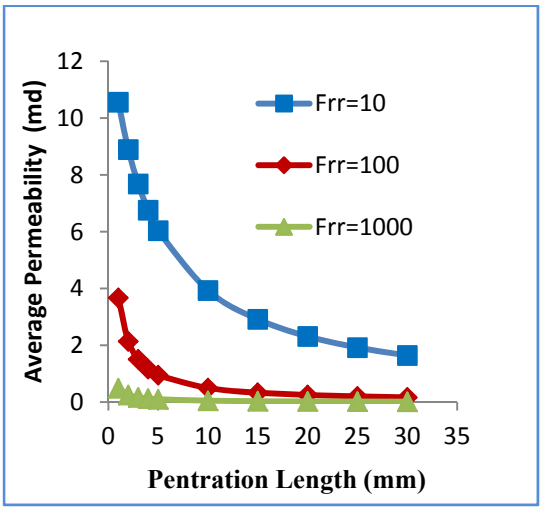

Figure 10-8 Average permeability results.
(1 mm = 0.04 inch)

Table 10-1 Core Permeability before and after Filtration Tests (Liquiblock 40K Gel)

No	D/cm	L/cm	A/cm^2	μ/cp	K_b/md	K_a/md	$K_{reduction}$(%)
Exp1(0.05% NaCl)	3.7	3.8	10.74	1	13	7.8	0.40
Exp2 (1% NaCl)	3.7	4.1	10.74	1	27	14.45	0.46
Exp 3(0.05% NaCl)	3.7	4.1	10.74	1	29	14.80	0.48
Exp4 (10% NaCl)	3.7	3.8	10.74	1	56	22.4	0.60

(1 cm = 0.4 inch)

Table 10-2 Core Permeability before and after Filtration Tests (DQ Gel)

No	D/cm	L/cm	A/cm^2	μ/cp	K_b/md	K_a/md	$K_{reduction}$ (%)
Exp1(0.05 %NaCl)	3.7	3.7	10.74	1	10	10	0
Exp2 (1 % NaCl)	3.7	3.9	10.74	1	13	13	0
Exp3 (10% NaCl)	3.7	4.1	10.74	1	8	8	0

(1 cm = 0.4 inch)

11. Technology Transfer Efforts and Impact to Small Producers

11.1. Technology Transfer Efforts

We submitted periodic, topical, and annual reports that gave details of accomplishments during the reporting periods. This final technical report summarizes work performed in this project. One website (http://web.mst.edu/~baib/PPG.htm) was built to report our research results.

Listed below are the publications and presentations from this research project:

11.1.1. Peer Reviewed Journals

1. Zhang, H.; Bai, B. "Preformed Particle Gel Transport through Open Fractures and its Effect on Water Flow," SPE 129908-PA, *SPE Journal*, 6(2), June 2011, pp. 388-400.
2. Zhang, H., Challa, R., and Bai, B., "Using Screening Test Results to Predict the Effective Viscosity of Swollen Superabsorbent Polymer Particles Extrusion through an Open Fracture" *Industrial & Engineering Chemistry*, Vol 49, 2010, 12284-12293.
3. Wu, Y., Tang, T., Bai, B., "An experimental study of interaction between surfactant and particle hydrogels", *Polymer* 52 (2011), 452-460.

11.1.2. Producer Oriented Journal/publications

4. Bai, B. Preformed Particle Gel for Conformance Control, a weekly lead story, March 21, 2011, JPT online http://www.jptonline.org/index.php?id=739

11.1.3. Conference Papers with Presentations

5. Elsharafi, M., and Bai, B., "Static Filtration Tests to Evaluate the Damage of Preformed Particle Gel on Non-Swept Zones/Areas during Conformance Control Treatments," a paper accepted by the 5th North African Mediterranean Petroleum and Geosciences Conference & Exhibition being held in Tripoli, Libya, 28-30 March 2011.
6. Zhang, H.; Bai, B. "Preformed Particle Gel Transport through Open Fractures and its Effect on Water Flow," paper SPE 129908 presented at SPE Improved Oil Recovery Symposium, 24-28 April 2010, Tulsa, Oklahoma, USA.
7. Wu, Y. and Bai, B, "Modeling Particle Gel Propagation in Porous Media," paper SPE 115678 presented at the SPE Annual Technical Conference and Exhibition, 21-24 September 2008, Denver, Colorado, USA.
8. Bai, B., Liu,Y.,"Case Study on Preformed Particle Gel for In-Depth Fluid Diversion", paper SPE113997 presented at the 2008 SPE Improved Oil Recovery

Symposium to be held in Tulsa, OK, April 21-23, 2008.

9. Bai, B. and Wu, Y. "Preformed Particle Gel for Conformance Control," a paper presented at the conference of Missouri Energy Summit, April 2009, Colombia, Missouri.

11.1.4. Other Presentations

10. Bai, B., "Preformed Particle Gel for Conformance Control," Presented at SPE Applied Technology Workshop (ATW)"Chemical Flooding-EOR" held in Penang, Malaysia, 16-19 January 2011 (Lead Discussion)
11. Bai, B: "A Novel EOR Process-Forced Imbibition through Combining Preformed Particle Gel Conformance Control and Surfactant Treatment," Presented at SPE Applied Technology Workshop (ATW)"Chemical Flooding-EOR" held in Penang, Malaysia, 16-19 January 2011
12. Bai, B. "Preformed Particle Gel for Conformance Control," RPSEA Small Producer Program Showcase - Permian Basin Focus held in Midland, Texas, Feb 3, 2010.
13. Bai, B., "Preformed Particle Gel for Conformance Control," presented the PTTC workshop "Technologies Targeting Mature Properties-RPSEA Small Producer and SWC" held in Tulsa, Oklahoma, August 25, 2010
14. Bai, B., "Preformed Particle Gel for Conformance Control," presented at a PTTC workshop held in Wichita, Kansas, August 26, 2010

11.1.5. Filed Provisional Patent

15. Bai, B., Wu, Y., "Method of Enhanced Oil Recovery," 10MST011prov, Filed in July 09, 2010.

11.1.6. Submitted SPE Abstracts

16. Muhammed, F., and Bai, B. "A Novel Enhanced Oil Recovery Process - Forced Imbibition by Combining Preformed Particle Gels and Surfactant Treatments." Paper submitted to *Journal of Petroleum Science and Engineering* (In Revision).
17. Elsharafi, M., and Bai, B, "Minimize Damage on Unswept Oil Zones/Areas During Preformed Particle Gel Conformance Control Treatments," a paper planned to submit to *SPE Reservoir Engineering and Evaluation*. (in preparation)
18. Zhang, H. and Bai, B. "Preformed-Particle-Gel Propagation through Semi-Transparent Fracture Models," a paper submitted to the 2012 SPE Improved Oil Recovery Conference to be held in Tulsa, OK (also plan to submit to *SPE Journal*).

11.2. Potential Impact to Small Producers

One out of every six barrels of crude oil produced in the United States comes from stripper wells. Excess water production, when accompanied by low oil production, results in wells becoming unprofitable to operate and leads to early well abandonment and unrecoverable oil. Based on reported successful usage elsewhere, PPG treatments have great potential to reverse this trend of decreasing oil production and increasing water production. Results from field application of PPG can provide an increase of several times the previous oil production for several months, even a couple of years, and reduce the water/oil ratio by more than a factor of 2. These treatments typically have ranged from injection of PPG of 2,000 – 30,000 lb of product as a suspension of fine particles. Chemical efficiencies have been very good – as low as 1 bbl incremental oil per pound of PPG chemical. Because the cost of PPG may be $2 - $4/lb, this becomes more attractive economically with current high oil prices. The DOE has estimated that the EOR target for the U.S. to be about 377 billion barrels of oil. Simple technologies like PPG injection are well suited to address the vast reserves of light oil left after mature waterfloods. If this process could just unlock 1% of this oil bypassed by waterflooding, this would represent a potential of 3.7 billion bbl of increased domestic reserves.

11.3. Likely Environmental Impacts

A significant improvement may be achieved by the successful application of PPG in terms of reduced requirements for fresher water sources and reduced volumes of produced water. Specifically, the volume of salt water produced is reduced significantly by selectively plugging water thief zones using PPGs. The general theme of lower volumes of water in hydrocarbon production is a major goal for several U.S. agencies, such as RPSEA, DOE, and EPA. Excess water production is a dominant reason for the abandonment or low profit in stripper wells. Production of salt water has also resulted in serious environment issues. If the oilfield water is classified as a hazardous waste, it would contribute over 98% of the waste produced in this country. Even if only 1% reduction in water production is achieved, $50-100 million could be saved annually and a substantial positive environmental impact could be realized.

Another advantage of the PPG technology is that it is an effective plugging agent that may be used in virtually any source of make-up water. Some other waterflood

conformance agents demand relatively fresh water as a make-up solution. The PPG technology can use almost any produced water as make-up, so there is no need to use fresh water.

12. Conclusions and Recommendations

12.1. Conclusions

This project has developed methods to optimize preformed particle gel treatments to increase oil recovery and reduce water production. The following are conclusions for this whole research program. More details can be found in the appropriate chapters.

12.1.1. Field Application Review for PPG Treatment (Chapter 2)

- Field applications of several PPG conformance control treatments at various reservoir conditions were summarized. To date, PPGs have been applied in more than 3,000 wells with various reservoir conditions, including:
  - Mature water-flooded reservoirs without natural or intentionally-made hydraulic fractures
  - Naturally fractured reservoirs
  - CO_2 flooded reservoirs
  - Polymer flooded reservoirs
- PPGs were applied in reservoirs with temperatures ranging from 30–110 ºC (86–230 ºF), and formation water salinities from 2,900 – 300,000 ppm.
- Treatment weights ranged from 6,600 – 88,000 lbs/well, and were commonly between 17,600 – 33,000 lbs per well.
- Negative effects from treatments were rarely found.
- A key benefit for PPG treatments is that we can use real-time monitoring results of PPG injection (pressure vs injection rate) to adjust initial treatment designs so that a better conformance control treatment can be achieved.
- A detailed example was presented to show how to better select well candidates, design treatment and operation, execute PPG injection, and evaluate performance.

12.1.2. Quantifying Particle Gel Propagation in Fractures (Chapters 3-7)

Lab experiments were run to quantify PPG propagation through fractures and fracture-like channels by using four models: screen models, tube models, transparent fracture models, and semi-transparent fracture models. Results of these experiments can guide the selection of best particle gels for specific reservoirs. The results indicate that

PPG injectivity increases with fracture width and flow rate; it decreases with brine concentration, on which the PPG swollen ratio is dependent. Increasing particle sizes and injection rates cannot significantly increase injection pressure. Fracture models showed that PPG propagated like a piston along a fracture during injection and a gel pack formed in the fracture after PPG placement. Gel packs are permeable and their permeability can be controlled by particle strength and size, and by formation pressure; thus, they can be used to optimize PPG design.

12.1.3. Developed a Novel PPG Treatment Process (Chapter 8)

A new technology called forced surfactant imbibition was initiated by combining PPG with surfactant. The method was developed based on a study of the compatibility of particle gels and surfactants. Surfactants can greatly decrease gel strength, thus the injectivity of particle gels can be significantly improved by the use of proper surfactants. Most surfactants studied were not absorbed into particle gels. Certain surfactants can significantly reduce gel strength; however, gel strength can be recovered after the surfactants have been removed. This technology has potentially large benefits in improving PPG treatments.

12.1.4. Developed a Series of Commercial-Available PPG Products (Chapters 9-10)

A series of customized, well-characterized laboratory scale PPG products were successfully synthesized for laboratory performance testing. These products covered a wide range of particle size and chemical characteristics. The experiments provide improved characterization of particle performance under a range of conditions, so that we can design better field PPG treatments for a large range of well conditions. The swelling capacity of these products was evaluated as a function of salt type, concentration, and temperature. Results indicate that the swelling ratio is generally significantly higher in a sodium chloride rather than in a calcium chloride brine. The PPG-8B product exhibits gradual swelling, taking as many as five days to swell to its maximum extent at room temperature. The PPG-9B product is better suited for lower temperature conditions, but it takes less time to swell to its full extent. More detailed performance statistics are reported in tables in Chapters 9 and 10.

12.1.5. Preliminary Results-Formation Damage caused by PPG (Chapter 11)

The possibility of damage caused by PPG to unswept reservoir areas was investigated in the lab. Preliminary results show that certain millimeter-sized gel particles neither penetrate into conventional rock with a permeability of less than 100 md nor form gel cake on the surface of the rock; thus, they do not damage unswept zones if the particle type and size are properly selected. This lack of damage may explain why PPG treatments in field applications have rarely had negative effects on oil production.

12.2. Recommendations

Numerous works have been done to find ways to optimize PPG treatment in this project. Information from this project will definitely help customers to design a suitable particle gel treatment. A specification form for PPG treatment design is listed in Appendix A (DATA SHEET FOR WELL CANDIDATE SCREEN WITH PPG CONFORMANCE CONTROL) for those who are interested in applying the PPG treatment technology.

It will be very useful to implement the technology if further work can be performed:

1. A new gel treatment concept “Gel-Pack” was initiated to optimize particle gel design in the project. Further work need to carry out to understand what factors impact permeability and compressibility of a “Gel-pack”, which will improve PPG treatment design.

2. An improved particle gel treatment concept, called forced imbibition through the combination of PPG and surfactant treatments, was developed during the project. Further research should be performed to understand the enhanced oil recovery mechanisms and to provide methods to optimize a field application design for this novel enhanced recovery process.

3. Preliminary investigations were made to find out whether particle gels damage non-swept areas/zones in reservoir rock. However, further research should be performed to systematically understand what factors impact the damage and to develop ways to minimize PPG damage to rock matrix or low permeability non-swept oil zones.

4. Preformed particle gels have been successfully applied to control CO_2 flooding conformance. However, no experimental work has been reported on how CO_2 may

impact the behaviors of a given particle gel, or to what extend that particle gel can block CO_2 flow paths.

APPENDIX.

DATA SHEET FOR WELL CANDIDATE SCREEN WITH PPG CONFORMANCE CONTROL

Input Worksheet for data necessary to screen candidate wells for PPG conformance control.

The following worksheet contains information that would be necessary to screen your wells for possible candidates for PPG conformance control.

Contact Information:

Name Title
Telephone Email

Well Information:

Well Type: Injection Well or Production well?
Operator:
Field name:
Location:

Reservoir and Production History Information

The following information is either necessary or useful in evaluation of PPG conformance control for a particular application. Starred information is critical, other information is just helpful.

A. Reservoir Description

1. Formation Name:
2. Size of study area*:
3. Lithology*:
4. Initial oil in-place:
5. Initial oil saturation, Soi* (%)
6. Connate water saturation, Swc* (%)
7. Drive mechanisms*:
8. Reservoir heterogeneity (Naturally fractured or not)*
9. Reservoir temperature:*
10. Formation water salinity (mg/L):*
11. Divalent concentration in formation water*:
12. Reservoir pressure (psi):
13. Oil viscosity at reservoir, cp*:
14. Permeability heterogeneity (Permeability variation coefficient)*:
15. Permeability anisotropy (orientation)*:
16. Sedimentary sequence--distribution of vertical permeability increasing or decreasing within each layer?
17. Average Permeability (md)*

18. Average Porosity (%)

B. Production/Injection History in Candidate Area

1. Current water cut (%)*
2. Current oil recovery (% of OOIP)*
3. Cumulative oil Production (bbl)
4. Cumulative water production (bbl)
5. Average Net Pay Zone thickness *
6. Producer-Injector spacing*
7. Injection water source
8. Injection water salinity*

C. Information for an injection well that is target for conformance control treatment

1. Completion method*
2. Completion Interval(s)*
3. Injected fluids (water, CO_2 or other)*
4. Cumulative injected volume (bbl)
5. Current injection rate (bbl/d)*
6. Wellhead Injection Pressure (psi)*
7. Bottom hole pressure (psi)
8. Net Pay thickness*
9. No. of Injection Zones
10. Injection Profile*
11. Tubing string inside diameter
12. Fractures present/details?
13. Thief zone(s) thickness

D. Information for producers in communication with target injection well

1. Distance between producers and injectors
2. Cumulative oil production
3. Cumulative water production
4. Current oil rate/day*
5. Current water rate/day*
6. Net zones (thickness)
7. Thief Zones (thickness)
8. Fluid level (distance above perfs)
9. Decline rate (%)

E. Related information

1. Previous Conformance control applications (reservoir)
2. Tracer injection and explanation (reservoirs)
3. Sand production
4. Wellbore schematic
5. Completion Diagram
6. Well work history
7. WOR vs cumulative oil production
8. Cumulative oil production vs cumulative water production
9. Comments on the thief zones

If you are interested in having Missouri University of Science and Technology evaluate your field, please contact Dr. Baojun Bai at baib@mst.edu or 573-341-4016.

Nomenclature

Variables

$PI\ (t)$ = pressure index, MPa

$P(t)$ = pressure at the time t after a well is shut in, MPa

T = shut in time, min, usually T is set as 90 minutes

e_1 = oil price, $/t

e_2 = produced water treatment cost, $/m^3

e_3 = PPG price, $/ton

e_4 = operation cost for PPG injection, $

e_5 = well service cost due to PPG treatment, $

e_6 = well testing costs, $;

Q_p = dry PPG particle cost, $/ton

ΔQ_o = incremental oil, ton

ΔQ_w = decreased oil, ton

R = profit-to-investment ratio

ΔP = the pressure drop

ΔP_w = the pressure drop during the water injection

ΔP_g = the pressure drop during the gel injection

r = the internal radius of the tube

v = the velocity

n = flow index

K = consistency constant, Pa·s^n

n_a = apparent flow index

K_a = apparent consistency constant

q = injection flow rate

L = fracture length or tube length

h = fracture height

w = fracture width

k = permeability, md

k_b = rock permeability before gel treatment

k_a = rock permeability after gel treatment

k_{avg} = average permeability of the damage section plus non-damage section

F_r = resistance factor

F_{rr} = residual resistance factor

PG_{exp} = experimental pressure gradient

PG_{cal} = calculated pressure gradient

G' = storage modulus, Pa

G'' = loss modulus, Pa

T = the torque exerted on the sample

v = the volume of surfactant hydrocarbon core, nm^3

l = the length of surfactant hydrocarbon chain, nm

a_0 = effective area of surfactant hydrophilic group, nm^2

n_c = the number of carbon atoms of hydrocarbon chain without methyl groups

n_{methyl} = the number of methyl groups in the hydrocarbon chain

m = the number of ethylene oxide groups

T = the torque exerted on the sample

r = the length of the lever arm

ΔT = temperature shift, K

D_p = pore size of the swollen hydrogel particle, nm

Greek Symbols

γ = shear rate, s^{-1}

τ = shear stress, Pa

μ = the viscosity of liquid, cp

μ_{PPG} = effective viscosity of swollen particle, cp

μ_w = water viscosity, cp

μ = frictional coefficient

ε_a = absolute average relative error, %

Subscripts

A = apparent

avg = average

cal = calculated

exp = experimental

eff = effective

w = water

PPG = swollen particle gel

References

Abbasy, I. et al. Laboratory Evaluation of Water Swellable Materials for Fracture Shutoff. Paper SPE 111494 presented at 2008 SPE North Africa Technical Conference and Exhibition in Marrakech, Morcco, 12-14 March 2008.

Al-Anazi, H.A. and Sharma, M.M. 2002. Use of a pH Sensitive Polymer for Conformance Control. Paper SPE 73782 presented at the SPE international Symposium and Exhibition on Formation Damage Control, Lafayette, Louisiana, 20-21 February 2002.

Al-Assi, A.A., Willhite, G.P., Green, D.W., and McCool, C.S. 2009. Formation and Propagation of Gel Aggregates Using Partially Hydrolyzed Polyacrylamide and Aluminum Citrate. *SPEJ* 14 (3): 450-461. SPE-100049-PA. doi: 10.2118/100049-PA.

Allain, C.; Salome, L. Gelation of Semidilute Polymer Solutions by Ion Complexation: Critical Behavior of the Rheological Properties versus Cross-link Concentration. Macromolecules. 1990, 23, 981.

Arhuoma, M.; Dong, M.; Yang, D.; Idem R. Determination of Water-in-Oil Emulsion Viscosity in Porous Media. Ind. Eng. Chem. Res. 2009, 48, 7092.

Aslam, S.; Vossoughi, S.; Willhite, G.P. Viscometric Measurement of Chromium (III)-Polyacrylamide Gels by Weissenberg Rheogoniometer. Proceedings of the AIME SPE/DOE Symposium on Enhanced Oil Recovery, Tulsa, Oklahoma, April 15–18, 1984; SPE Paper 12639.

Bai, et al. Case Study on Preformed Particle Gel for In-Depth Fluid Diversion. Paper SPE 113997 presented at SPE/DOE at the 2008 SPE/DOE 16th Symposium on IOR held in Tulsa, OK, U.S.A., April 20–23.

Bai, B., et al. Conformance Control by Preformed Particle Gel: Factors Affecting its Properties and Applications, *SPEREE*, Aug 2007, 415-421.

Bai, B., et al. Preformed Particle Gel for Conformance Control: Transport Mechanism through Porous Media. *SPEREE*, April 2007, 176-184.

Bourgoyne, A., et al. Applied Drilling Engineering; Society of Petroleum Engineers: Houston, TX, 1991.

Broseta, D. et al. Rheological Screen of Low-Molecular-Weight Polyacrylamide/Chromium (III) Acetate Water Shutoff Gels. Proceedings of the SPE/DOE Symposium on Improved Oil Recovery, Tulsa, Oklahoma, April 3–5, 2000; SPE Paper 59319.

Buchholz and Graham, *Modern Superabsorbent Polymer Technology*, Wiley-VCH, New York, 1998, pp. 1-152.

Chauveteau, G., Omari, A., Tabary, R., Renard, M., and Veerapen, J. New Size-Controlled Microgels for Oil Production. Paper SPE 64988 presented at the 2001 SPE International Symposium on Oilfield Chemistry, Houston, Feb 13-16.

Chauveteau, G., Tabary, R., Renard M. and Omari, A. 1999. Controlling In-Situ Gelation of Polyacrylamides by Zirconium for Water Shutoff. Paper SPE 50752 presented at the SPE International Symposium on Oilfield Chemistry, Houston, Texas, 16-19 February 1999.

Chauveteau, G., Tanary, R., Le Bon, C., Renard, M., Feng, Y. and Omari, A. In-depth Permeability Control by Adsorption of Soft Size-Controlled Microgels. Paper SPE 82228 presented at the 2003 SPE European Formation Damage Conference, The Hague, The Netherlands, May 13-14.

Cheung, S.,et al. A Swelling Polymer for In-depth Profile Modification: Update on Field Applications. Paper presented at SPE Applied Technology Workshop of "Chemical Methods of Reducing Water Production," San Antonia, Texas, USA, March 4-6, 2007.

Coste, J.-P., Liu, Y., Bai, B., LI, Y., Shen, P., Wang, Z., and Zhu, G. In-Depth Fluid Diversion by Pre-Gelled Particles. Laboratory Study and Pilot Testing. Paper SPE 59362 presented at 2000 SPE/DOE Improved Oil Recovery Symposium, 3-5 April, Tulsa, Oklahoma.

Du, Y. and Gong, J. P. in Surface Friction and Lubrication of Polymer Gels, ed. G. Biresaw and K. L. Mittal, CRC Press, Boca Raton, Florida, May 2008, ch. 11, pp.223-246.

Ershagi, I. et al. 1986. Injectivity Losses under Particle Cake Buildup and Particle Invasion. SOC. Petrol. Engr. paper No. 15073, California Regional Meet., Oakland, CA, April 2-4.

Frampton, et al. Development of a Novel Waterflood Conformance Control System. Paper SPE 89391 presented at the 2004 SPE/DOE 14th Symposium on IOR held in Tulsa, OK, U.S.A., April 17–21.

Friedmann, F., Hughes, T.L., Smith, M.E., Hild, G.P., Wilson, A., and Davies, S.N. 1999. Development and Testing of a Foam-Gel Technology to Improve Conformance of the Rangely CO2 Flood, *SPEREE* 2 (1): 4-13. SPE-54429-PA. doi: 10.2118/54429-PA.

Ganguly, S., Willhite, G.P., Green, D.W., and McCool, C.S. 2001. The Effect of Fluid Leakoff on Gel Placement and Gel Stability in Fractures. Paper SPE 64987 presented at SPE International Symposium on Oilfield Chemistry, Houston, Texas, 13-16 February 2001.

Hild, G.P. and Wackowski, R.K. 1999. Reservoir Polymer Gel Treatments To Improve Miscible CO2 Flood. *SPEREE* 2 (2): 196-204. SPE-56008-PA.

Huh, C., Choi, S.K., and Sharma, M.M. 2005. A Rheological Model for pH-Sensitive Ionic Polymer Solutions for Optimal Mobility-Control Applications. Paper SPE 96914 presented at the SPE Annual Technical Conference and Exhibition, Dallas, Texas, 9-12 October, 2005.

Kakadjian, S.; Rauseo, O.; Mejias, F. Dynamic Rheology as a Method to Quantify Gel Strength of Water Shutoff Systems. Proceedings of the International Symposium on Oilfield Chemistry, Houston, Texas, February 16–19, 1999; SPE Paper 50751.

Larkin, R. and Creel P. Methodologies and Solutions to Remediate Inter-well Communication Problems on the SACROC CO2 EOR Project-A Case Study. paper SPE 113305 presented at 2008 SPE/DOE Improved Oil Recovery Symposium held in Tulsa, OK, 19-23 April 2008.

Liang, J-T. and Seright, R.S. 1993. Gel Placement in Production Wells. *SPEREE* 8 (4): 276-284. SPE-20211-PA.

Li, Y., Liu, Y., Bai, B. Water Control Using Swollen Particle Gels. *Petroleum Drilling and Production Technology*, Vol 21(3), 1999. (in Chinese)

Liu, Y., Bai, B., Wang, Y. Applied Technologies and Prospects of Conformance Control Treatments in China. *Oil & Gas Science and Technology*, 65(6), 2010, pp 859-878.

Liu, Y.Z. et al. Application and Development of Chemical-Based Conformance Control Treatments in China Oil Fields. Paper SPE 99641 presented at the 2006 SPE/DOE Symposium on Improved Oil Recovery, Tulsa, Oklahoma, USA, April 22-26.

McCool, C.S., Li, X., and Willhite, G. P. 2009. Flow of Polyacrylamide/Chromium Acetate System in a Long Conduit. *SPEJ* 14 (1): 54-66. SPE-106059-PA.

O'Brien, W.J., Stratton Jr., J. J; Lane, R.H. 1999. Mechanistic Reservoir Modeling Improves Fissure Treatment Gel Design in Horizontal Injectors, Idd El Shargi North Dome Field, Qatar. Paper SPE 56743 presented at SPE Annual Technical Conference and Exhibition, Houston, Texas, 3-6 October 1999.

Pearson, D.S.; Graessley, W.W. The Structure of Rubber Networks with Multifunctional Junctions. *Macromolecules*. 1978, 11, 528.

Pritchett, J., Frampton, H., Brinkman, J., Cheung, S. Morgan, J., Chang, K.T., Williams, D., Goodgame, J. Field Application of a New In-Depth Waterflood Conformance Improvement Tool. Paper SPE 84897 presented at 2003 International Improved Oil Recovery Conference in Asia Pacific, 20-21 October, Kuala Lumpur, Malaysia.

Prud'homme, R.K. et al. Rheological Monitoring of the Formation of. Polyacrylamide/Cr3+ Gels. *SPEJ*. 1983, 23, 804.

Prud'homme, R.K.; Uhl, J.T. Kinetics of Polymer/Metal-Ion Gelation. Proceedings of the AIME SPE/DOE Symposium on Enhanced Oil Recovery, Tulsa, Oklahoma, April 15–18, 1984; SPE Paper 12640.

Pyziak, D. and Smith, D. Update on Anton Irish Conformance Effort. Paper presented at the 6th international conference on production optimization---reservoir conformance-profile control-water and gas shut-off, Houston, Nov 7-9, 2007.

Ramazani-Harandi M.J.; Zohuriaan-Mehr M.J.; Ershad-Langroudi A.; Yousefi A.A.; K. Kabiri. Rheological Determination of the Swollen Gel Strength of the Superabsorbent Polymer Hydrogels. *Polym. Test*. 2006, 25, 470-474.

Riccardo Po, J. Macromol. Sci., Rev. Macromol. *Chem. Phys*, 34, 1994, 607-662.

Rosen., M. J. Surfactants and Interfacial Phenomena. Wiley-Interscience, 3rd Ed., 2004.

Rousseau, D., Chauveteau, G., Renard, M., Tabary, R., Zaitoun, A., Mallo, P., Braun, O. and Omari, A. Rheology and Transport in Porous Media of New Water Shutoff/Conformance Control Microgels. paper SPE 93254 presented at the 2005 SPE Int. Symp. On Oilfield Chemistry, Houston, TX, USA, Feb 2-4.

Seright, R.S. 2004. Conformance Improvement Using Gels. Annual Technical Progress Report, Contract No. DE-FC26-01BC 15316, US DOE, Washington, DC (September 2004).

Seright, R.S. Gel Placement in Fractures Systems. Paper SPE 27740 presented at SPE Enhanced Oil Recovery Symposium, 17-20 April, 1994, Tulsa, Oklahoma.

Seright, R.S. 1999. Gel Treatments for Reducing Channeling in Naturally Fractured Reservoirs. *SPEPF* 14 (4): 269-276. SPE-59095-PA.

Seright, R.S. 1988. Placement of Gels to Modify Injection Profiles. Paper SPE 17332 presented at SPE Symposium on Enhanced Oil Recovery, Tulsa, Oklahoma, 16-21 April 1988.

Seright, R.S., et al. A Comparison of Different Types of Blocking Agents. SPE 30120 presented at the European Formation Damage Conference, May, 1995.

Seright, R.S. Use of Preformed Gels for Conformance Control in Fractured Systems. Paper SPE 35351, *SPEPF*, 2, 1997.

Seright, R.S. Gel Propagation through Fractures. *SPEPF*, 11, 2001, 225-232.

Seright, R.S. Washout of Cr (III)-Acetate-HPAM Gels from Fractures. Paper SPE 80200 presented at the 2003 SPE international Symposium on Oilfield Chemistry, Houston Feb 5-7.

Seright, R.S. and Liang, J-T. 1994. A Survey of Field Applications of Gel Treatments for Water Shutoff. Paper SPE 26991 presented at SPE Latin America/Caribbean Petroleum Engineering Conference, Buenos Aires, Argentina, 27-29 April 1994.

Seright, R.S; Martin, F.D. 1993. Impact of Gelation pH, Rock Permeability, and Lithology on the Performance of a Monomer-Based Gel, SPERE 8(1), Feb 1993, 43-50.

Smith, D., Kemp, M.K., McBee, M., et al. The successful Evolution of Anton Irish Conformance Efforts. Paper SPE 103044 presented at the SPE Annual Technical Conference and Exhibition, 24-27 September 2006, San Antonio, Texas, USA.

Smith J. E. The Transition pressure: A quick Method for Quantifying Polyacrylamide Gel Strength. Paper SPE 18739 presented at SPE International Symposium on Oilfield Chemistry, Houston, Texas, 8-10 February 1989.

Sydansk, R.D. and Moore, P.E. Gel Conformance Treatments Increase Oil Production in Wyoming. *Oil & Gas J*. (Jan. 20, 1992) 40-45.

Sydansk, R. D. and Seright, R. S. 2007. When and Where Relative Permeability Modification Water-Shutoff Treatments Can Be Successfully Applied. *SPEPF* 22 (2): 236-247. SPE-99371-PA.

Tang, C.J. Profile Modification and Profile Modification plus Oil Displacement Technique in the High Water Cut Oilfield in Zhongyuan Oilfield. *Petroleum Geology & Oilfield Development in Daqing*, Vol. 24(1), 2005. (in Chinese)

Thurston, G.B.; Ozon, P.M.; Pope, G.A. Viscoelasticity and Gelation of Some Polyacrylamide and Xanthan Gum Solutions. Proceedings of the American Institute of Chemical Engineers Spring National Meeting and Petro Expo, Houston, Texas, March 24–28, 1985; Paper No. 62B.

Vetter, O. J., et al. 1987. Particle invasion into porous medium and related injectivity problems. SOC. Petrol. Engr. paper No. 16255, Intl. Symp. On Oilfield Chem., San Antonio, TX, Feb. 4-6.

Woods, P., Schramko, K., Turner, D., Dalrymple, D.,1986. In-Situ Polymerization Controls CO_2/Water Channeling at Lick Creek. Paper SPE 14958 presented at SPE Symposium on Enhanced Oil Recovery, Tulsa, Oklahoma, 20-23 April 1986.

Zaitoun, A., Tabary, R., Rousseau, D., Pichery, T., Nouyoux, S., Mallo, P., and Braun, O. Using Microgels to Shutoff Water in Gas Storage Wells. Paper SPE106042 presented at 2007 SPE Int. Symp. On Oilfield Chemistry, Houston, TX, USA, 28 Feb - 2 March.

Zhang, H. and Bai, B. Preformed Particle Gel Transport through Open Fractures and its Effect on Water Flow. Proceedings of the SPE Improved Oil Recovery Symposium, Tulsa, Oklahoma, April 24–28, 2010; SPE Paper 109908.

SI Metric Conversion Factors

Å x 1.0*	E-10	= m
atm x 1. 01325	E+05	= Pa
bar x 1.0*	E+05	= Pa
bbl x 1. 589873	E-01	= m^3
bbl x 1.364	E-01	= metric ton
cp x 1.0*	E-03	= Pa · s
ft x 3.048*	E-01	= m
ft^2 x 9.290304*	E-02	= m^2
ft^3 x 2.831685	E-02	= m^3
ft/D x 3.528	E-06	= m/s
ºF x (ºF - 32)/1.8		= ºC
gal x 3.785412	E-03	= m^3
lb x 4.536	E-04	= metric ton
lb/gal x 1.20	E-01	= g/cm^3
in. x 2.54*	E+00	= cm
$in.^2$ x 6.4516*	E+00	= cm^2
$in.^3$ x 1.6387	E+01	= cm^3
$in.^3$/hr x 1.6387	E+01	= cm^3/hr
lbm x 4.535924	E-01	= kg
md x 9.869233	E-04	= μm^2
ppb x 1.0*	E+00	= µg/L
ppm x 1.0*	E+00	= mg/L
pound x 0.45359	E+00	= kg
psi x 6.894757	E+00	= kPa
psi/ft x 2.262059	E+01	= kPa/m
bbl/(psi•day) x 2.3059	E+01	= m3/(MPa•day)

*Conversion factor is exact.